Sediment-Triggered Migration and Floodplain Habitat Development in Meandering Rivers

Joshua Ahmed

2017

Thesis submitted as partial fulfilment for the degree of Doctorate of Philosophy

Summary

Meandering rivers create some of the most intricate and diverse regions on the planet. Lateral migration excavates floodplain material from the outer banks of meanders and subsequently deposits it at the hydrodynamically calmer inner bank region, creating point bars. Point bars are constructed by the progressive attachment of sediment in the form of scroll bar deposits: sediment shoals up and becomes deposited on the margins of the bar, increasing its aerial extent, which becomes stabilised by vegetation once regular inundation ceases. Point bars have the potential to affect flow as it is routed through the meander by both increasing the curvature of the bend and topographically forcing water to flow outwards, increasing boundary shear stress and rates of bank erosion.

A combination of remotely-sensed data, GIS, and a 2D morphodynamic flow model was used to examine the role of externally-imposed sediment supply on point bar growth and floodplain evolution in the Amazon Basin. Externally-derived sediment supply is important since it provides the material used to build point bars – of course supplemented by internal sediment sources. A simulated reach on the Sacramento River, USA was used to investigate the role of increased sediment supply on bar growth and meander evolution through time.

It is demonstrated that rivers characterised by high sediment loads have greter migration rates, rates of cutoff production, and larger populations of oxbow lakes driven by the maintenance of a steady-state sinuosity on the rivers through time. Channel sinuosity increases with migration rate, although the rate of sinuosity increase is determined by the type of meander deformation: downstream translating bends increase their length more quickly than their upstream translating or extensional counterparts. Point bar growth was observed to occur under high sediment loading conditions when modelled using a 2D morphodynamic model. The bar sequestered sediment at the upstream head of the bar causing it to grow

upstream. This increased the distance of outer bank subjected to bank erosion and also increased to magnitude of bank erosion. a sediment-driven control on sinuosity increases manifested through bend deformation style, and the simulated growth of point bars in the presence of enhanced sediment loading which resulted in increased rates of bank erosion. These results are of significance for meandering theory and particularly indicate the importance of point bars in effecting the morphodynamic evolution of meandering rivers.

Notice of Submission	
Candidate's last name	Ahmed
Candidate's first name(s)	Joshua
Candidate's student number	0838970
School	School of Earth & Ocean Sciences
Title of degree	PhD
Full title of thesis	Sediment-triggered migration and floodplain habitat development in meandering rivers
Is this a resubmission?	NO
Is a Bar on Access or library deposit required?	Bar on Access: NO Library deposit: NO
Candidate's signature		Date	

Dedicated to the haters, and to myself

Acknowledgements

First and foremost, I would like to thank my original supervisors without whom this project would be a mere shell of the final product, José, Eli, thanks for the enthusiastic conversations, ideas, and the knowledge you imparted to me along the way. My gratitude also goes to TC, my final supervisor, but always a fantastic source of knowledge and guidance. I must also thank Tom Dunne for his contributions to the thesis, his knowledge and expertise as a geomorphologist, hydrologist and simply as a scientist are second to none. Huge thanks to the #GeomorphLadsOnTour: Rhodri, Alex, Huw, and my predecessors, with whom I had the pleasure to share an office with: Kate and Pauline. I would also like to thank my family for their support during the creation of this masterpiece.

The journey has been long, longer than many, but shorter than a select few of Earth students out there (Piers, whoOoO?). Countless memories have been created over the past five years with several generations of PhD student: first came the 'Ciborowski' era, the students who demonstrated to me and inspired (perhaps?) me to become a PhD student (Jake, Elaine, Paola, James, Tracy, Pauline and Luca), many of whom I never spoke to outside of being an ignorant student, but some of whom I can call "friends" – oooh, PhD friends. Next, the 'Final Years' era (Hayes, Knight, Wild, Manton, Olu, Simon, Butler, Young, Wilson et al.) a great bunch with whom the chaotic mantra of 'Friday at Five' was truly embraced. Those mad weeks in the first term were a great induction to PhD life and a chance to integrate with some of the older generations week after week in the Pen and Wig, Lloyds, Live Lounge, Ten Feet Tall, and, of course, Full Moon. The countless "Jager Bombs" were a horrible, yet necessary end to the week. Then, the "Year Above" era, led by the likes of Coombs, Kirkham, Deaney, Olivier, Lawton, Lee, Hughes, Piedade, and Morgan. Although not as social as their 'Final Year' counterparts, a select few were always keen to come along for the ride (Coombs), whilst the others were always a staple in

the 'viva room' (now PhD Common Room) for an extended lunch session. Then, came my year: the legendary group of Charidemou, Pyle, Price, Bubeck, Kaigama, Jhan, and later on, Bates – albeit for a short time. Not being based in the same office could have isolated me from the madness of PhD life, but luckily coming up for lunch each day ensured I was integrated with the goings on of the department. A PhD can be a lonely experience if you let it be, if there's one piece of advice I would give to a new starter it would be to ensure you step away from the work once in a while and embrace the social side of PhD life. There's not many people in the department who would say no to a 30-minute stroll around the park on a sunny day! The following generation were somewhat tame compared to the years previous, but a nice bunch nonetheless. Phillips, Mikis, Horton, Loocke, Thomas, Mithan and more were added to the mix, and have since become associated with the onset of the Great Friday at Five Depression. The following year's cohort was certainly a large one: Hodge, Nairn, Detlef, Sparkes, Ward, Mattos, Gooday, Mitchison, Kennedy, Karykowski, and Stephenson et al. The F@5 decline continued under their management, but lunchtimes became busier, and on the odd occasion, the pub sessions would become larier. October 2015 saw the additions of Guice (G^2), Jillings, Nuber, Bennett, Martin, Poniecka, and Piga (although based in LDN for the majority of the time). Once again, this new intake were poor organisers sending F@5 further into decline. One merit of their work however, was their ability to organise Christmas parties (primarily the work of Bennett and Jillings), which did fuse the PhD years together.

October 2016 – the year of the rowdy. The 'bunch of undergrads' as they were coined by an unnamed member of the PhD community brought a new dynamic to the department. Enter, Panton, Williams, Brims (Grims), Hall, Reedman, Gore, Wang, Francis, Gillies, Price, Roelofse and Zhang. F@5 made a surging return reminiscent of the 'old days' when I began my PhD – the routine somewhat similar to those days, too. The only notable difference was the end location, Welsh Club. Being in the same

position as the 'Final Years' when I started, I now understand their willingness to sesh. The rowdy Pen and Wig sessions continued on to Cuba Revs, Live Lounge, and more often than not, Welsh Club (the home of Aled and the birthplace of the universal 'give me straws' hand sign). A few outings to the Sesh-U (SU) were also reminiscent of the old days when we ventured there for a Drink-The-Bar-Dry event in 2013. Needless to say, the adventures had post-5pm were always memorable and certainly an integral part of PhD life. Remember, the spontaneous nights are always the best ones (cheers to that!).

During my tenure in Cardiff I've had the fortune to travel (relatively expense-free) to many destinations: in my first year, I travelled to the affluent region of Windsor where I stayed – with full board – at Cumberland Lodge (where the filmed the King's Speech). This was also where I met many fellow geomorphically-minded colleagues from across the UK, many of which were familiar faces at conferences over the years (Strick, Ye, Biddy). In summer 2013 I travelled to Minneapolis to the National Centre for Earth-Surface Dynamics (NCED); here I met future friends for the first time (including a young(er) Dan Hobley), legendary geomorphologists (Chris Paola and Gary Parker), and learnt about experimental techniques commonly used in geomorphology. This experience taught me a lot, but also made me realise how little I knew – a common and reoccurring feeling felt throughout the PhD process. I have also been lucky to attend every BSG conference since commencing my PhD having met countless colleagues and legends over the years at Royal Holloway, Manchester, Southampton, and Plymouth. In addition to UK-based conferences, I've also visited Vienna twice for EGU and ventured across the pond to San Francisco for AGU, also on two occasions. As if that wasn't enough I've presented at a Quaternary Research Association conference in Exeter and a BGS conference in Edinburgh – where I was mistakenly given a keynote lecture slot. Once again, I would like to state the importance of attending conferences for two reasons: first, presenting your work in

front of your peers is a great way to network and build a reputation for yourself, which may be useful when it comes to moving beyond your PhD. Second, the social aspect of conferences is great. Meeting people with similar interests is how research ideas are created! Additionally, conferences give you the chance to explore a different place for **free**! You can also tack on a little holiday at the end of the conference: a highlight was certainly road-trippin' to VEGAS via Lake Tahoe, Reno, Bishop, and Death Valley over three days after AGU '16. Those landscapes were textbook, and Las Vegas… what a place!

Despite not being able to conduct any PhD-related fieldwork, which was one real downside of my project, I've managed to head out and relive many of my undergraduate fieldtrips. Who'd have thought they'd be so fun? I suppose the wandering around occasionally imparting knowledge to clueless students for a wage is rather appealing. I also managed to set up my own field campaign, the data from which will hopefully yield a manuscript and form a longer-term project. The tales from those two trips will be forever etched in my mind, particularly one or two events, which will (hopefully) remain undisclosed. Thanks to Michael, Matthew, Bob, Henry and James for assisting me on those trips.

One of the real privileges of being a PhD student (as if there wasn't already enough) is demonstrating. Being able to inspire and direct the learning of the next generation of scientists is an honour. Yes, it's supposed to be somewhat of a chore, but the satisfaction in helping someone understand something they otherwise wouldn't is a truly rewarding experience. Remember, you were probably in exactly the same clueless position they were when you were starting out! I've had the pleasure of getting to know many of our undergrads who are now more successful than I am. Shout out to all those I've helped, and the ones who humoured me with their banter over the years. In particular shouts to ECC (big up the Essex gang), Eleanor, Charlotte, Craig, Millie, Zoe, Beth, Elliot, Emma, Alex, Andy, Leroy, Ben, Alice, Kate,

Lilly, Harry, Callum, Tom, Josh, Adam, Scott, Ed, Luke, Ben, Chris, Izzy, Emily, Meg, Sam, Callum, Emily, Emily, Jake, Mitch, and of course Dan. The #CU_EES gang with whom I spent many hours with on fieldwork, teaching and demonstrating, and my tutees who had the pleasure of me being their tutor for a year.

All-in-all my 9-year career in Cardiff has been a truly memorable one. I've seen lecturers come and go (Rich Walker/Eli Lazarus), legends retire (John Parkes), and some people who've been as omnipresent as myself (Simon). The staff in this school have helped support me during my undergrad, PhD and during my time as a tutor, so a special big up to Jose, TC, Simon, Jenny, Alan, Liz, Henrik, Johan, Paul, Huw, Alun, Paul, Andrew, Andrew (Kerr), Ian, Jo, Christine, and Simon (Feely). I would be remiss if I didn't name some of the iconic (some may say Hall of Fame worthy) members of the department who have made this experience a thoroughly enjoyable one: Miros, Henry, Pricey, Pyle, Kirkham, Hayes, Wild, Manton, Rob, Paola, Margit, Loocke, Bethan, Micky, G^2 (although I'm sure he won't appreciate being in such an arbitrary list), Hennie, Hodge, Grims, Panton, Williams, Hall, Sir Jamie of Price, and of course, the legendary ANABEL - OH MY GOD! All of whom I am happy to call friends. A big thanks is also extended to Mr Trudson and to Trudy for their support and effort in the early days and particularly for their insightful RE-views.

Before I finish, I've also got to take a moment to thank BBC Radio 1, BBC Radio 1Xtra, Capital Xtra and Beats 1 for the many hours of entertainment they have provided me with over the years. Music has always been, and will continue to be, a huge motivator in my work. Big respect to DJ Stalkerseal for his magnificent mixes. The mixtape battles between Stalkerseal and DJ Killer Wales were game-changing. A special thanks to the Mundane Bulletin – you writers are something else! To the clubs, pubs and bars, and festivals that have provided an alternative venue to the office: Glam, Revs, Revolucion de Cuba, Live Lounge, 10 Feet Tall, Buffalo, Clwb Ifor Bach, Full Moon, Walkabout, Tiger Tiger, Pulse, Y Plas/Solus, X-Festival, Wireless,

Hospitality in the Park, Owain Glyndwr, Hopbunker, Gatekeeper, Central Bar, Kokos, Gassy Jacks, The Vulcan, The Woodville, The Flora, The Crwys, and of course, The Pen and Wig. Thanks to EasyGym for their wonderful facilities which, in addition to keeping me in fantastic shape, would spark the idea for what became a *Geology* manuscript.

Some final lessons every PhD student should remember are:

- You **ARE** entitled to holidays.
- You have an incredibly flexible work schedule. Don't feel obliged to work the same 9-5 day when you can make use of the day for the gym, soaking up the sun, running errands. As long as you meet your expectations, you'll do fine!
- Get involved with things in the department and speak to people.
- Enjoy this time, it will be over before you know it (unless you 'do-a-me').

And finally, to close, I adapt a famous excerpt from Dr Dre's 'Forgot about Dre':

"What cause I been in the lab, with a pen and a pad, tryna get this damn thesis off, I ain't havin' that, this is the millennium of Geomorphic Josh, it ain't gonna be nothin' after that, so give me my damn doctorate, and F*** science you can have it back."

and, Kendrick Lamar's DNA*:*

"I got geomorphology, morphology inside my DNA"

Table of contents

Chapter 1

Chapter 2

Chapter 3

Chapter 4

Chapter 5

Chapter 6

List of Figures

Chapter 1

Chapter 2

Chapter 3

Chapter 4

Chapter 5

List of Tables

List of Variables

τ (N m^{-2}) - shear stress

Θ - Shield's number

ρ (kg m^{-3}) - Density of water

ρ_s (kg m^{-3}) - Density of sediment

τ_C (N m^{-2}) - Critical shear stress

τ_B (N m^{-2}) - Boundary shear stress

g (m s^{-2}) - Gravitational acceleration constant

h (m) - Depth of water

H (m) - Water level

S - Channel bed slope

D_{50} (m) - Median grain size

A (m^2) - Area of polygon

P (m) - Perimeter of polygon

S_{FA} (Mt yr^{-1} m^{-1}) - Suspended sediment flux per channel width

S_F (Mt yr^{-1}) - Sediment flux

C_W (m) - Channel width

M (ch-w yr^{-1}) - Meander migration rate

M_L (m) - Meander elongation rate

f - Fractional change in channel length due to cutoff

L (m) - Characteristic length of channel removed by cutoff

n - Number of cutoffs

V (m) - Valley length

S_i (yr^{-1}) - Channel sinuosity

l_0 (m) - Length of year 1 channel centreline

σ (m^2) - Meander symmetry index

S^* (yr^{-1}) - Change of channel sinuosity

p - Mass flux in the x-direction

q - Mass flux in the y-direction

t (s) - Time

h (m) - Water depth

H (m) - Water level

R_s - Radius of curvature of the streamline in the x-direction

R_n - Radius of curvature of the streamline in the y-direction

C - Chezy coefficient

C_{BF} - Bankfull Chezy coefficient

a - Resistance coefficient

b - Resistance power

E - Eddy viscosity

Q_{Curv} - Mass fluxes in the y-direction in a curvilinear coordinate system

P - Mass fluxes in the x-direction in a curvilinear coordinate system

Q_{BF} (m^3 s^{-1}) - Bankfull discharge

Q (m^3 s^{-1}) - Discharge

I_s - Helical flow intensity

Tanδ_s - Angle of deviation between downstream and cross-stream flow components

ζ - Helical flow parameter

ε - Helical flow calibration constant

κ - Von Karmen's constant

Φ - Non dimensional sediment transport rate

S_{tl} - Engeund and Hansen (1967) total sediment load

R (m) - Hydraulic radius

H - Manning's n

u (m s^{-1}) - Velocity

z (m) - Elevation

E_L (m) - Entrance ramp length

S_s m^3 s^{-1} m^{-1}) - Sediment transport in the x-direction

S_n (m^3 s^{-1} m^{-1}) - Sediment transport in the y-direction

G - Transverse slope coefficient

α - Transverse slope power

e - Longitudinal slope coefficient

ζ - Struiksma longitudinal slope value

Q_{BL} (Mt yr^{-1}) - Reach-averaged bedload sediment transport rate

φ - Transverse slope bank erosion coefficient

ψ - Ratio of sediment transport at the outer bank

B_E (m yr^{-1}) - Bank erosion rate

Chapter 1

Introduction and Literature Review
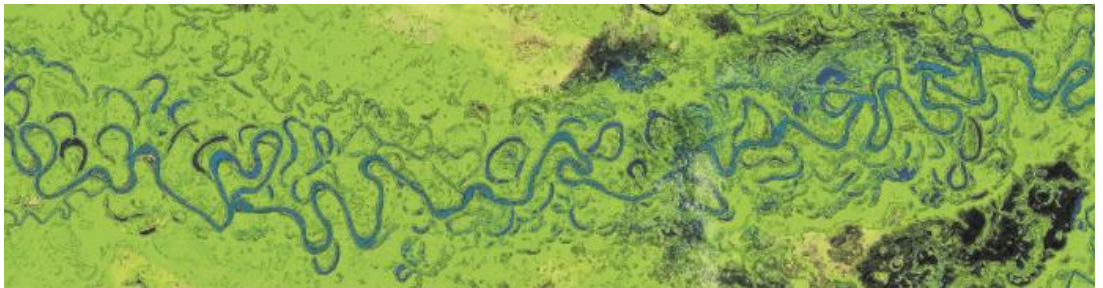
1. Introduction

Meandering rivers are some of the most important natural features on the planet; their movement across the landscape orchestrates the exchange of sediments, nutrients and water across the fluvial-terrestrial interface, ultimately facilitating the development of highly biodiverse riparian landscapes (Tockner and Stanford, 2002). The appealing aesthetics of meandering rivers reflect the complex processes governing the evolution of these features many of which remain poorly understood.. Over the past 50 years geomorphologists have identified a suite of key mechanisms operating in meandering channels. However, the complexity and variety of landscapes in which these rivers are found makes it difficult to understand the fundamental controls governing their development (Hickin, 1974; Latrubesse et al., 2005; Marani et al., 2002). Relationships have been identified between the dynamism of these channels with respect to variations in bend curvature (Hickin and Nanson, 1975; Ikeda et al., 1981), the composition of river bank materials (Constantine et al., 2009; Thorne, 1991), the presence of vegetation (Abernethy and Rutherfurd, 1998; Micheli et al., 2004), and fluctuations in discharge (Braudrick et al., 2009). The purpose of this thesis is to improve our understanding of how in-channel sediments (i.e., those supplied to the channel either by mass wasting events, anthropogenic disturbances, or episodic floodplain scouring associated with cutoff events) interact with flow hydrodynamics as they are routed, and transiently stored, through the channel network, and how these interactions affect meander and floodplain evolution. This will be achieved by using a combination of remote sensing techniques, GIS (geographic information systems), and numerical modelling.

1.1 Literature Review - meandering: from inception to cutoff and beyond

1.1.1 Meander initiation

Sinuous planforms have been observed in an array of landscapes across the planet as well as extra-terrestrially (Fagherazzi et al., 2004; Howard, 2009; Lazarus and Constantine, 2013). Despite their prevalence, their formation is still not fully understood. Several theories have been proposed for the onset of meandering including early theories involving the dissipation of energy in the channel (Langbein and Leopold, 1966; Leopold and Langbein, 1962; Yang, 1971a). The concept of entropy was introduced by Leopold and Langbein (1962) to describe landscape evolution in terms of energy distribution: in a river system energy is distributed uniformly as it routes sediment and water through the system to base level, in an attempt to reach equilibrium. Langbein and Leopold (1966) discussed the concept of equilibrium in river systems further stating that the process of channel lengthening, and increasing concavity, usually occurred downstream in the system. The process of lengthening acts to distribute energy more uniformly through the length of channel. Increasing volumes of water are conveyed through the channel with distance downstream causing the energy budget of the system to increase; to account for this increased energy the channel must lengthen to maintain a uniform energy distribution. (Langbein and Leopold, 1966). Average slope must also be maintained as the channel adjusts. Numerous channel paths can be selected which would provide the same slope and length as the original channel. A random walk model can be implemented to predict the new path between two points along the river given the specific conditions of the new path. The study demonstrated that sine-generated curves present good models for river meanders since this shape allows the river to do the least amount of work over its length (Langbein and Leopold, 1966). Yang (1971a,b) disputed theories for minimising or maximising the energy per unit mass of

water citing that the total energy is dictated by stream relief, not by channel course. Therefore, in the absence of tectonic activity, changes in energy cannot occur. Instead, Yang (1971b) proposed the law of least time rate of energy expenditure as fulfilling the conditions of channel meandering in streams with, and without sediment (Yang, 1971a). Similarly, theories considering the minimisation of energy expenditure, or maximum energy efficiency, in transporting sediment through the channel were advocated to explain the appearance of fluvial systems.

Equilibrium channel patterns with regard to channel width, depth, flow velocity and slope were predicted using theories of continuity and conservation of momentum (Bettess and White, 1983). Bettess and White (1983) postulated that if channel slope was equal to valley slope, the river would be straight. If the valley slope exceeded channel slope a meandering or braided pattern will emerge, and channel aggradation will occur. Resulting channel patterns are a reflection of the system trying to attain equilibrium conditions by expending the lowest stream power per unit length of channel (Bettess and White, 1983). Nanson and Huang (2008) demonstrated that routing of sediment and water through alluvial channels is governed by the least action principle. This theory states that when the channel cross section reaches its maximum sediment transport capacity per unit of available stream power, the flow conditions are at an optimum. Therefore, channel patterns appear to be the result of energy efficiency in which the maximum volume of sediment can be transported with the least amount of energy expenditure (Chang, 1979).

Gorycki (1973) used an inclined plate coated in a hydrophobic layer, (after experiments by Tanner, 1960), to demonstrate the development of a meandering pattern by altering the depth of flowing water over a plate with a sufficiently rough surface. The interaction between the flow filament and the rough channel boundary causes a velocity reduction and the development of sinuous channel flow, which after maturation begins to show dimensional metrics similar to those reported for natural

streams (Leopold et al., 1964). An important aspect of this experiment was that it did not require the presence of sediment to become sinuous; this is important since many systems (e.g., rivers in glaciated landscapes, lava flows and tidal meanders) develop sinuous planforms in the absence of a sediment supply. However, following the addition of sediment to the experiment (represented by carbide granules), the material behaved in accordance with observations on natural rivers. Specifically, material accumulated at the inner banks as point bar deposits and overdeepened sections formed at the concave banks (Gorycki, 1973). Lazarus and Constantine (2013) established a relation between the relative resistance of the floodplain and the valley slope using a Brownian walk cellular topography model. The model suggests that where the valley slope is sufficiently large, the flow can overcome any resistance imposed by floodplain roughness. In environments where the roughness prevails over the valley slope, the flow path is dictated by the roughness elements. The ability of channelised flow to excavate material from exposed (unvegetated/non-cohesive) floodplains will result in relatively straight planforms as opposed to those with a degree of roughness that allow a sinuous flow, and eventually channel, to form (Lazarus and Constantine, 2013). Evidence to support roughness-driven sinuosity development can be found along the Sacramento River, USA, where the conversion of forested floodplains to planted orchards resulted in a dramatic decrease in reach sinuosity from 2.20 to 1.40 over a 24-year period (Lazarus and Constantine, 2013).

A substantial field of research has developed on identifying a possible resonance phenomenon that operates within meandering rivers driven by typical wavelength of bends and that of topographic perturbations in the alluvial bed in an attempt to reconcile the linear bend and bar theories (Blondeaux and Seminara, 1985; Colombini et al., 1992; Frascati and Lanzoni, 2009; Garcia and Niño, 1993; Ikeda et al., 1981; Lanzoni and Seminara, 2006; Seminara et al., 2001; Whiting and Dietrich, 1993; Zolezzi and Seminara, 2001). It was previously argued that the formation of unstable

alternate bars was the only requirement for meandering; however, the migration of these bars through the channel is too fast to allow for bank erosion to occur at the opposite side of the channel. Moreover, the wavelengths of these bars are typically much shorter than those describing the meander planform (Parker, 1976; Whiting and Dietrich, 1993). Incipient meandering has also been purported to develop from natural instabilities arising as flow traverses across an erodible bed (Dietrich and Smith, 1983). The patterns of sediment transport associated with bed slope and shear stress cause small amplitude fluctuations to develop which are inherently unstable at dimensions much smaller than the channel (Blondeaux and Seminara, 1985). However, for a given set of flow conditions, there exists a stable wavenumber (wavelength normalised by channel width) at which alternate bars no longer amplify and propagate (i.e., grow and migrate downstream). If the channel adopts the same characteristic wavenumber then the curvature-induced alternate bar formation and sinuous flow pattern will be reinforced and cause resonance, which may ultimately allow for a meandering planform to develop (Blondeaux and Seminara, 1985).

Although the linear model has had much success in its ability to estimate the location of peak bed and bank scour and in predicting long-term channel change (e.g., Sun et al., 2001b), the non-linear nature of meandering complicates and dampens these effects (Bolla Pittaluga et al., 2009; Seminara and Tubino, 1992). A non-linear model was proposed by Bolla Pittaluga et al. (2009) which closely replicated the bed topography and position of maximum boundary shear stress in a modelled cross section based on a real meander on the Cecina River, Italy. The non-linear model performed better than the linear model, which tended to overshoot the location of scour maxima and minima and displayed a rapid flow transition zone near the apex. In agreement with the theory suggested by Seminara et al. (2001) and Zolezzi and Seminara (2001), the channel does select a wavelength at which the meander growth rate peaks and this is dependent on the amplitude of the initial perturbation, given a

set of dimensionalised parameters (grain size, channel aspect ratio, and shear stress).

1.1.2 Sediment transport and channel beforms

The evolution of a meander bend's planform geometry is the result of the interactions between discharge and sediment transport. Alluvial material is a fundamental component of all meandering river systems whether they be in tropical, temperate, or arid climates. An intimate relationship exists between rivers and the hillslopes from which they are derived; not only because these slopes route water to the channels, but also because these hills deliver sediment to the channel through mass wasting events (Benda and Dunne, 1997; Sutherland et al., 2002). The proximity of these hillslopes to the channel will determine how effective sediment transfer from the land to the channel is, whilst the mechanical characteristics of the material will control its residence time at the channel boundary (Rice, 1994). The ultimate destination for the sediment supplied to the channel by hillslopes is the coast and rivers form the conduit through which this material is transported and stored (Milliman and Syvitski, 1992). Alluvial material is mobilised during transient periods when the fluid shear being imparted to the individual grains in the river bed is sufficiently high enough to overcome the gravitational resisting forces of the grains. This relationship is commonly described by the Shields equation:

$$\theta = \frac{\rho g h S}{(\rho_s - \rho) g D_{50}} \qquad (1)$$

Where τ is shear stress, p is density of water, g is gravitational acceleration constant, h is flow depth, S is slope, ρ_s is density of sediment, and D is a characteristic sediment size (Shields, 1936). Therefore a large control on the mobility of the bed substrate is discharge (Frey and Church, 2009), although characteristics of the material (e.g., size, shape, and exposure to flow) are also of importance (Knighton, 1998).

Reconfigurations of the river's bed and banks is accomplished primarily by the transport of bed material, whilst the finer suspended material is more important for the vertical growth of the floodplain (Church, 2006; Mertes et al., 1996). Sediment mobility is dependent on the prevailing flow conditions and bed configuration. Homogeneous river beds have a clear division between fine and coarse configurations in that the former require less energy to mobilise them. However, heterogeneous beds are more complex in that the organisation of grains, and the relative exposure of individual grains, will determine whether a grain moves (Wiberg and Smith, 1987). The critical shear stress of a bed comprised of larger grains over a matrix of finer material will be less than that of a bed of coarser material with smaller grains filling interstices between the grains (Wiberg and Smith, 1987). Wiberg and Smith (1987) described the process in terms of grain angle of repose, whereby finer particles that were deposited between larger ones were shielded from the flow, thus limiting mobilisation. The development of a coarse bed surface layer is also related to the settling dynamics of fine material between coarse grains in conjunction with upstream sediment supply (Dietrich et al., 1989). It was observed that if the flow is more competent than the sediment supply, the bed becomes coarser – through selective erosion of finer sediments – and bedload pulses become less frequent. Further, the interstitial filling by fine grains results in locally increased flow velocities, which induces flow convergence downstream; this encourages greater sediment transfer resulting in active transport zones bounded by inactive zones (Dietrich et al., 1989).

The mechanics of sediment transport have direct consequences for channel morphology: as grains are transported from one place to another, accumulations are formed and altered by channel flow dynamics (Kasvi et al., 2012). Straight and meandering rivers have a characteristic pattern of deeps and shallows along their course spaced periodically at approximately five to seven channel widths (Leopold

and Wolman, 1957; Leopold et al., 1964). Keller (1971b) clarified the terms pool, riffle and bar after inconsistencies in the literature when referring to different morphological units. The pool is a topographically low area created through fluvial scouring of the bed; the riffle is a topographically high accumulation of coarse material between pools; finally, point bars are sedimentary accumulations at the convex bank adjacent to pools. Riffles have a symmetrical cross section whereas bars have an asymmetrical profile (Keller, 1971b). The regular spacing of these bedforms changes as channel sinuosity increases and the in-stream conditions become unstable without the addition of multiple bedform units. As the channel adds more units, the channel geometry becomes ever more complex with meanders developing multiple regions of curvature maxima resulting in what are commonly termed double-headed meanders (Brice, 1974; Hooke, 1977; Hooke, 1984; Hooke and Harvey, 1983; Lewin, 1972)

The development of pools and riffles only occurs in river beds composed of material coarser than sand (e.g., gravel) (Richards, 1976). However, the pool-riffle sequence is ubiquitous among both alluvial and bedrock channels, despite different characteristics being present in each (Keller and Melhorn, 1978). Bedload material is sorted by size between the pool and riffle whereby coarser material is found to be deposited on riffles, and finer material is dropped in the pools (Keller, 1971a; Leopold et al., 1964). Keller (1972) proposed a five-stage model for alluvial channel development in which a straight channel characterised by asymmetrical shoals (incipient bars) marks the initial channel structure. Stages two through five describe the progressive development of sediment accumulations at equidistant points, and the growth of point bars in addition to increasing sinuosity. Rivers are not required to develop through each consecutive stage and may move ahead to later stages. Stage one asymmetrical shoals provide a mechanism for scour by inducing flow convergence in channel bends and deposition through flow divergence in straight segments; this promotes the formation of incipient pools and riffles, respectively

(Keller, 1972b). Although the model provides a useful description of stream evolution the many potential results of interactions between channel forms and processes fail to be encompassed by the simple five stages. Notwithstanding, the model does provide a framework for potential stream evolution as energy variations prompt the channel to move to a new state of equilibrium (Keller, 1974; Langbein and Leopold, 1966; Lewin, 1976; Yang, 1971a).

The distribution of sediment in this manner has been ascribed to the velocity reversal hypothesis: the theory attributes changes in flow intensity through the pool-riffle sequence in transporting sediment. At low flows, bed velocities are lower in the pool than over the riffles (as interpreted from the appearance of turbulent white water over riffles at low flow and their absence over pools). However, with increasing discharge, bed velocities in the pool rise at a greater rate than those over the riffle; when the pool velocity is equal to the riffle the velocity reversal occurs. Once the pool velocity exceeds the riffle velocity, coarse material is mobilised and transported from the upstream riffle, through the pool, and deposited on the downstream riffle (Keller, 1971a; Keller, 1972a). In the event of rapidly falling flow velocity, coarse material in the pool will not be evacuated, and will reside in the pool until the next velocity reversal (Keller, 1971a).

Carling (1991) described the absence of a velocity reversal in most studies attempting to explain the characteristic oscillation in bed elevation (Carling, 1991). Work by Sear (1996) using tracer particles in pool-riffle sequences in the River North Tyne, UK, concluded that the observed patterns of scour and fill can be explained without the requirement of a reversal hypothesis. Instead, Sear (1996) proposed that sediment packing on the riffle induced by high frequency turbulent flows strengthens the alluvial structure of these features whereas pools, characterised by finer sediment, have little opportunity to form a resistant configuration. Therefore, pool sediments will be mobilised more easily at any given flow than those on a riffle (Sear,

1996; Wiberg and Smith, 1987). High grain mobilisation at the pool head results in scour, whilst the pool tail may be subject to some aggradation, although aggradation is dominant on the coarse, resistant riffles (Sear, 1996). A new theory reconciling changes in stage with variations in bed shear stress, and thus sediment transport, was proposed attributing a phase shift of one quarter the pool-riffle wavelength in the upstream and downstream direction in response to increased and decreased discharge, respectively (Wilkinson et al., 2004). During high flows, riffle bars grow in amplitude whereas pools exhibit scouring. The results presented by Wilkinson et al. (2004) show that where there is a positive downstream gradient in sediment transport, bed scouring can be accomplished, therefore not requiring the presence of shear stress maxima. Conversely, negative longitudinal gradients in sediment transport are associated with aggradation. A reversal is supported with changing stage, although it is the shear stress phase shift reversal from a location dominated by scour at low flow, to an area dominated by sediment deposition at high flow, and vice versa (Wilkinson et al., 2004). Furthermore, width variations display a minimum and maximum up- and downstream of riffle crests. At low flow, channel widening occurs on riffles in conjunction with flow deflection by the crests (Millar, 1999), which directs flow to the bank toe, inducing scouring. In high flows, the widened channel over the riffles experiences low shear (as a result of the relationship between hydraulic variables (Leopold and Maddock, 1953)), whereas the pools experience high shear concurrently with increases in bar amplitude (e.g., upstream phase shift in shear stress) (Wilkinson et al., 2004).

1.1.3 The role of bedforms in sand and gravel bed river meanders

In sand-bed rivers, the fine-grained material comprising the bed is often well-sorted and easily entrained by the overriding flows. The ease at which the sediment becomes mobilised allows channel bedforms to develop (e.g., ripples, dunes, and antidunes). The development of channel bedforms initiates a complex feedback cycle

in which the interactions between flow and sediment on the bed influences flow resistance, therefore causing further perturbations to the flow structure at the channel bed. The characteristics of the bedforms (e.g., wavelength and height) are conditioned by the prevailing flow conditions and the grain size on the bed. Low flows in relatively fine sediments generate ripples that rapidly migrate downstream as sediment is transported from the stoss side, over the crest, and down the lee side of the bedform. Under higher flow velocities, ripples become superimposed upon dunes: dunes have greater vertical heights and longer wavelengths between crests and can cause considerable disturbance to the overlying flow structure. The downstream migration of these bedforms is governed by the form roughness introduced by their protrusion into the water column from the channel bed. With increasing flow velocities, the bed becomes flattened as the dunes are eroded. This gives rise to a mobile flat bed in which sediment sheets of alternating fine and coarse character are transported downstream; this causes strong pulses in downstream sediment delivery. Under some conditions antidunes develop in response to high sediment mobility and low bed resistance and approximate the characteristics of surface waves. These features migrate upstream eroding material from the lee side of the dunes and depositing material on the stoss side of the upstream dune (Bridge, 1993; Dietrich and Whiting, 1989; Fryirs and Brierley, 2012).

Gravel-bed rivers are governed by similar conditions with regards particle entrainment. That is, they require sufficient shear stresses to mobilise material from the channel bed. The contrast between sand-bed and gravel-bed rivers is that the latter require greater stresses to initiate sediment transport. Furthermore, gravel-bed rivers can armour their beds and increase the resistance of bed material to entrainment. The organisation of grains on the bed of these rivers is governed more by sedimentary characteristics than in sand-bed rivers where bedforms are controlled by the prevailing flow conditions. Coarse-grained material in gravel-bed rivers may

protrude above other grains forming a nucleus around which other grains are deposited. The stoss side of the protrusion is characterised by coarse grains while downstream of the obstruction is characterised by fine-grained wake deposits. The development of much larger gravel bedforms requires sufficiently high flows and often a large sediment supply to facilitate their growth (Dietrich and Whiting, 1989; Fryirs and Brierley, 2012).

The contrasting bed characteristics of these river types has implications for the routing of sediment in meander bends. Sand-bed rivers are more mobile and sediment transport correlates closely with patterns of shear stress: where the shear stress is highest, the coarsest grains are found and where shear velocities are low, finer sediment is observed (Dietrich and Whiting, 1989). The presence of dunes also directs sediment across the channel in their troughs where both inward and outward currents are channelled. The currents transfer fine sediments to the inner bank and coarse sediments to the outer bank (Dietrich and Smith, 1984; Dietrich and Whiting, 1989). In gravel-bed rivers, the zone of maximum shear stress – although still directed toward the outer bank by planform curvature – does not coincide with the arrangement of grains on the bed and zone of maximum sediment transport. The margin of the point bar is characterised by finer material, which is easier to entrain than the coarse bed fraction in the centre and outer regions of the channel (Dietrich et al., 1989; Dietrich and Smith, 1984; Dietrich and Whiting, 1989). Therefore, particle arrangement on the bed and the presence of bedforms are critical in the routing of sediments through the meanders of sand and gravel bed rivers.

1.1.4 Controls and effects of meandering

The characteristic asymmetrical cross section of meander bends can be attributed to the interactions between channel geometry, flow morphodynamics, and sediment transport. Curvature-induced flow oscillation from the inner (convex) bank to outer (concave) bank establishes a cross-stream pressure gradient as the water surface

becomes elevated at the outer bank (Dietrich and Smith, 1983; Dietrich et al., 1979; Odgaard, 1984). Steep transverse water surface gradients increase the boundary shear stress at the outer bank, particularly at the bank toe, where sediment is excavated by downwelling fluid, and transported obliquely across the channel bed (Fig. A) (Bathurst et al., 1977; Dietrich et al., 1979).
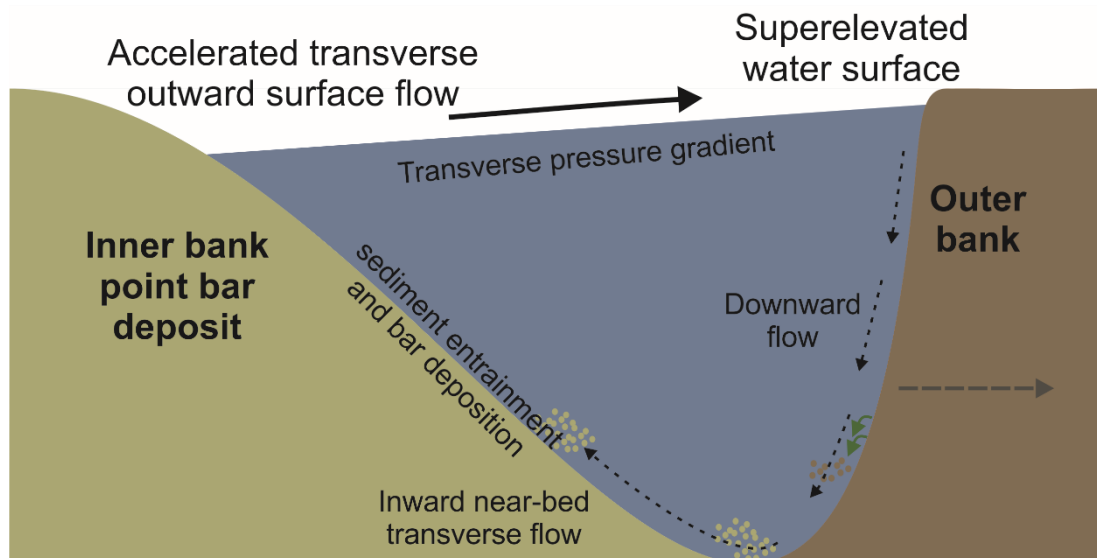
Figure A Cross-sectional schematic of sediment and flow routing in a meander bend. A transverse pressure gradient is created by the curvature-induced superelevation of water at the outer bank. Material is excavated from the bank by downwelling fluid that forms the descending limb of fluid circulation in the meander. Fine sediment is swept inward by the near-bed inward flowing water to be deposited on the point bar.

Bed material sorting occurs in concert with the crossing of the zone of maximum boundary shear stress, which crosses from the inside to outside banks. Coarse material is transported into the pool at the concave bank by strong transverse currents and the rolling of grains down the steep laterally sloping point bar margin via obliquely oriented channel bedforms (Dietrich et al., 1979; Hooke, 1975; Jackson, 1975). Concurrently, fine bed material is transported obliquely towards the inner bank in the downstream section of the meander by a weaker trough-wise current operating in topographic lows on the channel bed (Fig. 1) (Dietrich and Smith, 1984; Dietrich et al., 1979; Nanson, 1980).
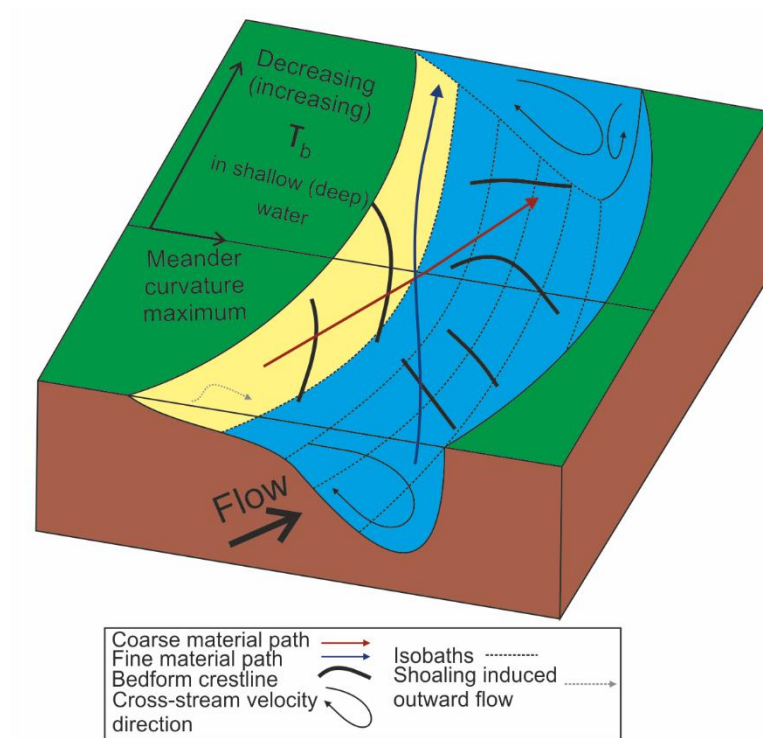
Figure 1 Bed and channel morphology in a meander bend adapted from Dietrich and Smith (1984). T_B is the boundary shear stress.

This mechanism of oblique trough-wise flow is also responsible for the exchange of sediment from point bar to point bar as channel curvature alternates downstream (Dietrich et al., 1979). Failure of this near-bed current to supply sediment to the inner bank can result in erosion of the bar (Lotsari et al., 2014). Such a condition may arise during low and high discharge events when secondary flows have been observed to be weaker (Bathurst et al., 1977). A strong dynamic feedback exists between the orientation of bedforms in the bend, the strength of trough-wise currents generated around these bedforms, and the advection of sediment to the bar and pool regions. Adjustments of the orientation of bedforms to more oblique angles with respect to the planform geometry can increase downstream sediment transport, thereby supplying greater sediment to the dune troughs. If the transverse currents operating in these dune troughs is sufficiently large to advect large proportions of fine sediment to the bar, shoaling will result. This shoaling will force the high-velocity core outward toward

the concave bank, decreasing downstream sediment transport due to the migration of the zone of maximum boundary shear stress into the pool. A reduction of lateral sediment export to the bar will permit erosion of the bar margin, which will ultimately lead to the inward migration of the high-velocity core (Dietrich et al., 1979). The zone of maximum boundary shear stress fully transitions across the channel just downstream of the bend's point of maximum curvature; the slight downstream offset results from flow inertia in the channel. Bank erosion is focused where the zone of maximum shear stress impinges the outer channel bank (Dietrich et al., 1979; Frothingham and Rhoads, 2003). Accordingly, bank erosion rates tend to be higher when channel discharges are of a higher magnitude (Gautier et al., 2007; Hooke, 1979; Lotsari et al., 2014). Many authors have stipulated the significance of meander curvature in forcing bank erosion purporting that a 'golden ratio' between the radius of curvature and average channel width of between two and three results in peak rates of retreat (Hickin and Nanson, 1975; Hudson and Kesel, 2000; Leopold and Wolman, 1960; Nanson and Hickin, 1983). As meanders grow, their curvatures continue to increase until a point at which the rate of expansion diminishes resulting from reduced cross-stream momentum transfer which limits bank erosion (Furbish, 1988; Handy, 1972; Lewin, 1972). Sharper bends can facilitate more rapid erosion as the high-velocity core is transferred across the channel more quickly (Ferguson et al., 2003). Sharp changes in curvature, often associated with confining media, can permit outer bank bench deposit formation: more rapid changes in planform curvature cause flow divergence in the upstream portion of the meander, inner bank erosion and fine sediment deposition at the outer bank, over time leading to bar formation (Lewin, 1978; Nanson and Page, 1983). Contrary to the view that bend curvature exerts a strong control on bank erosion, field observations have shown that resultant near-bank velocities do not vary in a consistent way with changes in curvature (Engel and Rhoads, 2012; Lotsari et al., 2014).

1.1.5 Knickpoints in meander evolution

Knickpoints are rapid localised changes in channel gradient that form in response to changes in tectonism (e.g., following uplift), climate (e.g., eustatic sea level change), the delivery of large sediment loads, or lithologic controls (e.g., faults) (Bishop et al., 2005; Whittaker and Boulton, 2012). Knickpoints can either be mobile or static in nature. The former case results from an erosion signal being propagated upstream through the channel network from an initial change downstream (e.g., sea level fall). In the latter case, a structural feature may confine the gradient change to a localised area along the river (e.g., a fault) (Crosby and Whipple, 2006). Bedload sediment supply was observed to be an important control on the retreat of knickpoints on a reach in Taiwan where uplift limited sediment supply to suspended load (Cook et al., 2013). Cook et al. (2013) suggest that the absence of bedload was responsible for the stalling of knickpoint retreat. Evidence from the modern landscape can be used to infer the propagation of knickpoints and understand how the erosion signal is manifested within varying substrates, as the knickpoint migrates upstream. Strath terraces – depositional surfaces through which the channel incises to reach its new gradient – indicate the former level of the river before channel incision. Additionally, unstable hillslopes deliver large pulses of sediment to the channel as it adjusts to accommodate the new gradient. Vertical channel incision increases the gradient of hillslopes causing them to oversteepen and increasing the likelihood of failure; this process can still be ongoing long after the initial propagation occurred (Gallen et al., 2011). Relict oxbow lakes have been documented across the Waipaoa Basin, New Zealand, purportedly in response to upstream knickpoint propagation between ~18 ka and the present (Crosby and Whipple, 2006). These observations may be pertinent for large river systems such as those in the Amazon Basin where changes in tectonism and climate may have initiated knickpoint migration and for which evidence may be interpreted from unstable hillslopes and large populations of oxbow lakes (Mertes et al., 1996).

1.1.6 Modelling channel change

Predicting long-term channel change by simulating the physical relations derived from field observations has led to the development of many morphodynamic models. One of the earliest and most prolific models was that developed by Ikeda et al. (1981) and Hasegawa (1977) with modifications made by Parker et al. (1982). The model allows erodible banks to be modified by the channel flow as a function of the near-bank flow velocity and an arbitrary erodibility coefficient, which is determined by the mechanical properties of the bank material. Pizzuto and Meckelnburg (1989) found a linear relation between lateral migration rate and the velocity perturbation (the difference between the flow velocity at the outer bank and the cross-sectionally averaged flow velocity) at the concave bank. Furthermore, they observed that areas of the bank colonised by Silver Maple tree species were more resistant to erosion than banks hosting other species (Pizzuto and Meckelnburg, 1989). These early formulations of the bank erosion equation, which underpinned many morphodynamic models (e.g., Howard, 1992; Howard and Knutson, 1984; Sun et al., 2001a; Sun et al., 2001b; Sun et al., 1996) applied a passive width adjustment parameter which maintained a constant channel width as the outer bank migrated. Parker et al. (2011) acknowledged the limitations of this model approach and devised a new model in which the two components (bank erosion and bar sedimentation) were decoupled and able to communicate with one another to establish an approximately constant width by balancing bar growth (controlled by vegetal colonisation) with bank erosion modulated through slump bank generation (Asahi et al., 2013; Eke et al., 2014a). The significance of maintaining width variations has been demonstrated experimentally as well as in the field (Luchi et al., 2010a; Luchi et al., 2010b; Zolezzi et al., 2012) and suggests that feedbacks between small spatial oscillations in channel width and curvature can be indicative of channel pattern thresholds that alter the flow structure through meanders that allow for the inception of mid-channel bars, which can further induce channel width and curvature oscillations. Modulating lateral bank retreat by

slump block failures has been verified by field observations that have demonstrated the physical presence of these cohesive blocks, usually derived by slides or cantilever failures induced by the removal of non-cohesive sediment at the bank toe (Darby et al., 2002; Osman and Thorne, 1988; Thorne, 1982; Wood et al., 2001). Before further bank retreat can take place, the slump blocks must be eroded. The length of this process is governed by the geomechanical properties and vegetation density of the blocks (Asahi et al., 2013; Motta et al., 2014). Furthermore, slump block production creates irregular bank line topography which alters the near-bank flow field through form roughness interactions; this typically diminishes near-bank shear stresses (Darby et al., 2010; Kean and Smith, 2006a; Kean and Smith, 2006b; Leyland et al., 2015), although localised flow steering towards embayments can elongate bank line depressions until a critical width is achieved at which point flow recirculation causes shear stress reductions (Hackney et al., 2015).

Experimental meandering channels have given insights into the process of sediment transport, settling and erosion in scaled channel settings with varying degrees of success. Most meandering patterns can only be generated and maintained in the presence of added cohesion in the form of fine-grained sediment (to simulate the role of clays) or vegetation (Braudrick et al., 2009; Iwasaki et al., 2016; Murray and Paola, 2003; Peakall et al., 2007; Schumm and Khan, 1972; Smith, 1998; Tal and Paola, 2007; Tal and Paola, 2010). In the absence of floodplain cohesion, the channel rapidly expands leading to the development of a braided channel. However, experiments conducted by Van Dijk et al. (2012) and Van de Lageweg et al. (2013) adopted a different strategy based on principles of instability discussed by Lanzoni and Seminara (2006). It is widely accepted that meandering channels are unstable systems driven by perturbations in planimetric evolution or external factors (e.g., sediment loading, base level change, discharge variations) (e.g., Furbish (1991)) . Lanzoni and Seminara (2006) proposed that most rivers convey this instability

convectively. Convective instabilities are created at discrete cross sections and are persistent: the perturbation extends from the source in one direction – in meandering rivers, most commonly downstream (Bolla Pittaluga et al., 2009). Adopting this strategy, a flume fitted with a transversely migrating sediment and water input was used to generate a convective instability that propagated downstream and triggered meandering (van de Lageweg et al., 2014; van Dijk et al., 2012). The authors justified this by equating the transverse inlet to an upstream meander that migrated into the downstream reach. In the absence of an upstream perturbation (i.e., static inlet), meandering ceased after the development of an equilibrium channel pattern; this is consistent with previous observations (Smith, 1998; van Dijk et al., 2012). Although the methodology seems justified (as verified by Schuurman et al. (2016)), issues with the upscaling to real river systems remains questionable, particularly in the absence of vegetation and suitable bank cohesion, which permitted rapid rates of bank retreat in their experiments (Schuurman et al., 2016; van Dijk et al., 2012).

1.1.7 The significance of point bars

An question that still remains in fluvial geomorphology as to whether the point bar deposits on the inside of meander bends promote bank retreat at the adjacent bank, or whether they are the result of channel migration and reduced sediment transport capacity as a constant channel width is maintained (Dietrich and Smith, 1983; Gautier et al., 2007; Hooke, 2007; van de Lageweg et al., 2013). Early evidence presented by Dietrich and Smith (1983) suggest that flow acceleration driven by the topographic presence of the point bar increase fluid advection towards the concave bank, facilitating stronger helical flow and greater sediment evacuation, resulting in faster rates of lateral retreat. The presence of the point bar reduced the flow depth downstream (at the inner bank) causing a reduction in the downstream velocity component in exchange for an increased outward velocity component directed towards the outer bank; this observation was verified by many field studies (Dietrich

and Smith, 1983; Jackson, 1975; Kondrat'yev, 1968; Leopold and Wolman, 1960; Lotsari et al., 2014; Rominger et al., 2010). Furthermore, the measurements made by Dietrich and Smith (1983) revealed that where point bars were present in the channel cross section, the shoaling-induced transverse flow component penetrated further across the channel than when the bar was absent, commonly only crossing to the centreline. The topographic effect of bars during varying stages has been examined and shown to be dependent on the local cross-sectional characteristics: meanders that maintain a constant width up to bankfull stage increase depth and scour over the point bar, whereas cross sections that maintain a shallow depth over the bar continue to outwardly direct flow (Kasvi et al., 2012; Thorne et al., 1985). The efficacy of these outwardly-directed convective accelerations was also documented up to bankfull stage on the Merced River, California (Legleiter et al., 2011). The growth of point bars has been monitored experimentally as well as in nature and reveal that where the bars are present (following flow divergence and sediment deposition), discrete units of sediment emerge from transversely-oriented bed currents and flow shoaling to create discrete scroll bar units (Dietrich and Smith, 1984; van de Lageweg et al., 2014). These units are characterised by a ridge and swale topography that unless filled with fine sediment can be exploited to form cutoffs (Braudrick et al., 2009; Grenfell et al., 2012; Jackson, 1976; Nanson, 1980). Sediment is carried to the margins of the bar and typically accumulates downstream of the bend apex, thereby increasing the longitudinal as well as lateral extent of the bar (Hickin, 1969; Legleiter et al., 2011; Pyrce and Ashmore, 2005). The efficacy of bars to outwardly-advect fluid towards the outer bank depends on sediment recruitment on the bar, which facilitates its growth in extent as well as amplitude, and the ability of the bar to persist within being eroded by large flood events (Dunne et al., 2010). The bar must be rapidly colonised by vegetation which will reduce flow velocities over the bar, thereby preventing scour and allowing for further sediment capture as well as increasing stability through root cohesion (Asahi et al., 2013; Nicholas, 2013; Parker et al., 2011;

Schuurman et al., 2016). The importance of colonising vegetation on point bar stability was modelled by Schuurman et al. (2016) in which they compared the results of three morphodynamics models. They concluded that the conversion of bars to floodplain through the vegetation growth was paramount for effective flow deflection and without this condition the topographic presence of the bar alone was not capable of deflecting channel flow towards the outer bank and triggering bank erosion (Dietrich and Smith, 1983; Schuurman et al., 2016). Allmendinger et al. (2005) suggested that grassed floodplains were more effective at keeping pace with outer bank erosion than forested ones, which resulted in narrower channels. Evidence derived from satellite imagery of the Kinabatangan River, Borneo suggests that where floodplains are converted from natural riparian forest to cultivated crop, rates of bank retreat are enhanced (Horton et al., In Press).

1.1.8 Meander cutoff processes

The ultimate fate of meander bends is to be cutoff by one of two mechanisms: neck cutoffs, more commonly observed on more dynamic rivers, occurs where two meanders converge; alternatively the bend can be terminated by a chute cutoff, where the river incises the floodplain over a distance longer than approximately a single channel width, to bypass the meander (Constantine et al., 2010b; Gay et al., 1998; Hooke, 2004; Howard and Knutson, 1984; Zinger et al., 2011). Cutoffs are the primary mechanism by which meandering channels maintain a steady-state sinuosity through time and have been argued as a self-organised process by which the river keeps its length in check (Stølum, 1996; Stølum, 1997; Stølum, 1998). The inevitable development of cutoffs is the result of a number of conditions: first, the effect of increasing meander amplitude as it migrates through time is to lower the channel gradient, thereby reducing the flow and sediment conveyance through the channel; second, high-magnitude flows can traverse overbank and begin incising material from either the up- or downstream part of the meander helping to facilitate the development

of a cutoff. Whether a cutoff develops or not will be depend on the prevailing flow conditions in the channel, the difference between the valley (floodplain) and channel slope, and the mechanical properties of the banks, including the presence or absence of riparian vegetation, (Camporeale et al., 2013; Constantine et al., 2010b; Erskine et al., 1982; Fisk, 1947). Multiple cutoffs can also be generated where skewed meanders - meanders oriented up- or downstream – migrate towards one another until they converge; this process was observed along the Ob River, Russia and attributed to increased flood frequency and sediment supply (Słowik, 2016). In large meandering rivers with rapid rates of bend extension it was observed that where the channel becomes wider-at-bends, and where vegetal colonisation cannot keep pace with bend extension, the likelihood of chute cutoff formation increased (Grenfell et al., 2012; Grenfell et al., 2014). Alternatively, rivers carrying high fluxes of bed material can cause the channel to shoal and flow can be forced over the bar and directed into depressions where prolonged scour and excavate a chute channel (Peakall et al., 2007). Following separation, these abandoned channels can either be rapidly infilled by bedload sequestration or slowly terrestrialised by overbank flows that deposit fine-grained material within the depression (Constantine et al., In Review; Constantine et al., 2010a; Dieras et al., 2013). Bends with high divergence angles (the angle formed between the mainstem and abandoned channels) are more likely to remain unfilled following plug formation due to the low flow and sediment conveyance through the abandoned channel; this is most common for neck cutoffs. Chute cutoffs have lower diversion angles, therefore sustaining bedload transport and infilling more rapidly than neck cutoffs (Constantine et al., In Review; Constantine et al., 2010a). The resulting lentic (still water) environments generated by isolation are periodically reconnected to the channel by flood events during which fish can migrate between the two environments, while fine-grained sediments transport organic compounds and contaminants to the oxbow lake effectively filtering them from the main channel (Dennis et al., 2009; Glinska-Lewczuk, 2005; Terezinha Costa et al., 2006; Walling et

al., 2003). Single-thread tie channels also supply sediment-rich water to lacustrine floodplain environments assisting nutrient transfer and facilitating sedimentation (Rowland et al., 2009). These periodic inundations are responsible for maintaining the supply of nutrient-rich fluid to the riparian species that colonise the banks of meandering rivers, which attract a plethora of specially adapted species to these habitats ascribing significant value to them (Costanza et al., 1998; Naiman and Decamps, 1997; Naiman et al., 1993; Tockner and Stanford, 2002).

1.1.9 Sedimentation processes and floodplain development

The constantly changing nature of meandering rivers makes it difficult to interpret their histories beyond a finite length of time due to the phenomena of 'signal shredding' (Jerolmack and Paola, 2010). Migrating bends incise into deposits laid down during former periods of channel activity preserving the prevailing conditions of the system at that time and allow inferences to be made from the resulting sequence stratigraphy. Lateral incision by migrating meanders effectively destroys these sedimentary archives resulting in temporal hiatus' in the stratigraphic record. The more mobile the river is, the more likely it is to contain these stratigraphic hiatuses. Novel dating techniques have improved our understanding of floodplain formation through overbank discharge events that deliver large amounts of suspended sediment to the floodplain (Aalto and Nittrouer, 2012). Aalto et al. (2003) described how climatically-driven flood events in the southern Amazon Basin resulted in the delivery of discrete packages of sediment to the floodplain by extracting a number of sediment cores and using ^{210}Pb dating to ascertain the age of the material. During La Niña events (cold phases of the El Niño-Southern Oscillation – ENSO), rapid-rise floods trigger levee breaches resulting in discontinuous crevasse splay deposits accumulating the floodplain. These sediment packages differ from those laterally continuous deposits of uniform depth associated with periodic overbank floods. A distinct lateral gradient is created from the channel margin where high-energy flood waters deposit the most

material while momentum losses limit the volume of sediment deposited in the distal floodplain (Swanson et al., 2008). The patterns of sedimentation with distance from the channel may also be controlled by the density of vegetation; reduced vegetation densities with progression into the distal floodplain facilitates greater rates of accretion close to the channel (Nanson and Beach, 1977). Since vertical floodplain growth requires water surface expansion above the bankfull depth, there is a finite elevation over which flood waters can accomplish this and facilitate floodplain accretion (Singer and Dunne, 2001; Wolman and Leopold, 1957). Although it is argued that frequent overbank flows are responsible for the majority of floodplain accretion, it has been suggested that, at least on the Mississippi River, episodic events that cause the greatest vertical floodplain growth (Shen et al., 2015). Mechanistically, episodic events are able to facilitate large vertical increases in floodplain topography through crevassing; that is, by breaching levees present at the channel margins (Aalto et al., 2003; Shen et al., 2015). Furthermore, reoccupation of negative floodplain relief (e.g., tie channels, scroll bars, floodplain channels and relict channels) can provide an efficient means of transporting sediment long distances away from the mainstem channel and infilling the distal portion of the floodplain (David et al., 2016; Lewin and Ashworth, 2014; Lewin et al., 2016; Slingerland and Smith, 2004). Sediment deposited in the distal floodplain was observed in the Amazon at distances up to 2.5 km away from the main channel (Aalto et al., 2003). Although overbank sediment advection is possible under the right flow conditions, it can be hindered by the water surface elevation on the floodplain (Lewin et al., 2016). Where water levels are high due to prior inundation (e.g., from rainfall, overbank flow or rising groundwater) sediment-rich water may be unable to penetrate the floodplain due to the presence of a substantial subaerial water body (Lewin et al., 2016; Mertes, 1997).

Channel and floodplain evolution rely on a multitude of factors: from the climatic setting of the catchment that enforces the hydrological regime responsible for

debauching, transporting and depositing sediment, to the geological setting of the catchment which will ultimately determine external sediment supplies, large-scale catchment characteristics (e.g., slope and area) and the routing of water through the landscape. The interactions between flow, sediment and the surrounding environment facilitates the growth and decay of some of the world's most dynamic and biodiverse features.

1.2 Areas of Investigation

The overall aim of this thesis is to describe and evaluate the relationship between in-channel sediments (e.g., macroscale bedforms) and meandering dynamics, which ultimately influences floodplain habitat creation. The thesis is divided into three distinct sub-hypotheses that will explore various aspects of the overarching question to gain insight into the significance of sediment supply on the evolution of meandering channels. Below is an outline of the three hypotheses examined in this thesis:

Chapter 3

This chapter will examine **whether externally imposed sediment supplies influence channel dynamism** as manifested by accelerated rates of meander migration and cutoff production. In order to achieve this, a suite of freely-available Landsat images supplied by the USGS and NASA through the Earth Explorer online facility will be manipulated using ArcGIS software.

Chapter 4

This chapter will examine **how meander migration and sinuosity are related and how external sediment supplies may contribute to this process**. A mixture of high and low temporally resolved Landsat imagery will be used to calculate changes in channel sinuosity and rates of migration to quantify their relationship through time.

Chapter 5

This chapter will examine **the mechanistic relationship between external sediment supplies, point bar deposition, and meander migration using a 2D morphodynamic model (MIKE 21c)**. A model will be used to simulate how the channel bathymetry responds to increases in sediment supply, and how this influences lateral migration at the opposite bank.

Chapter 2

The Amazon Basin
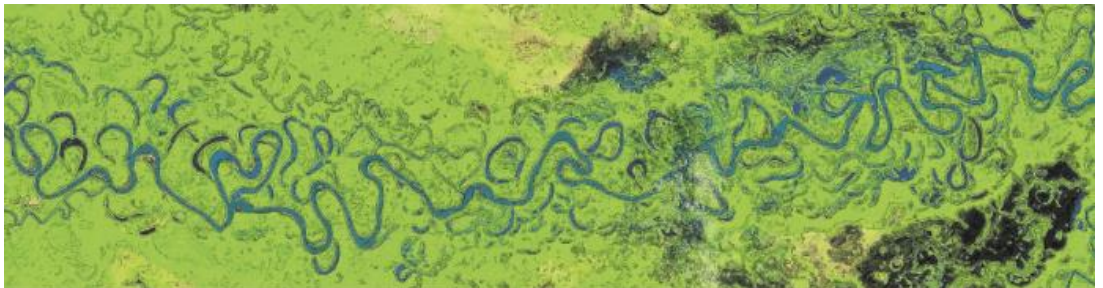
2. Amazon Basin: Site Description

The Amazon Basin comprises the largest freshwater catchment on the planet draining an area of ~ 6×10^6 km^2 and discharging 20% of global freshwater whilst also supplying 1200×10^6 tons of suspended sediment to the Atlantic Ocean (Meade, 1994; Richey et al., 1989). Since the Amazon Basin is relatively pristine, with few anthropogenic disturbances, it is a desirable location to study variations in nutrient and sediment routing, channel evolution, and changes in precipitation and discharge, all in response to the potential impacts of climate change and human modification (Aalto et al., 2006; Aufdenkampe et al., 2001; Costa and Foley, 1999; Davidson et al., 2012; Mayorga et al., 2005; Richey et al., 1990; Richey et al., 1986; Safran et al., 2005). The basin is strongly affected by gradients in rainfall as reflected by discharge routing times to the mainstem and the resulting water surface slope between the upstream and downstream mainstem gauging stations (Manacapurú and Óbidos) (Meade et al., 1985). The basin contains a legacy of past climatic and geological changes that have assisted in the development of the substantial diversity displayed by the modern-day landscape (Salo et al., 1986; Sioli, 1975). The highly active meandering rivers within the basin are responsible for reworking sediments deposited during the Holocene as well as more recent topography formed over the past one hundred years (Lewin and Ashworth, 2014).

2.1 Geological History

The Amazon Basin is comprised of several physiographic provinces (**Fig. 2**) which, through time, have caused the drainage patterns of the Amazon to change. In the north and south east are two Precambrian Shields formed of metamorphosed crystalline rocks over several orogenies between 600 and 3500 million years ago (Myr) These delineate the margin between the sub-Andean foreland basin and Andean Cordillera in the west of the continent and the Atlantic coast in the east. Connecting the Andes to the Atlantic Ocean is the Central Amazon Basin, a Miocene-Holocene rift basin through which the Amazon mainstem flows under considerable influence from several structural arches that constrain channel development in places (Dunne et al., 1998; Hoorn et al., 1995; Mertes et al., 1996). The development of these arches and structural highs is due to folding and tilting of the basins driven by
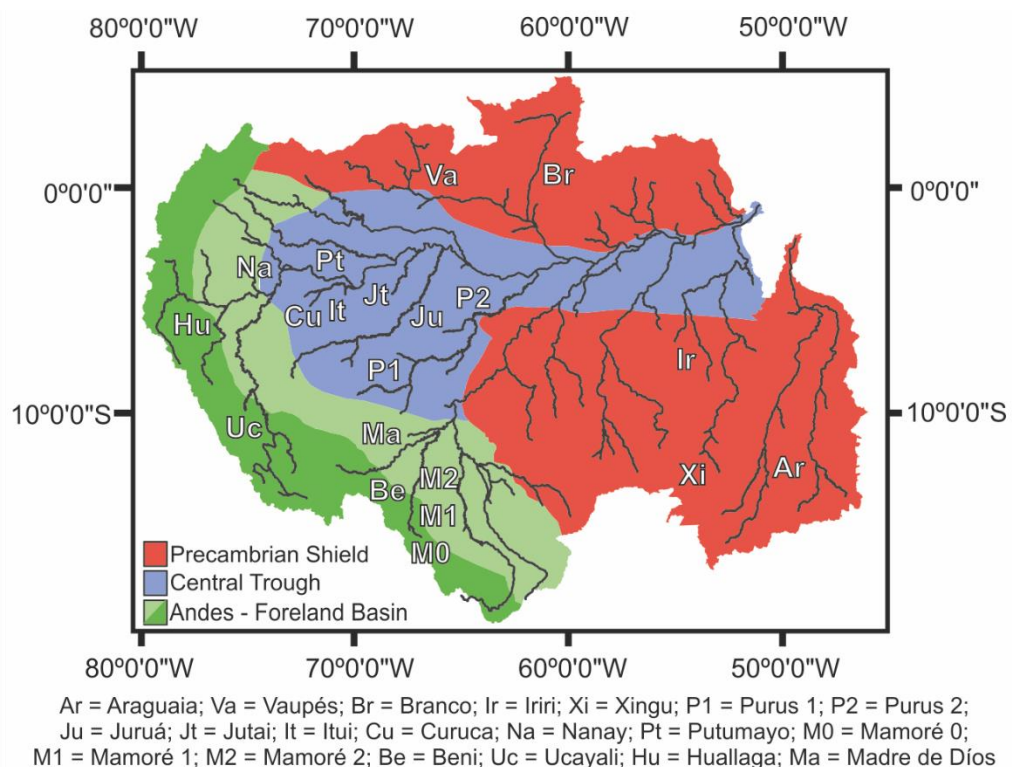
Figure 2. The Amazon Basin. The three main physiographic provinces are symbolised and labelled in the key. All 20 study reaches described in Chapter 3 are labelled with a two-letter abbreviation that is described below the map. A drainage network is also displayed in black. Detailed images of the reaches and information about each reach and their exact location can be found in Appendix 1.

mantle plume activity between the shields (Cox, 1989). Before the uplift of the Andean Orogen the Amazon drained from east to west

with large marine embayments extending from the west into the central Amazon (Hoorn et al., 1995; Hoorn et al., 2010; Mertes and Dunne, 2007). The rise of the Andes between the Oligocene and Pliocene (34 – 5 Myr) closed the westward and north-westward draining outlets into the Gulfs of Guayaquil and Maracaibo, respectively (Mertes and Dunne, 2007) and forced the river to flow eastwards to the topographically lower Atlantic mouth fixed in place by a graben dating back to the opening of the Atlantic Ocean (Potter, 1978). The current drainage alignment where the majority of the basin discharges into the Atlantic has existed since the early Pliocene shortly after the rivers of the Central Trough (e.g., Rio Juruá and Rio Purus) became erosional and began re-shaping the sediments deposited from the uplifting Andes (Latrubesse et al., 2010).

The Andes are the second highest mountain belt in the world with peak elevations in excess of 6000 m (Baby et al., 2009). Their formation is attributed to the convergence of the Nazca and South American plates predominantly during the Miocene era (Isacks, 1988), although early uplift of the Andes is estimated to have begun in the Lower Cretaceous Period during the Albian (Mégard, 1984). The characteristic bent geometry of the Andean Cordillera (Bolivian Orocline) developed in the late Cenozoic (~ 15 Myr), is hypothesised to have been the result of crustal thickening of the South American plate caused by the subduction of the older-aged low buoyancy Nazca plate, which altered the shear gradients along the trench (Barke et al., 2007; Capitanio et al., 2011; Isacks, 1988). Plate convergence generated a retroarc fold-thrust belt onto which the uplifting Andean peaks have been supplying sediment to the adjacent foreland basin since the upper Oligocene (Baby et al., 2009). The foreland basin is partitioned into several second-order intra-foreland basins, all being actively filled by sediment supplied by different river systems arising in the Andes (Decelles and

Hertel, 1989). Petrographic analyses of the riverine sediments in the Madre de Díos River highlighted the Andean source of the material, although some evidence also suggest the presence of a significant volume of Tertiary and Quaternary foreland basin fill (Decelles and Hertel, 1989).

River classification is strongly controlled by physiographic origin; for example, rivers draining the sediment-abundant Andean foothills are designated white water rivers with a loamy (brown-yellow), turbid appearance. They contain approximately 90-95% of total suspended sediment in the basin (Meade et al., 1985). Clearwater rivers that drain the cratonic highs of the Brazilan and Guiana Shields are relatively transparent with a yellow-green appearance and low sediment yields. Blackwater rivers such as the Rio Negro drain the Brazilian Plains and are transparent, although they can be slightly dark in colour. The colouration of these rivers results from acidic leaf-litter leachate derived from the adjacent floodplain. In general, these rivers tend to have low sediment yields but can have high quartz-dominated bedloads (Archer, 2005; Sioli, 1975; Sioli, 1984).

During the Pleistocene glaciation (~ 11.5 Kyr) sea levels were substantially lower than at present. Accordingly, rivers incised their valleys to compensate for the imposed disequilibrium. Following subsequent sea level rise, rivers with low sediment fluxes were unable to balance sedimentation, thus formed large flooded valleys (rias) characterised with depositional islands proximally upstream. These islands are clearly exhibited by the clear and blackwater rivers in eastern Amazonia (e.g., Rios Tapajós, Negro and Xingu) (Archer, 2005; Sioli, 1984). An explicit examination of the impact of human disturbance on the Amazon Basin has not been studied, however, Latrubesse et al. (2009) observed a 31% increase in bedload sediment transport between 1960 and 1990 which was attributed to significant deforestation in the middle Araguaia River. Conversely, Dunne et al. (1998) considered human-induced land use change to have limited impacts on the sediment budget of the Andean rivers as

background sediment loads were already high. This disparity clearly illustrates the varied physiographic provinces that exist across the Amazon and how their sensitivity to external forcings contrasts. This observation may be particularly important when considering future changes imposed by climate and humans.

2.2 Climate and Hydrology

The Amazon Basin traverses several degrees of latitude from 10˚N to 19˚S with the Andean Cordillera extending along the entire western margin of South America and being characterised by peak elevations exceeding 6 km. South America is bounded by both the Atlantic and Pacific Oceans to the east and west of the continent, respectively. These basin characteristics contribute to the diversity in climatic conditions observed throughout the Amazon Basin. The Intertropical Convergence Zone (ITCZ), a continuous equatorial low pressure zone, persists to the north of South America and delivers large sums of rainfall to the Andean Cordillera and the western sector of the basin. Sub-tropical high pressure cells in the Atlantic also contribute to the climatic conditions of the basin: the expansion of the South Atlantic cell in the austral winter reduces rainfall over the central Amazon before contracting in September and, in concert with the South American monsoon, delivers high levels of moisture to the Amazon (Barry and Chorley, 2010; Gerreaud and Aceituno, 2007). Furthermore, interactions between the Andes and moisture-laden air from the ocean induces orographic rainfall which can exceed 3 m yr^{-1} in places (Whipple and Gasparini, 2014).

Quasi-periodic fluctuations of surface pressure in the Equatorial Pacific induce a coupled oceanic-atmospheric phenomenon approximately every two to seven years. The El Niño-Southern Osciallation (ENSO) is an interaction between sea surface temperature and the overriding atmosphere between the mid- and western Pacific during which large volumes of heat and moisture are exported from the ocean into the atmosphere. These large transfers of heat and moisture disrupt Rossby waves in

the upper-atmosphere and the Hadley and Walker convection cells. The Amazon Basin is affected by both El Nino (EN) and La Nina (LN) events during which higher moisture fluxes are received by different sectors of the basin. During LN events larger moisture fluxes are received by the south-western part of the basin over the Peruvian and Bolivian Andes (Bookhagen and Strecker, 2010). These positive rainfall anomalies elevate river discharges and trigger widespread flooding of the adjacent floodplains (Espinoza et al., 2014; Marengo et al., 2012; Marengo et al., 2013). Conversely, EN events tend to produce low-magnitude floods compared to LN events, but cause river levels to be higher than during the normal annual flood cycle (Bookhagen and Strecker, 2010). El Niño events are often associated with droughts in the northern part of the basin the intensities of which are directly related to the strength of the climatic perturbation. Although ENSO events have been attributed to large-scale flood events, it has also been acknowledged that the migration of the ITCZ to more southerly positions (driven by warmer sea surface temperatures in the Pacific) can increase rainfall over Amazonia and enhance river discharges (Marengo et al., 2012). The predominant cause of extreme floods in the Amazon is the timing of peak discharges: usually the northern and southern tributaries reach peaks at different times due to slightly differing hydro-meteorological regimes dampening the mainstem floodwave (Marengo et al., 2012; Tomasella et al., 2011). Early onset of peak discharges in northern tributaries in 2009 coincided with the floodwave generated by the southern tributaries resulting in the highest ever recorded water level at Manaus (29.75 m) (Marengo et al., 2012). Aside from floods, the Amazon also experiences extreme droughts (e.g., 1998 and 2005) (Marengo et al., 2008b; Meggers, 1994). Although droughts are linked to EN events and reduced moisture export from the Pacific Ocean, they have also been linked to other climatic anomalies. The 2005 drought caused fires that destroyed vast areas of forest, caused water bodies to completely evaporate, and severing crucial transport links along the river. This was the linked to reduced intensity of the north-east trade winds, which transport

moisture from the Atlantic Ocean to Southern Amazonia. This coupled with lower than usual humidity and higher surface air temperatures resulted in the extreme drought (Marengo et al., 2008a; Marengo et al., 2008b). Hydro-meteorological extremes are intensified when one or more factors occur simultaneously such as the 2010 drought in southern Amazonia in which the end of an EN event was met with a weaker moisture export from the North Atlantic (Marengo et al., 2011).

Extreme drought events in the Amazon Basin cause detrimental socio-economic (e.g., for fishing and agriculture) as well as biogeochemical (e.g., nutrient exchanges between waters and vegetation) effects (Schöngart and Junk, 2007). Seasonal floods are responsible for connecting the river to its floodplain which is a necessary component to maintain the ecological functioning of the Basin's flooded forests. These interactions also allow fish species to occupy the flooded forests and oxbow lakes situated within them. Fish species richness is shown to be greater in lakes located closer to the active channel and within floodplain forests although these habitats may be particularly at risk due to increasing land use conversion (Cox et al., 2008; Davidson et al., 2012; Finer and Jenkins, 2012; Lobón-Cerviá et al., 2015). It is estimated that 30% of the Amazon's mainstem flow is derived directly from the floodplain where an exceptional amount of water can be stored (Alsdorf et al., 2010; Richey et al., 1989). The floodplain topography effectively directs this discharge (at rates of ~ 5500 m^3 s^{-1}) from the channel into the floodplain and until stage levels become so high that flows are entrained parallel to the main channel (Alsdorf et al., 2007; Alsdorf et al., 2010).

The ultimate purpose of the Amazon River (in a natural sense) is to export sediment and water from the uplands to the Ocean. The Amazon is one of the largest exporters of both sediment and water to the global ocean and in doing so is a key source of nutrients for biogeochemical cycles (Mayer et al., 1998; Milliman and Meade, 1983; Milliman and Syvitski, 1992). Despite discharging a sediment load several times

larger than that of the Mississippi (Blum and Roberts, 2009; Milliman and Meade, 1983), the Amazon does not have a subaerially exposed delta; the reason for this is that ocean currents in the Atlantic are too strong to facilitate vertical growth of the delta above the surface. Nevertheless, a large subsurface delta exists, whilst a large proportion of sediment is transported along the coast in a northerly direction to the Amazon Fan (Allison et al., 1995; Kuehl et al., 1986; Nittrouer et al., 1986a; Nittrouer and DeMaster, 1996; Nittrouer et al., 1986b; Nittrouer et al., 1995). The Amazon Fan is the third largest mud-dominated deep-sea fan extending 4800 km downslope from the shelf break and exhibiting a maximum thickness of c. 4-5 km (Damuth et al., 1988; Maslin, 2009). During glacial periods, sediment is supplied to the fan at a rate 20 to 1000 times greater than during interglacial periods when the sediment is transported away by the sea ((Mikkelsen et al., 1997; Nittrouer and DeMaster, 1996). The complex morphology of the fan provides a sedimentary archive by which geological and climatic changes in the Amazon Basin can be interpreted from rates of sediment supply to the fan ((Damuth et al., 1988; Maslin, 2009)).

Chapter 3

Sediment supply as a driver of channel migration in the Amazon Basin
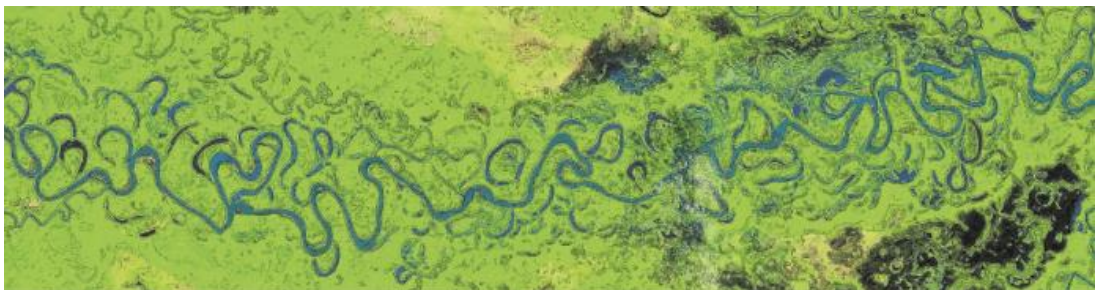
Contributed to a Nature Geoscience publication – Constantine et al. (2014)

3. Motivation

A simple visual examination of three rivers from three different physiographic provinces in the Amazon Basin should be sufficient to emphasise the potential significance of varying sediment supplies on meandering channel behaviour. Shield rivers carry sediment loads several orders of magnitude lower than those fed by the rapidly denuding Andes while those in the Central Trough exhibit intermediate sediment loads.
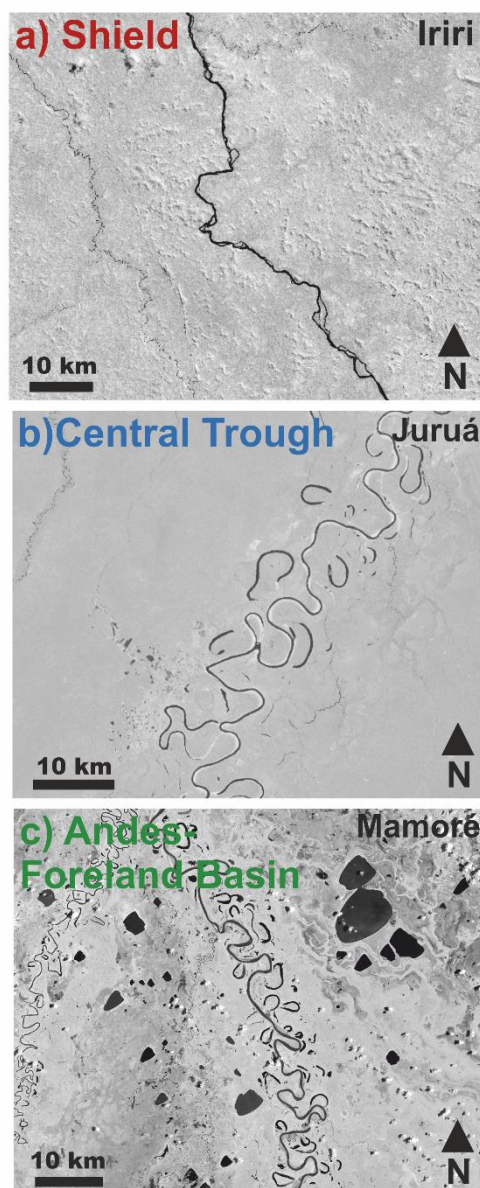
Figure E1. Rivers from the Shield, Central Trough, and Andes-Foreland Basin displayed as monochrome Landsat 7 images. The river names are displayed and colours correspond to those used in the plots presented later.

3.1 Abstract

Meandering rivers are ubiquitous across the planet; however, the processes governing their development and evolution still remain somewhat elusive. The channel centrelines of 20 meandering reaches across the Amazon Basin were monitored between 1985 and 2013 to assess their rates of movement and the number of channel cutoffs generated. The Amazon is comprised of four physiographic provinces, each delivering different volumes of sediment to their respective basins. Sediment flux data, as reported in the literature, correlates positively with channel evolution. Reaches draining the highly erodible Andes supply large fluxes of sediment to the channel network, elevating the rates of channel migration and meander cutoff. Conversely, reaches draining the highly eroded Precambrian shield show lower rates of channel mobility. Furthermore, reaches with large sediment fluxes show relatively stable sinuosities through time despite their high migration rates. This suggests that reaches with higher migration rates must produce more channel cutoffs to maintain a steady-state sinuosity through time. Therefore, greater populations of oxbow lakes suggest that floodplains of highly dynamic rivers have larger volumes of potential valley storage accommodation space. This correlates well to the number of relict oxbow lakes observed in the floodplains of these rivers. Our results cannot be explained by differences in channel slope, and highlight the importance of sediment supply in modulating the ability of meandering alluvial rivers to reshape the floodplain environment through river migration. Sediment supply would be radically reduced by the construction of large dams proposed for the Amazon Basin.

3.2 Introduction

Meandering rivers form some of the most dynamic and biodiverse landscapes on Earth; their geometry undergoes constant adjustments in response to externally-mediated forcings. Meander migration extracts sediment from the floodplain and disperses it in both the cross-stream and downstream directions, where it is periodically transported and sequestered. Although much research has focused on the conveyance of sediment derived from within the system (internally-sourced), little research has been dedicated to the role of externally-derived sediment and how it interacts with the channel. Sediment supply can be adjusted by both natural and anthropogenic processes: mass wasting events regularly supply sediment to the channel network and are often initiated by discrete storm events (Benda and Dunne, 1997). The denudation of mountain belts by sub-aerial processes (e.g., freeze-thaw or chemical weathering) also delivers material to the channel network where it is subsequently transported downstream. Longer-term processes such as the growth and retreat of glaciers or orogenesis can also deliver vast amounts of sediment to river channels as it is excised from the landscape.

Anthropogenic factors are also responsible for, and often accelerate, sediment transfers to river channels; this is primarily driven by changes in land-use such as the conversion of natural forest to agricultural land. Deforestation is a common and widespread issue in the Amazon, which has been observed to increase the alluvial sediment supply as unconsolidated sediment is transported to the channel by runoff (e.g., Rio Araguaia; (Latrubesse et al., 2009). Furthermore, deforestation of the Tocantins and Araguaia River basins in south-east Amazonia has been modelled to increase river discharge by 25% in the absence of any increases in rainfall (Coe et al., 2009; Coe et al., 2011). Basins not affected by deforestation will be impacted indirectly by atmospheric feedbacks that act to distribute water around the Amazon, potentially altering the hydrology of rivers across Amazonia more widely (Coe et al.,

2009). Deforestation also poses a threat to river water quality and ecology through the exposure and erosion of contaminant-rich soils (Mainville et al., 2006). The removal of vegetation exposes the soil, which becomes degraded following conversion from forest to agricultural land, and increases the likelihood of erosion. Increased rates of Mercury-enriched soils, deriving from volcanic activity, pose a threat to riverine ecology as this soil becomes exposed and is vulnerable to transport by overland flows (Mainville et al., 2006).Sediment transport is a sporadic process with sediment undergoing storage in either the channel bed or on the adjacent floodplain as determined by the size-distribution of the material in question. Bed material is periodically transported when flow conditions exceed the thresholds for granular motion. The geometry of meandering rivers causes areas of transport and stagnation to be varied: the inner meander bends are sites of sediment accumulation due to lower flow velocities, whereas the outside of the bend is characterised by sediment removal (Leopold and Wolman, 1960). The cross-sectional asymmetry of meanders, and the flow within them, results from curvature-induced centrifugal forces resulting from the curved nature of the channel (Dietrich et al., 1979). Flow enters in the upstream portion of the meander, crosses from the inner to outer bank, reaching a maximum just downstream of the bend apex. This curvature-induced outward flow advection creates a cross-stream pressure gradient, which creates helicoidal flow characterised by outward flow at the surface and inward oblique flow at the bed, which carries eroded sediment from the cut-bank to the downstream end of the point bar (Braudrick et al., 2009; Dietrich and Smith, 1984; Dietrich et al., 1979; Frothingham and Rhoads, 2003; Odgaard, 1987).

The presence of point bars has been observed to displace high-velocity fluid entering the meander towards the outer bank as it shoals over the top of the bar (Dietrich and Smith, 1983; Legleiter et al., 2011). The growth of bars has been modelled experimentally and shown to grow through sediment accumulation at the downstream

(tail) of the bar and at the lateral margins as flow shoals over the bar, or as near-bed currents deliver sediment from the eroding concave bank (Dietrich et al., 1979; Pyrce and Ashmore, 2005). Additional sediment, derived from the landscape, increases the availability of material which, in non-transport limited scenarios, can accumulate in the channel and enhance the growth of bedforms (Dunne et al., 2010). Since the growth of these bedforms is driven primarily by sediment supply, in concert with the prevailing flow conditions, it is logical to suggest that point bars provide a mechanistic link between sediment supply and channel behaviour.

The construction of reservoirs interrupts the natural transfer of sediments downstream which can result in river bed degradation as flows capable of transporting sediment remove all the fine material leaving a coarsened channel bed. Moreover, this loss of material results in the cessation of channel bedforms and can lead to decreased biodiversity as the ecological functioning of the river deteriorates (Rollet et al., 2014). In addition, discharge controls imposed on seasonally flooded wetland environments like the Amazon will likely reduce the supply of nutrient-rich sediment to the adjacent floodplain causing a reduction in riparian diversity, too (Kingsford, 2000). A total of 153 large-scale dams (>2 MW) are proposed for the Amazon Basin with plans to site many of them in the Andes-Foreland Basin region (Finer and Jenkins, 2012). For this reason, it is important to assess the role of in-channel sediments on the behaviour of freely meandering channels to ascertain the importance and understand the possible changes that may result from dam construction. The Amazon Basin is an ideal study site to conduct this study since it remains relatively pristine and is characterised by a number of physiographic provinces that supply varying sediment loads to the rivers that drain them.

This chapter will examine the role of sediment supply on the evolution of meandering rivers across the Amazon Basin. Twenty river reaches spanning the basin were selected based on their physiographic location and data availability. An analysis of

channel migration rates, populations of oxbow lakes and rate of oxbow lake generation were all examined in relation to sediment fluxes to determine the role of sediment supply on channel dynamism.

3.3 Methods

A series of georectified Landsat images obtained from the United States Geological Survey's (USGS) Earth Explorer were used to digitise channel centrelines between 1985 and 2013 for 20 Amazon River reaches (**Fig. 2; Chapter 2**). Each reach was monitored between three and five times over the course of the 28-year period depending on image availability. The channel width was determined by measuring the straight-line distance across the bankfull channel, perpendicular to the banks using the most recent imagery. This was completed a minimum of 15 times per reach to ensure an accurate channel width was determined. The measurements were only made at straight sections of the reach uninfluenced by islands or tributaries; meander bends were avoided to prevent the channel width being skewed towards larger values caused by erosive processes in the bends. The average was taken and rounded to the nearest 10 m to improve calculations at latter stages of the analysis. Since the pixel resolution of the imagery is 30 m, the rounding is thought to be negligible in the context of the uncertainty introduced by the imagery. To overcome complications with mid-channel bars and channel islands, where the flow bifurcated, the channel with the largest conveyance was used to determine channel width, and delineate the channel path. For cases where islands divided the flow equally, the entire channel width was measured from outermost bank to innermost bank; therefore, this technique may systematically overestimate the channel width on these rivers (e.g., Rio Branco).

Meander-belt widths were determined by measuring the longest distance between relict oxbow lakes in the adjacent floodplain. These measurements were taken at randomly placed cross sections oriented perpendicular to the channel using the most

recent satellite imagery available on Google Earth©. Measurements of the meander-belt width were used to indicate the freedom of the channel to migrate within its floodplain. Narrow meander-belts are indicative of channel confinement, either imposed geologically or otherwise (Caputo, 1991). Additionally, the images were inspected for human interference, subsurface geological activity (e.g., areas of uplift), and sections of channel narrowing. The influence of subsurface geology was inferred from the surface as no seismic data was available for the analysis. Channel flow direction is a useful indicator for the presence of localised areas of uplift (as is present in the downstream part of the Rio Beni). The uplifted channels drain radially outwards from the locally elevated surface.

Digitising channel centrelines consisted of delineating the bankfull channel boundary characterised by the vegetation line – an indicator of high water mark – on each side of the channel, and generating a mid-channel point. These points were synthesised for the entire channel length at intervals of approximately one channel width. In areas of complex channel geometry, for example in some meander bends, the point density was increased to capture the channel form more accurately. The bankfull channel margin was used to limit the complexities of mapping the wetted channel margin with variations in water stage between satellite image dates, and limited hydrological data to complement the imagery. After creating a temporal record of channel centrelines, eroded-area polygons were constructed by intersecting two centrelines from subsequent years (Constantine et al., 2009; Micheli et al., 2004). The purpose of generating polygons was to deduce the minimum annual rate of channel migration between the two time periods using equation 1:

$$M = \frac{A_i}{P_i n} \quad (1)$$

Where A_i is the area of the ith eroded-area polygon, P_i is one-half the perimeter of the ith polygon – or the average centreline length between years and n is the number of

years between images (**Fig. 3**). The minimum rate of channel migration is derived since the direction of channel shift may have reversed at least once between the images (Constantine, 2006). A reach-averaged annual rate of channel migration is derived with the mean weighted such that shorter polygons are discounted relative to long polygons; this is calculated using equation 2 (Constantine, 2006).

$$\overline{M} = \frac{\sum_i^n M_i P_i}{\sum_i^n P_i} \tag{2}$$
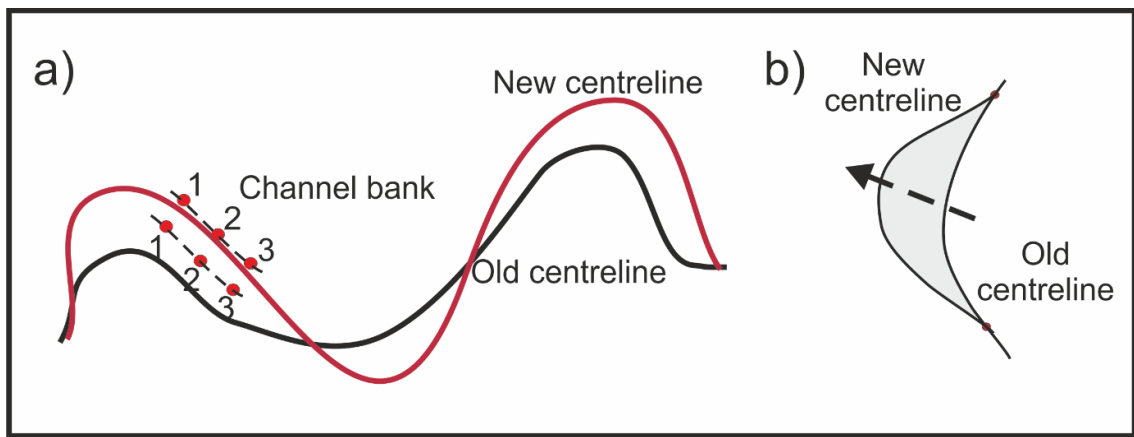
Figure 3 a) Centreline derivation from equidistant points, and b) eroded-area polygon generation from centreline intersection.

Polygons that were indicative of cutoffs were removed from the migration rate calculation as these introduced anomalously large rates of migration that did not take place. All efforts were made to maintain any migration that is likely to have occurred before the segment was cutoff. Similarly, periods where the dominant flow channel altered, for example those channels which bifurcate around large mid-channel islands or bars, were removed from the analysis for the same reason.

Both the frequency and type of meander cutoff were documented between consecutive image dates and normalised by channel length to allow inter-reach comparisons to be made. A neck cutoff was classified as the convergence of two limbs of a meander neck induced by the continual outward migration of the limbs.

Chute cutoffs were determined as reductions in channel length facilitated by meander bypass (Erskine et al., 1992; Gay et al, 1998; Lewis and Lewin, 1983). Channel sinuosity was calculated as the ratio of channel centreline length to the sum of the channel-belt axis lengths (Brice, 1964). This method was selected because it accounts for changes in valley orientation thus deriving a more accurate metric for sinuosity than simply taking a straight-line valley distance. In addition to establishing a cutoff inventory, the number of observable oxbow lakes in the floodplain was documented. Oxbow lakes were characterised as any arcuate open water bodies within the active meander belt. This definition was expanded to include partially-infilled and fully infilled lakes that could still be identified from the imagery by their shape or differing vegetation cover to the surrounding floodplain. The rate of oxbow lake infilling relates to their proximity to the channel and access to sediment (Constantine et al., 2010a). The total number of lakes was normalised by the length of channel in units of channel widths to account for differences in reach length.

Channel slope was calculated using a series of point elevations measured from processed Shuttle Radar Topography Mission (SRTM) Digital Elevation Model (DEM) data. The version four (V4) processed data differs from the original collected and processed by NASA and the USGS in that it has been subjected to a number of void filling algorithms to provide seamless elevation for the entire globe at a resolution of 3-arc seconds (~ 90 m) (Jarvis et al., 2008; Reuter et al., 2007). Water surface elevations were extracted from the channel centreline at intervals of 10 km. The decision to use a 10 km interval spacing was made since it scales well with the length of the study reaches (> 100 km) and allowed for repeat slope measurements along each river. Channel surface elevations were extracted – since SRTM data cannot penetrate the water surface – and used as a surrogate for bed elevation. It is assumed that under uniform flow conditions channel surface slope accurately represents channel bed slope (Leopold et al., 1964).. Each collection of slope measurements

was averaged to derive a reach-averaged slope with the uncertainty described by the standard error of the population of reach slopes.

Sediment fluxes were compiled from the literature (see **Table 1**) as documented during extensive field surveys of the Amazon. Sediment fluxes for reaches without any reported values were derived by developing a linear model between the drainage basin area and the corresponding sediment flux for all the reaches draining similar physiographic provinces (**Fig. 4**). A linear regression equation was derived for the relationship which could then be used to estimate sediment flux from upstream drainage areas of the reaches. Sediment fluxes were subsequently normalised by channel width and converted into fluxes per width of channel using equation 3.

$$S_{FA} = \frac{S_F}{C_W} \quad , \tag{3}$$

where S_F is sediment flux in units of Mt yr^{-1} and C_W is channel width in m. The purpose of normalising sediment flux by channel area was to account for the fact that larger channels can convey larger sediment fluxes. Fluxes reported in the literature are for total suspended sediment (TSS); this metric includes both the sandy bedload sequestered on point bars, and the silty washload that passes through the channel and is deposited overbank during floods without being deposited on point bars (Filizola and Guyot, 2009). Since sediment load measurements remain sparse across the Amazon, the use of TSS in this study is a surrogate of bedload sediment fluxes. The coarsest fractions of sediment are unable to be conveyed continuously by channel flows and are deposited, accumulating in regions of the channel with low flow velocities. Resultantly, the coarse bedload forms the substrate constructing the point bar. Methods for collecting sediment flux data within the literature varied significantly and so may introduce uncertainties to the fluxes that were used in this study. For example, the data compiled from Filizola and Guyot (2009) represented sediment collected using a depth-integrated sampler (after Meade et al., (1979)) that was

subsequently filtered and homogenised to generate a single sample for each site. The final TSS values were calculated after relating sediment load measurements to local discharges and performing regression analyses for three different calculations of TSS. The values adopted in the present study was that which was deemed most representative by Filizola and Guyot (2009). Sediment flux data taken from Dunne et al. (1998) was collected at approximately 4-monthly intervals between 1981 and 1984 with additional samples taken in 1988, 1990, and 1991. The samples were depth and width integrated and collected from the mouths of the tributaries to the Amazon mainstem. Measurements from Guyot et al. (1996) corrections based on the data collected by the hydrological agencies in Bolivia and Brazil to generate TSS estimates, while Armijos et al. (2013) created a sediment rating curve from sediment samples taken at various depths of the channel every day days. A regression equation was used to estimate TSS fluxes for the Ucayali River after formulating a statistically robust correlation between the rating curve and observations of flow and sediment flux on the river (Armijos et al., 2013). Although variable techniques were used to measure TSS across the study reaches, many were internally corrected for variations and the majority of values had already been converted into measurements of TSS, therefore supporting the use of this data as an accurate estimate of reach suspended sediment flux.
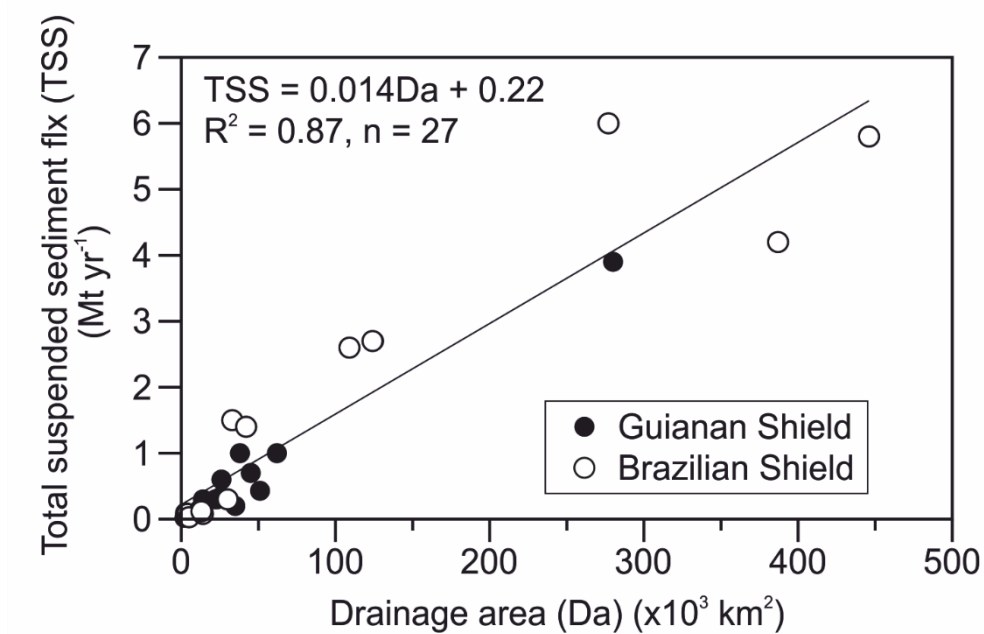
Figure 4. Drainage area-TSS flux for 26 reaches draining the Guiana and Brazil Shields. Reach data points are plotted from those reported in Table 1 of Filizola and Guyot (2009). A linear regression equation has been provided.

Table 1 Suspended sediment load data for Amazonian study reaches and locations of gauges

Reach (Abbreviation)	Total suspended sediment flux (Mt yr^{-1})	Sediment gauge coordinates
Araguaia at Aruanã (Ar)[a]	15	14:55:00 S, 51:05:01 W
Vaupés at Taraqua (Va)[b]	0.70	01:6:51.6 N, 69:40:34 W
Branco at Caracaraí (Br)[b]	2.7	01:49:42 N, 61:07:49 W
Iriri (Ir)[c]	0.056	
Xingu (Xi)[c]	0.33	
Purus1 at Seringal Fortaleza (P1)[b]	103	07:43:10 S, 66:60:00 W
Purus2 (P2)[d]	32	03 :58 :34 S, 61 :28 :10 W
Juruá (Ju)[e]	12	04:44:00 S, 70:18:00W
Jutai at mouth (Jt)[f]	2	02:44:40 S, 66:47:22 W
Itui at Seringal do Itui (It)[c]	0.28	04:44:00 S, 70:18:00 W
Curuca at Santa Maria (Cu)[c]	0.35	04:40:48 S, 71:28:12 W
Nanay (Na)[g]	0.91	
Putumayo (Iça) at mouth (Pt)[h]	24	03:08:13 S, 67:58:29 W
Mamoré0 at Paracti/Puerto Villarroel (M0)[j]	13	16:50:19 S, 64:47:30 W
Mamoré1 (M1)[k]	82	
Mamoré2 at Puerto Ganadero (M2)[l]	64	14:51:00 S, 65:02:53 W
Beni at Rurrenabaque (Be)[m]	212	14:27:01 S, 67:31:36 W
Ucayali at Requena (Uc)[n]	205	05:00:58 S, 73:58:53 W
Madre de Díos at Miraflores (Ma)[m]	71	10:54:27 S, 66:08:59 W
Huallaga at Chazuta (Hu)[o]	71	06:34:12 S, 76:07:12 W

a. Study reach is between two sediment gauges: Aruanã (14:55:00 S, 51:05:01 W) and Luís Alves (13:12:55 S, 50:35:04 W). An average sediment flux was calculated from the fluxes reported at these gauges by Lima et al. (2005).

b. Sediment flux reported by Filizola and Guyot (2009).
c. Total suspended sediment fluxes reported by Filizola and Guyot (2009) for all rivers draining the Brazilian Shield were plotted against drainage area to allow sediment fluxes to be estimated from linear regression equations (Fig. 2a).
d. A sediment flux was interpolated from the sediment flux-drainage area relationship with values reported by Filizola and Guyot (2009) at Labrea (07:15:26 S, 64:47:55) (68 Mt y^{-1}) and by Dunne et al. (1998) at Aruma-Jusante (04:43:36 S, 62:08:52 W) (25 Mt y^{-1}) gives a sediment flux for P2 (Fig. 2b).
e. The study reach begins 200 valley km (Vkm) downstream of Eirenupé sediment gauge where Filizola and Guyot (2009) recorded a flux of 12 Mt y^{-1}. Dunne et al. (1998) recorded a flux of 15 Mt y^{-1} at Gaviao, 153 Vkm downstream of the study reach. The values observed by Dunne et al. (1998) are generally larger than those of Filizola and Guyot (2009) because they sampled the full flow depth. The observed difference between these sediment fluxes is within the uncertainty of the measurements themselves.
f. Sediment gauging station is 356 Vkm downstream of the end of the study reach as sampled by Dunne et al. (1998).
g. The total river length is 316 km, which, using the global length-area relationship described by Mueller (1994) translates to a drainage area of 14500 km^2. Sediment flux was calculated using the yield per unit area (62 t km^{-2} yr^{-1} from the Rio Orthon at Caracoles (2 Mt y^{-1}) (Guyot et al., 1996). Both basins drain Tertiary and Quaternary sediments in actively deforming parts of the Andean foreland basin (Decelles and Hertel, 1989; Räsänen et al., 1992).
h. Flux reported by Dunne et al. (1998) from CAMREX gauging station at the mouth of the R. Ica (Putumayo).
j. The sediment flux at the confluence between Rio Chimoré and Rio Mamoré is calculated by summing the flux at Paracti (~4 Mt y^{-1}) (17:13:02 S, 65:49:11 W) and Puerto Villarroel (9 Mt y^{-1}) as reported by Wittmann et al. (2009) and Guyot et al. (1996), respectively. An assumption is made that there is little storage between Paracti and the confluence with the Mamoré.
k. The flux entering M1 is calculated by summing the flux into M0 and one-half the flux recorded at Abapo (18:54:35 S, 63:24:00 W), as reported by Guyot et al. (1996). The flux at Abapo is reduced by 50% since approximately this percentage of suspended material is deposited in the floodplains of rivers crossing the foreland basin of Eastern Bolivia (Guyot et al., 2007; Guyot et al., 1994; Guyot et al., 1996).
l. Sediment flux reported by Wittmann et al. (2009).
m. Sediment flux reported by Guyot et al. (1996).
n. Sediment flux reported by Guyot et al. (2007).
o. Sediment flux reported by Armijos et al. (2013).

3.4 Results and Discussion

Rivers were grouped into three classes as determined by their dominant sediment-source regions: the Andes (Andes-Foreland Basin), the Central Amazon Trough, and the Brazil and Guiana Precambrian Shields (Shields). Two-tailed t-tests and Kruskal-Wallis tests (KW) were used to quantify the significance of the differences observed between rivers draining these three distinct physiographies. Spearman's rank correlation coefficients (ρ) and Kendall rank correlation coefficients (τ_B) were used to specify the significance of correlations between the assessed variables. Average annual rates of channel migration are found to be statistically significantly different for reaches draining the Andes-Foreland Basin when contrasted with rates calculated for rivers in the Central Trough and Shields (t-tests: $\alpha < 0.001$; KW: $\alpha < 0.001$). On average, rivers draining the Andes-Foreland Basin had migration rates 4.54 and 5.54 times larger than those observed for rivers draining the Central Trough and Shields, respectively. Migration rates varied over two orders of magnitude for the 20 study reaches with the lowest rates being observed on rivers draining the Shields (e.g., Rio Branco: 4.4×10^{-3} ch-w yr^{-1}) (**Fig. 5**).
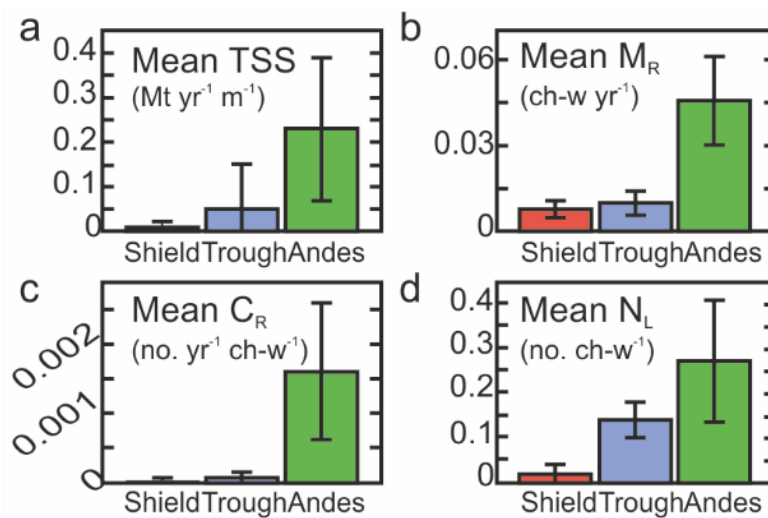
Figure 5. Summary of mean statistics for TSS (total suspended sediment load), M_R (average annual meander migration rate), C_R (average cutoff production rate), and N_L (number of oxbow lakes in the floodplain) symbolised by physiographic province

Cutoff rates were statistically different for rivers draining the Andes-Foreland Basin when compared to rivers draining the other physiographies (t-tests: $\alpha < 0.001$; KW: $\alpha < 0.001$). The total number of cutoffs observed on Andean rivers ranged from between two and 19, with the majority occurring along the Rio Beni and Rio Mamoré (19 and 32). The Araguaia was the only Shield reach to develop a cutoff over the study period. From the Central Trough reaches, the Purus2, Jutai and Putumayo did not produce any cutoffs over the observed study period. Cutoff rates were substantially lower (Shields: > 50 times slower; Central Trough: 17 times slower) on the Shield and Central Trough reaches compared to their Andes-Foreland Basin counterparts.
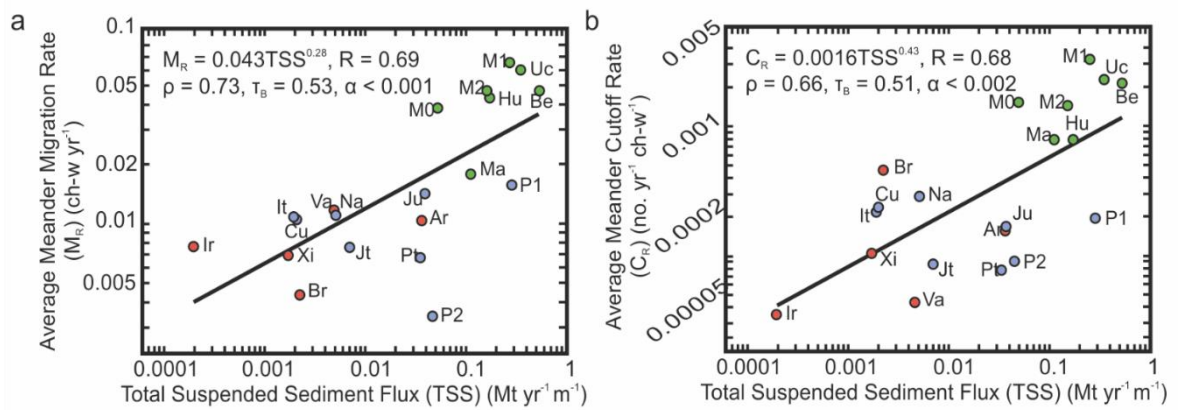
Figure 6 a) Regression between TSS and M_R; b) Regression between TSS and C_R. Symbols are consistent with the colours used throughout the chapter and labelled with reference to the study site map. A Pearson (ρ) and a Kendall Tau (τ_b) correlation was calculated for each plot and is presented with the corresponding statistical confidence level (α).

The dominant cutoff mechanism (i.e., chute or neck) was found to vary between reaches; 77 cutoffs were documented across all 20 study reaches with just over half being chute cutoffs (52%). The majority of the chute events occur on the cutoff-rich reaches (Mamoré, Beni, and Ucayali), although they are almost equally as prevalent as neck cutoffs along the Beni and Mamoré0 reaches (**Table 2**).

Table 2. Cutoff inventory for the Amazon Basin

Reach Name	Period	Cutoff Sum	Neck	Chute	% neck of total	% chute of total
Araguaia	1986-2013	1	1	0	100.00	0.00
Vaupés	1987-2009	0	0	0	0.00	0.00
Branco	1990-2007	0	0	0	0.00	0.00
Iriri	1985-2013	0	0	0	0.00	0.00
Xingu	1996-2013	0	0	0	0.00	0.00
Purus1	1987-2013	2	2	0	100.00	0.00
Purus2	1987-2011	0	0	0	0.00	0.00
Juruá	1991-2011	3	3	0	100.00	0.00
Jutai	1988-2010	0	0	0	0.00	0.00
Itui	1984-2013	2	2	0	100.00	0.00
Curuca	1994-2010	1	1	0	100.00	0.00
Nanay	1987-2010	1	1	0	100.00	0.00
Putumayo (Iça)	1991-2009	0	0	0	0.00	0.00
Mamoré0	1986-2010	13	7	6	53.85	46.15
Mamoré1	1986-2010	26	10	16	38.46	61.54
Mamoré2	1986-2010	11	2	9	18.18	81.82
Beni	1987-2013	19	10	9	52.63	47.37
Ucayali	1993-2010	11	3	8	27.27	72.73
Madre de Díos	1988-2013	3	1	2	33.33	66.67
Huallaga	1995-2013	2	0	2	0.00	100.00

An examination of channel slopes shows that no robust relationship exists between channel slope and channel mobility. Channel slope was found to be relatively consistent within the uncertainty of the data for all 20 reaches; there was no relationship between channel slope and physiographic province (**Fig 7**). It could be expected that rivers with greater slopes would exhibit higher rates of mobility associated with increases in stream power, and therefore shear stress (Grenfell et al., 2012; Schumm and Khan, 1972). However, our results reveal no consistent causative relationship between average channel slope and migration rate ($\rho = 0.35$, $\tau = 0.33$, $\alpha > 0.16$) (**Fig. 7**). Perhaps, this is a result of uncertainty in the data (derived from SRTM) of water surface slope, which does not accurately resolve the patterns of channel slope on the channel bed (Jarvis et al., 2008). The absence of a slope-

driven increase in channel mobility suggests other factors are primarily responsible

for the trends observed (e.g., sediment availability).
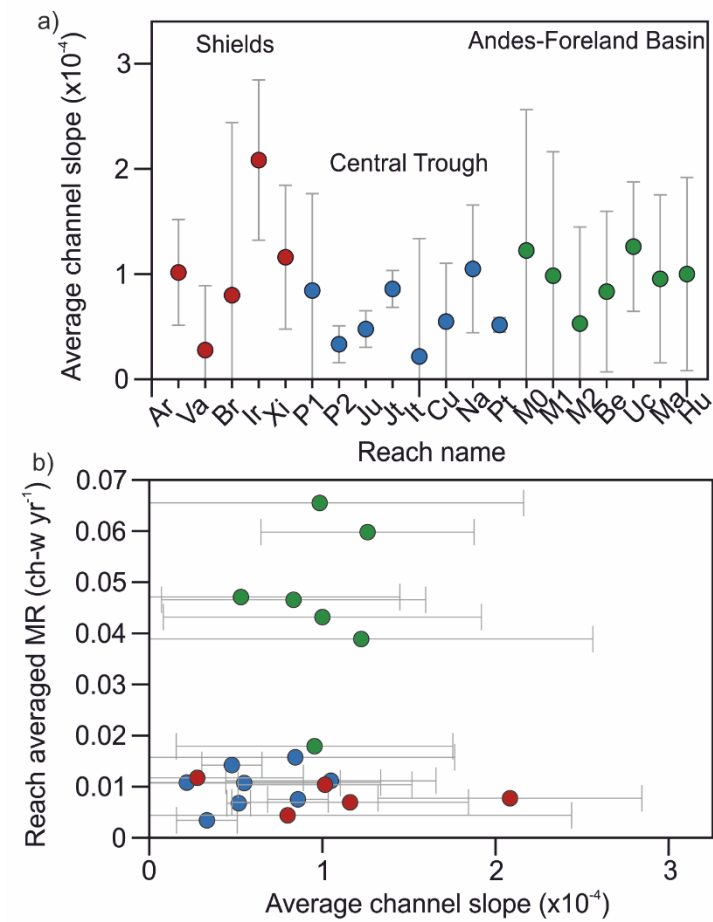
Figure 7 a) Measurements of average channel slope from SRTM DEM.; b) M_R as a function of average slope. Error bars indicate ± 1StdError about the mean value as determined from repeat measurements of channel slope over the reach length

Estimated TSS fluxes for the seven Andes-Foreland Basin rivers were found to be statistically discrete with regards the rivers draining the alternative physiographies (t-tests: $\alpha < 0.001$; KW: $\alpha < 0.005$) (**Fig. 5a**). Rivers draining the Andean mountains carry an order of magnitude more sediment than those draining the Central Trough and Shields. It is these sediment-rich rivers which were also observed to migrate the most rapidly and produce the most oxbow lakes. A count of the total number of discernible oxbow lakes in the floodplain of these rivers showed a similar upward trend; the largest number of observed lakes were found in the floodplains of rivers draining the sediment-rich Andes-Foreland Basin rivers, whilst considerably fewer lakes were documented in the floodplains of the Central Trough and Shields (t-tests: $\alpha < 0.001$; KW: $\alpha < 0.005$) **Fig. 8**).
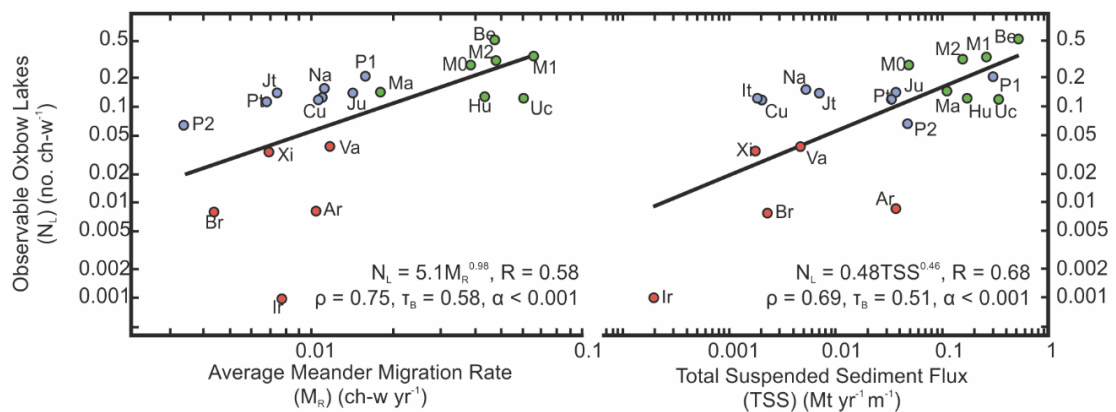
Figure 8 a) N_L plotted as a function of M_R; b) TSS versus N_L. All symbolisation is consistent with the previous figures in the chapter. A Pearson (ρ) and a Kendall Tau (τ_b) correlation was calculated for each plot and is presented with the corresponding statistical confidence level (α).

Changes in total reach sinuosity revealed that many of the reaches maintained a relatively stable sinuosity over the 28-year study period. Sinuosities were shown to deviate by ±7% on 18 of the 20 reaches; the Ucayali and Mamoré0 showed an approximate decrease of 17% over the same period.
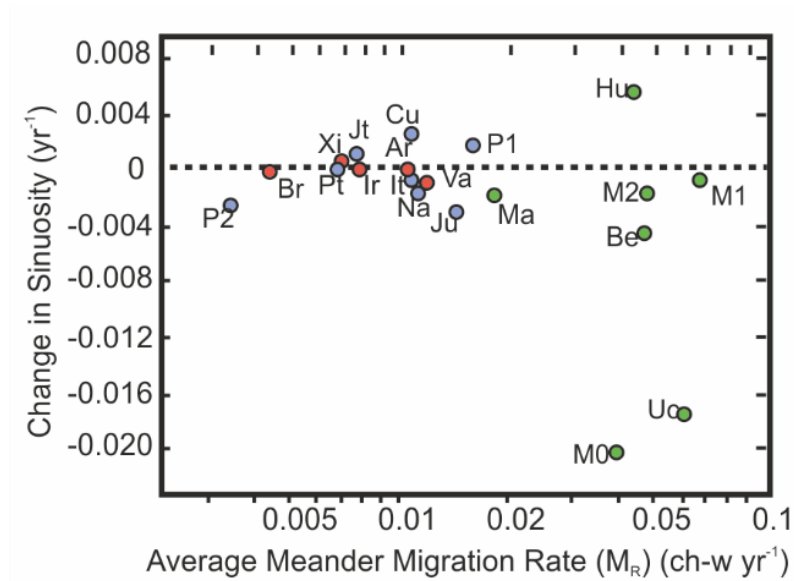
Figure 9. Average annual rate of change in sinuosity plotted against M$_R$.
The black dashed line indicates a steady state sinuosity of 0.

The results suggest that rivers rich in alluvial bed material (i.e., those located in the Andes-Foreland Basin region) migrate across their floodplains more rapidly than those in sediment-poor provinces (**Fig 6a**). It has been shown experimentally that enhanced sediment loads can trigger more rapid channel migration (Dunne et al., 2010; Wickert et al., 2013). A potential mechanism linking higher sediment loads to increased channel mobility can be conceived through the sequestration of bed material on point bars. Since point bars accumulate at the inner bank of meander bends, their growth and orientation can disrupt the passage of flow through the meander, and therefore influence the distribution of shear stress (Dietrich and Smith, 1983). Computer-generated models of meandering channel dynamics show that in

the absence of point bars the distribution of flow velocity in the bend is characterised by high flow velocities at the inside of the bend, and more suppressed flows at the outside. This observation is a function of the relative distance the flow has to travel around the bend (Abad and Garcia, 2009a). As point bars develop, flow entering the bend is deflected outwards, both as a function of bend curvature and due to topographic steering by the accumulated sediment. It has been suggested that a larger topographic extent of the point bar can effectively steer this high-momentum fluid, at a greater velocity, towards the outer bank, thereby increasing boundary shear stress and encouraging bank erosion (Abad and Garcia, 2009c; Dunne et al., 2010; Legleiter et al., 2011).

Testing the theory that larger point bar footprints should correlate with greater channel mobility, if indeed there is a link between sediment retention, bar growth and bar-driven topographic steering, was achieved using a small section of the Rio Mamoré. For our study the Mamoré was split into three reaches; between M0 and M1 the Rio Grande joins the Mamoré. The significance of this tributary relates to the very high suspended sediment load it carries directly from the Andes (~136 Mt yr^{-1}) (Guyot et al., 1994). Although the sediment load is initially very large, approximately 50% of this is deposited as the Grande traverses across the Foreland Basin resulting in a final estimated load of ~69 Mt yr^{-1}, which combines with the ~13 Mt yr^{-1} already present. Examining the Mamoré from satellite imagery clearly reveals that downstream of confluence, the aerial extent of point bars becomes greater (**Fig. 10**).
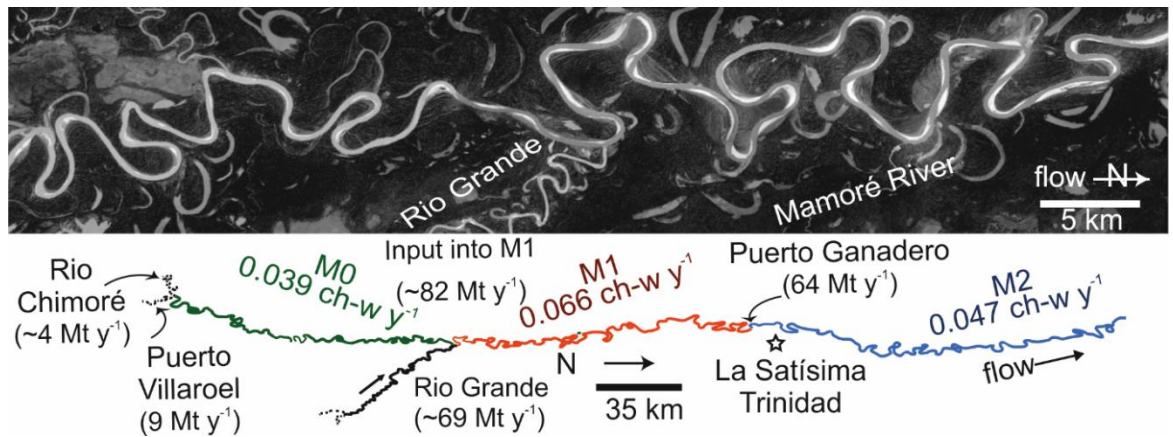
Figure 10. Enhanced point bar development on the Rio Mamoré downstream of the confluence with the Rio Grande. A 2013 Landsat image of the Rio Mamoré reveals larger point bar extents downstream of where the river receives a large supply of sedimentary material from the Rio Grande. Migration rates increase following the input and decrease further downstream, although remain higher than before the input.

Moreover, there is an approximately 1.7-fold increase in channel migration downstream of the confluence further supporting the potential linkage between sediment and channel mobility. At the beginning of reach M2 there is a roughly 29% decrease in channel migration rate which is inferred to be a result of in-channel sediment sequestration and overbank deposition during floods. It appears that the overloaded channel is sequestering material on the bars explaining their increased footprint downstream of the confluence. The decrease in channel migration is consistent with the reduced sediment load (~64 Mt yr^{-1}).

The total number of cutoffs produced for each river was also found to be consistent with the upward trend in sediment flux (**Fig. 6b**). Rivers within the Andes-Foreland Basin were more likely to produce cutoffs than those in the Shields or trough. These observations support the theory that as rivers migrate more, as they do in the Andes-Foreland Basin, the bends become ever more likely to converge into one another since the alluvial valley within which they traverse is only finitely wide. A second argument that supports these observations is related to channel sinuosity: as the river migrates, the average meander wavelength increases, which causes the slope of the

channel to diminish and sinuosity to increase. Sediment transport relies on the channel's ability to convey water at a suitable velocity to entrain the bed material. As the channel slope decreases, the capacity for sediment transport diminishes due to slower flow velocities, therefore supporting in-channel sedimentation. Theoretically, Stolum (1996) postulated that the maximum sinuosity that can be attained by a river is ~3.14, but many natural rivers have much lower values (van Dijk et al., 2012). The high-magnitude discharge (i.e., above bankfull) events may also promote the development of cutoff events along the tributaries since the yearly annual floods raise water levels by several metres which gives rise to overbank flow and extensive flooding (Junk and Furch, 1993). Since just over half of the cutoffs documented were chutes, which are typically formed by flow exploiting low-lying topography (Constantine et al., 2010b; Gay et al., 1998; van Dijk et al., 2012; Zinger et al., 2011), it is likely that the discharge variability is responsible for promoting some of the cutoff incidences documented in the Amazon.

The high frequency of cutoff events along the sediment-rich reaches links well with the hypothesis of excess sediment being sequestered on point bars: larger bars conveying high-momentum fluid to the outer bank will increase boundary shear stress, sediment entrainment, and channel migration. More rapid movement of the channel precludes the generation of cutoffs. Indeed, the previous explanation is only really valid for the generation of neck cutoffs. However, more rapid bar growth and associated lateral migration may leave swales (depressions) exposed within the point bar complex for high discharges to exploit, perhaps facilitating the development of chute cutoffs. This is particularly applicable to reaches where the rate of vegetation colonisation on point bars is insufficient to keep pace with lateral migration (Nicholas, 2013). Alternatively, the high sediment loads conveyed by rivers in the Andes-Foreland Basin may be unable to effectively transport the entire sediment load, and so, results in bed aggradation. The deposition of material on the river bed effectively

reduces the channel's capacity and increases the potential for overbank flows, which may result in floodplain scour and chute development (**Fig. 11**). Indeed, high-magnitude flood events, which increase bed shear stress, will be able to periodically entrain the alluvium deposited on the bed, once again increasing the channel capacity.
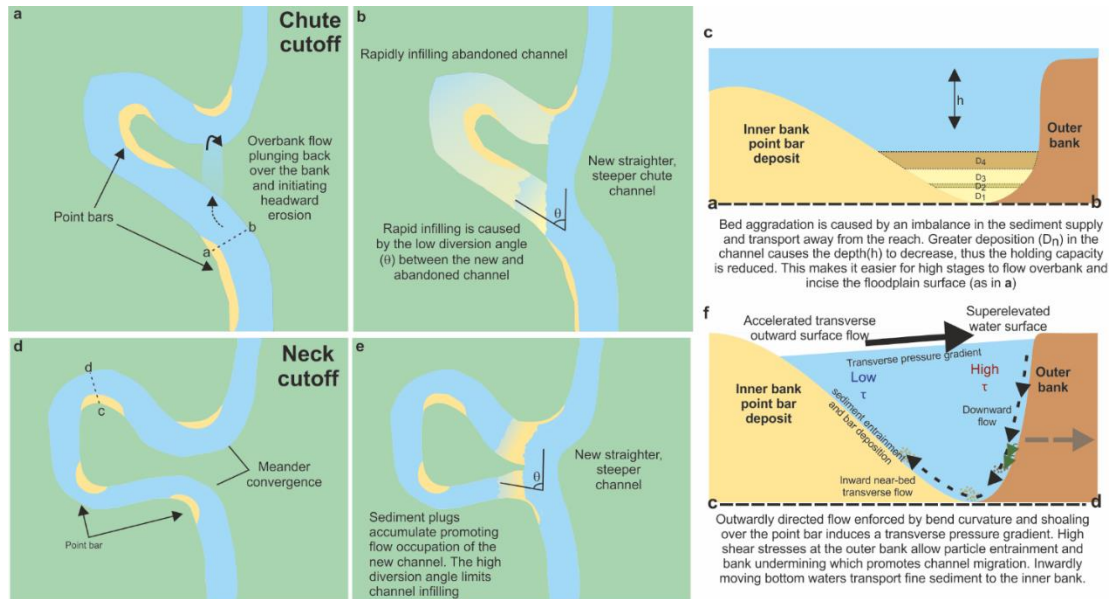
Figure 11. Schematic of cutoff dynamics driven by sediment loading. a) Chute cutoff development caused by overbank flow and floodplain scour; b) Chute cutoff channel and abandoned chute undergoing rapid infilling by diverted channel bed material; c) Mechanism of chute initiation by overbank flow induced by in-channel sedimentation; d) Neck cutoff development caused by progressive channel migration; e) Shortened channel and abandoned neck plugged by sediment at the ends but remains open due to low sediment diversion; f) Neck cutoff development mechanism enhanced by point bar sedimentation which increases outward flow and lateral migration rate.

An assessment of the long-term pattern in channel sinuosity revealed little variation over the ~28-year study period, despite the numerous incidences of cutoff, and high rates of channel migration (**Fig. 9**). This stationary long-term sinuosity has been interpreted elsewhere as an equilibrium state between the processes that act to increase channel sinuosity (lateral migration), and those which curtail it (cutoffs). Since there is a positive correlation ($\rho = 0.77$, $\tau = 0.62$) between migration rate and cutoff rate, it suggests that the two processes are in an equilibrium state over sufficiently long time periods (Fig. 10). The fact that two of the Andean reaches (Ucayali and Mamoré0) show a slightly larger deviation (~17%) from the ±6% sinuosity change displayed by the other reaches suggests that these rivers were undergoing large changes in their planforms. This was confirmed by the temporal clustering of cutoffs along these reaches during the observation period.
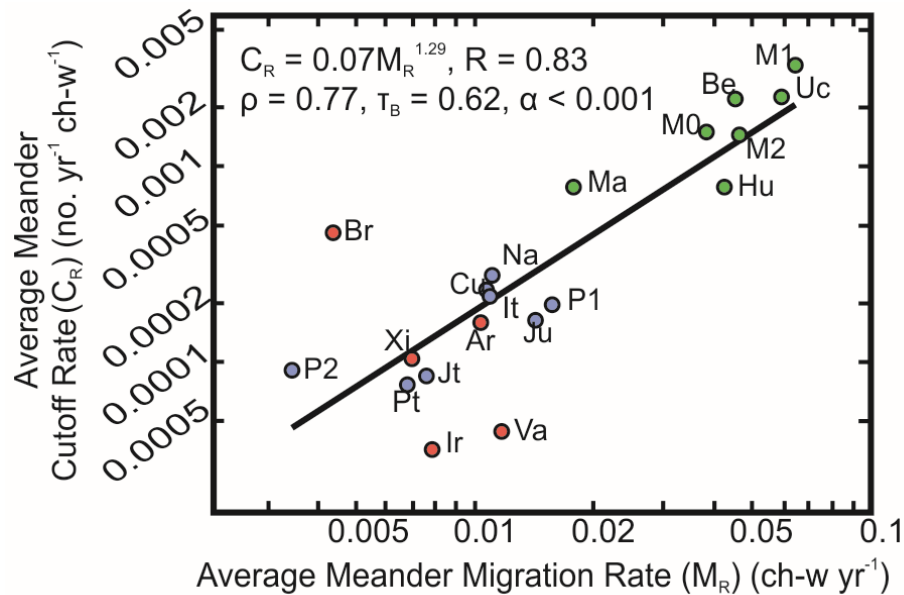
Figure 12. M_R plotted against C_R, Symbology is the same as that used in the previous figures. A Pearson (ρ) and a Kendall Tau (τ_b) correlation was calculated for each plot and is presented with the corresponding statistical confidence level (α).

Although high sediment fluxes are causing an increase in rates of lateral migration, the long-term sinuosity of the reaches is being maintained by a corresponding increase in the frequency of cutoffs produced. A greater frequency of cutoffs along Andes-Foreland Basin rivers should result in larger populations of oxbow lakes in their floodplains. Indeed, an assessment of the active floodplain adjacent to all 20 study reaches revealed similar patterns to those reported for cutoff and migration rates; that is, with increasing sediment flux, the number of oxbow lakes in the floodplain increases (ρ = 0.69, τ = 0.51) (**Fig. 8a**).

The significance of these findings and the inference that sediment flux has consequences for channel migration are manifold: first, increases in channel migration are important for those concerned with risk management. For example, the ability to forecast and predict where meandering channels will move in the future will inform those invested (economically or socially) in floodplain infrastructure (Gilvear et al., 2000). Second, meandering channels are responsible for generating biologically-rich riparian habitats colonised by specialist species that increase productivity and value through ecosystem services (Tockner and Stanford, 2002). Furthermore, the movement of river channels into established floodplains introduces a disturbance that allows for the generation of primary species which results in increased biodiversity (Salo et al., 1986). Importantly, the process of floodplain destruction through meandering introduces large amounts of organic material to the channel (particularly in heavily vegetated areas). This organic matter – comprised of lignin, cellulose and other macromolecules – is an important (often neglected) source of carbon dioxide produced by biological degradation in the channel (Aufdenkampe et al., 2011; Mayorga et al., 2005; Ward et al., 2013). Where there is rapid bank collapse and channel migration, it is expected that large amounts of potentially organic rich material will be recruited by the channel with the potential for it to be respired and released as carbon dioxide to the atmosphere. Indeed, some of this material will be deposited

during sedimentation in wetlands, or counteracted by the growth of new vegetation on the floodplain. Third, the sediment-triggered migration and generation of oxbow lakes may act as sites for sediment sequestration in the long-term as these floodplain depressions are filled with alluvial material. Finally, the proposed installation of 151 large (>2 MW) hydroelectric dams predominantly in the Andes-Foreland Basin of the Amazon (Finer and Jenkins, 2012), where it has been shown that the most dynamic rivers are situated, could result in significant fragmentation, and system destabilisation in the future. Sediment retention behind these engineered structures will reduce alluvium delivery to the lower reaches reducing potential sites for habitat development; and, reducing the ability of bedforms to sequester material to enhance dynamism. Furthermore, the supply of sediment to the floodplain during overbank flows will be reduced which will impact filling rates and terrestrialisation of oxbow lakes. Potential decreases in lateral mobility will diminish the complexity and diverse nature of floodplain composition along these highly dynamic rivers.

3.5 Conclusions

Rivers draining the Andes-Foreland Basin are rich in alluvial material typically an order of magnitude larger than those rivers that drain the Central Trough and Shields. These sediment-rich rivers show significantly higher average annual migration rates than those in alternative physiographies. As a result, the incidence of cutoff events is higher along these reaches, and the production of oxbow lakes is greater. There is a clear positive correlation between increasing sediment flux and channel migration, cutoff rate, and the population of oxbow lakes in the floodplain. We propose that rivers with large sediment supplies sequester alluvial material on point bars throughout the reach enhancing their topographic profile and facilitating the transverse displacement of high-velocity fluid to the outer bank; this results in accelerated rates of channel migration, and associated changes in channel geometry. These observations are important for risk analyses and estimating long-term sediment and organic material exchanges between river channels and their floodplains, and the creation of riparian habitats. Moreover, these findings suggest a mechanistic link between sediment supply and floodplain evolution. The dynamic nature of these channels and the habitats they create will be threatened by the installation of hydroelectric dams that will fragment this delicate system.

Chapter 4

Point Bars in the Evolution of Channel Sinuosity in the Amazon Basin

Written up and submitted to Geology
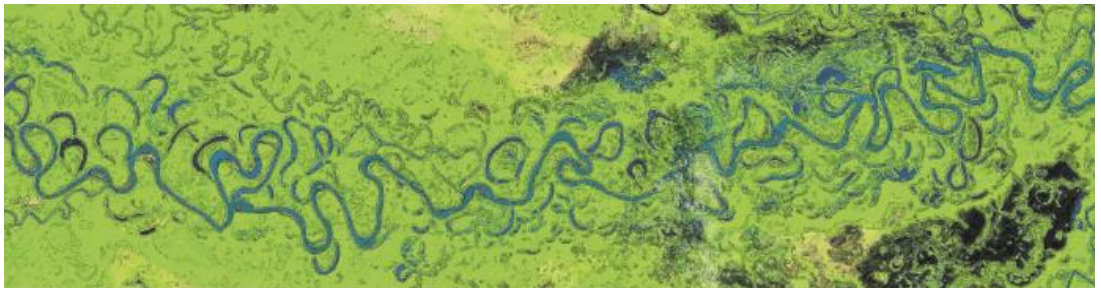
4. Abstract

External sediment supply is a fundamental component of alluvial river systems and in the long term provides the necessary substrate required for point bar growth. Despite this, a complete understanding of their function in meandering channels remains unclear. We quantified the relationship between the geometry of channel migration and the rate of change of sinuosity for 22 reaches across the Amazon Basin using an archive of Landsat images. Annual increases in sinuosity fit a power function with rates of channel migration. The relationship between the two variables can be explained, in part, by the predominant mechanism of bend deformation operating along the reach: bends that extend normal to the downstream direction increase their sinuosity more slowly than bends that translate downstream. Downstream translating bends are more common on rivers with high sediment loads, and appear to establish point bars with larger areal extents that expand throughout the meander. Upstream translating meanders are associated with compound meander development or the deposition of upstream sediment lobes. These observations suggest that the position of point bars within meander bends can influence flow routing so as to control the dominant direction of meander growth. Understanding the interactive relationship between sediment loading and meander dynamics will improve the accuracy of morphodynamic river models which has consequences for interpretations of floodplain stratigraphy as well as patterns of sediment cycling across the channel-floodplain interface.

4.1 Introduction

The sinuosity of single-thread meandering channels, expressed as the ratio between the length of the channel and valley length, has a theoretical maximum value of 3.14 (the sinuosity of a circle), although many channels fail to achieve this due to cutoff development (Constantine and Dunne, 2008; Stølum, 1996). Meander migration serves as the mechanism by which river channels continually adjust their sinuosity and overturn the valley floor through time. More sinuous channels access material stored in the distal floodplain and redistribute it to the channel, where it renews floodplain growth through point bar accretion at the inner banks of meanders (Lauer and Parker, 2008). Vegetal encroachment and continued sedimentation increase the bar surface area through time until it attains the bankfull height, although chute channel formation may preclude complete floodplain conversion (Braudrick et al., 2009). The likelihood of meander cutoff increases for channels with higher sinuosities, producing negative relief that enhances floodplain complexity through the creation of distinctive lentic environments, which also act as fine-grained sediment sinks (Constantine et al., 2014; Lewin and Ashworth, 2014). This intrinsic sediment reorganisation is responsible for the creation of diverse riparian habitats in which pioneer and mature plant species coexist in close proximity (Salo et al., 1986).

Still unresolved is the influence of externally supplied sediment on barform growth and planimetric channel evolution; this material is a fundamental component of alluvial river systems and its supply rate may be amplified by tectonism (Latrubesse and Restrepo, 2014) or changes in land use or climate (Latrubesse et al., 2009). Point bars facilitate the link between external sediment supplies and meander dynamics through their ability to sequester alluvial material and to divert flow. Point bar expansion increases the length and curvature of bends, increasing the cross-stream centrifugal force (Hickin and Nanson, 1975), and enhancing the cross-stream velocity component under some circumstances by topographic steering, increasing the

boundary shear stress at the outer bank (Dietrich and Smith, 1983; Legleiter et al., 2011). Extensive experimental work has yielded conflicting results regarding the effect of varying sediment supply on the planform evolution of meandering rivers. Some studies observed increased channel mobility due to increased sediment supply (Braudrick et al., 2009; Wickert et al., 2013), while others observed no effect (van de Lageweg et al., 2014). Field evidence has elucidated information about the role of point bars in perturbing flow and promoting meander growth (Lewin, 1976). Similarly, simulations of sediment transport and channel response suggested that meander cross sections receiving enhanced sediment supply experienced more rapid outward bar migration and lateral cutting at the bank toe (Dunne et al., 2010). Empirical evidence from the Amazon Basin also suggests that rivers carrying high sediment loads are more dynamic and appear to develop more extensive point bars than do low-sediment rivers (Constantine et al., 2014).

Empirical evidence is generated to quantify the relationship between channel sinuosity and meander migration, and identify sediment supply as an important component in this process manifested through point bar deposition. These findings suggest the need to further explore the role of sediment supply in the morphodynamic evolution of meandering channels within the channel-floodplain system.

4.2 Methods

Multispectral Landsat imagery from 1984-2014 were used to delineate bankfull channel margins of 22 reaches across the Amazon Basin (**Fig. 13**). Imagery for three reaches (Mamoré, Beni, and Madre de Díos) were obtained at a near-annual resolution, while the remaining reaches had a temporal spacing of ~10 years. All images were obtained from the USGS Earth Explorer facility. Imagery within the annual dataset were converted to normalised difference vegetation index (NDVI) format to be used within ArcGIS; the remaining reaches were compiled from a previous study (Constantine et al., 2014).
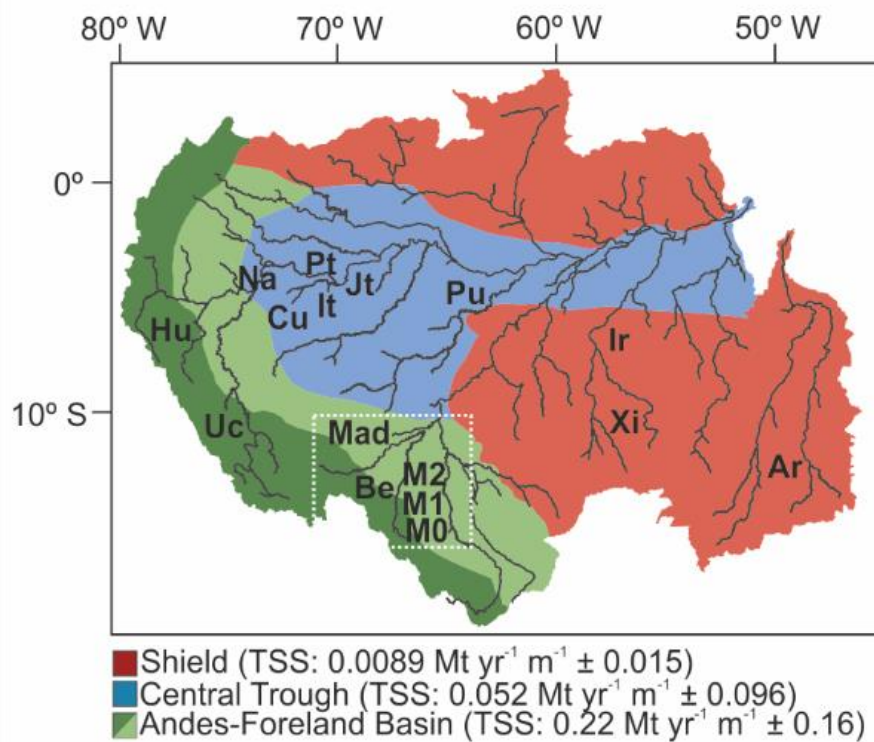
Figure. 13 Amazon drainage basin symbolised by physiographic province and labelled with reach abbreviations: Ar = Araguaia; Ir = Iriri; Xi = Xingu; Pu = Purus; Jt = Jutai; It = Ituí; Cu = Curuca; Pt = Putumayo; Na = Nanay; Hu = Huallaga; Uc = Ucayali; Mad = Madre de Díos; Be = Beni; M0 = Mamoré0; M1 = Mamoré1; M2 = Mamoré2. The average annual total suspended sediment flux (TSS; megatonnes per metre of river channel width) and associated standard deviations about the means are indicated for each province. All reaches are covered by an approximately decadally-resolved suite of imagery; reaches within the white dashed box are also covered by an annually-resolved dataset and are characterised by a number of sub-reaches. Detailed images of the reaches can be observed in Fig. 15C.

The bankfull channel boundary was delineated by selecting a representative pixel threshold at the channel-bank interface. The pixel characteristics were analysed to distinguish the limit of regular flow inundation and thus identify the bankfull channel boundary. The bankfull boundary was used to effectively normalise for variations in channel stage between images. The threshold selection, which characterises the interface between the channel and the floodplain, was achieved by trialling multiple test pixels and selecting the pixel value that best described the interface. Trials were carried out by selecting a pixel thought to be representative of the boundary and applying this to the entire image. If the boundary was regarded representative, it was used, if not, it was removed and an alternative was selected. Since many of the reaches were still connected to former channels and backwater lakes, careful removal of erroneous segments was required before the centrelines were digitised to prevent inaccurate boundary delineation.
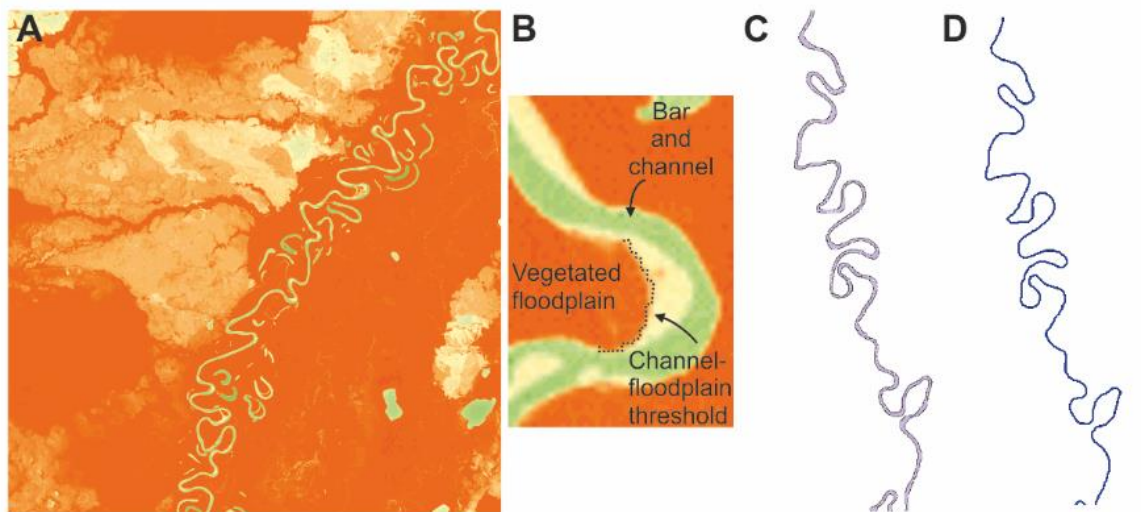
Figure 14. Methodology for semi-automated channel extraction from satellite imagery. A) NDVI image created by combining bands 4 and 5 from Landsat 8 multispectral imagery. The brighter oranges are indicative of high vegetation densities; greens and whites indicate bare sediment and water. B) An indicative threshold was found to distinguish floodplain from bare sediment and water indicative of the channel environment. C) Vectorised channel following filtering of connected features. D) Final centreline derived from the vectorised channel boundary.

The boundary was vectorised and used to generate centrelines for each year on record using the Planform Statistics Tools for ArcGIS (Lauer and Parker, 2008) **(Fig. 14)**; the centrelines were intersected and used to calculate reach-averaged migration rates normalised by the average channel width (ch-w yr^{-1}) (as explained in detail in Chapter 3) (Micheli et al., 2004). Channel width measurements (n > 20) were made along straight sections of river unaffected by flow-driven widening, and incidences of channel cutoff were omitted from the survey. The change in channel sinuosity with time (S^*, yr^{-1}) was thus calculated by measuring the total change in length between two sequential years and dividing by the original channel length and the time between images. To limit data loss on cutoff-bearing reaches multiple sub-reaches were created for the rivers in the high-resolution dataset (**Fig. 15**). The sub-reaches were at least 50 km long to ensure changes in length could be observed.
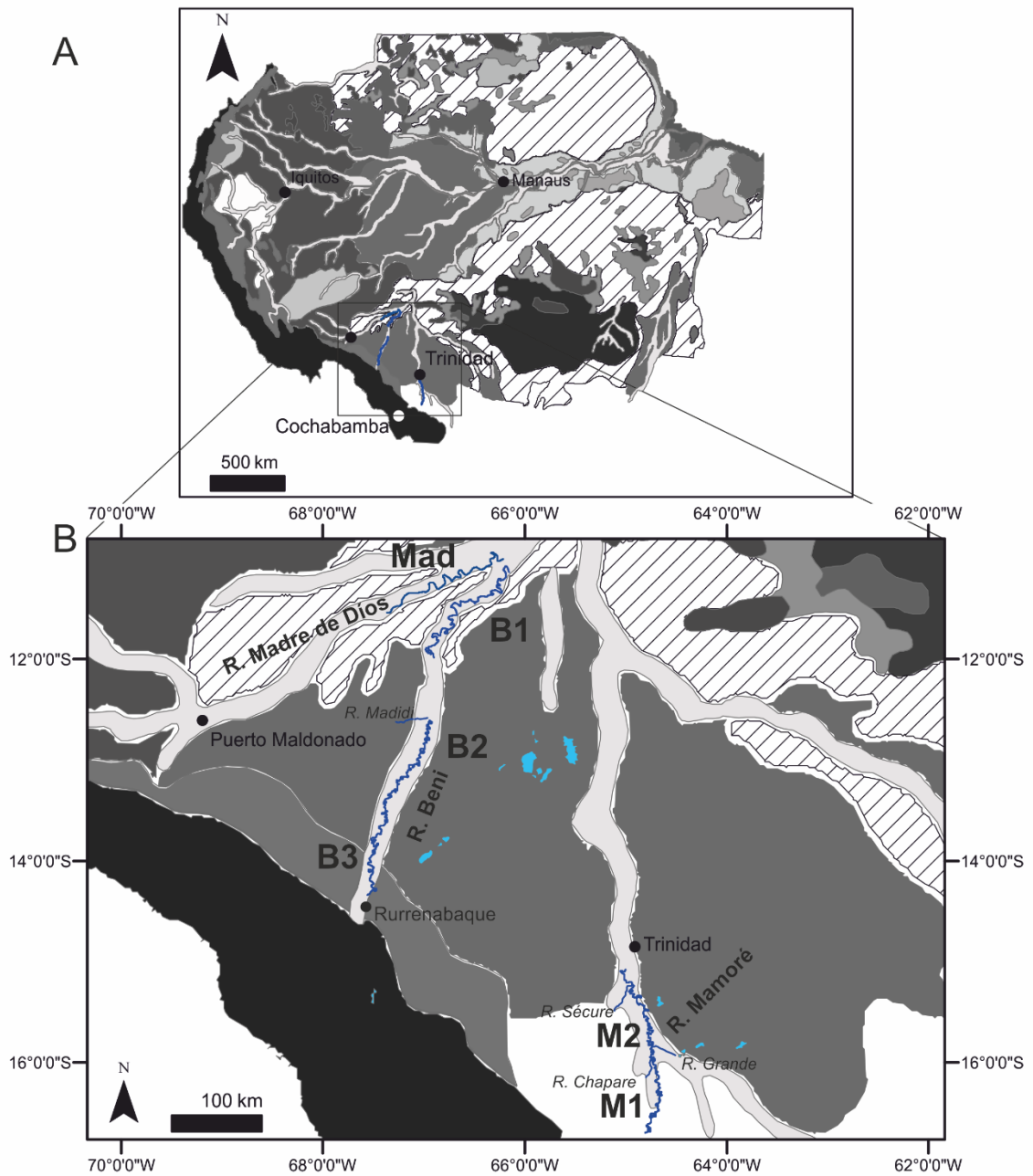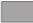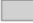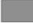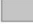
Figure 15 A) Labelled geological map of the Amazon Basin. B) A zoomed section of the Amazon Basin featuring the three rivers and 6 reaches under investigation. Mad = Madre de Dios; B1 = Beni 1; B2 = Beni 2; B3 = Beni 3; M1 = Mamore 1; M2 = Mamore 2. Major tributaries, towns and relevant gauging stations are labelled with the latter being represented by stars: GM = Guayaramerin, MF = Miraflores. The key for the geological map can be found in Fig 15C (below).

Geological Units

- Amazon planalto and associated uplands
- Andean Cordillera
- Bottomland complexes
- Coastal Lowlands
- Crystalline shield uplands
- Crystalline uplands with base-rich soils
- Eastern sedimentary Uplands
- Floodplain complexes
- Inselberg/Mountainous land complexes
- Loamy Plains
- Relict Valley of Roraima
- Relict Valleys
- Sandstone Table lands
- Sandy Plains
- Sedimentary uplands with base-rich soils
- Steeplands and valleys of the Selva Alta
- Water
- Western sedimentary Uplands

C

B1 R3 R2 R1 25 km

B2 R3 R2 R1 25 km

M2 R2 R1 R2

B3 R2 R1 25 km

Mad R3 R2 R1 25 km

M1 R1 25 km
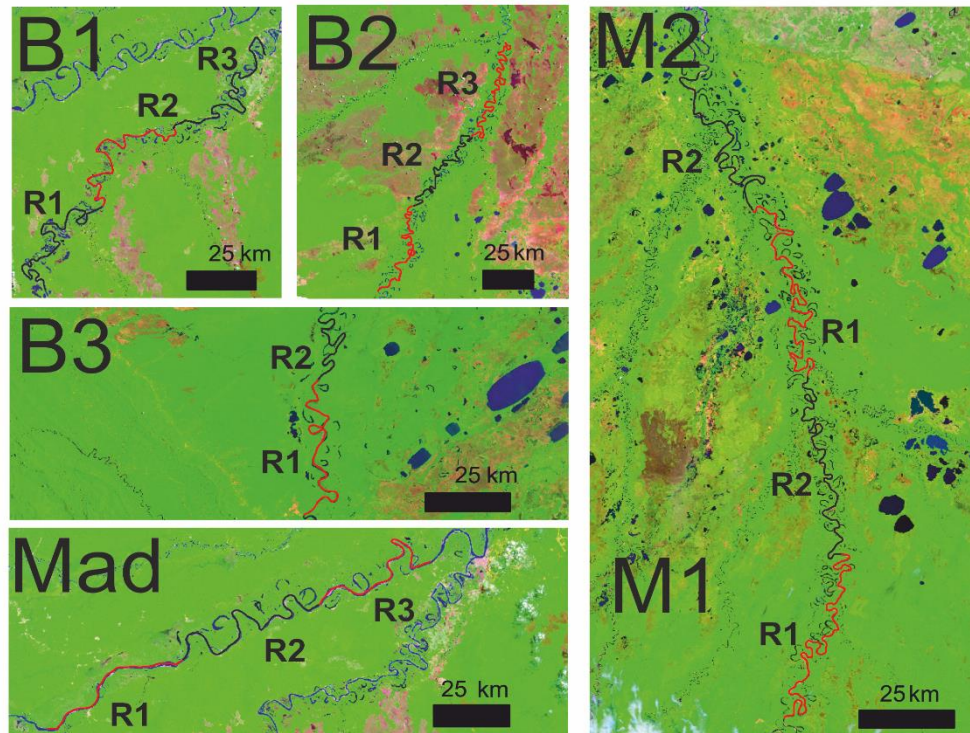
15C) Examples of each reach and sub-reach composites taken from Landsat 8 obtained from USGS Earth Explorer. Each sub-reach is labelled sequentially increasing in the downstream direction (denoted by the prefix R), and coloured alternatingly in red and black for ease of viewing. The top panel displays the geological key for Fig. 15A and 15B.

For reaches where direct length changes due to lateral migration could not be measured because of incidents of cutoff (decadal dataset; **Fig. 13 & Fig. 15**), the following relation derived by Constantine and Dunne (2008) was applied for estimating the rate of channel lengthening ($DM_L \, dt^{-1}$),

$$\frac{dM_L}{dt} = \frac{fL\dfrac{dn}{dt} + V\dfrac{dS_i}{dt}}{l_0} \quad (1)$$

where M_L is channel length, t is time, f is the characteristic fractional change in channel length due to cutoff, L is the characteristic length of channel removed by a single cutoff event, n is the number of cutoff events, S_i is the channel sinuosity, and V is valley length. Each of the variables was measured directly (**Table 3**) from the decadal dataset to derive $DM_L \, dt^{-1}$ and then normalised by the year one channel length (l_0) to be comparable to the annually-resolved data.

We define a meander symmetry index (σ) (**Fig. 16**) for characterising styles of meander deformation. We used the descriptors defined by (Hooke, 1984), in which $\sigma \approx 1$ defined extension, $\sigma < 1$ defined upstream translation, and $\sigma > 1$ defined downstream translation. Although the meander symmetry index does not directly assess bends that undergo other modes of deformation (e.g., rotation), the index does evaluate the broad direction in which a meander is eroding. Therefore, rotating bends will be included within the upstream or downstream translation categories. Other descriptions of meander deformation such as changes in radius of curvature were not measured for simplicity: the meander symmetry index was developed to allow for easy, quantitative descriptions of meander deformation based on the changing shape of the bends. Local curvature measurements were used to inform the division of meanders at inflection points.
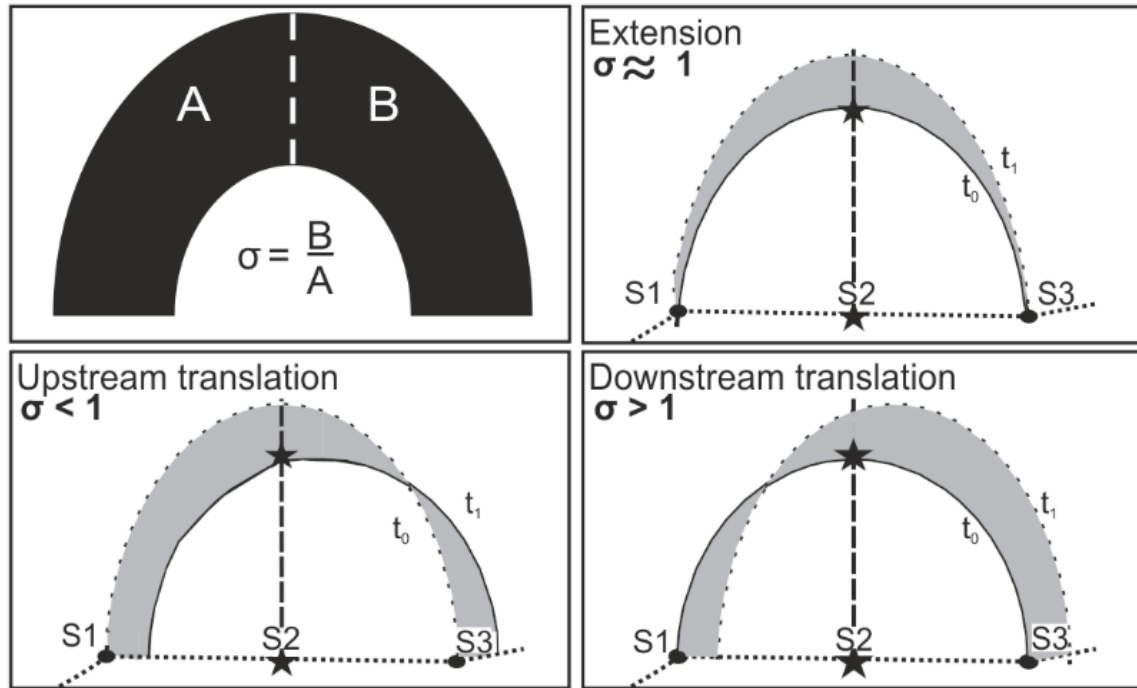
Figure 16. Meander symmetry index (σ) and exemplar scenarios. Clockwise from top-left: σ is calculated the ratio between the total eroded-area produced between the first (t$_0$) and final year (t$_1$) on record in the downstream (B) and upstream portions (A) of the meander. Each meander is divided through the bend apex (star-ended vertical dashed line) of the earliest centreline (t$_0$) and erosional areas are bounded by inflection points derived by connected reach segments (S$_{1,2,3,...n}$) along the t$_0$ centreline. Extension occurs when the ratio between down- and upstream eroded areas is close to one, downstream translation is where the ratio exceeds one, and upstream translation is where the ratio is less than one.

Meanders were individually analysed and characterised as the reach length between inflection points (where the sign of planform curvature changes). Eroded-area polygons were constructed for the meander between the earliest and latest dates on record bounded by the inflection points. Eroded-areas were then partitioned by the vertex intersecting the meander apex, producing two parts of the meander, one for the up- and one for the downstream portion. The ratio between the eroded-areas defined a σ value for every meander present during the earliest image on record. New meanders or those that were terminated by cutoff were omitted from the analysis. The minimum number of meanders used to calculate the characteristic σ for a reach was 7, but the majority (17 of 22) of reaches comprised at least 20. Average σ-values were used to classify the deformation style for each population of meanders along a reach. The calculated values of M_R and S^* were then correlated against total

suspended sediment flux (TSS) data compiled from various sources by Constantine et al. (2014) as an index of total sediment supply. Suspended sediment within the tributaries of the Amazon include both sandy bed-material, which is the material of bar formation, and silt-clay washload, which is transported through the channel and into floodplains without being sequestered in bars. The raw fluxes were converted to equivalent fluxes per channel width to account for the fact that wider channels can convey larger sediment loads.

Table 3 Measured parameters for Equation 1 used to calculate S* for the decadally-resolved dataset

Reach Name	DS/dt (yr^{-1})	Valley length (ch-w)	dn/dt (ch-w/yr)	L (ch-w)	f	dM/dt (ch-w yr^{-1})	S* (yr^{-1})
Araguaia	-8.58E-05	472.31	0.12	7.46	0.44	0.082	0.00013
Iriri	1.70E-05	1012.71	0.00	0.00	0.00	0.017	0.00001
Xingu	5.88E-04	559.44	0.00	0.00	0.00	0.329	0.00041
Purus1	1.80E-03	584.20	2.17	31.30	0.90	3.227	0.00248
Jutai	1.11E-03	532.38	0.00	0.00	0.00	0.589	0.00052
Itui	-6.81E-04	467.52	1.12	18.88	0.86	0.805	0.00079
Curuca	2.57E-03	532.39	0.06	3.38	0.30	1.431	0.00118
Nanay	-1.64E-03	307.72	0.55	13.69	0.92	0.042	0.00006
Putumayo (Iça)	1.28E-04	713.61	0.00	0.00	0.00	0.091	0.00007
Mamoré0	-2.03E-02	378.77	13.81	31.62	0.81	6.112	0.00635
Mamoré1	-7.87E-04	336.51	5.42	20.65	0.79	5.151	0.00736
Mamoré2	-1.60E-03	344.91	2.51	10.48	0.52	1.964	0.00302
Beni	-4.59E-03	345.14	6.16	12.89	0.65	4.577	0.00626
Ucayali	-1.75E-02	311.06	10.56	22.68	0.72	5.120	0.00782
Madre de Díos	-2.00E-03	205.13	0.97	12.17	0.67	0.561	0.00169
Huallaga	5.58E-03	210.17	0.25	5.38	0.41	1.419	0.00417

Table 4 - Meander symmetry indices for each study reach with number of meanders assessed (n), the reach-averaged σ-index and calculated standard deviation and skew of the meander populations indicated.

	Reach (n)	Average σ	Std Dev	Skew
Decadal series	Araguaia (35)	1.58	1.27	2.24
	Iriri (78)	1.18	0.75	1.05
	Xingu (58)	1.21	0.76	0.96
	Purus1 (66)	1.80	1.13	0.97
	Jutai (115)	1.20	0.91	2.25
	Itui (100)	2.07	1.82	2.81
	Curuca (112)	1.40	0.94	1.99
	Nanay (65)	1.34	1.23	2.23
	Putumayo (84)	1.28	0.95	2.95
	Mamoré0 (27)	1.94	1.45	0.77
	Mamoré1 (24)	2.35	1.93	1.54
	Mamoré2 (21)	2.09	1.65	0.83
	Beni (26)	2.41	3.03	2.85
	Ucayali (32)	1.57	1.21	1.36
	Madre de Díos (16)	1.39	1.11	2.13
	Huallaga (21)	2.67	2.08	1.02
Annual series	Madre de Díos (16)	1.21	0.72	0.79
	Beni1 (21)	2.78	2.43	1.01
	Beni2 (27)	2.60	3.21	2.92
	Beni3 (7)	3.55	3.29	1.65
	Mamoré1 (11)	2.33	1.93	0.97
	Mamoré2 (12)	2.32	1.73	1.24

4.3 Results and discussion

Measurements of 285 discrete lengthening and migration rates from across the Amazon Basin indicate that sinuosity changes (S^*) as a power function with respect to average M_R (**Fig. 17A**). Rivers draining the sediment-poor Shield and Trough regions lengthen significantly slower than those within the Andes-Foreland Basin (Kruskal-Wallis (KW): α < 0.02). There is no significant deviation between the lengthening rates observed between the annual and decadal Andes-Foreland Basin reaches (KW: α > 0.15), although no migration rates were resolved below 6.7×10^{-3} ch-w yr^{-1} due to the 30-m resolution of the imagery. This lower limit of meander migration equates to between 1.0 and 4.8 m yr^{-1} in real terms. Sinuosity change observed on the Beni 2, Beni 3 (B2, B3), and Mamoré (M1, M2) reaches were, on average, between three and seven times greater than those on the Madre de Díos (Mad) and Beni 1 (B1) reaches, and up to 47 times larger than rivers draining the Shields. Furthermore, increases in channel sinuosity were significantly larger on rivers with plentiful sediment supply (KW: α < 0.0002; Mann-Whitney: α < 0.0002) **(Fig 17B)**. The structural controls on the Mad and B1 reaches are likely to be responsible for the low observed rates of mobility in which erosion resistant Tertiary deposits constrain lateral migration (see **Fig. 18**) (Gautier et al., 2007; Roddaz et al., 2005; Schwendel et al., 2015). Shuttle Radar Topography Mission data demonstrate the confined nature of the active channel which abuts the resistant boundary at several points along the reach. Oxbow lakes are also observed along the boundary where they were eventually severed from the channel as migration ceased. Confinement of the channel prevents a freely meandering channel from evolving, therefore limiting the development of meanders as they would if allowed beyond their boundaries (Nicoll and Hickin, 2010). An analysis before absolute sinuosity change (Ω) and M_R to confirm the observed relationship between these two variables was not a result of autocorrelation (**Fig. 19**).
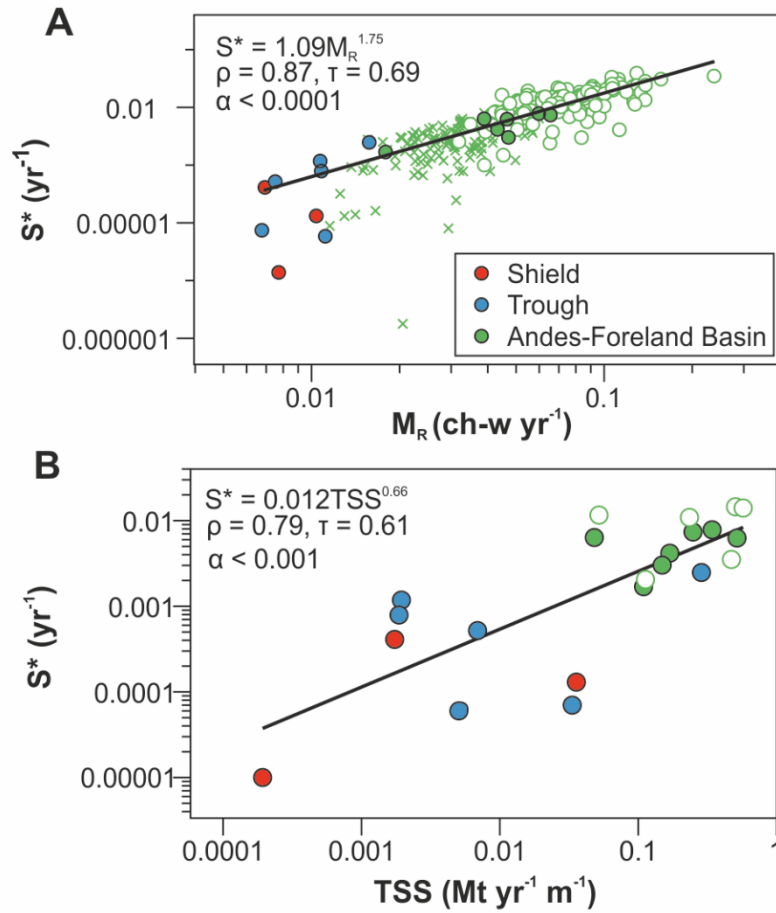
Figure 17. A) Average annual channel migration rate (*M_R*; channel widths per year) related to change in channel sinuosity with time (*S**; per year). Solid points are derived from the decadally resolved dataset and empty points indicate average *S** values calculated from the annually resolved dataset. Crosses indicate annually resolved data points from the Mad and B1 reaches that are laterally confined. The regression line was calculated using orthogonal distance regression to account for the variability in both MR and S*. B: Total suspended sediment flux (TSS; megatonnes per year per metre of channel width) plotted against *S**.
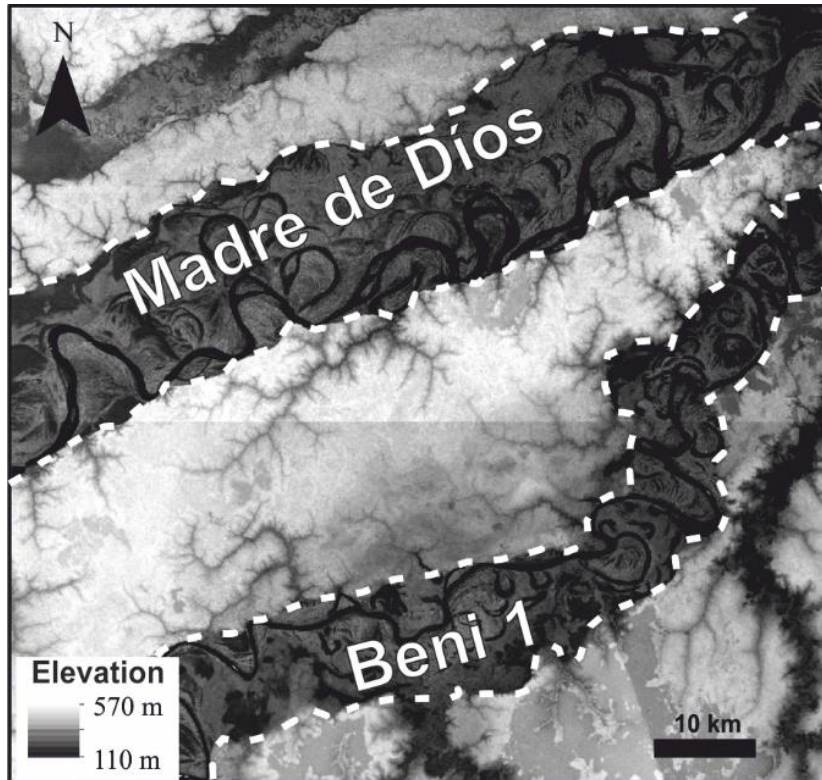
Figure 18. Shuttle Radar Topography Mission (SRTM) digital terrain model (DTM) of Mad and B1 reaches. Consolidated deposits as reported by Gautier et al. (2007) reduce rates of meander migration; this is consistent with our findings. The SRTM demonstrates the confined nature of the active river within the topographically lower valley with many instances of the river abutting against the boundary (white dashed line). Confinement of the channel prevents a freely meandering channel from evolving, therefore constraining the development of free meanders. A similar terrace material constraint on valley width along the mainstem Amazon leads to reductions in sinuosity, increases in channel gradient, and faster floodplain turnover rates (Mertes et al, 1996, Figs 6, 19; Dunne et al., 1998, p. 459). This imposed confinement does not occur in the B2 and B3 reaches as the valley widens considerably downstream of B1 towards the Andean front.
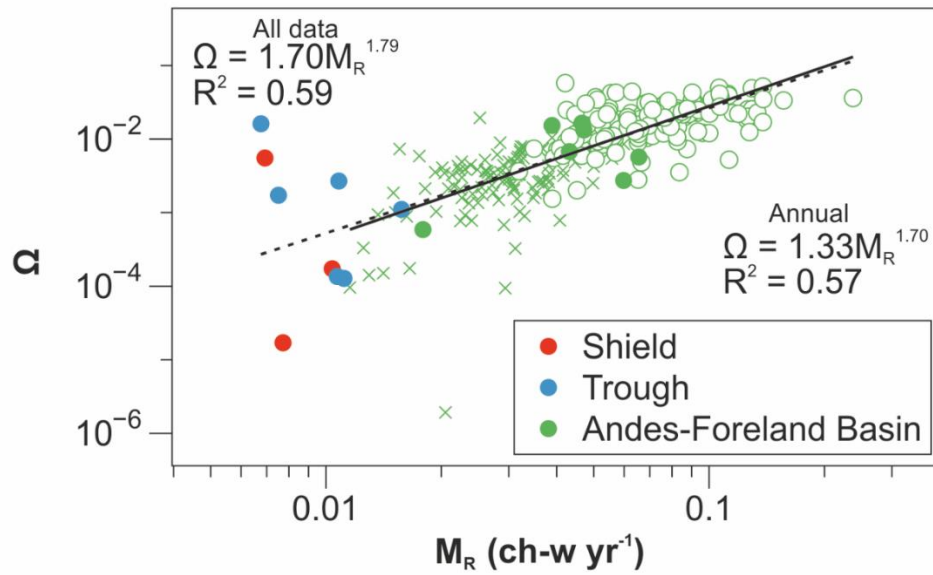
Figure 19. M_R plotted against absolute change in sinuosity (Ω). The total absolute change in sinuosity was plotted to show that a time-independent relationship exists between the two variables. Open circles indicate annually-resolved data points; closed circles are from the decadal dataset and described by the legend; green crosses are annually-resolved data for the Mad and B1 reaches for reasons described in Fig. 2. Regression lines are solid for all the data and dashed for the annual data.

variations in S^* are correlated with differences in meander deformation (Daniel, 1971; Kondrat'yev, 1968). Reach-averaged σ indices ranged from 1.20 to 3.55 with the majority of meanders within each reach being greater than 1.0 (average σ skew = 1.61) (**Table 4**). Individual meanders (12-54%) within each reach also displayed indices below 1.0, reflecting upvalley meander erosion. The meander symmetry index (σ) increases with S^* (**Fig. 20A**), with the largest average indices associated with rivers draining the Andes-Foreland Basin. On average, σ-indices in the Andes-Foreland Basin were significantly (KW: α < 0.05) larger than for rivers draining the Shield (1.64 times larger) and those draining the Central Trough (1.50 times larger). The reaches analysed using annual resolution imagery had larger σ-values (population average ($\bar{\sigma}$) = 2.51) than those recorded using the decadal time series ($\bar{\sigma}$ = 2.12) in the Andes-Foreland Basin: the annually resolved dataset can identify changes that may be obscured over longer timescales (e.g., directional change of channel migration). There was no coherent trend in σ with progression downstream on any reach. Frequency distributions of σ for rivers draining different physiographic

provinces (**Fig. 21**) illustrate that most meanders translate downstream (1.05 < σ < 5.0). The percentage of meanders exhibiting symmetry indices greater than 5.0 increased for rivers draining the sediment-rich Andes-Foreland Basin with some reaches showing values between 10.0 and 15.0. Upstream translating meanders (0 < σ < 0.90) comprise up to 50% of meanders in reaches draining the Central Trough and Shield, while a maximum of 33% are identified in Andes-Foreland Basin rivers (**Fig. 21**). Extensional meanders (0.90 < σ < 1.05) were consistently low in abundance along all reaches, although they become more prevalent in some of the higher sediment-bearing reaches (**Fig. 21; Panel C**).

Rivers with greater sediment supplies showed larger σ-values (**Fig. 20B**). Rivers draining the sediment-depleted shields and the Central Trough have normalized sediment supplies an order of magnitude lower than those that drain the Andes and flow into the Foreland Basin. Correspondingly, reach-averaged σ-values were lower in the regions relatively depleted in sediment supplies and were almost 150% larger in the sediment-rich rivers. These results suggest that there is a link between sediment supply and meander deformation, which is achieved by sediment sequestration on point bars. Rivers with greater sediment loads can deposit this material as water shoals over the point bar and momentum diminishes in the lee, or as material is transported across the channel by transverse near-bed currents (Dietrich and Smith, 1984; Frothingham and Rhoads, 2003). Experimental evidence suggests that point bars grow preferentially in the downstream direction as sediment is deposited at the tail or on the margins of the bar (Braudrick et al., 2009; Dietrich et al., 1979; Pyrce and Ashmore, 2005). Therefore, frequent deposition associated with greater sediment fluxes, should result in faster outward and downstream growth of the bar enabling displacement and retention of the high-velocity flow-field near the outer bank downstream of the meander apex facilitating erosion within this half of the meander . Downstream translational meanders experience quicker and more

sustained curvature-driven transfers of momentum to opposite sides of the channel and have well developed secondary circulation cells that facilitate the growth of longer more developed point bars that begin at the upstream inflection point (Abad and Garcia, 2009a; Abad and Garcia, 2009c). In the upstream translational case, flow momentum crosses over closer to the apex resulting in less well developed bars as high-velocity flows are sustained at the inner bank for longer (Abad and Garcia, 2009a; Abad and Garcia, 2009c). The growth of more expansive bar forms in downstream skewed (translational) meanders leads to enhanced boundary shear stresses and the potential for more rapid bank erosion (Abad and Garcia, 2009c).
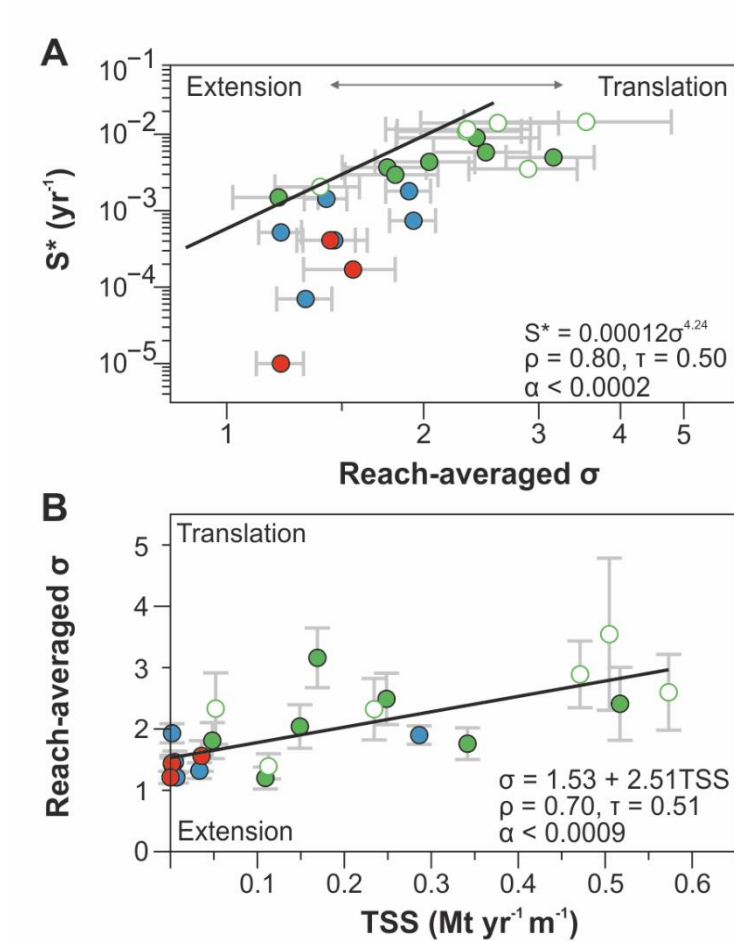
Figure 20. – A) Reach-averaged meander symmetry index (σ) plotted against the change in channel sinuosity with time (S*; per year). Error bars indicate the standard error about the mean of the reach-averaged σ values. Symbolisation follows that of Fig. 2A. The regression line is calculated using orthogonal distance regression to account for the variability in both variables. B) TSS plotted against σ. Error bars indicate the standard error about the mean of the reach-averaged measurements. Regression analysis was performed using ordinary least squares since the errors in TSS were undefined in the source literature.
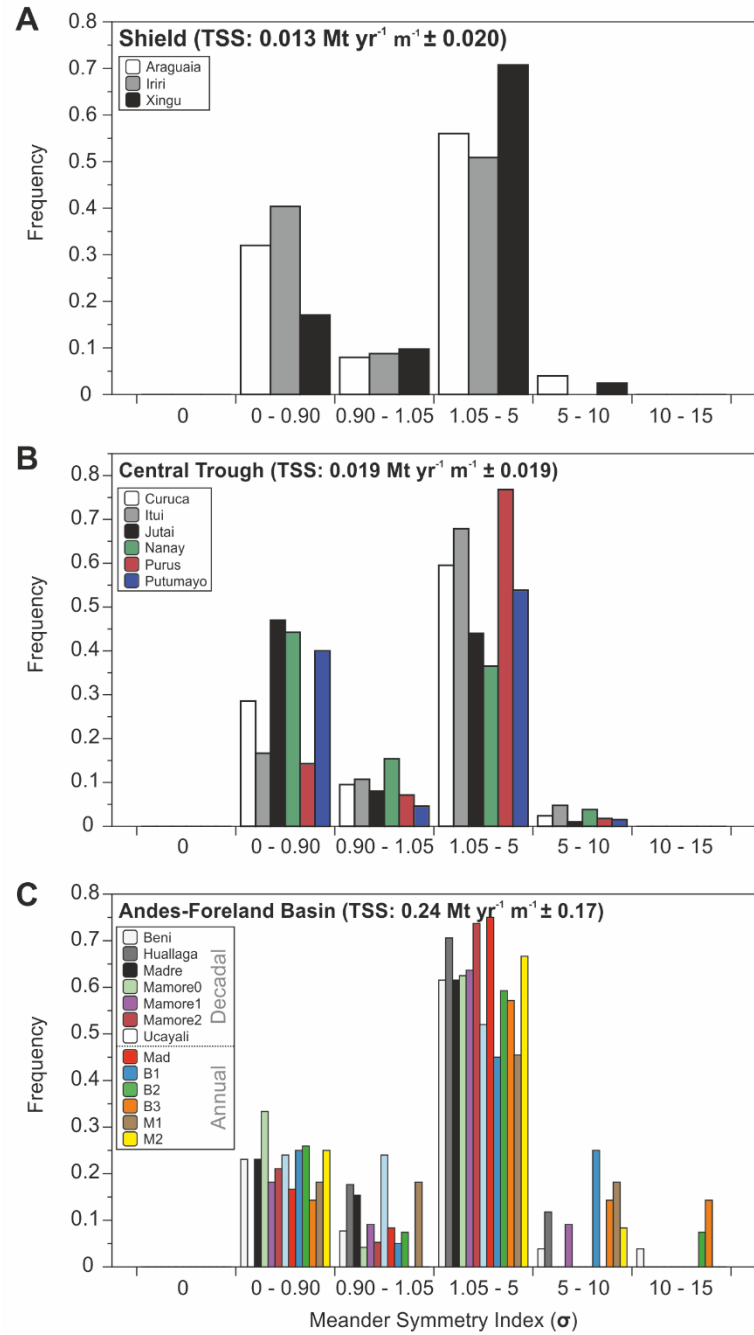
Figure 21. Frequency distributions of σ-index for rivers draining the A) Shield, B) Central Trough, C) Andes-Foreland Basin. The data was binned into upstream translating meanders (0 – 0.90), extending meanders (0.90-1.05), and varying degrees of downstream translating meanders (1.05-5; 5-10; 10-15) and normalised by the total number of meanders evaluated on the reach. The rivers within each physiography are symbolised and described by the legend. A width-normalised total suspended sediment flux and associated standard deviation are also presented for each physiography.

Upstream translating meanders develop when multiple zones of curvature maxima arise (i.e., compound meanders). These meanders often contain two distinct point bars, each associated with a localised area of outer bank erosion, possibly enhanced by complex floodplain topography (**Fig. 22**). Over time they mature into two separate meanders (Vermeulen et al., 2016). In non-compound meanders, sediment lobes are clearly identified at the upstream edge of the point bar (**USBB; Fig. 22**). These lobes were observed in both high and low sediment-bearing rivers and are capable of increasing local channel curvature facilitating flow redirection towards the channel banks. Similar sediment assemblages were documented on meanders in the Beatton River, Canada, in addition to rapid rates of bank erosion (Nanson, 1980).
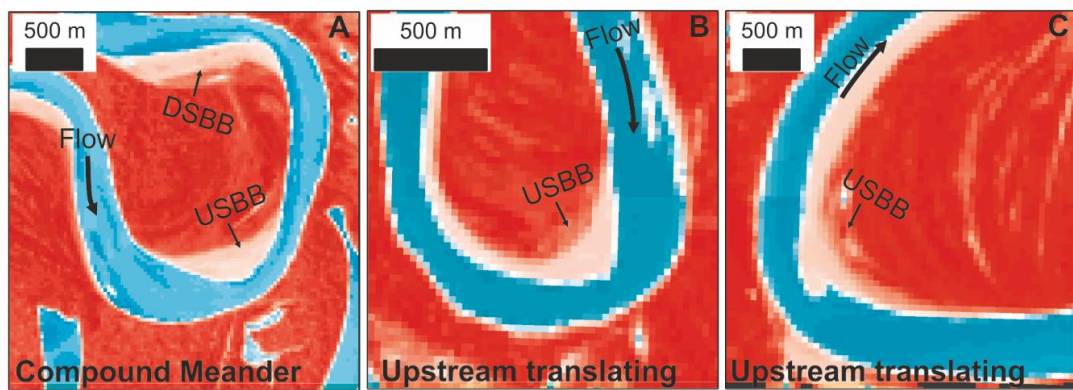
Figure 22. Point bar positions in upstream translating bends. Panel A shows a double-headed compound meander bend with point bars characterising each zone of curvature maxima. The bend moves predominantly downstream (downstream translating); however, the upstream bar bulge (USBB) is associated with localised channel widening. A downstream bar bulge (DSBB) induces downstream meander translation. Panels B and C illustrate bends experiencing upstream translation and have clear examples of USBB. Localised concentrations of sediment in the upstream portion of the meander will increase curvature and encourage shear-stress driven outer bank retreat as the flow-field migrates outward across the channel. Panel A is taken from the Rio Beni (-12.6 ^{O} N, -67.0 ^{O} W) while Panels B (-15.6^O N, -64.8 ^{O} W) and C (-15.3 ^{O} N, -64.9 ^{O} W) are from the Rio Mamoré. They are all displayed in modified NDVI format where the vegetation appears orange/red.

Changes in the sub-aerial extent of point bars was assessed to discern whether the style of meander deformation (i.e., extension or translation) was related to systematic patterns of bar growth. Three meanders from the Beni were used to display how meander deformation and bar deposition changed over the ~25 year study (**Fig. 23**).
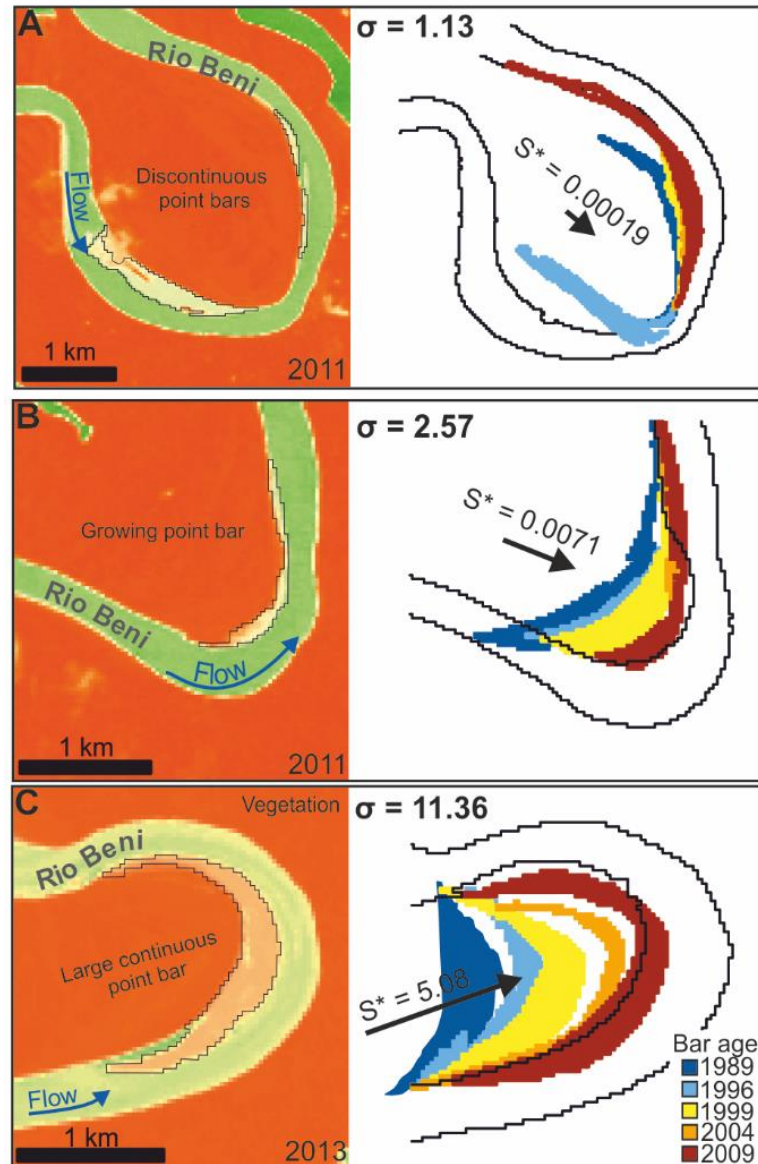
Figure 23. Bend deformation and point bar extents for three meanders on the Rio Beni. Subaerial point bar extents are outlined in black on Landsat imagery converted to display the normalised difference vegetation index (NDVI). The extents of point bars in five discrete years are displayed after extraction from Landsat imagery; warmer colours indicate younger deposits. σ-indices, direction of bend movement, and flow direction are all annotated. Each bend is prescribed an S* value calculated using the regression equation in Fig. 3A; the associated arrows indicate the relative rate of sinuosity increase.

In meanders with high σ-values, bars tended to be longer, continuous, and wider between inflection points. Conversely, extensional meanders ($\sigma \approx 1.0$) have narrower – sometimes discontinuous – bars with smaller surface areas (**Table 5**). Our observations are similar to those made in laboratory experiments by Abad and Garcia (2009b), who observed larger, well-developed barforms in downstream translational meanders than in upstream translational ones. Patterns of in-channel sedimentation clearly influence the planimetric evolution of meander bends, promoting sinuosity growth and the development of floodplain complexity; these processes are ultimately driven by upstream sediment supply.

Table 5. Subaerial bar extents for point bars displayed in Figure 23. Mean values are indicated by μ and geographical coordinates for the meanders are indicated in decimal degrees. Meanders A, B, and C correspond to the notations used in Figure 23. Changes in areal extent may result from imbalances between sediment erosion and deposition or variations in vegetation coverage and discharge. Estimates of river stage (Q_L; metres above sea level (masl)) between images are also given to account for differences in bar exposure when calculating bar areas. These were estimated using Fig 24.

Meander	σ-index	Year					μ	Meander location (Decimal Degrees)	
		1989	1996	1999	2004	2009		Lat	Long
		Bar area (km^2)							
A	1.13	0.28	0.32	0.22	0.10	0.42	0.27	-12.8	-66.95
B	2.57	0.36	0.22	0.35	0.21	0.24	0.28	-12.89	-66.99
C	11.36	0.41	0.37	0.41	0.22	0.52	0.39	-13.09	-67.13
Q_L		161.77	162.62	163.76	162.23	159.89			
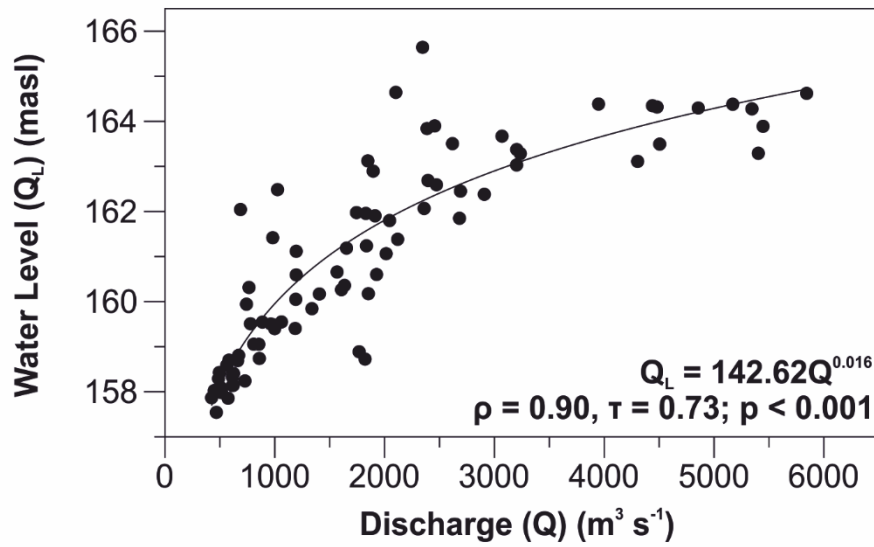
Figure 24. Discharge plotted against estimated water level at Rurrenabaque gauge. Water level estimates are made using satellite altimetry; the measurements are subject to uncertainty associated with necessary atmospheric corrections. Further information can be sourced from the Ore-Hybam website: http://www.ore-hybam.org/index.php/eng/Tecnicas/Station-limnimetrique-virtuelle.

4.4 Conclusions

In the absence of cutoff events, meander deformation is responsible for increases in channel sinuosity: the mechanism of meander deformation exerts an important control on how quickly channel sinuosity increases. Empirical observations derived from satellite imagery show that reaches with downstream-skewed (translational) meanders grow more quickly than extensional meanders and their growth may be driven by sediment availability, which is ultimately manifested through alluvial sequestration on point bars. As bars grow, alluvial material is sequestered downstream of the apex facilitating the longitudinal growth of the bar; their presence in the channel displaces high-momentum fluid across the channel to induce bank erosion. The meander symmetry index (σ) indicates how meanders evolve and suggests a possible linkage between external sediment supplies and channel behaviour, a topic that remains unresolved. An improved understanding of the relationship between sediment loading and in-channel processes is important for synthesising accurate predictions of channel change, which facilitate insights into the development of alluvial stratigraphy, sediment and nutrient exchanges across the channel-floodplain interface, and the construction of riparian habitats.

Chapter 5

Point bar responses to variable sediment loading: morphological implications for channel geometry
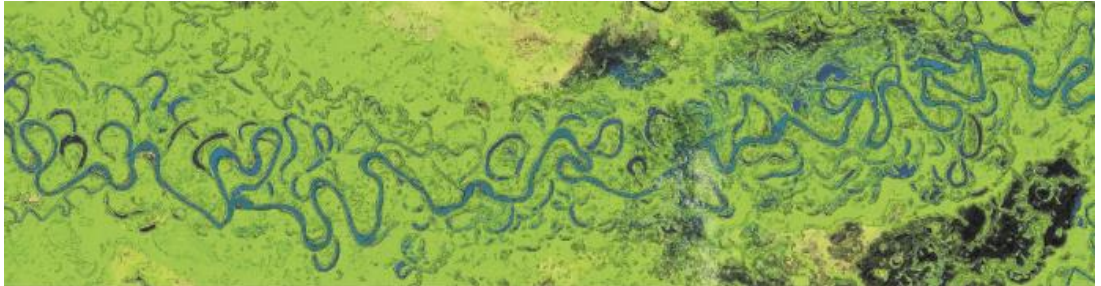
5. Abstract

The inner banks of meander bends are characterised by low-level alluvial platforms known as point bars. These features have been suggested to form the mechanistic link between enhanced sediment supply and channel evolution. Here we demonstrate by use of a 2D hydrodynamic model (MIKE 21c), that point bar growth is stimulated by increased sediment supply along a gravel-bed reach of the Sacramento River. The point bar was observed to grow upstream as coarse sediment was deposited at the bar head, in the upstream entrance of the meander. As the point bar grew, increases in the magnitude of boundary shear stress was observed along the outer bank of the meander. Moreover, increases in the longitudinal extent of the bank subjected to erosion was also observed as the bar grew. Sediment calibre, the length of the study reach, and the omission of suspended sediment transport were identified as important controls on the development of bars in these simulations. We demonstrate that point bars serve as sites of sediment storage and have the ability to alter channel hydrodynamics if supplied with the optimum substrate to facilitate growth. Future changes to catchment-wide sediment supplies in the future may enhance or reduce the ability of bars to sequester this material as the composition of material changes with climate or human interference, permenantly altering the long-term evolution of meandering river systems.

5.1 Introduction

The debate as to whether point bars introduce a sufficiently large perturbation to the high-velocity flow field, thereby forcing bank erosion, or whether point bars form in response to width-driven velocity reductions remains unresolved (Dietrich and Smith, 1983; Eke et al., 2014a; Lewin, 1976; van de Lageweg et al., 2014). Point bars are classified as a complex of individual scroll bar units characterised by undulating ridge-and-swale topography with very little permanent vegetation cover (Allen, 1965; Nanson, 1980). Bars are ubiquitous features along single-thread, as well as multi-

thread, channels and are the result of interactions between sediment transport and flow hydrodynamics (Allen, 1965). Their formation is driven by sediment deposition using material supplied from the eroding outer banks of meanders and their growth may act to reinforce bank retreat further (Lewin, 1976). Coarse-grained material concentrates at the bar head where flow velocities are high prior to the curvature-induced transfer of momentum across the channel. Fine-grained material characterises the bar tail in the downstream portion of the meander, supplied by inward moving bed currents that extend the bar longitudinally downstream (Bluck, 1971; Braudrick et al., 2009; Dietrich and Smith, 1984; Hooke, 1975; Nanson, 1980). Sediment can be sequestered on the bar surface and at the margins as flows shoal over the topographically elevated surface and cause a rapid decline in velocity. This process is further enhanced by gravitational movement of grains down the steep point bar face (Dietrich and Smith, 1984; Pyrce and Ashmore, 2005). Discrete sheets of sediment migrate across the channel and shoal up onto the point bar constructing additional scroll bar deposits, these deposits become fully amalgamated following the deposition of fine sediments and vegetal colonisation, although failure to achieve this before large flood pulses can trigger chute channel formation (Dietrich and Smith, 1983; van de Lageweg et al., 2014; van Dijk et al., 2012).

Meandering rivers intrinsically balance floodplain destruction with renewal through the redistribution of alluvial material across the channel (Lauer and Parker, 2008). This process revitalises riparian habitats by increasing biodiversity and heterogeneity both at the surface – through the distinct zonation of plant species and creation of lacustrine environments – and subsurface, where distinct floodplain architecture is created by variable patterns of sedimentation (Peakall et al., 2007; Salo et al., 1986; van de Lageweg et al., 2013). The presence of bars in the channel can distort the flow field propelling it towards the outer bank and encouraging bank erosion (Dietrich and Smith, 1983). Until recently, numerical models have struggled to resolve whether

bar-push (where point bar accretion precedes bank retreat) or bank-pull (where bank erosion induces inner bank deposition) control the planform evolution of meandering rivers as they have relied heavily upon outer bank erosion to stimulate the process (Ikeda et al., 1981; Parker et al., 1982; Sun et al., 1996). Parker et al. (2011) identified the severe weakness of implementing passive inner bank migration to satisfy the condition of constant channel width as the outer bank retreats, and proposed a new decoupled approach in which two sub-models, one describing each bank, could evolve independently, while still maintaining communication. Relative changes in channel width were controlled primarily by the balance between outer bank erosion – modulated by slump block armouring – and, inner bank sedimentation stabilised by vegetal encroachment (Asahi et al., 2013; Eke et al., 2014b; Parker et al., 2011). This method allowed for more realistic planform evolution and the emergence of short-term width oscillations as imbalances between the two processes occurred, as is commonly observed in reality (Zolezzi et al., 2012). Rates of bank retreat are strongly dependent on the geotechnical properties of the floodplain, which in turn is determined by the sedimentary composition of the banks, vegetation density, and antecedent soil moisture conditions (Thorne, 1982). Cohesive banks are typically more resistant to erosion, and so, require persistently high flow velocities to debauch the material. The failure mechanisms along cohesive river banks tends to be by cantilever or gravitational slumping, whereas granular entrainment tends to be the dominant process of bank erosion along non-cohesive banks (Osman and Thorne, 1988; Thorne, 1982). Vegetation density reinforces banks by increasing soil cohesion, although the degree to which this effect reduces rates of erosion is dependent on species and the depth to which the roots penetrate the bank (Allmendinger et al., 2005; Constantine et al., 2009; Pizzuto, 1994; Thorne, 1990). Once material is deposited at the bank it must decay and be transported away before further bank retreat can prevail (Thorne and Tovey, 1981). Therefore, bank erosion rates are limited by the mechanical properties and geometry of slump blocks

deposited at the outer bank toe, which allows for short-term oscillations in the local channel width through time (Eke et al., 2014b; Leyland et al., 2015).

Here we provide evidence to support the hypothesis that rivers rich in riverbed sediment (both bedload and suspended load) more expansively develop their point bars, driving rates of outer bank erosion. We accomplish this by modifying the sediment supply to a meandering reach on the Sacramento River, USA, by adjusting the upstream channel slope using a 2D morphodynamic flow model (MIKE 21c). The link between point bar growth and sediment supply has been suggested by previous studies, however an evaluation of the mechanism by which these two interact is only supported by indirect evidence (Ahmed et al., In review; Braudrick, 2016; Constantine et al., 2014; Dunne et al., 2010). An understanding of how point bar growth responds to increased sediment supplies is required considering that future climate changes are likely to generate larger volumes of sediment from the landscape through enhanced rates of erosion – assuming a wetter climate (Nearing et al., 2004). Furthermore, human-induced landscape change such as riparian habitat conversion are likely to further amplify the transfer of sediments from the land and into river channels (Latrubesse et al., 2009), thus warranting further exploration of these dynamic interactions.

5.2 Study Site

The Sacramento River drains an area of 68,000 km^2 in northern California, USA, encompassing the Sierra Nevada, Cascade, and Klamath mountain ranges in the east and north of the catchment (**Fig. 25**) (Norris and Webb, 1990). Comparatively modest contributions to discharge are gained from tributaries draining the Coast Ranges to the west, while substantial sedimentary inputs are sourced from this region (Michalkova et al., 2011). The River is sourced in the southern part of the Cascade Range near Mount Shasta and subsequently descends through the structurally-controlled Sacramento valley to San Francisco Bay, over a distance of approximately

500 km (Larsen et al., 2006). Geologically, the Klamath Mountains are the oldest, comprised of faulted metamorphic terranes interspersed with volcanic intrusions dated between the early Paleozoic and Jurassic period (~500 – 150 Ma). The Sierra Nevada is of similar age and composition associated with subduction during the Paleozoic, while the Cascade Range is dominated by younger (Upper Eocene to Quaternary) volcanic sequences overlying compacted sedimentary rocks. The eroding banks of the Sacramento River reveal heterogeneous mixtures of semi-consolidated fluvial sands and gravels interbedded with volcanically-sourced sands, silts and clays (Buer, 1994). The gravel-bed river actively migrates across the ~ 100 km wide alluvial plain at rates of up to 39 m yr^{-1}, although reach-averaged rates are typically between 4.3 and 6.4 m yr^{-1}, and strongly influenced by land use type (Larsen et al., 2006; Michalkova et al., 2011; Micheli et al., 2004).

Extensive conversion of riparian forest to agricultural land is thought to have increased the erodibility of the floodplain, facilitating the development of chute cutoffs, which enforce an upper limit to sinuosity development along the channel length (Constantine et al., 2010b; Micheli and Larsen, 2010). Constantine (2006) suggested that vegetation density was not a major control on bank erosion, but, rather, the geotechnical properties of the bank were of more importance. This has been purported to be related to the root penetration depth, where if root penetration is shallow compared to bank height, erosion will occur unabated (Constantine et al., 2009; Van De Wiel and Darby, 2007). The wider unfarmed floodplain is characterised by riparian forest within oxbow lakes and grassland species with the highest vegetation densities found along the channel-floodplain boundary (Buer, 1994). Much of the river is confined by artificial levees, rock revetment, and resistant geological boundaries which limit channel mobility (Buer, 1994; Constantine, 2006). Although the levees confine channel movement, they are set back from the active channel at between 0.75 and 2.5 km to allow some transverse movement of the channel

(Constantine, 2006). Our study reach (at River Mile (RM) 166) is not affected by levees, although they are present adjacent to, and downstream of the reach.
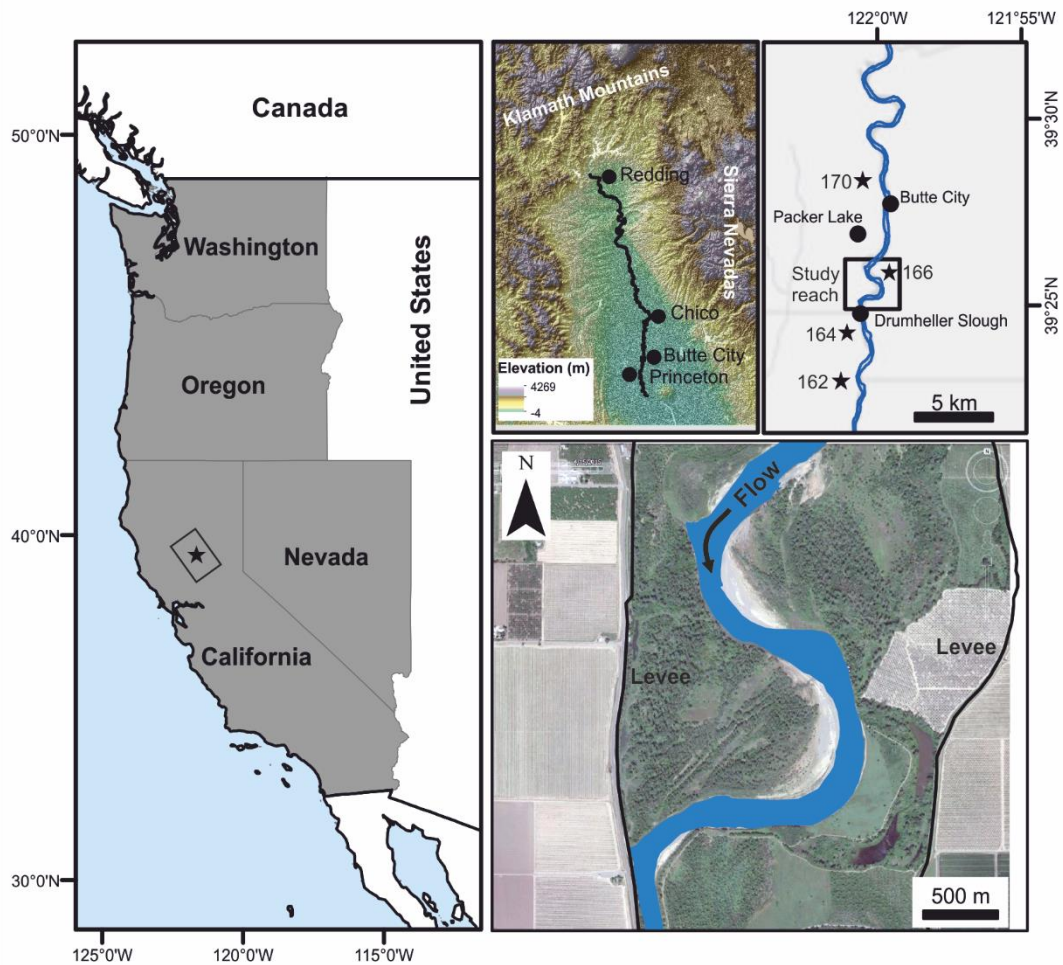
Figure 25. Study area map. From left to right: The Sacramento River reach in northern California denoted by a black star. Topographic map of the Sacramento Valley. The Klamath Mountains and Sierra Nevadas border the north and east of the Valley. Notable areas are marked and labelled with black markers. Top right: Extended river reach labelled with notable sights along the river and black stars for river mile (RM) locations. The study reach is enclosed within the black square. Bottom right: Study meander with levees marked in black.

Moisture fluxes from the Pacific Ocean rise and condense over the steep mountain ranges surrounding the Sacramento Valley. A longitudinal rainfall gradient between the lowland valley and the mountains is evident with annual totals 0.50 and 1.78 m yr^{-1} in each area (Buer, 1994). Average annual discharge (2010-2017) is 269.51 $m^3 s^{-1}$ (US Geological Suvey (USGS) gauge 11377100), however, annual maxima can be as high as 3000 $m^3 s^{-1}$ and commonly coincide with the annual snow melt and large

winter storms, although these peaks have been suppressed by the presence of dams (Buer et al., 1989; Constantine et al., 2010b). The installation of multiple dams in the upper catchment since the 1940s has effectively dampened high magnitude flows and increased average low flows by regulating channel conditions throughout the year (Buer et al., 1989). The altered flow regime has reduced downstream rates of sediment transport along the river (Singer, 2008b). Despite reductions in flow magnitude, bank erosion has remained high due to land use changes (Micheli et al., 2004). Bank erosion positively enhances the Sacramento River by supplying coarse material to the channel which creates habitats for fish and macroinvertebrates (Buer et al., 1989; Florsheim et al., 2008). Long-term average bedload transport fluxes are between 0.1 and 1.0 megatons per year (Mt yr^{-1}) (Singer and Dunne, 2004). Suspended sediment fluxes are estimated to be 12 Mt yr^{-1} (USGS gauge 11389500).

5.3 Model development and methods

5.3.1 Modelling strategy

Initially, the model will be rigorously tested to ensure it responds in accordance to the general theory of river meandering as described in the literature. Tests will be undertaken to assess the hydrodynamics (e.g., flow routing, upstream and downstream discharge and water levels, and secondary circulation) and timesteps over which they operate are suitable for the desired experiments. Additionally, the model morphodynamics will be tested to assess the model response to changes in grain size, bank erosion parameters, channel bed slopes and resistance parameters. Following the parameterisation stages, the model will be used to investigate the two key questions: first, the model will be used to assess the effect of added sediment load on channel morphology. This will be accomplished by running a number of experiments in which the sediment load is adjusted and then evaluating changes in the channel cross section and channel bed. Second, the model will be used to

quantify the effect of added sediment supply on the channel planform. Channel planform changes will be analysed by quantifying changes in the magnitude and distance of bank over which bank erosion takes place in response to added sediment delivery to the channel.

A number of shorter duration experiments will be conducted to examine the sensitivity of the model to changes in grain size, bed slope, bed resistance, and helical flow. These experiments will not be run to equilibrium as would be desired to understand the full effect of changes in these parameters on bed development. The rationale for not running each of these experiments to equilibrium is two-fold: first, the time required to run these experiments is large. Second, the purpose of running these simulations is to understand the effect of changes in the parameters on bed development, therefore, running the model for a sufficiently long time so as to gain insight into how the bed responds to these changes will allow for appropriate targeted modelling in later experiments.

5.3.2 Model overview

A two-dimensional hydrodynamic flow and sediment modelling package (MIKE 21c) produced by the Danish Hydrological Institute (DHI) was used to conduct a range of experiments in which sediment supplies were adjusted to assess the feedbacks between point bar evolution and channel geometry. The model uses a curvilinear grid to evaluate the flow hydrodynamics in two directions (horizontal and vertical) by solving the vertically-averaged St. Venant equations of continuity and conservation of momentum. Three assumptions are assumed: 1) lateral exchange of momentum due to fluid friction and wall effects along the river banks are neglected; 2) vertical velocity gradients are neglected, and; 3) the rigid lid approximation is adopted whereby the water surface is considered as an impermeable, shear stress free surface. Therefore, the model is suitable for shallow, gently varying topography within wide, mildly curved channels with small Froude numbers (DHI, 2014c). The depth-averaged (2)

shallow water Navier-Stokes equations governing the curvilinear hydrodynamics within MIKE 21c are as follows:

$$\frac{\partial P}{\partial t} + \frac{\partial}{\partial s}\left(\frac{p^2}{h}\right) + \frac{\partial}{\partial n}\left(\frac{pq}{h}\right) - 2\frac{pq}{hR_n} + \frac{p^2 - q^2}{hR_s} + gh\frac{\partial H}{\partial s}$$

$$+ \frac{g}{C^2}\frac{p\sqrt{p^2} + \sqrt{q^2}}{h^2} = RHS$$

$$\frac{\partial q}{\partial t} + \frac{\partial}{\partial s}\left(\frac{pq}{h}\right) + \frac{\partial}{\partial n}\left(\frac{q^2}{h}\right) + 2\frac{pq}{hR_s} - \frac{q^2 - p^2}{hR_n} + gh\frac{\partial H}{\partial s}$$

$$+ \frac{g}{C^2}\frac{q\sqrt{p^2} + \sqrt{q^2}}{h^2} = RHS$$

$$\frac{\partial H}{\partial t} + \frac{\partial p}{\partial s} + \frac{\partial q}{\partial n} - \frac{q}{R_s} + \frac{p}{R_n} = 0 \qquad (3)$$

Where s and n are curvilinear coordinates, p and q are mass fluxes in the s and n directions, H is water level, h is water depth, g is the gravitational acceleration constant, C is the Chézy roughness coefficient, and R_s and R_n are the radii of curvature of the s and n lines, respectively, and RHS is right hand side (described below).

The Reynolds stresses – a component of the RHS can be described by the following:

In the p-direction,

$$\frac{\partial}{\partial x}\left(E\frac{\partial p}{\partial x}\right) + \frac{\partial}{\partial y}\left(E\frac{\partial p}{\partial y}\right) = \frac{\partial}{\partial s}\left(E\frac{\partial p}{\partial s}\right) + \frac{\partial}{\partial n}\left(E\frac{\partial p}{\partial n}\right) + \frac{2E}{R_s}\frac{\partial q}{\partial s} + \frac{2E}{\partial s}\frac{q}{R_s} + \frac{2E}{R_n}\frac{\partial q}{\partial n} + \frac{2E}{\partial n}\frac{q}{R_n} \qquad (4)$$

In the q-direction,

$$\frac{\partial}{\partial x}\left(E\frac{\partial Q_{curv}}{\partial x}\right) + \frac{\partial}{\partial y}\left(E\frac{\partial Q_{curv}}{\partial y}\right) \qquad\qquad (5)$$

$$= \frac{\partial}{\partial s}\left(E\frac{\partial Q_{curv}}{\partial s}\right) + \frac{\partial}{\partial n}\left(E\frac{\partial q}{\partial n}\right) + \frac{2E}{R_s}\frac{\partial p}{\partial s} + \frac{2E}{\partial s}\frac{p}{R_s} + \frac{2E}{R_n}\frac{\partial p}{\partial n} + \frac{2E}{\partial n}\frac{p}{R_n}$$

100

The RHS also combines information about Coriolis force and atmospheric pressure (DHI, 2014c).

5.4 Grid development

The initial grid was developed from a small section of the Sacramento River between Butte City and Princeton, California, USA. A bathymetric survey collected by the U.S. Army Corps of Engineers (USACE) was used to develop a digital elevation model (DEM) for the reach by interpolating the survey points into a triangulated irregular network (TIN) enforcing constrained Delauney triangulation. The program's grid generation suite requires banklines to be input from which a grid is developed. Grid lines were digitised around an aerial photograph of the River obtained during the time of the survey. Multiple sub-grids were joined together to ensure the meander geometry could be captured accurately while satisfying the orthogonality requirements of the model domain. The grids were each created and orthogonalised independently before being joined and undergoing one final orthogonalisation. The curvilinear grid is generated using an implicit finite difference approximation and Stone's strongly implicit procedure (Stone, 1968). This method efficiently solves the partial differential equations governing the fine resolution elliptical grid. A filter then smooths the grid boundaries according to a curvature threshold in which boundary points that exceed the prescribed curvature threshold are subjected to the running average. The corners of the grid remain fixed in position during this process (DHI, 2014c).

Due to several complications with model stability during the initial runs the reach length was reduced to a single bend (**Fig. 26**). An artificially straight entrance with an almost flat bed was appended to the start of the bend to dissipate any anomalous entrance flow conditions associated with the curved nature of the bend. The straight

ramp was developed from the original bathymetry after removing the upstream bend from the grid. The bed of the straight ramp was then conditioned with the slope estimated from prior field surveys on the Sacramento River – approximately 0.00033 (Constantine et al., 2010a). The ramp bed was uniformly flat with no superimposed bedforms (**Fig. 26**). The grid is approximately 2760 m long and 270 m wide with grid cell dimensions of 154 and 30 in the J and K (X and Y) directions, respectively. The grid resolution is 30 m (J-direction) for the straight entrance ramp (~ 1300 m) and then increases to 15 m resolution. The K-axis has a continuous resolution of 10 m. The initial point bar present in the bathymetry has a maximum lateral extent of ~ 180 m and a longitudinal length of ~1,100 m, meaning our grid is of sufficient resolution to observe processes occurring over the bar and pool area. A border of land cells was created along each of the longitudinal channel boundaries and set at an elevation of 30 m. The floodplain was not modelled in the study; all processes were confined

within the channel boundary. The grid was completed by joining the initial surveyed channel bathymetry to the orthogonalised grid.
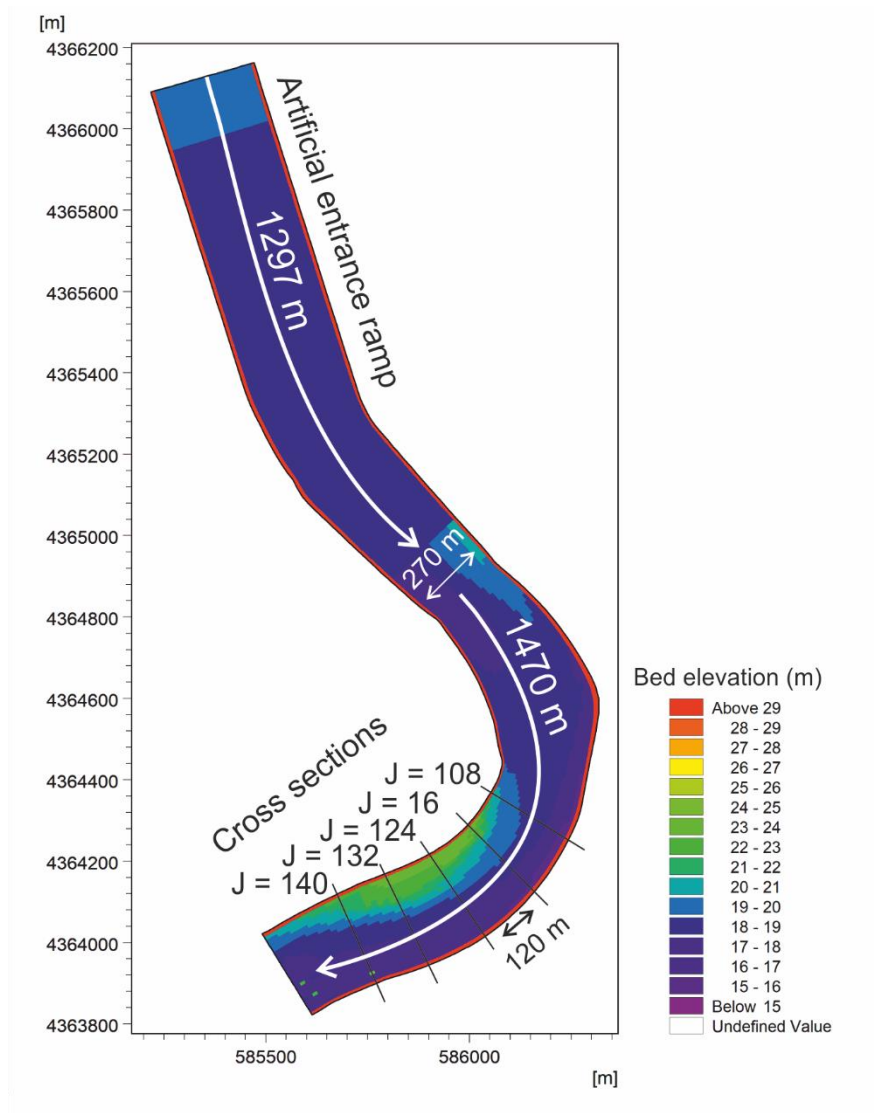
Figure 26. Topographic map of the study reach in physical space. The map is symbolised by elevation. The artificial entrance ramp is labelled and the cross sections used for analysis are displayed. The spacings between cross sections is indicated as is the length of the original surveyed bathymetry downstream of the entrance ramp.

5.5 Boundary conditions

The upstream and downstream boundary conditions at the channel bed are characterised as being flat. No changes in the channel bed level are possible at these boundaries to maintain constant conditions. A notable limitation is introduced at the upstream boundary as a result of the prescribed flat entrance condition. In nature,

103

meanders are characterised by an asymmetrical cross section that develops in response to curvature-driven flow oscillations across the channel. A flat channel bed in place of an asymmetrical one means the flow hydrodynamics may not have evolved to the same level as that of a real meander. Ideally, the addition of multiple meander bends would be effective in minimising this effect as was originally envisioned for the modelling campaign (Fig. 26). However, the selection of a flat bed for the present model will still generate insight into the response of the channel to enhanced sediment supply, although the results should be treated with caution as they may not fully represent the conditions present in typical meandering rivers.

5.6 Model Parameters

5.6.1 Helical flow

Channel flow is subjected to several forces as it transitions from a straight to a curved geometry. Curvature-induced centrifugal forcing transfers high-momentum fluid from the inner to outer banks elevating the water surface slope towards the outside of the meander. The outward-driven flow momentum increases boundary shear stresses at the outer bank and causes a reduction at the inside of the bend. To compensate for the increased water surface slope, a near-bed inwardly-oriented flow component is created by descending fluid at the concave bank. This secondary circulation cell is responsible for transporting sediment across the channel towards the point bar as a proportion of the downstream-oriented main flow component is deflected inwards (Dietrich and Smith, 1984; Dietrich et al., 1979; Hooke, 1975). Helicoidal (secondary) flow is modelled by two factors: 1) the intensity (i_s), which is calculated by,

$$i_s = u \, \frac{h}{R_c} \quad (6)$$

where u is the main flow velocity, h is the water depth, and R_c is the meander radius of curvature; and, the angle of deviation between the downstream and cross-stream flow components ($\tan\delta_s$) is defined as,

$$\tan\delta_s = \zeta\,\frac{h}{R_c} \qquad (7)$$

where,

$$\zeta = \varepsilon\frac{2}{\kappa^2}\left(1 - \frac{\sqrt{g}}{\kappa C_{BF}}\right) \qquad (8)$$

and κ is von Karman's constant (0.4), g is gravitational acceleration constant (9.81 m s^{-2}), C_{BF} is the bankfull centreline-derived Chézy number, and ε is a calibration constant – in our case, 0.1 – and remains constant over the entire grid area. The ζ parameter was calculated to be 1.0 with our constant α value. The radius of curvature of the streamlines is calculated as the cross product of the downstream velocity vector and the acceleration vector (DHI, 2014c). Helical flow estimates are used to inform the deflection of bed material across the channel, and therefore have large implications on the process of bar building and planform change. The greater the helical flow intensity, the greater the inward deflection of flow momentum. As a result, more sediment is conveyed across the channel towards the point bar instead of being transported by the downstream flow component (DHI, 2014c).

5.6.2 Sediment transport

Non-dimensional sediment transport rate (Φ) for the model is calculated from Equation X,

$$\Phi = \frac{S_{tl}}{\sqrt{(\rho_s - \rho)g\,d_{50}^3}} \qquad (9)$$

Where, ρ_s is the density of sediment, ρ is the density of water, d_{50} is the median grain size, g is gravitational acceleration (9.81 m s^{-1}), and S_{tl} is the total load sediment transport formula of Engelund and Hansen (1967). Sediment transport was modelled using the Engelund and Hansen (1967) total load model that partitions bedload and suspended load into two fractions. Our model only explicitly models bedload transport since suspended load (typically with grain diameters of 0.5 mm or less) is not predominantly responsible for point bar growth and only constitutes ~ 30% of overall bedload material (Singer, 2008a). The model describes sediment transport by the following relationship,

$$S_{tl} = 0.05 \frac{C^2}{g} \; \theta^{\frac{5}{2}} \sqrt{(\rho_s - \rho) \, g \, d_{50}^3} \qquad (10)$$

where, C is the Chezy coefficient and θ is the Shields parameter. The model is intended for use in sand-bed rivers and so the decision to model sediment transport in a gravel-bed river like the Sacramento may introduce some discrepancies between observations of bed mobility in the field and estimates made using the model. The decision to use the model was based on recommendations presented by DHI (2014c). An informal test of sediment transport using the Meyer-Peter and Muller (1948) model was also undertaken and revealed no significant difference between rates of sediment transport using the two models. These results suggested that the use of the Engelund and Hansen (1967) model should not produce results too divergent from those outputted using the Meyer-Peter and Muller (1948) model.

A second limitation associated with the Engelund and Hansen (1967) transport model is that it does not include a sediment entrainment threshold. Sediment mobility is related to stream power at the bed. Therefore, with insufficient stream power the model is unable to entrain sediment and make changes to the bed. Alternative sediment transport models use a critical threshold over which grains are mobilised. This potential difficulty in entraining grains under moderate flow conditions may

prevent sediment being routed onto and around the meander, thereby limiting channel bed evolution.

The up- and downstream boundary conditions are constrained by bed level change to reduce complexity associated with imposing estimated field-observed rates of sediment transport on the model. The model boundaries are forced to maintain a constant bed level elevation, thus preventing any erosion or deposition at either boundary. The depth of alluvial material on the bed was arbitrarily set to be 100 m so as to permit sediment excavation in the absence of a bedrock boundary. Bedload transport rates respond immediately to changes in local hydraulic conditions, but are also strongly affected by the deviation between longitudinal and transverse flow components (conditioned by helicoidal flow), and the transverse bedslope, which facilitates the downslope movement of material.

5.6.3 Flow resistance

Flow-induced friction at the channel bed is described by the Chézy equation,

$$C_{BF} = \frac{1}{\eta} \, R^{\frac{1}{6}} \qquad (11)$$

where C_{BF} is the bankfull centreline-derived Chézy coefficient, η is Manning's roughness coefficient (0.035), and R is the hydraulic radius, which approximates as the channel depth. This parameter contributes to the chosen sediment transport formula (in the present case, Engelund and Hansen (1967)), and as such exerts a strong influence on rates of sediment transport in the model. The Chézy value is squared in the Engelund and Hansen (1967) formula meaning that slight increases in this parameter have a large overall effect on sediment transport. For this reason, a sensitivity analysis was undertaken to tune sediment transport values to those measured in the field.

5.6.4 Sub-grid turbulence

Sub-grid turbulence is modelled by specifying a constant eddy viscosity across the model reach, which is then integrated into the momentum equations (Equations 4 & 5). Velocity-based eddy viscosity is applied in the present model as the flow depth is less than the transverse grid spacing and does not remain spatially constant. Eddy viscosity describes the turbulent-driven, vertically integrated and sub-grid scale fluctuations in shear stress across the channel domain and controls short wavelength oscillations in shear stress (DHI, 2014a). This is then entered into the equations for conservation of momentum and mass where it contributes to the distribution of momentum.

5.7 Hydrology

Hydrological data for the reach was obtained from the USGS (gauge number 11377100 at Red Bluff) for January 2010 – January 2017 (**Fig. 27**), which was used to generate a long-term hydrograph (max length 200 years). This allowed us to simulate channel change over multiple decades with realistic water levels and discharges without acquiring a long-term historic record. Discharge was routed through the upstream channel boundary at 15-minute intervals governed by the flow record, while the downstream boundary was forced with a complementary water level record for the same period from the same gauge. To prevent model instabilities associated with overbank flood flows, we imposed an upper hydrological limit on discharge and water levels based on the estimated bankfull discharge of Constantine et al. (2010a). Discharges greater than 1869 $m^3\,s^{-1}$ were given the designated bankfull value and corresponding water level (25.13 m) to maintain within-channel flows.
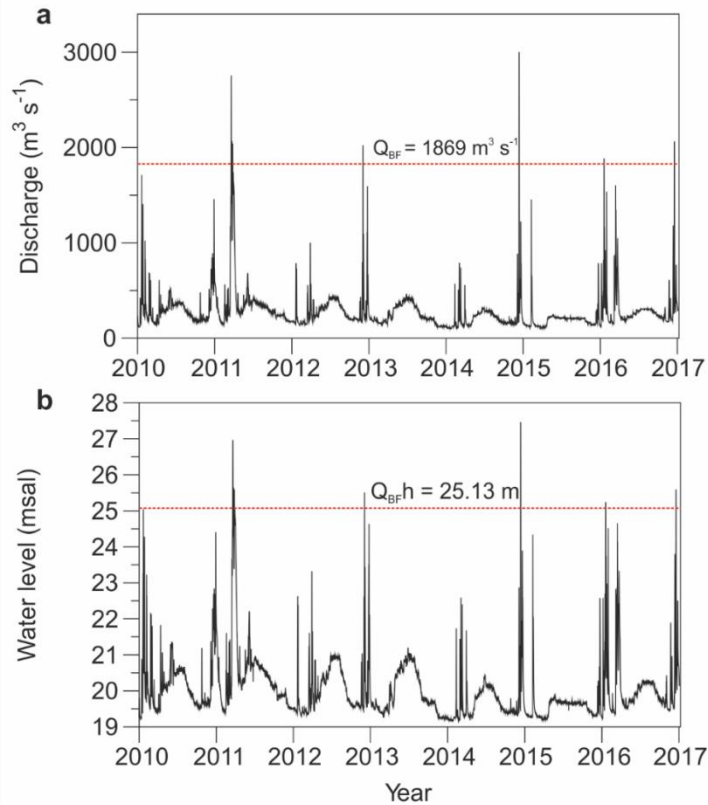
Figure 27. Hydrological characteristics of the Sacramento River. a) Discharge record from USGS gauge 11377100 near Red Bluff. The estimated long-term bankfull discharge (Q_{BF}) is indicated by a red dashed line. This is also the limit of simulated flow discharge. b) Water level record from the same USGS gauge with the bankfull water limit indicated in red. This was the simulated water level limit.

We inspected discharge routing through the modelled channel at equally spaced cross sections and compared these discharges to those specified at the input boundary to identify any significant temporal lags in flow (**Fig. 28**). We found that the time-averaged discharge (i.e., the discharges at every timestep over the simulation period) at each of the six cross sections was statistically similar (Student's t-test: $p > 0.68$). The maximum offset between the input discharge and modelled discharge was 23.08 m^3 s^{-1} at J = 70. This small variation (~8% of average annual Q) between observed and modelled discharges indicates that the model was routing discharge reliably and so the hydrodynamic conditions were suitable for the model.

109
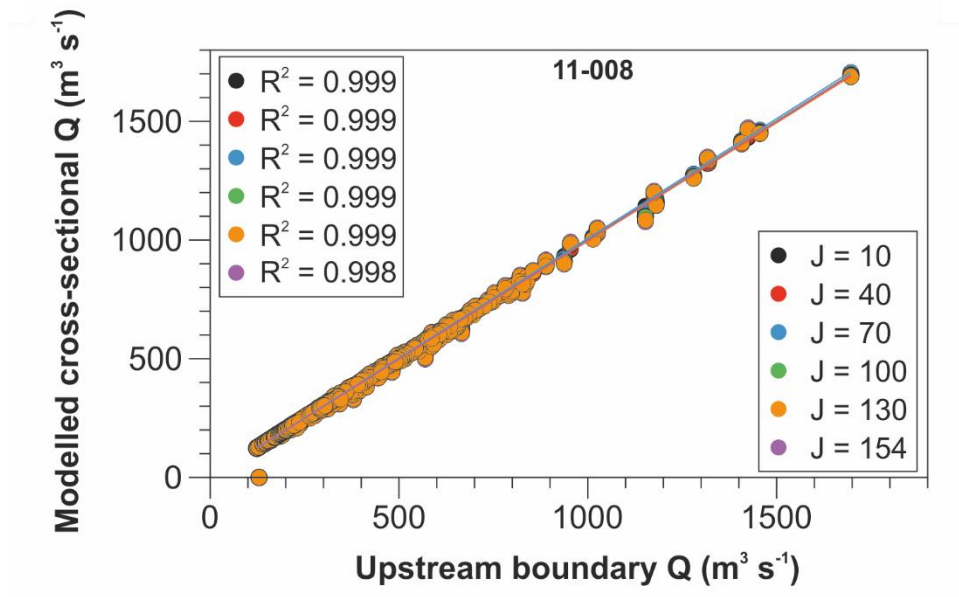
Figure 28. Discharge calibration for initial model setup. Discharges routed through the upstream boundary were plotted against the modelled discharge at six cross sections in the model domain indicated by the location along the J-axis for experiment 11-008. Linear regression statistics are indicated on the plot.

Flow velocities were inspected at the outer bank and at the channel centreline for five different discharges to assess how downstream currents velocities responded to increases in discharge (**Fig. 29**). The measured values were compared to the cross-sectionally averaged downstream flow velocity reported by (Constantine et al., 2010a) as simulated using HEC-RAS. As expected, the flow over shallow areas of the channel (primarily bar deposits) diminishes while the deeper areas of the channel are subject to greater velocities. During higher discharges, when the water is deeper, both the pools and bars experience greater flow velocities facilitating greater fluxes of sediment. The relationship between discharge and flow velocity can be described by a power function in which the exponents fall within well-defined values reported in the literature (e.g., Leopold et al., 1964) (**Fig. 30**).
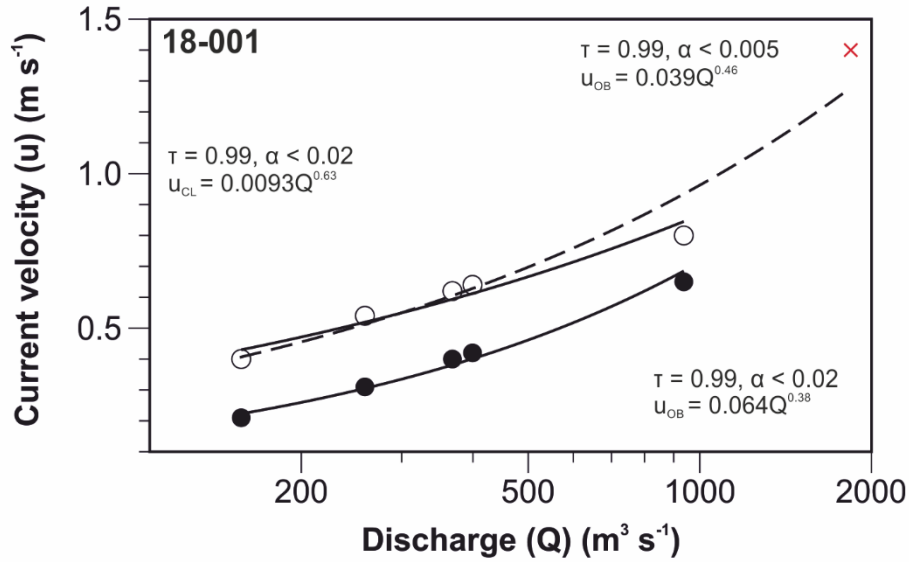
Figure 29. Depth-averaged downstream flow velocities for varying discharges. The downstream velocity flow structure for five different discharge events in an initial conditions channel. Flow is from left to right and a legend describes the downstream flow velocities.
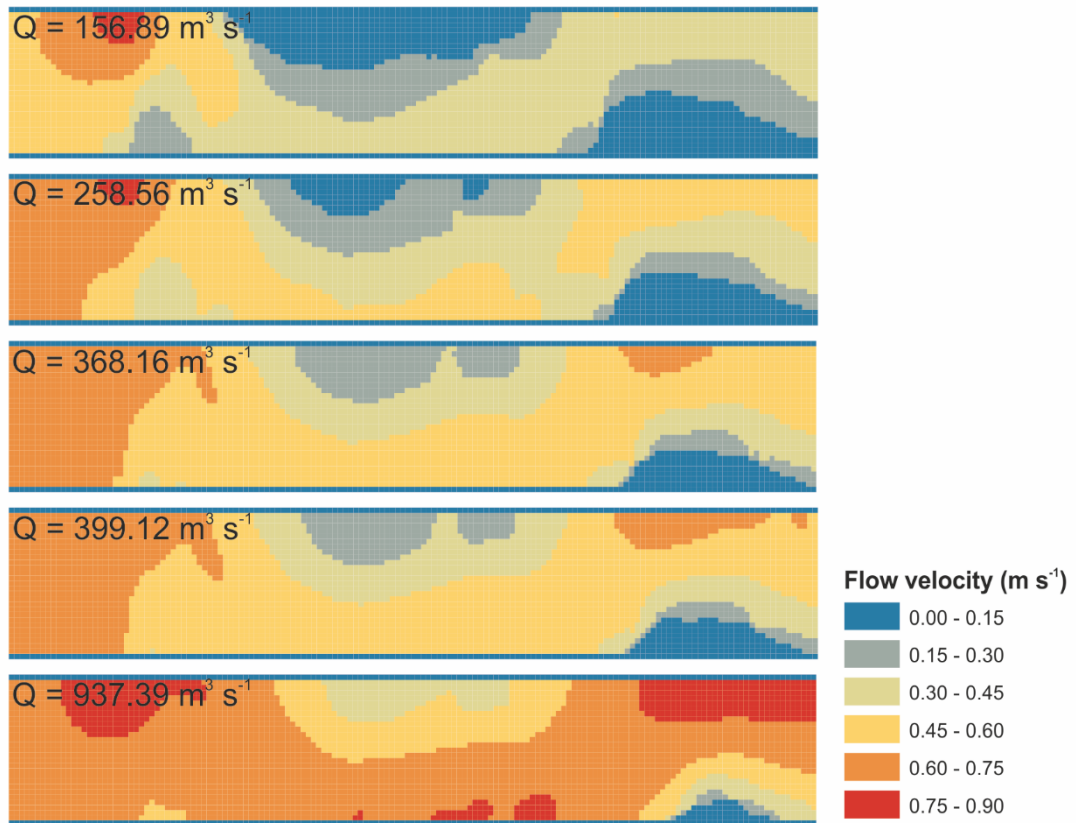
Figure 30. Relationship between discharge and downstream flow velocity. Measurements of flow velocity at five different discharges plotted against corresponding flow velocities at the channel centreline (u_{CL}; solid circles) and at the outer bank (u_{OB}; open circles). The red cross marks the measured velocity for bankfull discharge as simulated by Constantine et al. (2010a). Power law regression lines were fitted to each distribution with appropriate statistics indicated. The dashed line represents the line of best fit for u_{OB} including the bankfull value (red cross).

5.8 Entrance slope conditions

To simulate changes in sediment supply the bed slope was adjusted over the distance of the artificial entrance ramp (~ 1297 m). The initial flat-bed entrance topography used in the simulation to create initial conditions bathymetry was adjusted to facilitate various increases in bed slope according to Equation (**12**),

$$\partial z = SE_L \quad (12)$$

where, z is bed elevation (m), S is channel slope, and E_L is the entrance length (m). The topography produced during the initial conditions simulation was used as a constant starting bathymetry downstream of the entrance ramp and all hydrodynamic conditions were preserved to isolate sediment loading as the only adjustable variable in the simulations.

5.9 Parameterisation: Results and Discussion

Initially, model stability was assessed over a 1-year period at a general timestep of 10 seconds and a warm up period of 100 seconds. The warm up period is the amount of time over which the parameters are forced from zero to 100% of their true value (DHI, 2014b). A quasi-steady hydrodynamic integration strategy was adopted to reduce computing requirements by increasing the timestep over which flow is routed during the simulation (DHI, 2014c). Grid cells are defined as active channel or zones of deposition above the water surface as prescribed by the flood and dry thresholds (flood: 0.3 m; dry: 0.2 m). Cells defined as depositional are not included in calculations of sediment transport until they are inundated by enough water to become active channel cells. These parameters were set arbitrarily based on model specifications leaving a 0.1 m difference between them to ensure stability (DHI, 2014b). The channel boundaries were open at the up- and downstream ends of the model to allow for discharge to flow through the entire reach.

5.9.1 Initial conditions

The initial surveyed channel bed configuration was used to establish an equilibrium bed topography before any sediment load experiments were performed; the reason for this initial model run was to ensure the channel bed had developed a steady-state regime for the given flow conditions. The temporal sensitivity of the model was evaluated with respect to the time taken to develop equilibrium bed topography. It was determined that after a period of 200 years the channel had evolved to a sufficiently steady bed configuration for the given conditions (**Table 6**). We used a cumulative root-mean-square error calculation of bed level change across the entire model domain to determine the time at which changes in topography became relatively steady (**Fig. 31**). Indeed, changes in the bed configuration are expected to continue through time as the flow hydrograph continues to modify the boundary. However, the rate of these changes diminishes as a steady state topography develops.
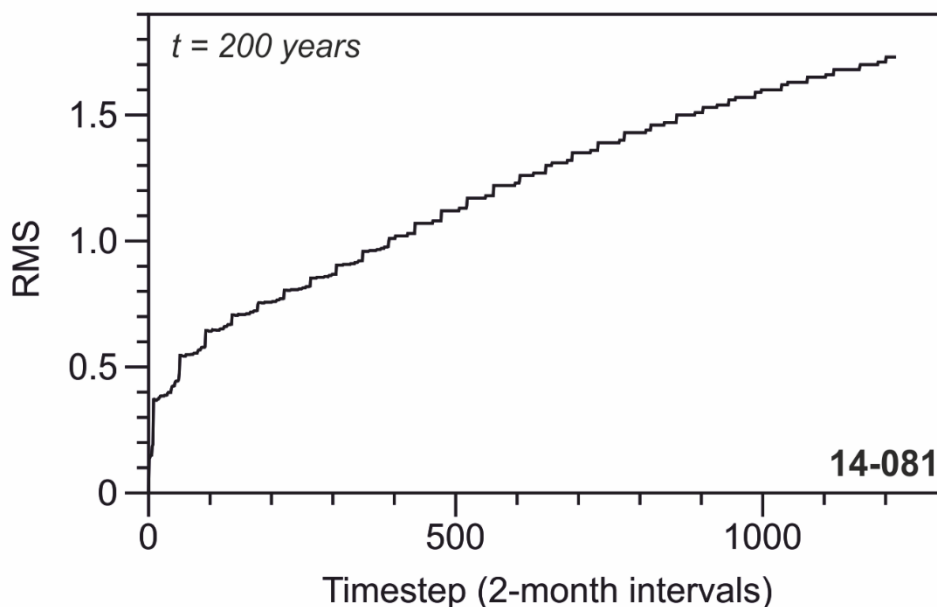
Figure 31. Cumulative root-mean-square error calculations for bed level change. Root-mean-square errors were calculated at each timestep for bed level change to determine when the changes in bed topography reached steady state. The x-axis is a proxy of time with each timestep representing ~2 months over a 200-year period. The experiment number is indicated in the lower right.

Table 6. Parameter table for initial conditions simulation (14-081)

Parameter	Value
Model run duration (years)	200
Wetting depth (m)	0.3
Drying depth (m)	0.2
Eddy Viscosity ($m^2\ s^{-1}$)	1
Chezy coefficient ($m^{0.5}\ s^{-1}$)	Depth-dependent
Helical flow intensity	0.1
Sediment grain size (d_{50}; mm)	13.5
Sediment porosity	0.3
Sediment density (kg m^3)	2650
Dimensionless boundary shear stress (θ)	0.07
Bedload sediment transport formula	Engelund and Hansen (1967)
Maximum rate of bank erosion (m yr^{-1})	6
Transverse slope coefficient (φ)	20
Sediment transport capacity for material removal (ψ)	0.1
Bank height (m)	LB: 3.2, RB:10.4

The rate of change over the first 100 months was most rapid as the channel bed adjusted to the prevailing flow conditions (**Fig. 31**). The resulting topography was used as the initial channel condition for the main model experiments. The sensitivity of morphological change to grain size conditions was investigated over a 1-year period with four different grain sizes (1 mm, 8 mm, 10 mm, and 13.5 mm) with all other parameters remaining constant. As expected, the bed became more active and reach-averaged sediment transport rates increased as the average grain size diminished (**Fig. 32**). When the grain size was reduced to 1 mm, the point bar experienced severe topographic damping by the end of the simulation with much of the channel becoming level (**Fig. 33**). The three remaining experiments demonstrated little morphological change over the short simulation period, but displayed an exponential decrease in mobility and little topographic change in the meander with increasing grain size (**Figs. 32 and 33**).
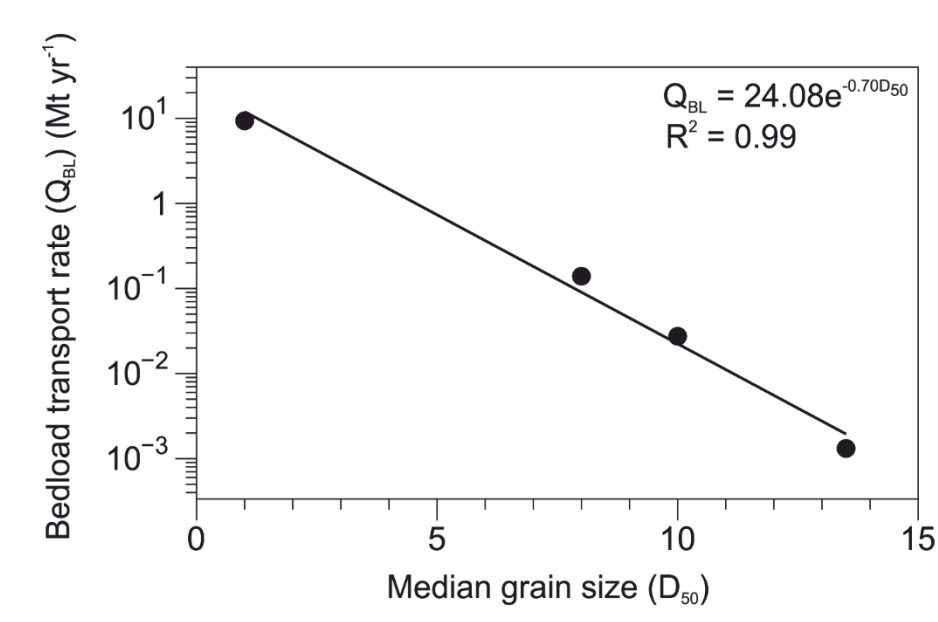
Figure 32. Relationship between grain size and bedload transport rates. The median grain size was set constant across the entire reach. Bedload transport rates are averaged over the reach and through time. The data are fitted by an exponential curve with the regression statistic and equation presented in the top right.

Increased sediment mobility associated with smaller grain sizes was useful for monitoring bedform evolution over shorter timescales. For our experiments we wanted to preserve the conditions observed in the field, therefore we held median grain size (D_{50}) at 13.5 mm (Constantine et al., 2010a) in the final experiments.
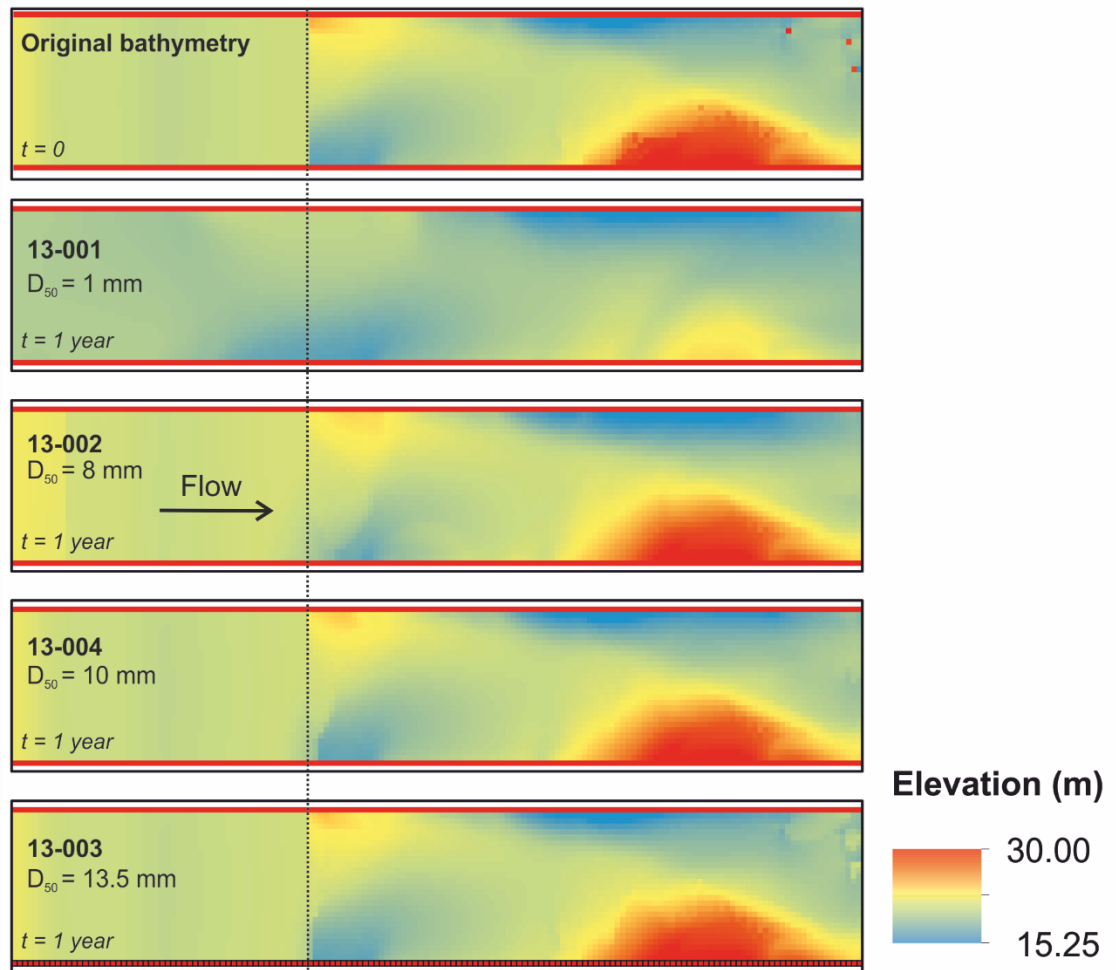
Figure 33. Bed level changes with changes in median grain size (D$_{50}$). The original bathymetry is shown in the top panel. Subsequent panels are labelled with the simulation number as well as the D$_{50}$ used and simulation period. The dashed line indicates the end of the entrance slope. Flow is from left to right.
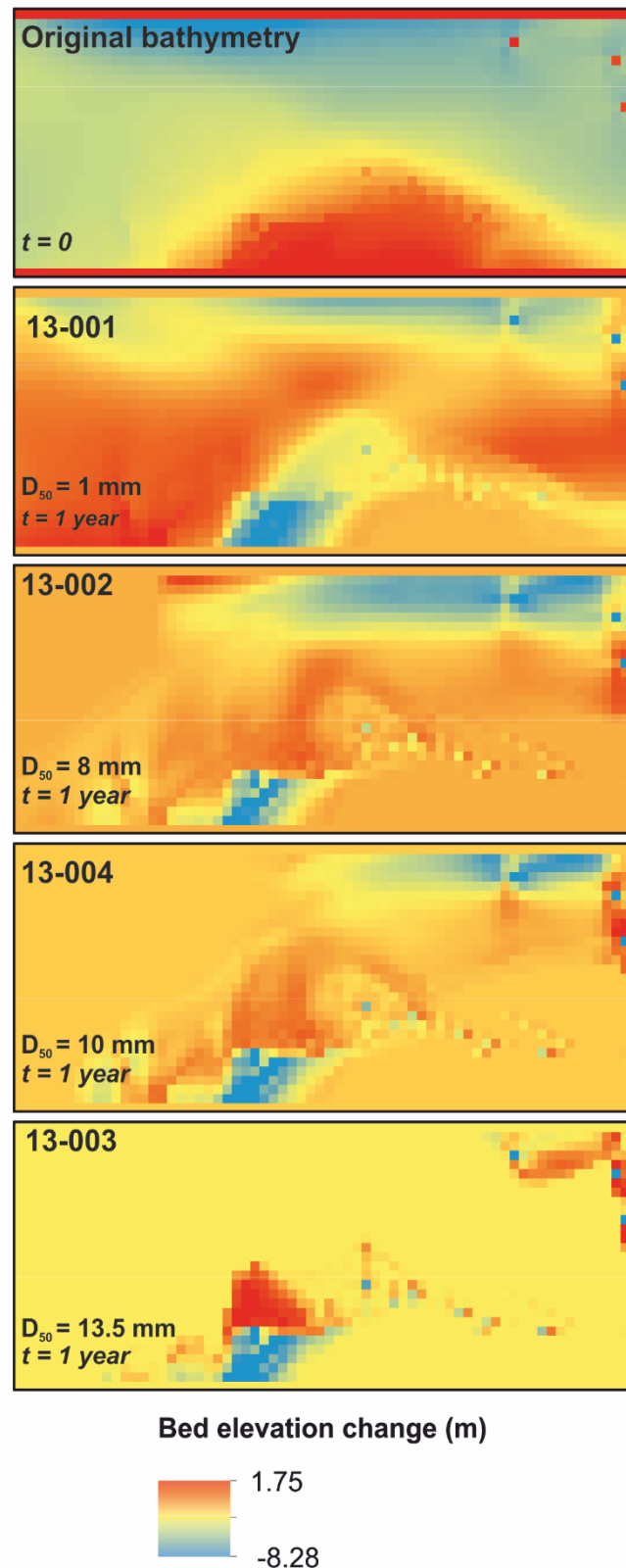
Figure 34. Absolute bed elevation changes (m) around the meander (downstream of the entrance ramp) with changes in D$_{50}$. The top panel shows the initial bed topography while the subsequent panels display the absolute changes in elevation from the initial topography for simulations with variable grain sizes. Flow is from left to right.

The hydrodynamic and morphodynamic models were decoupled to allow for time efficient long-term simulations to be conducted. The morphodynamic timestep was scaled up by multiplying the hydrodynamic timestep by a constant factor of 20 effectively increasing each timestep from 60 seconds to 20 minutes.

The resulting bathymetry that was subsequently used for the sediment loading experiments was characterised by two deeply scoured pools and a topographically lower point bar with a smaller sub-aerial extent (**Fig. 35**). The bed resistance parameters were deemed the most likely reason for the deeper pool, upstream scour pool and suppression of the point bar.
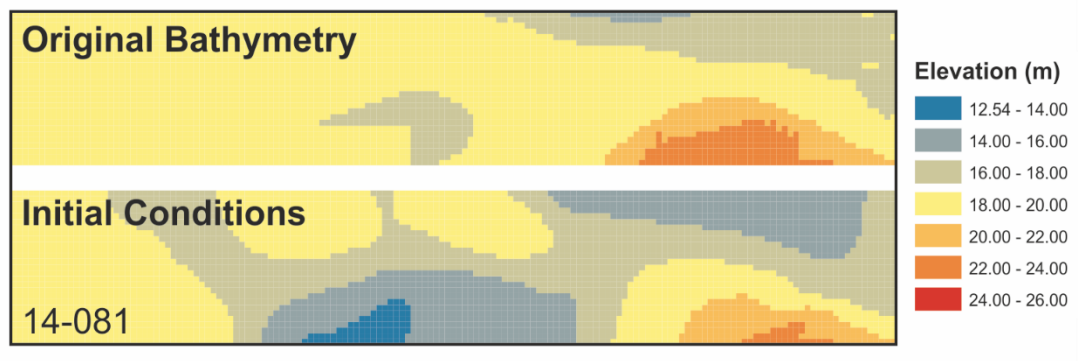
Figure 35. Bathymetry comparisons following initial conditions simulation. The top panel is the original surveyed bathymetry with artificial ramp while the lower panel is the bathymetry produced following a 200-year simulation run with the conditions prescribed in Table 1 after reaching equilibrium. The simulation number is displayed in the lower left and the flow direction is from left to right.
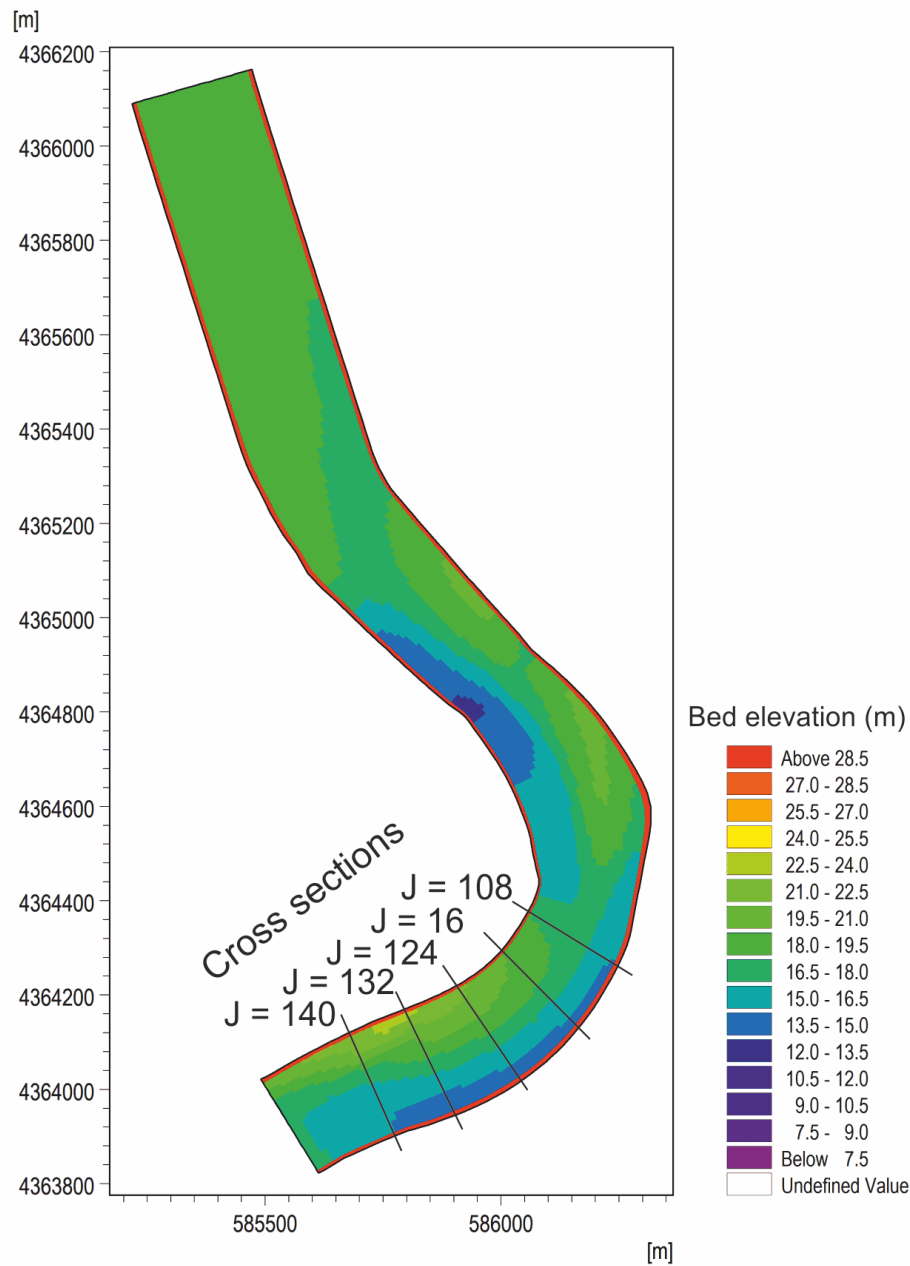
Figure 35E Initial conditions of the channel bed following model parameterisation. The model was run for a 200-year simulation in which the bed could evolve to equilibrium (see description of RMS). The cross sections used to assess channel bathymetry are marked and labelled. This figure is the same as the bottom panel of Fig. 44 except it is modelled in physical model space. Bed levels are symbolised according to the legend.

5.9.2 Helical flow

Helical flow intensities (i_S) were measured over a 5-year simulation at five different discharges at the outer most grid cells around the apex (using 8 cells about the apex). A strong correlation between discharge magnitude and i_S was observed where higher discharges created more powerful helical flow intensities. We also performed an analysis to examine how closely the simulated i_S was to estimated intensities calculated using equation 8 (**Fig. 36**). The model systematically overestimated i_S but simulated values on the same order of magnitude as the estimated values. Increasing the helical flow intensity by setting α to 1.0 did not produce bed topography significantly different to the case where α = 0.1 (**Fig. 37**, T-test: p > 0.99), although flow intensities were an order of magnitude larger than those predicted by Equation 8.
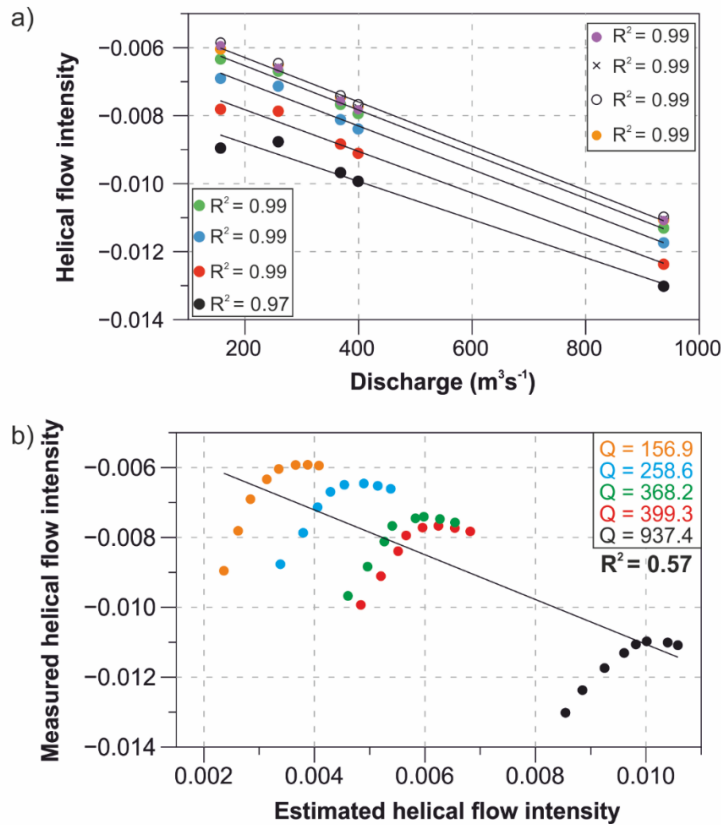
Figure 36. Helical flow intensities. a) The intensity of helical flow (i_s) was examined for five different discharges (Q) at the bend apex. The different symbols indicate the 8 grid cells around the apex that were used to inspect i_s. Correlation coefficients between Q and i_s are indicated for each grid cell by the legend. b) Estimated i_s calculated using equation 8 versus measured intensities simulated by the model. Each set of symbolised points are for 8 grid cells around the bend apex. Each colour corresponds to the discharge indicated in the

legend. A correlation coefficient is provided.
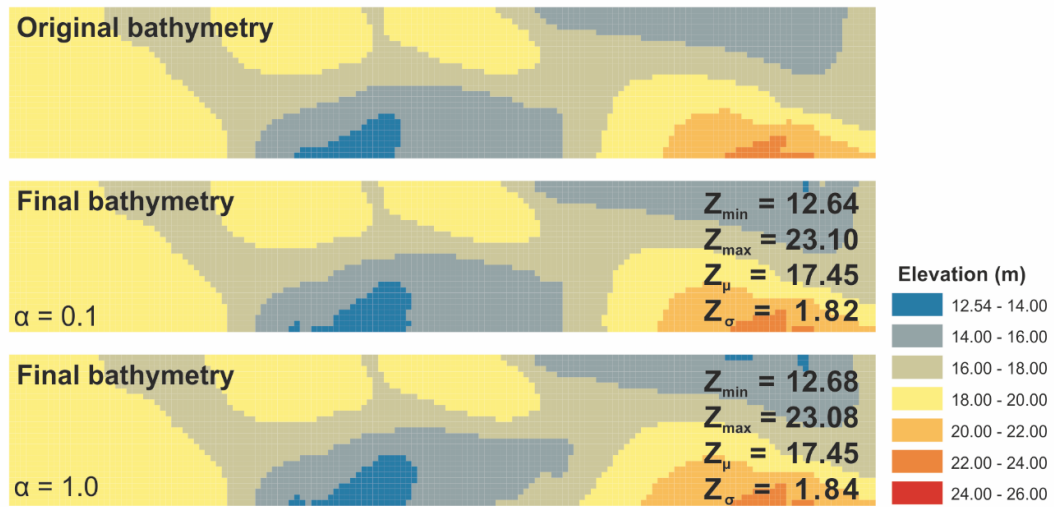
Figure 37 Channel bed comparisons for variations in helical flow calibration constants (α). The channel bed after a 10-year simulation was compared after using calibration constants of 0.1 (middle panel) and 1.0 (bottom panel). Minimum (Z_{min}), maximum (Z_{max}), mean (Z_{μ}), and the standard deviation (Z_{σ}) of bed elevations were measured across the entire grid domain for both scenarios and used to perform a T-test. Flow is from left to right.

5.9.3 Sediment transport

Sediment transport rates were calibrated according to estimated bedload gravel transport rates reported by (Singer and Dunne, 2004), which equated to 0.0009-0.07 Mt yr^{-1} at Butte City - approximately 4.5 km upstream. Estimates of the reach-averaged bedload transport rates (0.047 Mt yr^{-1}) were accomplished by calculating a grid-averaged sediment transport rate across each timestep of the simulation and calculating a temporally-averaged transport rate by multiplying the discharge rate by the sediment bulk density (assumed to be 2650 kg m^{-3}) over a one-year period. Our value is towards the upper limit of gravel transport rates observed by Singer and Dunne (2004) and is likely to be larger than expected due to the overestimated rates of transport in shallow areas of the channel.

The balance between inwardly-oriented near-bed sediment transport and outwardly moving gravitational sediment transport determines the net cross-sectional sediment export, and thus, morphological change in the meander. Therefore, the strength of these parameters will determine how the channel evolves through time. The sensitivity of the transverse and longitudinal slope parameters will affect the routing of sediment through each grid cell of the model and contribute to the total sediment transport in the downstream (s) and cross-stream (n) directions. Therefore, it is necessary to undertake some sensitivity tests of these variables to assess how they contribute to bed level evolution and attempt to ascertain an optimum combination of values.

We conducted a sensitivity analysis to determine the correct balance between these parameters for realistic channel bed evolution (**Figs 38 & 39**). Transverse sediment transport is described by,

$$S_n = \left(\tan \delta_s - G\theta^{-\alpha} \frac{\partial z}{\partial s} \right) s_{bl} \quad (13)$$

where, $\tan\delta_s$ is helical flow intensity, G controls the transverse slope steepness, and α is the transverse slope power. Longitudinal sediment transport is described by,

$$S_s = \left(1 - e \frac{dz}{ds} \right) \quad (14)$$

where the value of e was calculated empirically following Struiksma (1985), where,

$$e = \xi \frac{C_{BF}^2}{g}, \xi = 0.05 \quad (15)$$

Several G and α variables were trialled (**Table 8**) to ascertain the degree to which these parameters altered the channel bed. Lower values of G led to increased bed instability, whereas larger values made the bed more stable. As α was varied, there were minor changes in the morphological evolution of the bed, so a constant value of

0.5 was selected. The longitudinal slope factor (e) remained static throughout the experiments, although we did vary the parameter to assess how longitudinal sediment transport rates affected bed evolution. The longitudinal slope factor was observed to exert very little influence on the evolution of the boundary (**Fig. 40**) as is consistent with DHI (2014b): we used an empirically derived value for e calculated using equation **15**.

Table 7. Bed slope sensitivity analysis. G, α, and e are the slope parameters described in the text each assigned a value for each run. The minimum and maximum bed elevations at the end of each simulation are displayed. The standard deviations (σ) for min and max bed elevations is provided to describe the variation in elevation between runs.

	Parameter						
	G	**α**	**e**	**Run**	**Min Δbed elevation (m)**	**Max Δbed elevation (m)**	**Simulation Period (years)**
Value	0.5	0.5	7	12-001	-1.24	0.66	5
	1	0.5	7	12-002	-1.21	0.58	5
	1.25	0.5	7	11-015	-1.17	0.57	5
	1.5	0.5	7	12-003	-1.13	0.56	5
	2	0.5	7	12-004	-1.00	0.54	5
	3	0.5	7	12-005	-1.02	0.55	5
	1.25	1	7	12-006	-1.17	0.57	5
	1.25	0.5	5	12-007	-1.18	0.57	5
	1.25	0.5	2	12-008	-1.18	0.57	5
	1.25	0.5	8	12-009	-1.17	0.57	5
				σ	0.082	0.032	
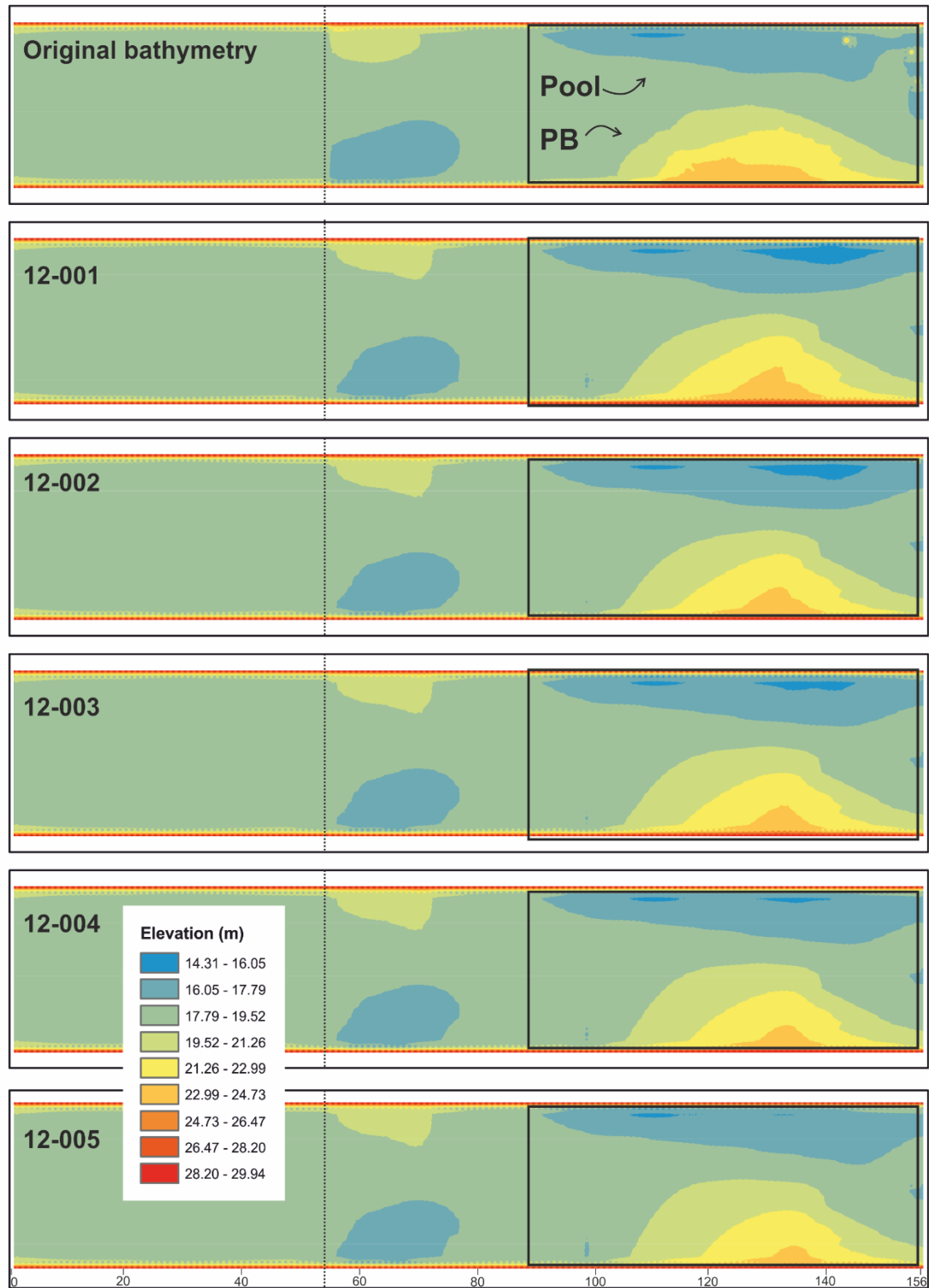
Figure 38. Channel bed changes in response to variations in the transverse slope coefficient. A straight plan view of the modelled channel with symbolised bathymetry for five experiments in which G was varied (Table 8). Distance in grid cells is shown beneath panel 12-005. The starting bathymetry is displayed in the top panel, the remaining panels display the bathymetry after a 5-year simulation. The dashed line at 53 indicates the end of the entrance slope. Flow is from left to right. The box shows the point bar (PB) and pool region which are labelled in the top panel.

124
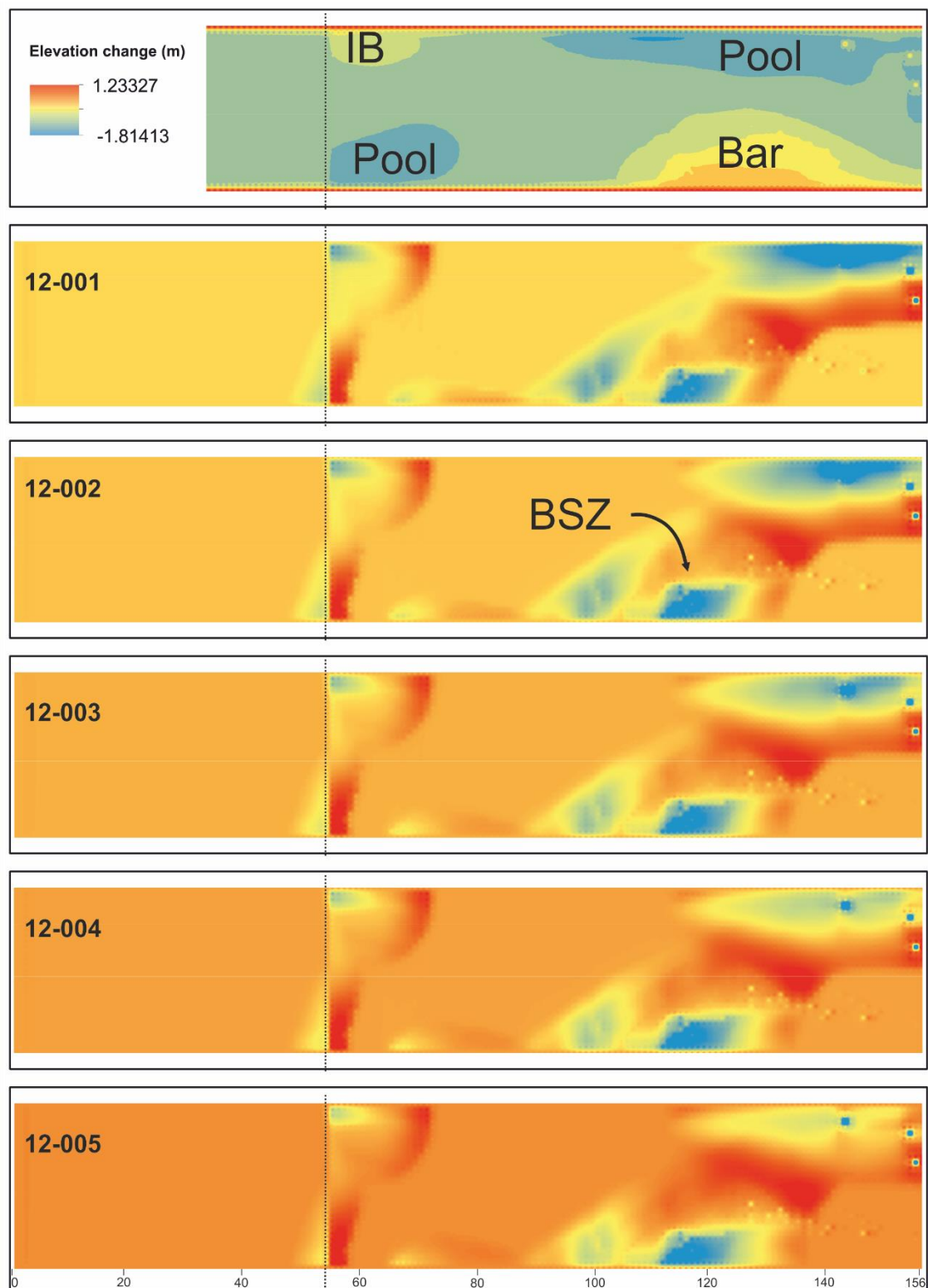
Figure 39. Changes in channel bed in response to variations of the transverse bed slope. A straight plan view of the modelled channel with symbolised changes in channel bathymetry for the five experiments displayed in Fig. 16. The top panel displays the starting bathymetry. The distance in grid cells is displayed beneath panel 12-005. The dashed line at 53 indicates the end of the entrance slope. IB is incipient bar; point bar and pool locations are also labelled in the top panel. BSZ is bar scour zone and IB is incipient bar. Flow is from left to right.

The range in absolute bed elevation change was greater for smaller transverse slope coefficients (**Table 8;** St Dev) resulting from the increased mobility of bedforms. Pool scour (top right of the panels in **Fig. 38**) was much more pronounced for runs with lower G values as was the scour induced by the transitioning high-velocity flow cell across the channel at the upstream margin of the point bar. Scour at the bar head appeared to be relatively independent of changes in G, given the almost constant size of the scour zone (labelled BSZ in panel 12-002 of **Fig. 39**). Our parameterisation phase suggested that an intermediate G coefficient should be used to satisfy the objectives of the experiments that permitted moderate scour in the pool and at the bar head and sufficient deposition in the region of the point bar. Therefore, a G value of 2.0 was selected.
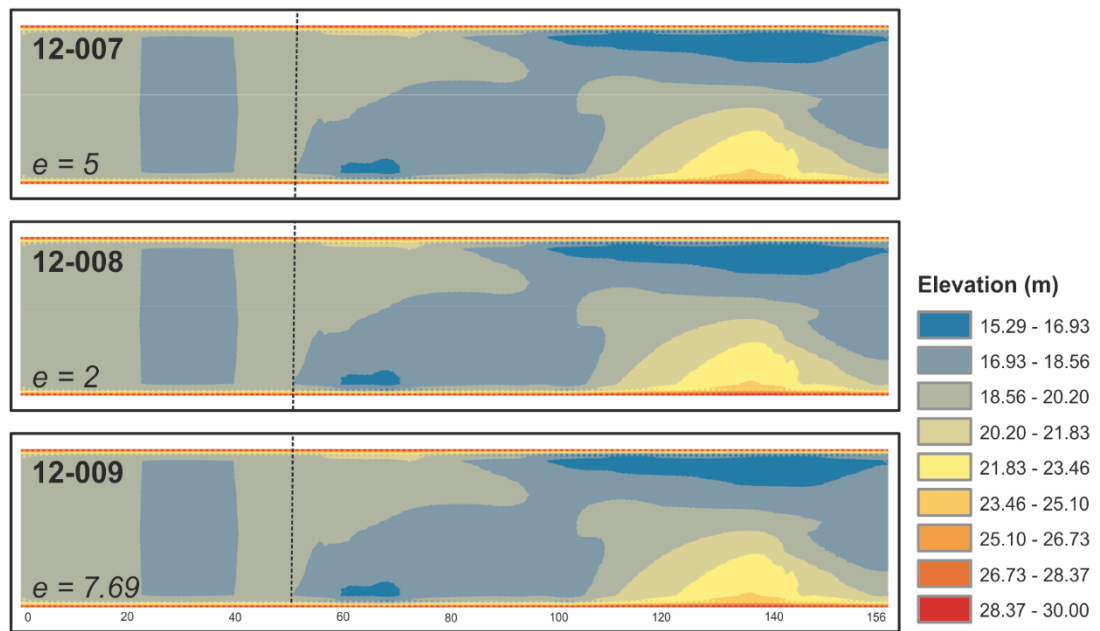
Figure 27. Bed elevation changes with changing longitudinal slope coefficient (e). Three 1-year simulations during which all conditions remained constant except e. The dashed line indicates the end of the entrance slope. The axis beneath the bottom panel describes the distance in grid cells. The flow direction is from left to right.

We tested five statistics to characterise the bed level changes: mean, median, minimum, maximum and standard deviation of the bed elevations downstream of the artificial entrance ramp (**Tables 8 & 9**). The values reported in **Table 8** – particularly maximum bed elevation values and standard deviation of bed elevations – confirm

our observations that for transverse slopes, increased G coefficients increase bed stability, and that bed levels are not very sensitive to changes in the longitudinal slope coefficient (e) (**Fig. 40**).

Table 8. Transverse slope coefficient (G) bed sensitivity statistics. Experiments are listed and correspond to those in Fig. 17. The statistics are measured for the absolute bed elevation across the entire channel bed, downstream of the artificial entrance ramp.

Statistic	12-001	12-002	12-003	12-004	12-005
Min	14.30	14.95	15.25	15.25	15.25
Max	23.77	23.70	23.65	23.61	23.49
Mean	18.68	18.67	18.67	18.67	18.66
Median	18.48	18.47	18.45	18.45	18.45
St Dev	1.61	1.57	1.52	1.49	1.44

Table 9. Longitudinal slope coefficient (e) bed sensitivity analysis. Experiments are listed and correspond to those in Fig. 18. The statistics are measured for the absolute bed elevation across the entire channel bed, downstream of the artificial entrance ramp.

Statistic	12-007	12-008	12-009
Min	15.25	15.25	15.25
Max	23.68	23.67	23.68
Mean	18.67	18.67	18.67
Median	18.46	18.46	18.46
StDev	1.55	1.55	1.54
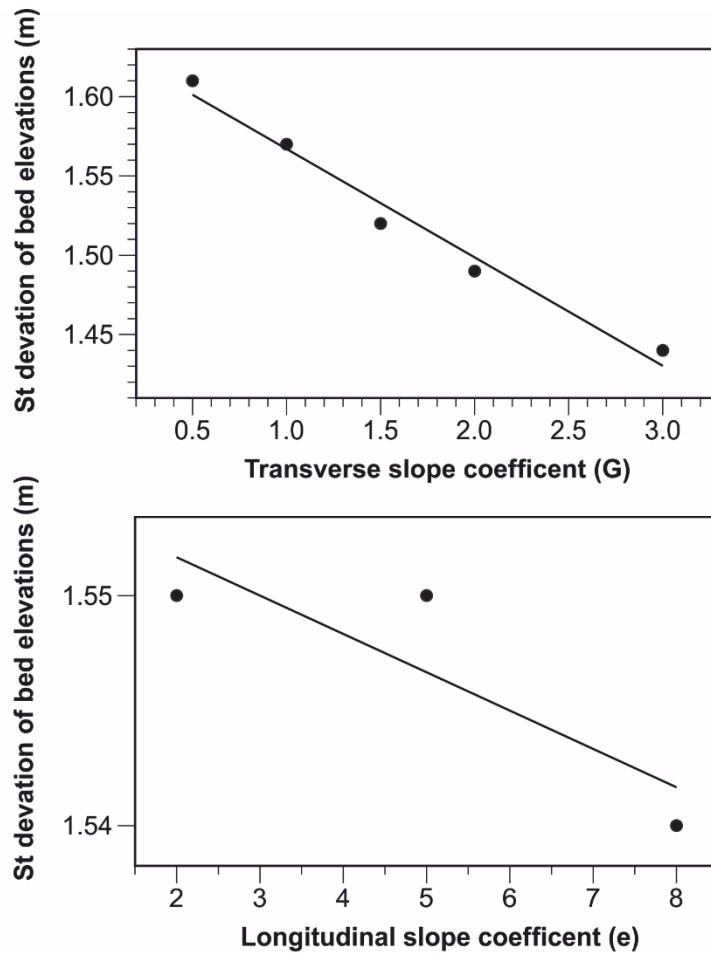
Figure 28. Effect of slope coefficients on channel bed elevations. A. The standard deviation of bed elevations across the model domain for a given transverse slope coefficient (G). B. The standard deviation of bed elevations across the model domain for a given longitudinal slope coefficient (e). Model runs were one-year in duration.

5.9.4 Flow resistance

The modelled channel depth was adopted from Constantine et al. (2010a), who estimated it to be 6.22 m at bankfull stage. This was applied as a constant value across the channel area, and tested to assess whether accurate rates of sediment transport were achieved. An evaluation of downstream sediment transport rates was performed by measuring a time-averaged transport rate across the model domain over the full simulation period to reveal that sediment transport rates were unrealistic (3.08×10^{-31} Mt yr^{-1}) (**Fig. 43**). This was corrected by simulating depth-dependent

Chézy roughness (C) after specifying a constant arbitrary initial roughness of 50 $m^{0.5}$ s^{-1} across the entire model domain, which was then updated according to,

$$C = ah^b \quad (16)$$

where a is the resistance coefficient and b is the resistance power. These parameters were chosen by predicting the resistance created by bankfull channel flow at the centreline (~ 6.22 m), which should represent the maximum depth possible at this location. The estimated bankfull pool depth (~ 11.2 m) was also used to inform the selection of these parameters for deeper areas of the channel. These parameters were then adjusted to facilitate appropriate sediment transport across the model domain (described later). A combination of a and b that permitted sufficient sediment transport in deeper regions of the channel as well as over the shallow bar area was achieved by trialling several combinations, whilst attempting to stay true to the estimated roughness using channel depth measurements. Ultimately, the depth-dependent equation will increase bed shear stresses over shallow regions of the channel, thereby increasing localised rates of sediment transport (DHI, 2014b).

Enhanced sediment transport over the bar as a result of increased resistance was reported to smoothen the crest (Talmon, 1992). A lower roughness limit was set at 27 $m^{0.5}$ s^{-1} to minimise unrealistic scouring of the bar. Several trialled a and b combinations (**Table 10**) revealed the complexity of achieving both realistic rates of sediment transport – to facilitate morphological changes – and limiting excessive scour of the point bar (**Fig. 44**). Reductions of either coefficient cause increased bed mobility and more pronounced changes to the channel bed (e.g., **Fig. 42**; right-hand panels 2-5). A compromise was met in which reasonable rates of sediment transport were achieved and a large part of the bar was maintained. Unfortunately, the bar suffered substantial scour at the head and channel-side margin, causing a reduction in its sub-aerial extent (**Fig. 44**). The downstream migration of the bar is unlikely to

cause any significant issues with further experimentation, although it has shifted the region of maximum outer bank scour further downstream. The reason for the excessive scour around the bar was due to the representation of flow resistance on the channel bed in the sediment transport equation. The strategy for selecting the parameters a and b in the Chezy equation was to assess the response of channel evolution to changes in each of the parameters by running simulations in which the parameters were sequentially increased and evaluated the sediment load from each experiment. Based on the results of these tests, an optimum combination of the parameters was used that approximated the observed bedload transport rate.

Table 10. Chézy coefficient combinations and corresponding bedload sediment loads.

Run	Roughness coefficient (a)	Roughness power (b)	Q_{BL} (Mt yr^{-1})
19-001	15	0.33	0.23
19-002	25	0.33	3.64×10^{-31}
19-003	12	0.5	0.13
19-004	12	0.8	0.0012
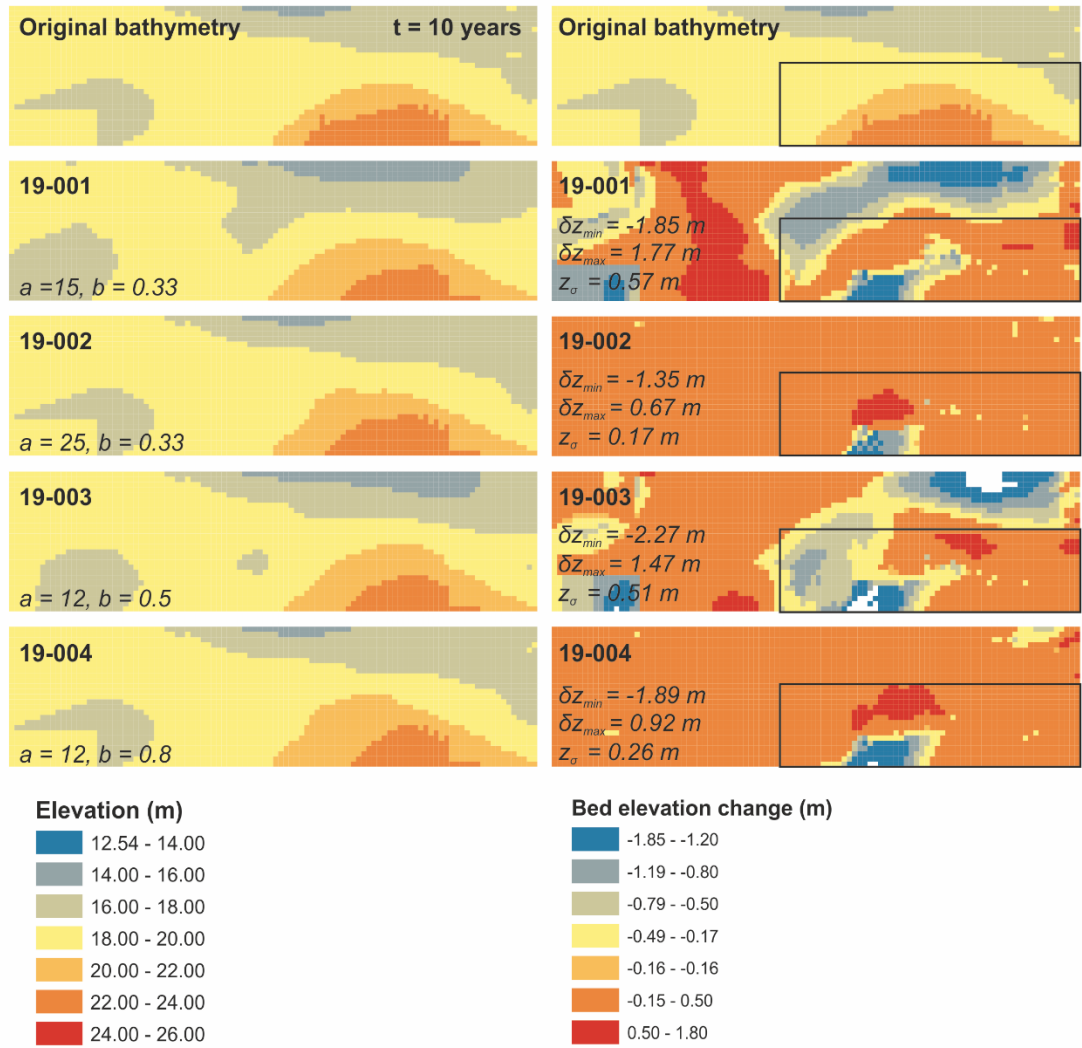
Figure 42. Sensitivity analysis of depth-dependent Chézy coefficients. A sub-set of simulations in which the sensitivity of bed morphology was tested for different combinations of the Chézy coefficients (a and b). Sensitivity is quantified using measurements of maximum bed level change ($δ_{max}$), minimum bed level change ($δ_{min}$), and the standard deviation of bed level changes ($δ_σ$). Simulation numbers and coefficient combinations are displayed. The simulation ran over a 10-year period from the initial surveyed bathymetry (t=0) with a gently inclined artificial entrance ramp with a slope of 0.00033. Flow is from left to right. The left-hand panels show the bathymetry at the end of the simulation while the right-hand panels display the bed level changes, beneath the top panel. Black rectangles indicate the bar region.
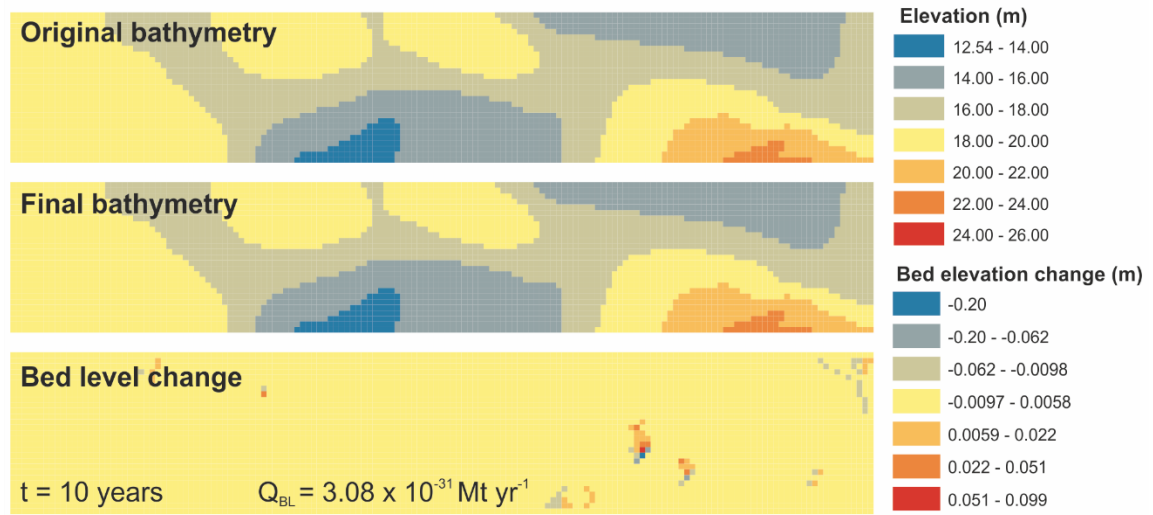
Figure 43. Channel bed changes under a spatially constant Chézy coefficient. The top and middle panels display the channel bathymetry at the beginning and end of a 10-year simulation. The bottom panel shows bed level changes that took place over this period. The reach-averaged bedload sediment transport rate (Q_{BL}) is indicated. Flow is from left to right.
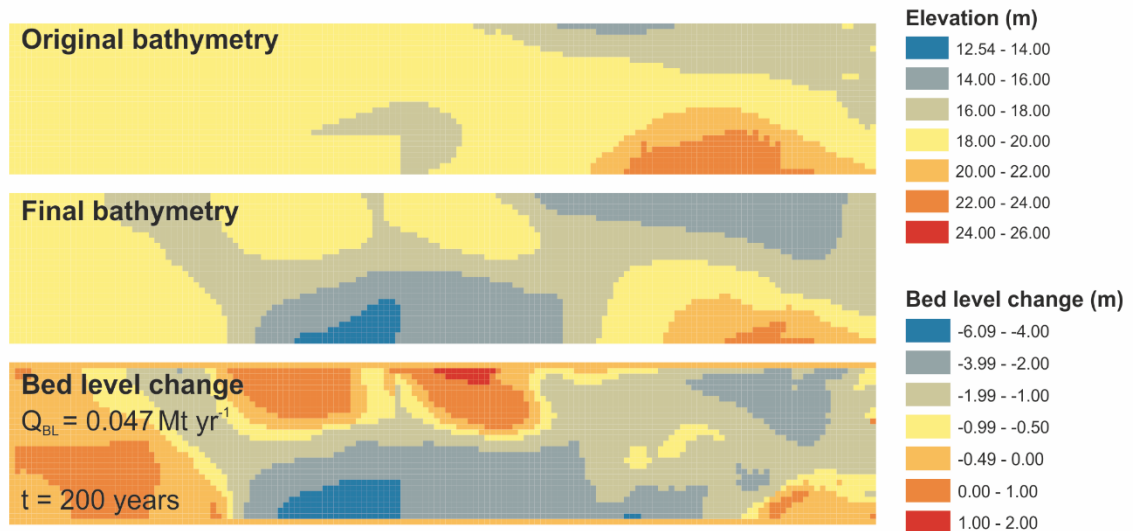
Figure 44. Channel bed changes under depth-dependent Chézy coefficient. The original bathymetry used to develop initial conditions is displayed in the top panel. The middle panel shows the resultant equilibrium bed topography and the bottom panel displays changes in bed elevation over the 200-year simulation period. The reach-averaged bedload sediment transport rate (Q_{BL}) is indicated. Flow is from left to right.

5.9.5 Bank erosion

Satellite images were collected between 2003 and 2015 at two-yearly intervals from

Google Earth© and used to calculate reach-averaged migration rates for the study

132

site. Images were georeferenced following standard procedures in ArcGIS with at least four ground control points (GCPs). Total root-mean-square error (RMSE), that is, the error calculated from the offset between the estimated locations of the points based on the position of the GCPs and the actual position of the points by use of a polynomial fitting algorithm, was minimised and never exceeded 4.09 m (2005 image). The inherent offset arises from the difficulty in identifying recognisable GCPs in the relatively rural landscape. Centrelines were digitised (**Fig. 47**) and used to generate eroded-area polygons which were subsequently converted to lateral migration rates following the methodology of Micheli et al. (2004) and Constantine (2006) (described in the Methods section of Chapter 3). The calculated migration rate (M_R) was used to calibrate the annual migration rate of the model banklines. Bank erosion is described by (**17**);

$$M_R = \ \varphi \frac{\delta z}{\delta t} + \ \psi \ \frac{S}{h} \qquad\qquad (17)$$

where M_R is the migration rate (m s^{-1}), z is the local bed elevation, S is near-bank sediment transport, h is local water surface level and φ and ψ are parameters used to calibrate the model based on field observations. The φ parameter describes the extent to which the transverse bed slope controls outer bank erosion and is set to 20 in the present study after calibrating model outputs with observed rates of retreat. The ψ parameter describes the ratio of sediment transported away from the outer bank following removal from the bank and is set to 0.1 (100% of the specified range), again following model calibration. Our simulated average annual rates of meander migration were lower than those calculated from the aerial photography, but on a similar magnitude to those reported by Micheli and Kirchner (2002) for dry meadow land (~ 1.50 m yr^{-1}). However, migration rate maxima were observed to be 17.34 m yr^{-1} along the model reach. A likely discrepancy between the observed rates of bank retreat and

the modelled rates is effective sediment transport in deeper portions of the river and the coarse floodplain substrate.

A cellular sediment conservation method is used to model bed level change, bank erosion, and planform evolution. Each cell that becomes inundated above the threshold for inclusion in the sediment transport equation is evaluated with respect to the sediment entering and leaving the cell. Subsequent to this, the bed level change is calculated which informs predictions of bank erosion by assuming the bank slope remains constant through time. Sediment eroded from the banks is included in the sediment continuity equations.
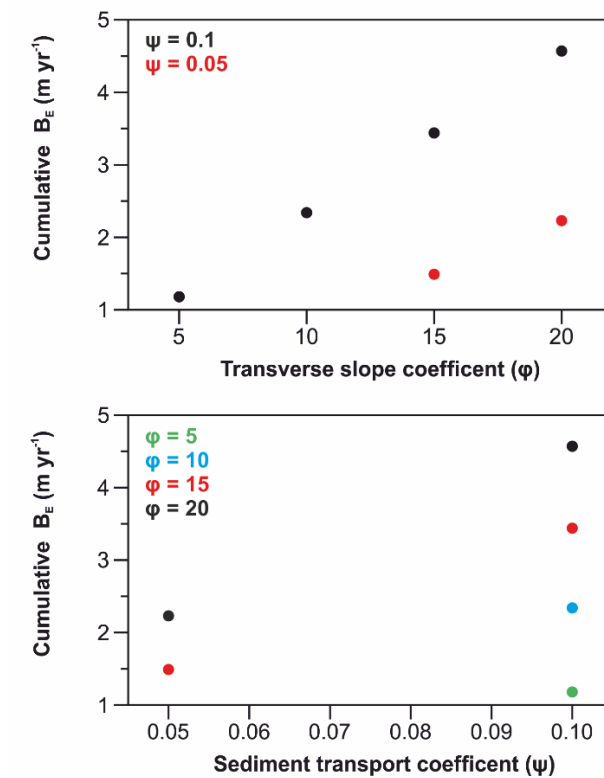
Figure 45. Sensitivity analysis of bank erosion coefficients. Top panel: Average cumulative outer bank erosion rates (B$_E$; m yr^{-1}) plotted for different transverse slope coefficients (φ). Point symbolisation is described in the plot. Lower panel: B$_E$ plotted against different sediment transport coefficients (ψ). Point symbolisation is described in the plot.

The simulations were performed on the equilibrium bed channel over a period of 10-years during which time all parameters were held constant except for φ or ψ. The channel had developed from an initial entrance slope of 0.00033 as estimated in the field. We assessed and compared the average rates of bank erosion along the erodible sections of the inner and outer banks for different combinations of coefficient

(**Fig. 45**). Assigning larger values to these coefficients effectively increases bank erosion as the effect of transverse bedslope, and the removal of sediment from the outer bank, become more pronounced. The model indirectly accounts for the role of slump block armouring through the ψ parameter, where higher values are indicative of weaker blocks. The bank height (H) was calculated from six USGS river cross sections at locations upstream of the study site. The average bank depth (10.40 m) was calculated from the cross sections using the latest date on record (August 1990) and input as the outer bank depth. Similarly, the inner bank depths were calculated to be the average depth at which the top of the inner bank met the point bar surface (3.20 m) in the same cross sections. The outer river banks tend to be vertical and at almost 90° (**Fig 46**). A maximum daily rate of bank erosion can be specified to ensure the river banks do not exceed observed rates of migration for the given flow conditions. Initially, this parameter was simply derived from the average annual rate of channel migration for the reach (6.88 m yr^{-1}), however, it yielded unrealistically small rates of bank retreat over the study period. A plausible explanation for this is that under variable flow conditions, bank erosion is a non-linear process: the most erosion will occur during high discharge events, since more material can be excavated as well as transported away from the bank toe, while more modest erosion will occur during low flow events (Gautier et al., 2007; Pizzuto, 1994). Therefore, a maximum daily rate derived from a yearly average is not feasible since greater than average rates of erosion are confined to periods of high flow. The bank substrate is considered to have the same characteristics as the material present in the river bed, which is not dissimilar from the observations made by Buer (1994). Indeed, this assumption implies there is no fine-grained material present in the bank, and that they are homogeneous in structure. The river banks in this region are comprised of Holocene alluvium and are characterised by an unconsolidated gravel base overlain with sands and silts, although the bank composition can be spatially variable with some banks missing a gravel base (Constantine et al., 2009). Banks with sandy bases

135

were observed to erode more quickly than banks comprised of gravel or characterised by cohesive channel fill deposits (e.g., clays) (Constantine et al., 2009). Despite these simplifying assumptions, the modelled process of bank erosion should not be adversely affected because changes in planform geometry were calibrated against changes detected using aerial photography.
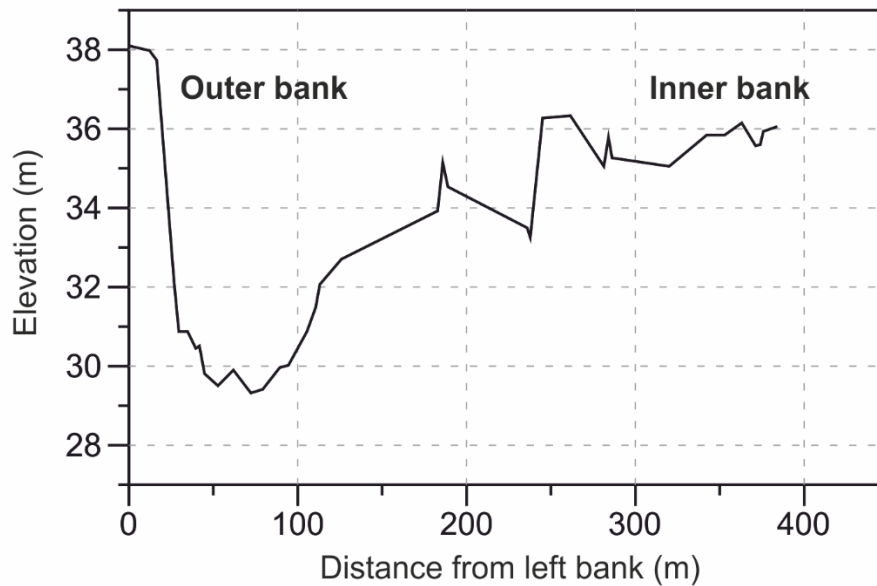
Figure 46. Example cross section at river mile (RM) 189.3 on the Sacramento River.

Erosion was concentrated along the outer bank (the left bank facing downstream); for this reason, we only simulated erosion along this axis. We acknowledge that erosion along the inner boundary is possible, particularly in the upstream part of the reach where the high-velocity core will be located at the right bank (oriented downstream). Realignment of the bank lines is not performed explicitly, but cellular erosion rates are calculated to elucidate how the channel planform changes through time. Maximum rates of migration mirrored patterns of average bank migration displayed in Fig. 45, with values ranging from 8.25 – 25.23 m yr^{-1}, where α was changed from 15 to 20 under a constant of 0.05, and 7.43 – 81.44 m yr^{-1} where α ranged from 5 to 20

in intervals of 5, when the ratio of sediment transported from the bank toe (β) was set to 0.1 (**Table 11**).
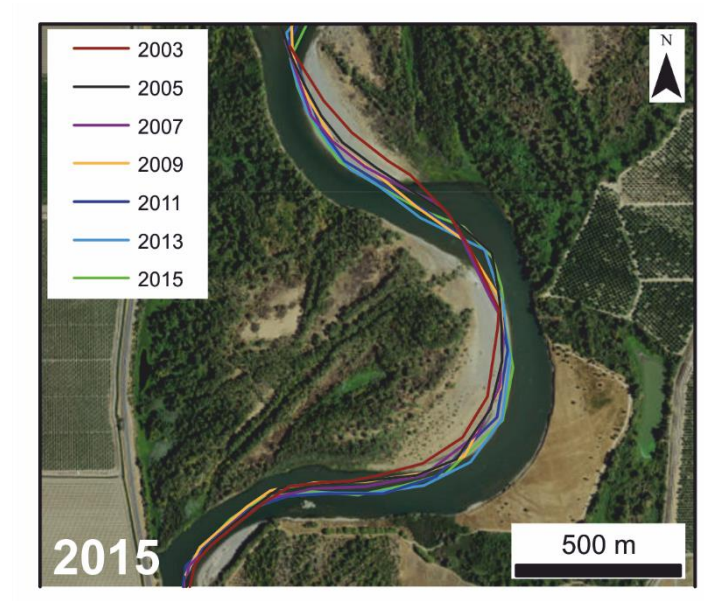
Figure 47. Channel migration inferred from centreline movement on the Sacramento River. Centrelines were created from satellite imagery at two-yearly intervals.

Table 11. Sensitivity of lateral migration to bank erosion coefficients. Bank erosion (B_E) is measured in metres.

Run	φ	ψ	Mean B_E (outer bank)	Max B_E (outer bank)
18-001	15	0.05	1.49	8.25
18-002	20	0.05	2.23	25.23
18-009	5	0.1	1.18	7.43
18-010	10	0.1	2.34	29.43
18-011	15	0.1	3.44	53.82
18-007	20	0.1	4.57	81.44

5.10 Enhanced Sediment Loading: Results and Discussion

5.10.1 Changes in bar morphology

Three experiments were carried out in which the entrance slope (~ 1300 m) was increased as a surrogate mechanism for increasing sediment supply to the channel. Sediment was excavated from the bed and transported downstream. The bed slope of the entrance ramp was increased on three occasions to simulate different sediment supply conditions (**Table 12**): the first experiment increased the slope by 21%, the second by 57%, and by 142% in the final experiment (**Figs 48-50**). Two metrics of reach-averaged sediment load were measured during each experiment. One measurement was made during the development of equilibrium bed conditions (over a ~100-year simulation) in which the bathymetry evolved from a gently-inclined entrance ramp with prescribed slope; the second metric measured sediment transport over a 10-year simulation, after the development of equilibrium bed topography as determined by the rate of change of bed elevations over the ~100-year simulation (**Figs 48-50**; top plot). The second method, although measured over a shorter period should provide more accurate estimates of sediment transport (**Table 12**) since the bed has adapted to the prevailing flow conditions, whereas the first metric measures transport rates associated with large changes in topography, produced as the channel evolves to equilibrium. All three sediment loading experiments exhibited the same pattern of deposition just downstream of the inclined channel ramp where the channel gradient decreased. Moreover, a large volume of material (**Figs 48-50;** deep red zone in lowest panel) was observed to be deposited in the region of scour at the inner bank upstream of the bend apex. The deposition of material at the downstream edge of the channel ramp persisted throughout the 100-year simulation reaching a maximum depth of 5.70 m during run 18-013. This did not create a sediment lobe 5.70 m deep since some of the material was used to fill the sediment trap. Further downstream sediment was deposited at the inner bank upstream of the existent point bar causing

longitudinal growth in the upstream direction (**Fig. 51**). The width of the bar remained relatively consistent (~ 90 m at its maximum and greatest elevation), although the margin was trimmed by approximately a single grid cell, equating to ~ 10 m in width, during the final scenario (18-013).

Table 4. Slope conditions and bedload transport rates (Q$_{BL}$) for sediment loading experiments.

Run	Simulation period (years)	Initial entrance slope	Q$_{BL}$ (Mt yr^{-1})
18-001	10	0.00033	0.084
18-015	10	0.00040	0.11
18-012	10	0.00050	0.12
18-013	10	0.00080	0.17

Figure 48. Evolution of equilibrium conditions for inclined bedslope of 0.0004. The top plot displays the cumulative RMS of bed level changes (m) across the entire model for each timestep of the simulation. The top panel shows the starting bathymetry with an imposed entrance slope of 0.0004. The middle panel shows the final equilibrium topography, while the bottom panel displays the net bed elevation change for the simulation period (129 years). Flow direction is left to right. The lower limit of the entrance ramp is delineated by a vertical dashed line in the top panel.
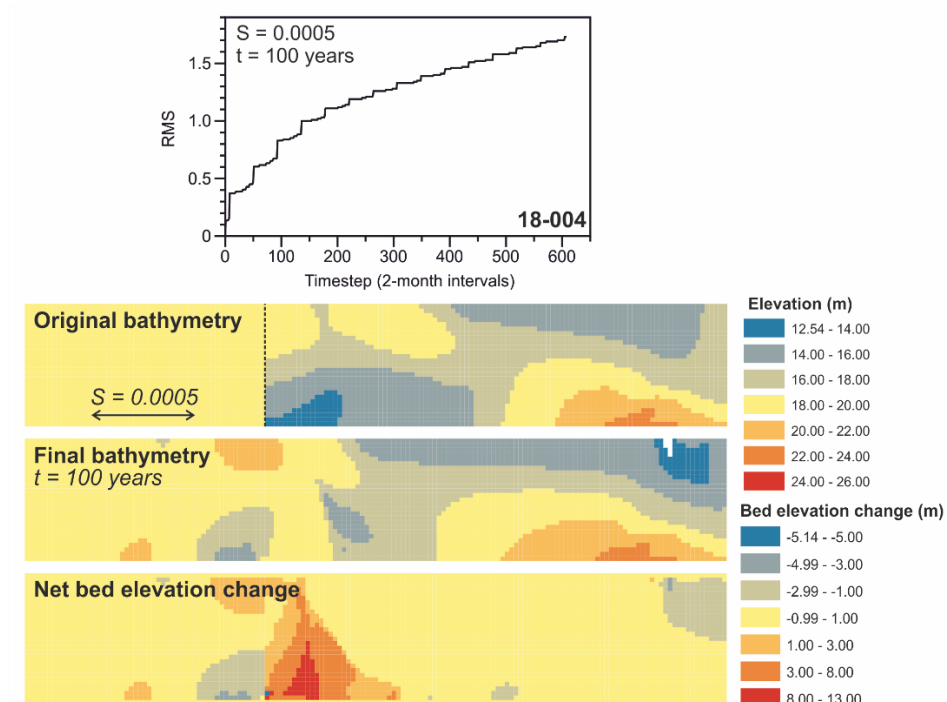
Figure 49. Evolution of equilibrium conditions for inclined bedslope of 0.0005. The top plot displays the cumulative RMS of bed level changes (m) across the entire model for each timestep of the simulation. The top panel shows the starting bathymetry with an imposed entrance slope of 0.0005. The middle panel shows the final equilibrium topography, while the bottom panel displays the net bed elevation change for the simulation period (100 years). Flow direction is left to right. The lower limit of the entrance ramp is delineated by a vertical dashed line in the top panel.
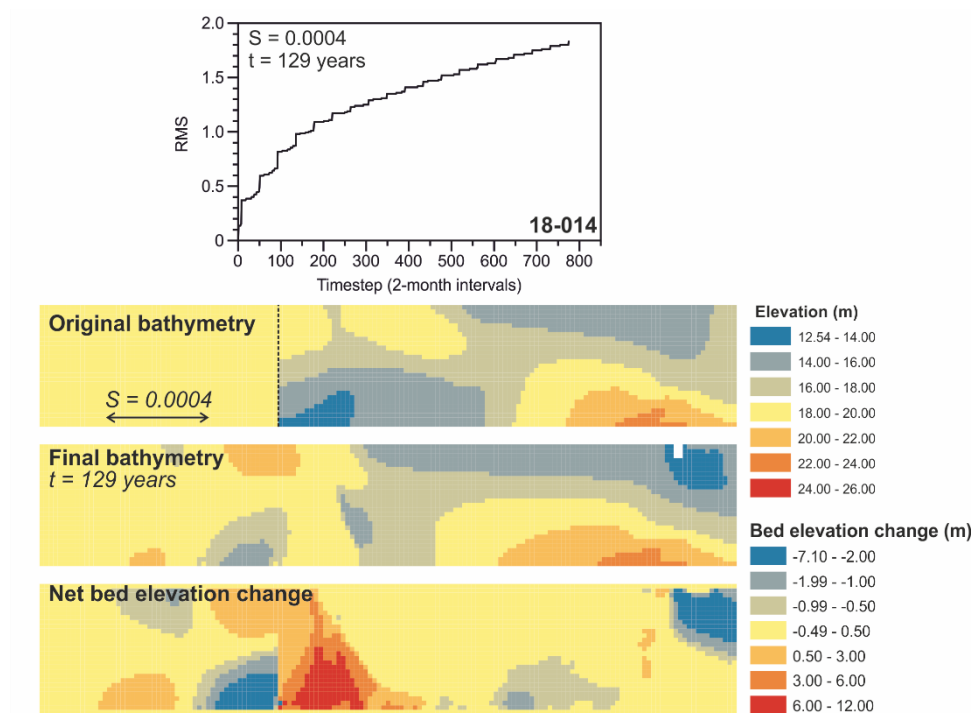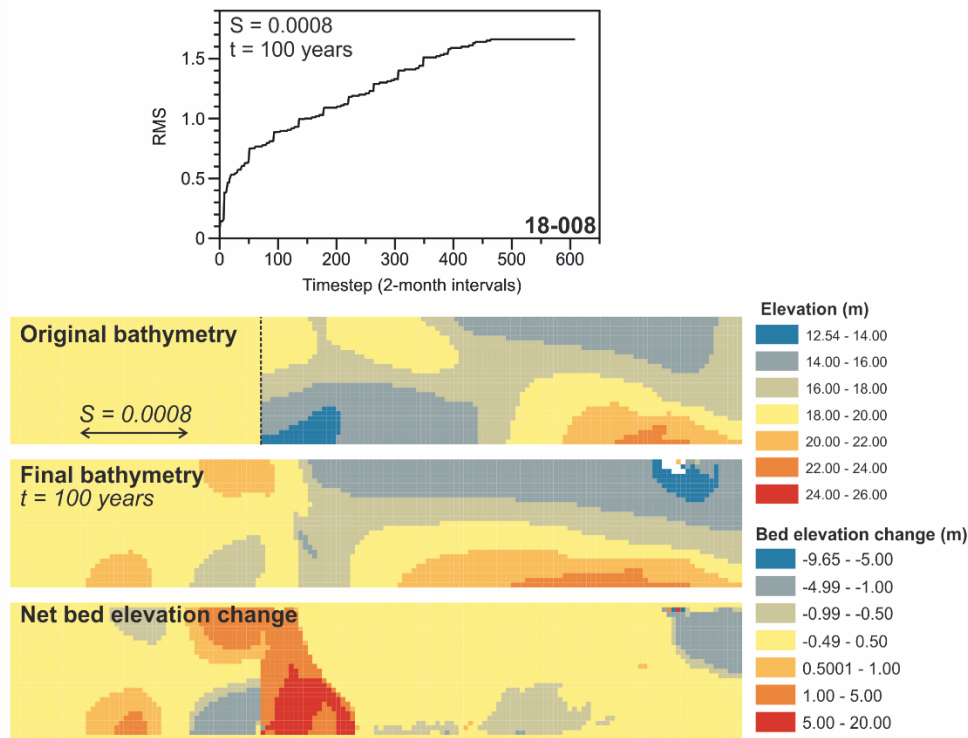
Figure 50. Evolution of equilibrium conditions for inclined bedslope of 0.0008. The top plot displays the cumulative RMS of bed level changes (m) across the entire model for each timestep of the simulation. The top panel shows the starting bathymetry with an imposed entrance slope of 0.0008. The middle panel shows the final equilibrium topography, while the bottom panel displays the net bed elevation change for the simulation period (100 years). Flow direction is left to right. The lower limit of the entrance ramp is delineated by a vertical dashed line in the top panel.

Point bars are typically observed to grow in the downstream direction resulting from the cross-stream transport of material from the eroding bank (Dietrich and Smith, 1984). Our simulations show upstream growth of the bar with some vertical growth of the bar, upstream of the central axis (defined as a division through the centre of the original bar normal to the channel). Vertical point bar growth is accomplished by the deposition of suspended material over the bar surface as the water depth – and hence flow velocity – diminishes (Ikeda, 1989). What is evident from our experiments is that the absence of suspended sediment limits the ability of bars to grow downstream as well as vertically because the shear stresses generated by the flow regime are insufficient to transport material up and across the bar surface. Instead, where bedload material is abundant (e.g., **Fig. 52**; S = 0.0008), the material is deposited at the inner bank of the meander, upstream of the existent bar, where flow velocities

decrease due to the curvature-induced cross-stream transfer of momentum (Hooke, 1975). The bar grows in the upstream direction and achieves a maximum increase of 3.50 m. Grain size analysis of point bar surfaces typically reveals a downstream fining as the material used to construct the bar changes from coarse material at the head to fine material at the tail (Bluck, 1982; Nanson, 1980). This characteristic grain size distribution arises primarily due to the distribution of shear stress in the channel and the selective capacity of near-bed currents to transport finer material towards the bar tail (Braudrick et al., 2009; Dietrich and Smith, 1984; Dietrich et al., 1979; van de Lageweg et al., 2014). Pyrce and Ashmore (2005) revealed how patterns of sediment deposition changed with the evolution of point bars: initially, coarse material accumulates at the bar head after being transferred from the adjacent upstream pool, this transport then diminishes, as flow and sediment transport increase in the deeper part of the channel, encouraging deposition along the outer margins and downstream region of the bar. These observations partially support the processes occurring in our simulations whereby the bar is still in a stage of development, infilling the sediment trap along the inner bank and then growing upstream with adjusting flow conveyance in the meander.

Bar aggradation at the head was accompanied by outward growth of the bar in the cross-stream direction. The lobe of material that developed in each of the simulations can be explained by the transport of grains down the transverse slope towards the pool. Since the slope was relatively steep (~ 0.1 – 0.3) the coarse grains are free to roll down the face, particularly during high-magnitude flow events that shoal over the upstream portion of the bar and mobilise material downslope with the flow filament (Dietrich and Smith, 1984; Hooke, 1975). Failure of the bar to grow downstream in the present study may arise for a number of reasons: first, the meander ends abruptly near to the most downstream extent of the bar not allowing any further growth to take place. Second, the coarse bedload and absence of suspended load in the simulations

appears to inhibit the inward transfer of material by helical flow to the downstream end of the bar. An examination of the bedload transport direction revealed that there is little inward moving vectors suggesting that either the helical flow is not effective enough to transport sediment against the steep transverse bedslope or the convey the coarse material inwards. If the channel length was to be extended further downstream perhaps the helical flow component would strengthen. The argument for this is that the deep pool that formed at the outer bank (**Fig. 51**; deep blue shading at downstream boundary) is where the strongest helical flow will develop (Dietrich et al., 1979; Frothingham and Rhoads, 2003), which would facilitate the inward movement of material to the downstream margin of the bar. Therefore, it is possible that the length scale of the bend inhibits accurate sediment redistribution downstream of the apex. Despite this shortcoming, the objectives of the study can still be investigated with regards sediment deposition at the bar head and what effect this has on channel hydrodynamics and bank erosion.
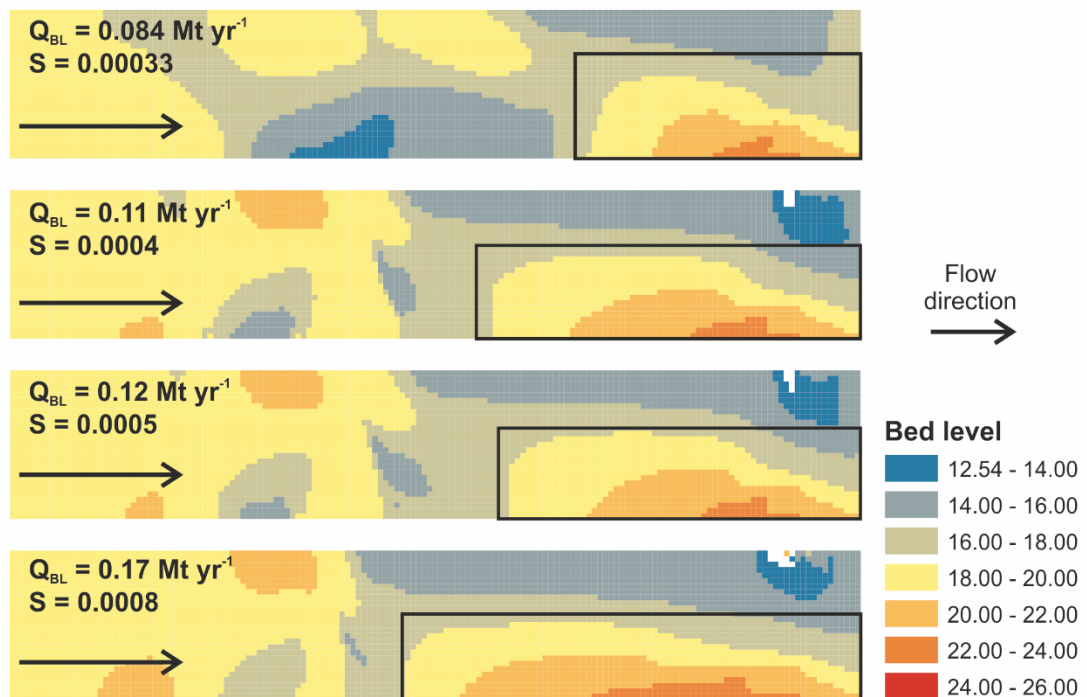
Figure 51. The response of channel bathymetry to changes in sediment supply. Point bars are indicated by black boxes on the right side of each panel. Flow direction is from left to right and the entrance slope conditions and sediment supplies are indicated for each run.

5.10.2 Shear stress distribution

We examined patterns of shear stress (τ) distribution across the channel for the different experiments as a means of a) quantifying whether increases in sediment supply caused coeval increases in shear stress, and b) to examine whether larger shear stresses were observed at the outer channel boundary as the point bar grew in size. We evaluated a number of metrics (τ_{Max}, τ_{50}, τ_μ, and τ_σ) to quantify the shear stress distributions in 10-year simulations using equilibrium bed topography. These metrics were all reach-averaged measurements for particular discharge events and clearly demonstrated the reliance of shear stress distributions on discharge. As expected, shear stress maxima were observed in the deepest part of the channel oscillating from side to side as the flow moved from the straight section into the meander. As the discharge magnitude increased, the zone of shear stress maxima migrated slightly downstream in the region opposite the point bar (**Fig. 52**; panel 5 'PB') attaining shear stresses between 1.20 and 2.60 times larger than in the lower discharge scenarios. This pattern of stress distributions was not consistent for all the sediment loading experiments; as the sediment load was increased there was an upstream migration of shear stress maxima at the outer bank. Each discharge shows consistently low shear stresses over the point bar, where stresses would need to exceed a critical shear stress (τ_C) of ~ 15 N m^{-2} as estimated using the Shields equation with the input model parameters (**Table 6**) to move the bed material.

$$\tau_c = \theta g(\rho_s - \rho)D_{50} \qquad (18)$$

The downstream migration of shear stress maxima with increasing discharge results from a delayed crossover of flow momentum due to less topographic influence of the point bar at higher discharges since it is able to move more directly downstream (Whiting, 1997). For the low discharge event (158.89 m^3 s^{-1}) during the high sediment load scenario (**Fig. 55**; panel 1), outer bank shear stresses are 4.2 times lower than in the high discharge scenario. A possible explanation for this is the substantial depth

difference and flow coverage of the bar between scenarios. During the high-magnitude discharge event, flow encroaches much further up the bar to within ~20 m of the inner bank whereas the flow is ~80 m from the top. Furthermore, flow depths at the concave bank are ~ 4 m deeper between scenarios. This demonstrates the stage dependence of shear stresses when interacting with point bars and the optimum range in which topographic deflections become important for outward flow momentum.

One important caveat associated with examining shear stress distributions in the present study originates from the changing bathymetric entrance conditions. Since our entrance slope was gradually inclined for successive experiments there was a slope-induced increase in shear stress which could have be misinterpreted as resulting from enhanced sediment loading alone. **Figures 52-55** show the reach distributions of shear stress, clearly highlighting the large values over the entrance ramp which increased in magnitude as the ramp became steeper.
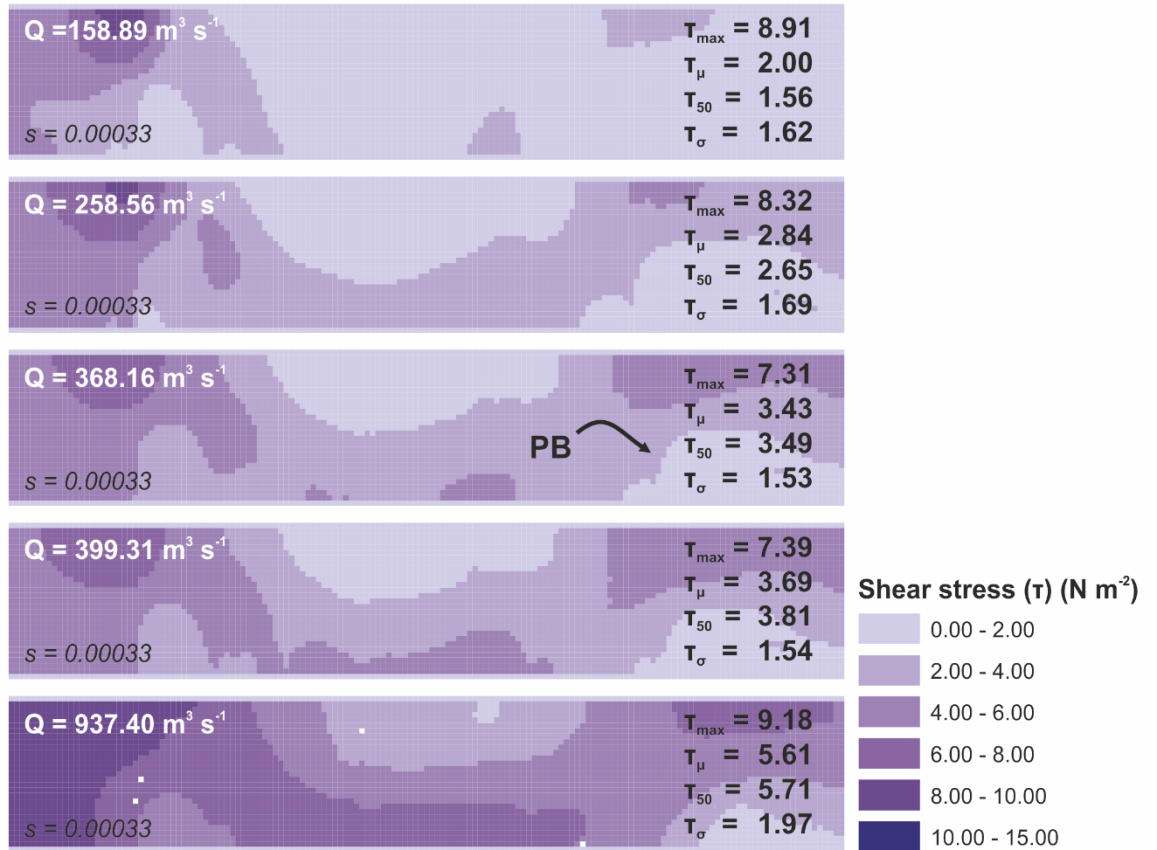
Figure 52. Shear stress distributions for changing discharges. The channel had an entrance slope of 0.00033 and developed equilibrium conditions. Discharge was routed through the model over a 10-year period and the shear stress maxima (τ_{Max}), mean (τ_μ), median (τ_{50}) and standard deviation (τ_σ) were evaluated across the model domain. Flow was from left to right. 'PB' locates the position of the point bar.
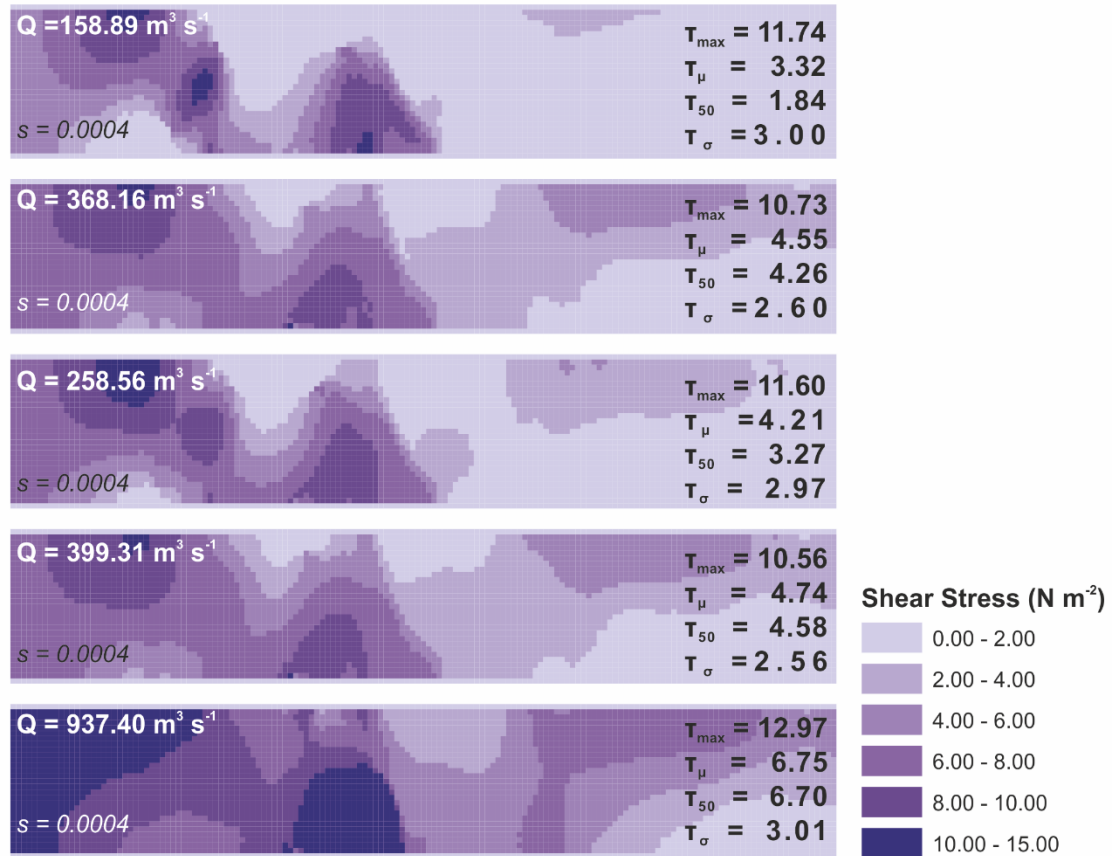
Figure 53. Shear stress distributions for changing discharges. The channel had an entrance slope of 0.0004 and developed equilibrium conditions. Discharge was routed through the model over a 10-year period and the τ_{Max} τ_{μ}, $\tau_{50,}$ and τ_{σ} were evaluated across the model domain. Flow was from left to right.
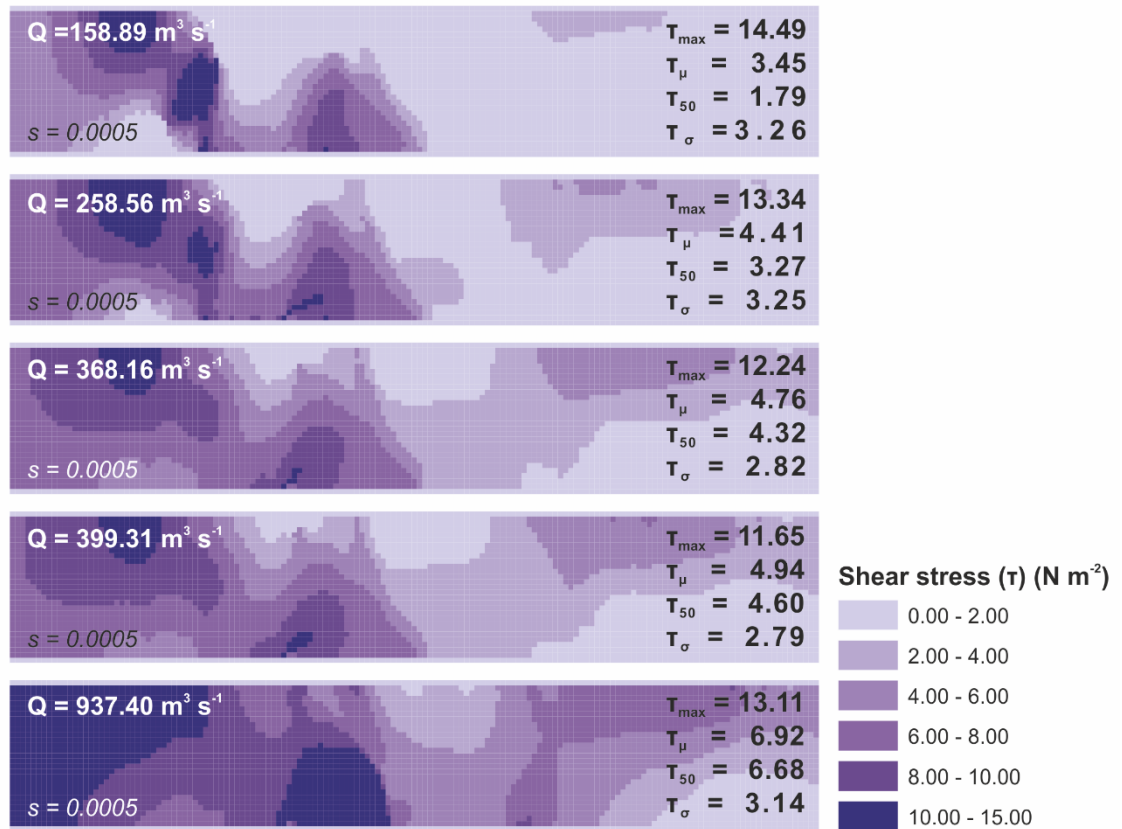
Figure 54. Shear stress distributions for changing discharges. The channel had an entrance slope of 0.0005 and developed equilibrium conditions. Discharge was routed through the model over a 10-year period and the τ_{Max} τ_{μ}, $\tau_{50,}$ and τ_{σ} were evaluated across the model domain. Flow was from left to right.
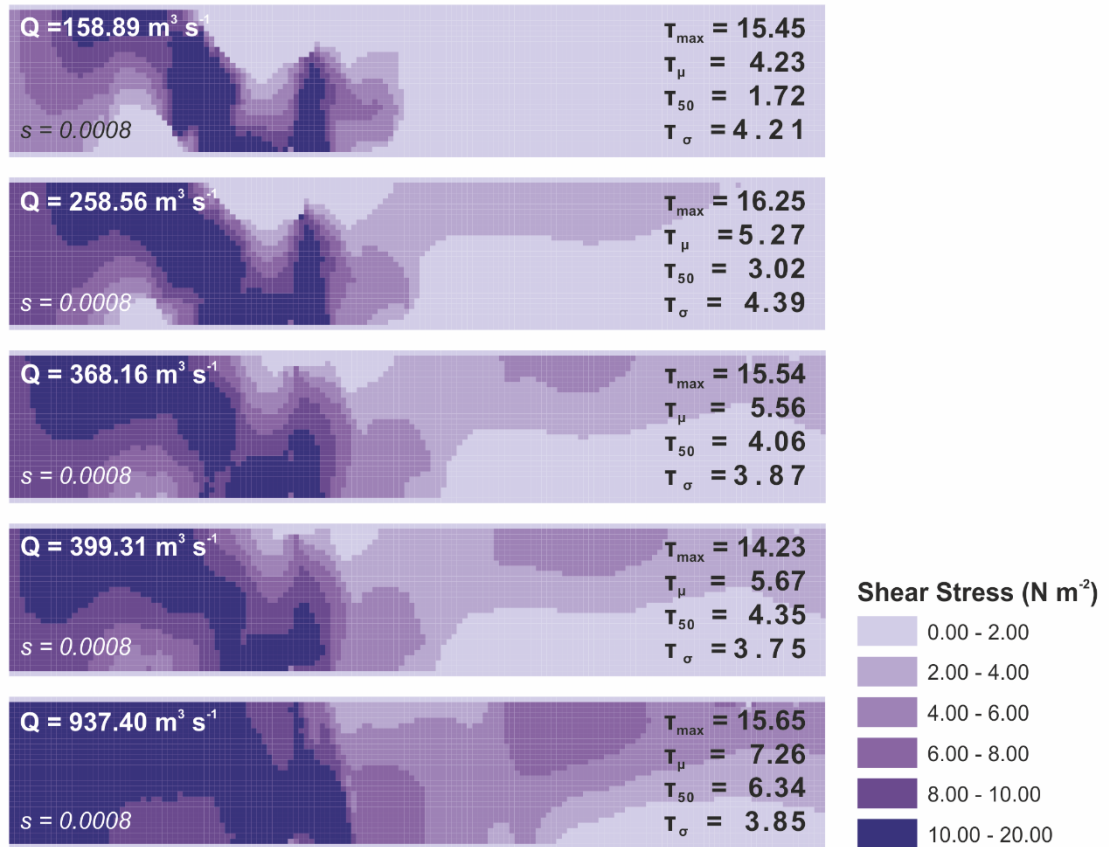
Figure 55. Shear stress distributions for changing discharges. The channel had an entrance slope of 0.0008 and developed equilibrium conditions. Discharge was routed through the model over a 10-year period and the τ_{Max} τ_{μ}, $\tau_{50,}$ and τ_{σ} were evaluated across the model domain. Note the scale change from the previous figures. Flow was from left to right.

Quantifying shear stress maxima independently of changes in channel slope was accomplished by examining the stresses residing at the outer bank opposite the point bar at five different discharge events. The same metrics as above were adopted to describe the outer bank shear stresses. The strong discharge dependence on the outer bank stresses was evident in the observations of the shear stress maxima (**Fig. 56**). There was no evidence of consistent increases in boundary shear stress at the outer bank as the sediment load was increased, although the largest mean, median, and maximum shear stresses were observed for the channel with a sediment load of 0.12 Mt yr^{-1} (S = 0.0005), perhaps further demonstrating the existence of an optimum channel-bar configuration in which the deflection of flow momentum is maximised.

149
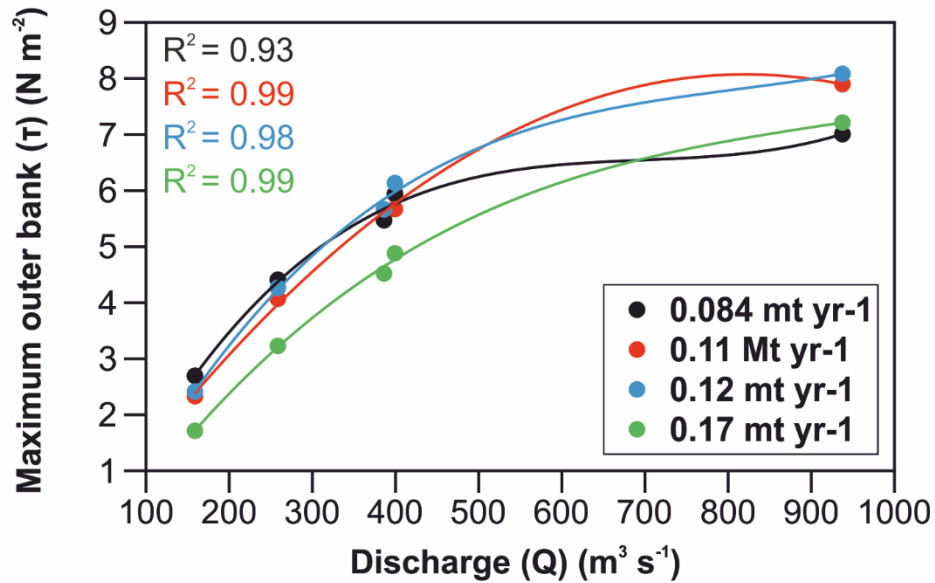
Figure 56. Shear stress maxima measured at the outer bank for five discharge magnitudes. Bedload transport rates indicative of sediment supply are used to symbolise the data and correlation coefficients. The data are fitted by logarithmic regression lines. The surveyed outer bank line was classified as being from the bend apex to the downstream boundary.

5.10.3 Cross sectional analysis

Regularly spaced cross sections (~120 m) from the bend apex to the downstream boundary were extracted to examine how the channel bed responded to elevated sediment supplies. The transverse bed slope became steeper as the channel adjusted to increased sediment loading by sequestering more material at the inner bank on the point bar. The degree to which sediment was deposited, and increased the transverse bed slope varied with distance. At cross section 108 the depth of alluvium increased by 3.62 m between the low and high sediment supply experiments, doubling the transverse bedslope from 0.015 to 0.030. At the subsequent cross sections the transverse slope became shallower with a minimum slope change in section 124 where the change between high and low scenarios was only 0.0056, although the channel centre was scoured (**Fig. 57**; J=124). The depth of sediment deposition for the surveyed cross sections with progression downstream declined

from 3.61 to 0.10 m with section 132 demonstrating erosion at the upper most part of the section by 0.42 m. The longitudinal decrease in sediment deposition with distance downstream of the bar head was caused by ineffective sediment transport over the bar surface due to diminishing flow depths – and velocities – which failed to entrain the coarse bedload material. The transverse slopes were similar in the central area of the bar (sections 116-124) for the first three sediment loads, but displayed large regions of scour in the channel centre when the load was increased to 0.17 Mt yr^{-1}. The simulated transverse slopes were of a similar magnitude to those calculated from the surveyed bathymetry produced by the US Army Corps Engineers (e.g., **Fig. 46**) ($S_{transverse}$ = ~0.030, at the same cross sections).

The cross-sectional response to sediment loading was different to the results presented by Dunne et al. (2010) who simulated channel change over a 30-year period in the Sacramento River using a flow and sediment transport model (FLUVIAL-12). Their results showed that changes in bank erodibility, manifested through an erosion coefficient, and changes in sediment supply, changed the cross-sectional evolution of the channel. Where the bank erodibility was held constant, and sediment supply was increased to 125% of the initial conditions, the cross section at the apex adjusted by reducing the depth to which scour occurred at the outer bank, increased the vertical height of the point bar, and increased the distance that the channel migrated by > 100 m. The rapid retreat of the bank and high sediment supply to the channel kept the pool shallow compared to the low sediment supply case where the pool was much deeper. Our results concur with the general notion that lateral retreat increases under greater sediment loading, although the depth of the bed did increase by ~ 3 m at the most downstream cross section as a pool was established (**Fig. 57**; J=140).
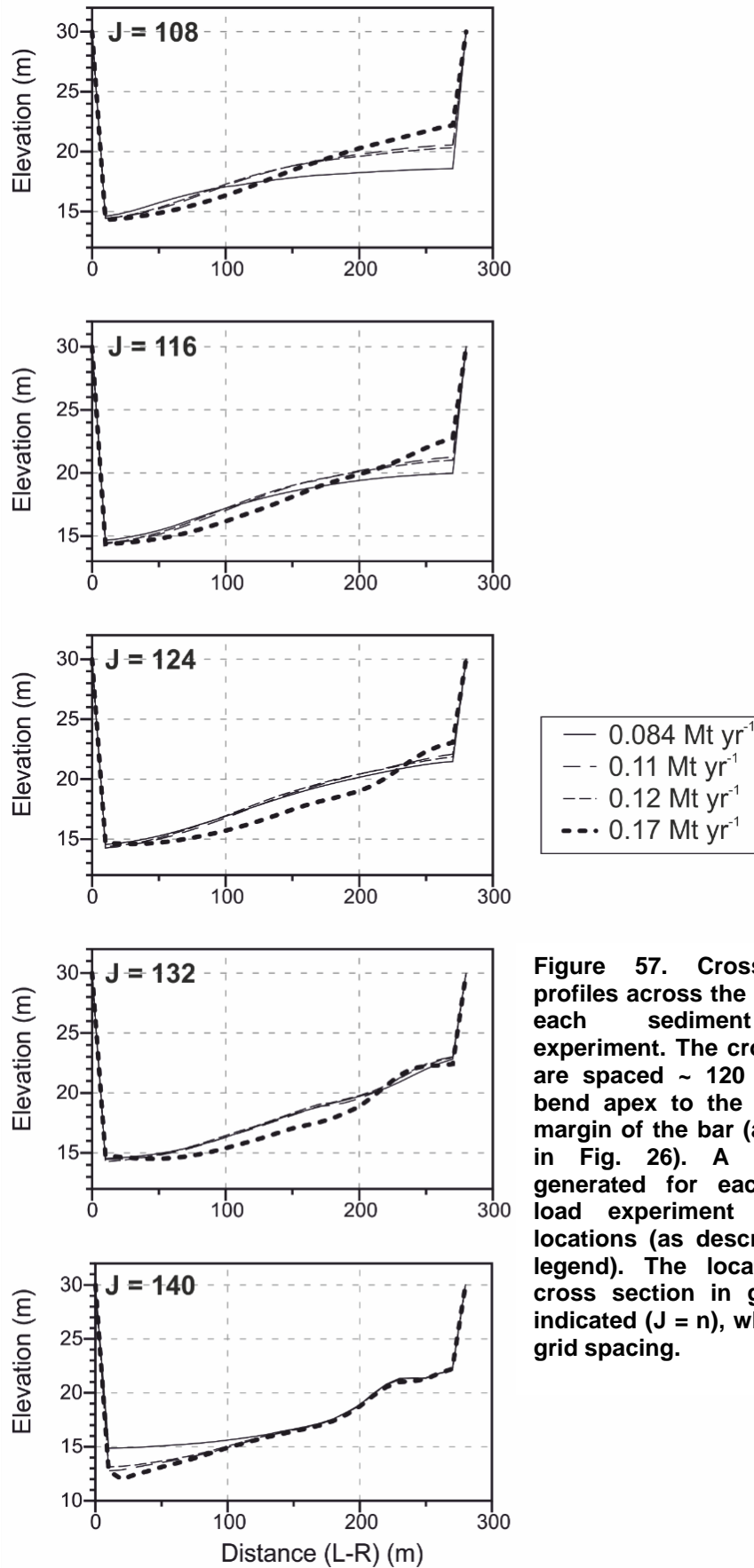
Figure 57. Cross sectional profiles across the point bar for each sediment loading experiment. The cross sections are spaced ~ 120 m from the bend apex to the downstream margin of the bar (as displayed in Fig. 26). A profile was generated for each sediment load experiment at all the locations (as described by the legend). The location of the cross section in grid cells is indicated (J = n), where n is the grid spacing.

5.10.4 Bank erosion

Rates of channel migration were shown to increase under elevated sediment loading conditions (**Fig. 58**). The additional sediment facilitated upstream point bar growth, which increased the curvature of the flow lines and permitted earlier transfer of flow momentum to the outer bank, which increased the length over which migration occurred (**Fig. 59**). In the low sediment simulations, the bar was smaller in extent and located in the downstream portion of the meander. The flow was outwardly-advected, due to planform curvature, and showed peak rates of migration towards the centre and downstream end of the channel, opposite the point bar (**Fig. 59**; top panel). As the bar grew in extent, this zone of maximum shear stress migrated upstream (**Figs 52-55**), correspondingly shifting the area of characterised by large rates of erosion further upstream. The peak rates of retreat remained in the downstream region of the channel where a deep scour pool had developed (**Fig. 51 & Fig. 59**) where the total retreat over the 10-year simulation varied from 8.25 to 74.19 m yr^{-1}. The average rates of retreat were also displayed an increasing trend with respect to sediment load, although the correlation was less clear due to, on average, greater rates of migration occurring in run 18-015 (Q_{BL} = 0.11) than where the load was 0.12 Mt yr^{-1} in the subsequent loading experiment (18-012). The similar sediment loads and channel bathymetry in these two simulations produced similar rates of maximum bank migration (**Table 13**), and so the average rates are likely to have been affected by natural variability in the data.

Table 13 Summary of bank erosion rates for different sediment loadings.

Run	Q_{BL} (Mt yr^{-1})	Average B_E (m yr^{-1})	Maximum B_E (m yr^{-1})
18-001	0.084	1.49	8.25
18-015	0.11	7.76	46.22
18-012	0.12	7.59	48.22
18-013	0.17	8.34	74.19
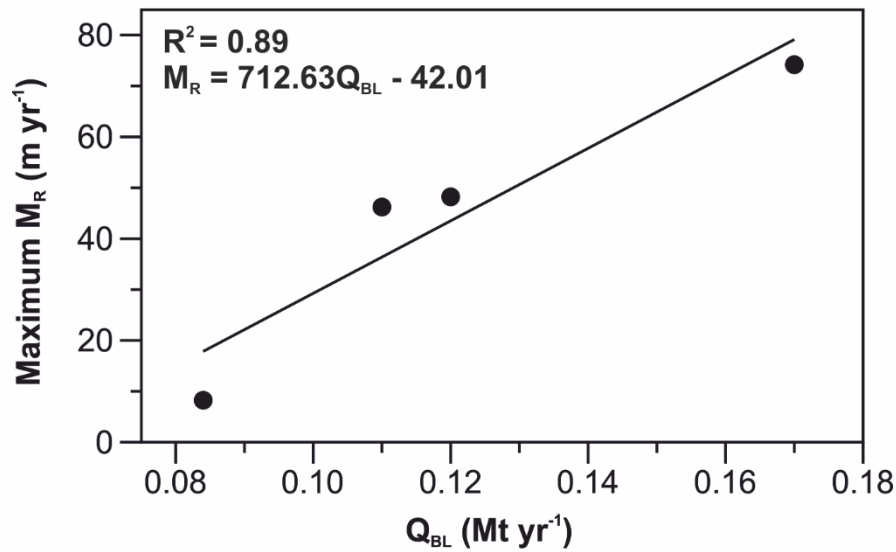
Figure 58. Maximum migration rates (M_R) as a function of sediment load (Q_{BL}). The data are fitted by a linear regression. The corresponding correlation coefficient and regression equation are indicated.

The distance over which erosion took place opposite the point bar increased from 660 m to 870 m between the low and high sediment scenarios (**Fig. 59**; 18-001 and 18-013), indicating the significance of bar extent in affecting the flow field and encouraging bank erosion. A second zone of bank retreat is clearly observed ~ 360 m upstream of the apex and represents an area of flow convergence just downstream of an incipient bar.
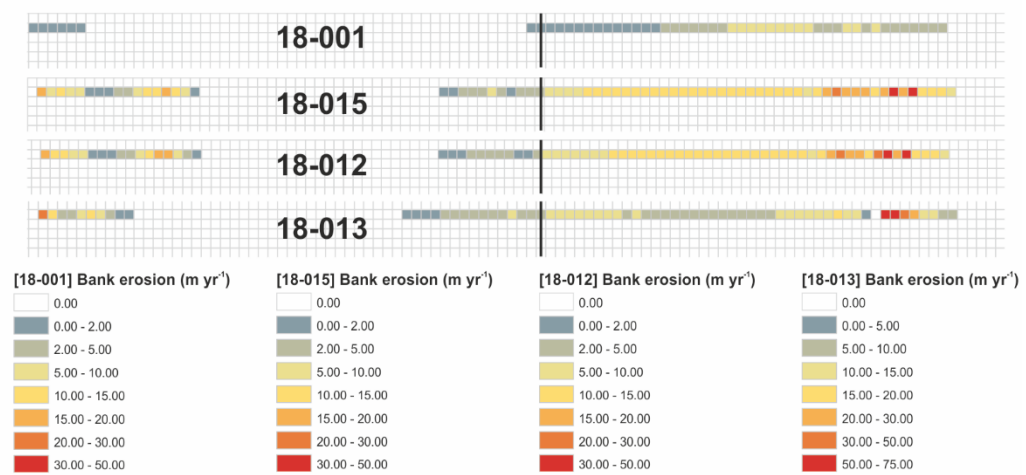
Figure 59. Extent and magnitude of outer (left) bank erosion for changing sediment loads. The four panels show the extent of outer bank erosion downstream of the artificial entrance ramp. Erosion values represent the cumulative bank erosion accomplished over the 10-year simulation period in each outer bank grid cell. Each panel corresponds to the conditions outlined in Table 7. Note the scale change for 18-013. Only the cells at the outer bank are permitted to erode. The final ~ 90 m of the bank are fixed for model stability and the cells beyond the eroding bank are fixed floodplain cells. The black vertical lines demarcate the bend apex.

155

5.11 Implications and considerations

The process-linkage identified between sediment loading, bar growth and channel migration has a number of interesting implications for long-term valley sediment storage and channel evolution. We demonstrated that the addition of alluvial material can trigger bar aggradation as the streamwise sediment flux becomes imbalanced. That is, the volume of material entering the reach is greater than the flux out of the reach. Under these conditions, the sediment entering the channel has two possible trajectories; the sediment is either stored in the bed, causing channel aggradation and point bar growth, or the sediment is distributed overbank during floods. Grain size is of paramount importance in the determination of sediment distribution through the channel network. Rivers characterised by coarse sediments are more likely to satisfy the conditions required for bed aggradation, since the material will have low settling velocities, thus depositing more readily than finer grained sediments. Therefore, the source region of sediments exerts a powerful control on the ability of meandering channels to sequester material, and ultimately change their appearance through time (Furbish et al., Unpublished). Catchments that deliver primarily fine-grained sediments to their rivers (i.e., heavily managed and agricultural regions (Owens et al., 2005)), will be less successful at producing changes in bed topography, since the material is able to pass through the channel without being deposited. Conversely, in rivers where the sediment calibre is high, changes in channel bathymetry may be slow and only possible during high-magnitude floods when flow velocities are large enough to entrain bed material. This latter point is demonstrated by the model results presented above, which clearly show poor mobility in a coarse bedload dominated river. Our results suggest that only under the right sediment loading conditions (i.e., where the channel substrate is not too large, and not too small) will bedforms be able to develop satisfactorily to affect the distribution of flow within the channel. A combination of both coarse and fine sediments is often advocated for achieving both

the longitudinal and vertical growth of point bars (Bluck, 1971; Braudrick et al., 2009; Lauer et al., 2016; Nanson, 1980). However, despite coarse bedload environments perhaps being less able develop downstream point bar growth, we demonstrated that upstream point bar growth – accomplished by sedimentation at the bar head – is also competent at deflecting the flow filament towards the outer bank, and increasing bank erosion.

Over long-term timescales bedload sediment is often cycled between the channel and floodplain, as point bars become colonised by vegetation and removed from the active channel, and subsequently re-excavated by lateral migration (Dunne and Aalto, 2013; Lauer and Parker, 2008). The reintroduction of sediment to the channel provides substrate from which point bars can be built; however, an added complication in this process is the ratio between fine and coarse material present in the floodplain. Floodplains characterised by large fine to coarse material ratios will liberate largely morphologically-insignificant sediment to the channel ineffective at stimulating bed topography growth. The history of the system will determine the composition of the floodplain as determined by both the source of sediment being supplied, and the flow conditions at the time. Added complexity is introduced by the dynamism of the system: if the channel experienced rapid rates of meander migration and produced large numbers of cutoffs, the floodplain is likely to be more heterogeneous, as the combination of coarse and fine-grained material becomes less spatially divergent (Constantine et al., 2014; Constantine et al., 2010a; Dieras et al., 2013; Dunne and Aalto, 2013). Moreover, floodplain heterogeneity, deriving from infilled oxbow lakes created by both neck and chute cutoff mechanisms, are sources of fine and coarse material loads, respectively. Floodplains able to supply morphologically-significant loads to their rivers have the ability to create a positive feedback loop in which enhanced loading by lateral migration leads to sediment deposition on bars, which alters the flow-field, accelerating the transfer of fluid momentum towards the outer

bank, thereby increasing bank erosion (Furbish et al., Unpublished). This process is likely to be limited by the speed at which inner bank sedimentation can keep pace with outer bank erosion, which is driven by vegetal colonisation and bank material properties (Eke et al., 2014a; Nicholas, 2013) – the latter being enforced by the historic composition of the basin.

As channel and floodplain management becomes increasingly more prevalent, the factors outlined above regarding optimum sediment calibres for effective bathymetric – and ultimately planform – evolution will diminish. Therefore, it is important to quantify the effect of sediment supply changes, and the structure of that particular sediment supply, to make accurate predictions as to how they interact with flow hydrodynamics to adjust the channel. These insights can then be used to inform policy makers of the wider implications that changes in land and river management may have on the functioning and behaviour of meandering rivers.

5.12 Limitations

The absence of suspended sediment transport in the model could be viewed as a shortcoming of the study since it does not reflect the observed sediment dynamics of the Sacramento River. We argue that for the purpose of this study, to achieve bar growth, bed material load was more important than suspended load, since the latter has the ability to move straight through the reach without being deposited. (Nicholas, 2013) proposed that in large sand-bed rivers, suspended sediment load was of importance because it was less affected by the transverse bed slope and controlled by the rate at which sediment settles out of the water column. The significance of this is that coarser material is more likely to be transported down the transverse bed slope towards the pool (which was confirmed by the present study), whereas finer material has the capacity to be deposited on the bar surface as flow velocities diminish (Nicholas, 2013). These observations were made for simulated large sand-bed rivers as opposed to coarse gravel bed rivers, so the application of this mechanism to the

material being transported by the Sacramento may not be as valid. The role of suspended sediment may also be important for smoothing topography: the model suffered from large areas of scour - primarily the result of excessive friction in shallow areas of the channel – these may have been subsequently filled by the deposition of fines during low flow periods (Braudrick et al., 2009; Lewin and Ashworth, 2014). Alternatively, given the alluvial resistance at the bed, this material may have been re-excavated more easily than the coarser material, therefore having no net effect on bed recovery.

The boundary conditions for sediment transport in the present model are imposed by bed elevation change, which was set to be constant through time (i.e., $\delta z \, dt^{-1} = 0$). To make the model operate more realistically, with regards sediment transport, it would be beneficial to simulate estimated rates of sediment transport as calibrated by field measurements. Adopting a constant, or temporally-varying, sediment transport rate at the channel boundaries could permit for simpler modelling campaigns in which the role of externally-imposed sediment supplies on channel morphology could be assessed. Although the present method of sediment transport should not cause any significant errors for model functionality, it did make constraining sediment transport my complex. This problem would be remedied by imposing a transport rate in future work. A further limitation – as described at the beginning of this chapter – was the flat entrance conditions which do not establish the correct flow characteristics in the channel for flow entering a meander bend. In nature, the asymmetrical channel cross section that begins downstream of the meander inflection point (straight between meanders) would initiate asymmetrical flow which is responsible for sediment sorting and transport in the bend. Failure to initiate these flow conditions may lead to irregular sediment transport, which could explain some of the deposition observed at the point bar head in the experiments.

The length of the study reach (as described in 'changes in bar morphology section) may have inhibited the development of effective secondary circulation, which would prevent the cross-stream transport of sediment failing to simulate downstream bar growth. Extending the channel to the original length would solve both the problem of meander length and afford the opportunity to monitor changes in sediment transport and flow hydrodynamics over multiple meanders with different geometries, therefore validating our observations further.

Time constraints during the development of the model limited the time available to conduct extensive testing of each of the parameters. The shortcoming of this was that not all tests were able to run to equilibrium as would be desired to conduct a rigorous evaluation of each of the parameter's responses to changing conditions. As an alternative approach, the variables were tested for various durations to acquire some insight into their effect on the evolution of the channel bed. This allowed for a targeted approach to parameterisation, and allowed the importance of certain parameters on channel bed evolution to be identified. Therefore, although not running each experiment for the full duration to establish equilibrium conditions, it was mitigated by adopting a targeted strategy to allow consideration of important variables to be undertaken, whilst still understanding the effect of each of the parameters on channel evolution.

Simulations were only performed under sub-bankfull flow conditions. A number of important processes occur during flood events, particularly overbank sedimentation - which facilitates floodplain growth (Aalto et al., 2003; Lewin et al., 2016) – and bedform evolution, which determines alluvial stratigraphy [nicholas 2016]. The absence of flood events may have limited channel bed movements and thus limited the accuracy of the results in comparison to what might be expected in natural channels.

5.13 Future research directions

Following multiple complications with the initial model development the author believes that a more successful modelling campaign could be achieved by developing the model from a flat-bed and with further refinement of the bed roughness parameter (manifested through the depth-dependent Chézy coefficient). Developing the channel bathymetry from a gently sloping flat-bed prescribed with the field-measured channel gradient may reduce the complexities involved with routing a hydrological record through a channel with predefined bathymetry. Approaching the model development in this manner reduces the applicability to the real-world; however, a reduced complexity model will still allow for insights into the processes operating, albeit in a semi-artificial channel. Further sensitivity analysis of the alluvial resistance factor should be completed to facilitate better patterns of sediment transport, this is particularly important for the bend entrance, where the present model struggled to replicate bar-induced flow shoaling. Incorporating suspended sediment into the model would make the simulations more realistic and perhaps resolve some of the issues related to scour, since the finer sediment could act to smooth out the bed topography when being deposited. Additionally, incorporating suspended sediment may replicate field-observed processes more accurately (e.g., downstream bar growth). Adding multiple grain size fractions to the model would allow for more reliable modelling of river bank erosion, which in the present study were assumed to be comprised of the same material forming the bed. This assumption means that the erodibility and transport of material from the bank would be more complex than in reality, thereby under predicting rates of bank retreat. Moreover, adding multiple grain size classes would permit an improved understanding of vertical bar growth, which relies on fine sediment deposition to raise the elevation of the bar above the level of frequent inundation – thus becoming a floodplain (Wolman and Leopold, 1957).

5.14 Conclusions

The mechanism linking enhanced sediment supplies to point bar growth and channel evolution in meandering rivers has only been evaluated indirectly. We conducted a number of experiments using a 2D hydrodynamic flow model in which we adjusted the sediment supply to demonstrate that increases in sediment led to point bar growth. The increase in point bar area was shown to affect the flow-field, whereby the magnitude of the outer bank boundary shear stress increased and expanded causing larger rates of bank erosion. The absence of suspended sediment load from the model precluded downstream bar growth contrary to observations of this process on meandering rivers in nature as well as in experimental settings. Instead, point bar growth occurred in the upstream direction as a result of significant sedimentation at the bar head. Since the presence of the bar still acted to increase bank erosion, the model demonstrated that there is a mechanism by which bar growth can act to perturb the flow field, and lead to more rapid rates of channel change. Our results highlight the importance of sediment composition in determining how point bars grow and indicate that future changes in sediment loading could have implications for the long-term evolution of meandering river systems, particularly if the material supplied has the aptitude to be deposited as bars.

Chapter 6

Synthesis and Implications
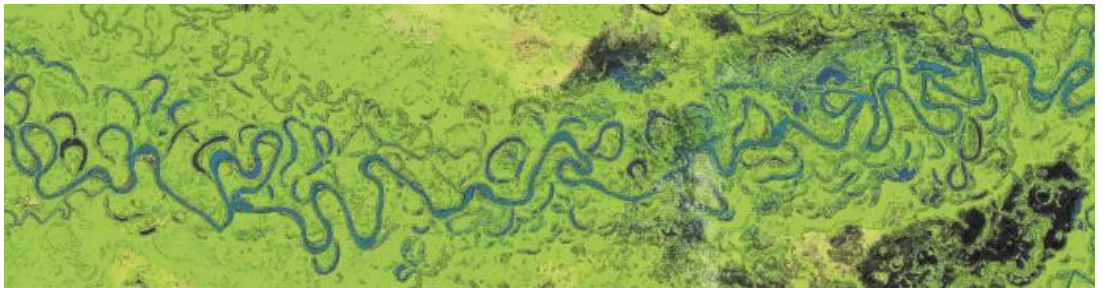
6. Overview

This thesis has considered the significance of externally-imposed sediment supplies on the evolution of single-thread meandering rivers and subsequent floodplain habitat creation. It is clear from the results I have presented in chapters 3, 4 and 5 that there is indeed a relationship between the availability of sediment and the rates at which floodplain material is overturned to produce renewed floodplain growth. In relation to the three sub-hypotheses stated in chapter 1 I have found the following:

Chapter 3

Externally imposed sediment supplies cause increased rates of channel migration and trigger more frequent cutoff events which help to maintain a steady-state sinuosity through time.

Chapter 4

Meander migration and channel sinuosity develop coevally in that greater rates of the former produce larger increases in the latter. This process is complicated by mechanisms of meander growth.

Chapter 5

Increasing the in-channel sediment load causes enhanced sediment deposition at the head of the point bar and is linked to accelerated rates of meander migration at the opposite bank.

6.1 Thesis Summary

A considerable proportion of the results from this thesis have been extracted from the Amazon Basin, effectively the world's largest outdoor laboratory. Multispectral Landsat imagery afforded me the fortune of extracting information regarding the change in position of a number of freely-meandering rivers from across the basin. Exploiting the large database of imagery between the early 1980s and the present, allowed me to accurately monitor channel change. This thesis identifies a number of hitherto poorly explored process linkages between externally-imposed sediment supplies (i.e., driven by climate, tectonism or land use change) and channel dynamism demonstrated to be manifested through point bar growth. The conclusions outlined below contribute further understanding to the complex interconnected processes that are manifested over short timescales on meandering rivers, but are driven by long-term changes of climate and landscape evolution.

Sediment is an inherent component of meandering channel systems across the world and has the potential to transform the state of systems from relatively stable to highly dynamic under the right conditions. I have demonstrated that rivers characterised by high sediment supplies – that is, where sediment supply is larger than sediment export – can increase the extent of their bedforms through sediment sequestration. The channel responds to this increase in bed storage by increasing the lateral export of fluid momentum, through increased channel curvature, and topographic accelerations, which effectively increases the boundary shear stresses at the outer bank, and accelerates bank erosion. This process is sensitive to both sediment availability, discharge magnitude, and the composition of the alluvial material in the channel. The latter component is important for the construction of point bars, which rely on shoaling-induced deposition and lateral sediment export at the channel bed to build the bar vertically and in the downstream direction.

6.2 Executive Chapter Summaries

6.2.1 Chapter 3 - Do externally imposed sediment supplies influence channel dynamism?

It was demonstrated that annually-averaged rates of channel migration can be explained, at least in part, by the relative abundance of sediment in the river. The Amazon is characterised by rivers draining exceptionally different physiographies: some regions are old and highly weathered, no longer supplying large amounts of sediment to the rivers draining their landscapes ($\sim$ <1 mt yr^{-1}). Other regions, particularly the geologically immature Andes, are denuding rapidly and supply large volumes of alluvium ($\sim$ 100 Mt yr^{-1}) to the rivers that traverse them (Aalto et al., 2006; Guyot et al., 1996). The results demonstrate that in rivers with high sediment loads (where total suspended sediment load (TSS) was used as a proxy for bedload material) the rate of meander migration was, on average, between 4.54 and 5.54 times greater on sediment-rich rivers than those draining the Central Trough or Shield. Likewise, rivers draining the Andes-Foreland Basin demonstrated many more incidences of channel cutoff (neck or chute) over the observation period than regions characterised by lower sediment fluxes. Cutoff rates (number of cutoffs, per year, per length of channel), were calculated to be 50 times lower for rivers in the Shields when compared to reaches in the Andes-Foreland Basin. The cutoff mechanisms were shown to be equally distributed between chute and neck, although some of the more sinuous rivers (Beni and Mamoré) displayed larger frequencies of neck cutoff. The significance of these observations lie in the long-term trend of channel evolution: meandering rivers continually increase their occupation within the floodplain through meander migration (Lauer and Parker, 2008). This process is limited from increasing infinitely by the formation of cutoffs, which develop as a function of floodplain conditions (e.g., antecedent moisture, topographic complexity, and material properties) and reach sinuosity (Camporeale et al., 2005; Darby et al., 2002; van Dijk

et al., 2012). In essence, the results demonstrate the inherent self-organisation of meandering rivers where they compensate for continued channel elongation by periodically severing lengths of channel from active service. An assessment of the long-term sinuosity (over ~25 years) revealed that, with very few exceptions, channel sinuosity remained constant, varying by ±7%. A survey of each of the study reach's floodplains for the presence of oxbow lakes supported the notion that the most mobile rivers generate larger numbers of cutoffs to maintain steady-state sinuosity. Examining the confluence between the Rio Grande and the Rio Mamoré revealed that migration rates increase by 69% following a 530% increase in sediment load (13 Mt yr^{-1} to 82 Mt yr^{-1}). I posited that this linkage is achieved through sediment sequestration on point bars, which appear larger downstream of this confluence from satellite imagery.

6.2.2 Chapter 4 – How are meander migration and sinuosity related, and how do external sediment supplies contribute to this process?

A combination of high-temporally (annual) and low-temporally (decadal) resolved satellite imagery to quantify the relationship between meander migration and sinuosity development across the Amazon Basin. Although it is widely accepted that the meandering process acts to increase the channel length (e.g., Constantine and Dunne, 2008; Lauer and Parker, 2008), it has yet to be quantified and evaluated with an emphasis on sediment supply. I developed a semi-automated method of extracting channel centrelines from satellite imagery, which were subsequently used to calculate reach-averaged channel migration rates. Changes in channel length were also calculated to deduce how length varied as a function of migration rate. To minimise complexity Cutoff-bearing reaches were omitted from the annual dataset so as to resolve only positive changes in length. The two parameters were found to be positively correlated, although the range of sinuosity changes for migration rates was quite large, which warranted further exploration of the variables. I developed an index for characterising the predominant direction in which the meander evolves based on the broad classification of Hooke (1984): the meander symmetry index (σ) describes how erosion is partitioned between the two halves of the meander about the apex and bounded by the inflection points. This metric was applied to the reaches to reveal that downstream-translating meanders lengthen more quickly than those that extend normal to the channel direction, and those that translate upstream. The mechanistic reason for this lies in the ability of point bars to sequester material being transported through the channel. Rivers carrying higher sediment loads are able to deposit more material in the lee of the bar as the flow shoals and moves outwards: inward moving near-bed flows also transfer eroded material to the downstream part of the bar, where it continues to grow downstream (Braudrick et al., 2009). Observations made in chapter 3 support the notion that larger point bars develop where an adequate supply

of bed material is inferred. Larger point bars have been associated with greater rates of lateral migration and channel scour (Abad and Garcia, 2009b; Constantine et al., 2014; Dunne et al., 2010), which I have demonstrated to be true. The novel finding in this study was that the position of these barforms are clearly important in determining the predominant direction of meander deformation, which in turn, regulates the rate of sinuosity growth. The position of point bars is clearly important for the long-term planimetric evolution of the channel, since bars have the ability to increase local centreline curvature and therefore outwardly-displace flow momentum, which is a principle driver of bank erosion (Dietrich et al., 1979; Hickin and Nanson, 1975). These results suggested that the enhanced construction of point bars have a number of consequences which will be discussed in the latter half of this chapter.

6.2.3 Chapter 5 – What is the mechanistic relationship between external sediment supplies, point bar deposition, and meander migration?

A 2D morphodynamic flow model was used to understand how a meander bend responded to increased sediment supplies, and particularly, whether this excess material was sequestered by the bar, or remains in the deeper portion of the channel or was exported downstream. I used real bathymetric data for a meander bend on the Sacramento River, USA, appended with an artificial inclined ramp to adjust sediment supplies to the reach in order to assess how the bathymetry and channel planform evolved over a 10-year period. The results suggested that for increases in sediment supply – accomplished by adjusting the slope of the entrance ramp – sediment would be deposited at the head of the point bar, increasing its longitudinal extent. The greatest increase in bar extent occurred where the sediment load was greatest (0.17 Mt yr^{-1}). The increase in bar area caused a coeval increase in rates of bank erosion at the outer bank. Moreover, the distance over which bank erosion took place along the outer bank was increased for the high sediment simulations. An examination of the shear stress distribution in the channel revealed that discharge was pivotal in determining stress maxima, and also the location at which the maximum stresses were focused. Higher discharges increased the boundary shear stresses and the extent of the maxima at the bank; this pattern is widely reported in the literature (e.g., Legleiter et al. 2011).

The upstream growth of the bar is contrary to the observations of point bar growth in both natural rivers and experiment ones (e.g., Braudrick et al., 2009; Dietrich and Smith, 1984; van de Lageweg et al., 2014), which typically grow downstream. The upstream growth of the point bar in these simulations was due to the coarse bedload and the absence of suspended sediment modelling: failure to model suspended sediment transport reduced sediment transport over the bar surface, which when the

material is deposited, raises the vertical elevation of the bar. Because the bedload was coarse (13.5 mm), and subjected to low flow velocities in the proximity of the bar head, the material was deposited with little transport over the surface of the bar. The absence of sediment delivery to the downstream end of the bar may be a function of the coarse bedload, steep transverse slopes, the channel not being long enough, or a combination of the three. Had the channel being longer, helical flow may have developed more strongly downstream and been more competent to transport bed material across the channel to the downstream margin of the bar.

The findings provide insights into the functioning of meandering channels under enhanced sediment supplies and suggest that the grain size distribution is an important consideration for the development of bedforms, and planform evolution, through time. This may be of particular significance in the future where drainage basins experience greater fluxes of sediment from the landscape to river channels in response to changing land use patterns and changes in climate.

6.3 Significance and wider implications

Fluvial geomorphologists have long-debated the cause and controls on meandering channel evolution with early theories dating back to Einstein (1926). As a community, authors have described the significance of curvature (e.g., Hickin and Nanson, 1975) – arguably the most important driver in meandering – as well as the role of discharge, vegetation density and floodplain bank composition (e.g., Allmendinger et al., 2005; Einstein, 1926; Gautier et al., 2007; Lazarus and Constantine, 2013; Thorne, 1982). What this thesis attempted to quantify was the effect of external sediment supplies on the planimetric evolution of meandering channels, not a novel idea, but a very important one. Although the supply and transport of alluvium is a common characteristic of meandering rivers, an understanding of how this material interacts with the surrounding flow is rather primitive. Early workers demonstrated a link between the emergence of point bars and the mobility of the channel (Lewin, 1976), as well as the influence of point bars on the force balance operating in the bends (Dietrich and Smith, 1983). Following this early work, the question of how a meandering system may respond to changes in sediment supply became somewhat dormant. Recently, experimental work trying to quantify this question has produced mixed results warranting further investigation over larger areas and longer timescales (Dunne et al., 2010; van de Lageweg et al., 2014). Using the Amazon as a test site, where sediment supplies differ on a regional scale, we were able to establish that where more sediment is found, greater mobility and dynamism was observed; this is in accordance with previous observations (Dunne et al., 2010; Wickert et al., 2013). The significance of increasing dynamism in sediment-rich environments can be addressed from several perspectives:

1) *Changes in climate and land use* – Observations of global air and ocean temperatures has revealed the unprecedented rise in temperature since the onset of combustible fossil fuels (ca. 1880) (Mann et al., 1999), with many

studies documenting the impacts of these changes on the planet (e.g., Riebesell et al., 2000). It has been suggested that the regional distribution of rainfall will be altered under a changing climate, with some areas likely to experience greater rainfall and others to receive less (IPCC, 2013). Additionally, the intensity of rainfall is predicted to also become more variable (Kendon et al., 2014), with more intense storms associated with climatic anomalies becoming more frequent. This is not true of everywhere, and has not been verified for the Amazon where extreme weather events are often linked to quasi-periodic atmospheric anomalies (e.g., ENSO) (Marengo et al., 2012). It is plausible to suggest that areas subjected to increased precipitation, be it in tropical or temperate landscapes, will likely experience increased rates of erosion, either through accelerated rates of weathering, or by physical entrainment (Knighton, 1998) or mass movement (Stoffel et al., 2014). In tropical environments where the geology permits, increased chemical weathering will prevail (Stallard, 1988); in colder environments, the impact of physical weathering will become more important (e.g., Hales and Roering, 2009; Matsuoka, 2008). The aforementioned erosional mechanisms increase the opportunity for enhanced sediment delivery to river systems, which after the findings of this thesis suggest there is potential for increased changes in planform structure. Areas affected by landsliding, either climatically- or tectonically-induced, have the aptitude to deliver vast volumes of alluvium to river channels which requires subsequent dispersion to facilitate the development of an equilibrium channel environment (Benda and Dunne, 1997; Dadson et al., 2004). These large additions of sediment may also increase the likelihood of overbank floods which may lead to cutoff development as the sediment transport capacity diminishes (Lane et al., 2007); this may pose a threat to floodplain infrastructure, encourage the

initiation of river avulsions, and control patterns of floodplain deposition (Edmonds et al., 2016; Lewin et al., 2016; Slingerland and Smith, 1998) . Changes to land use can also cause significant increases in sediment delivery to river channels: unconsolidated material is mobilised by overland flow where little vegetation is available to intercept the incoming rainfall or retard flow velocities at the surface (Boardman, 2015; Marshall et al., 2014; Rominger et al., 2010). As discussed above, if more intense storms arise with a changing climate, the likelihood of overland flow in poorly vegetated landscapes will increase (Walling, 2006). Deforestation along the Araguaia River, Brazil, increased sediment loads to the channel by an estimated 233 megatons (Mt) emphasising the rapid short-term response of the river to Anthropogenically-enhanced sediment loading (Latrubesse et al., 2009). Prolonged sediment loading could transform the river's channel pattern from one type to another as the conditions required for effective sediment transport are not satisfied (Kleinhans, 2010).

2) *Stratigraphy* – The stratigraphic record grants geologists an insight into the past where inferences can be made about the earth surface conditions at the time. Understanding the present-day functioning of meandering river systems is important for interpreting historical sequences of sediment and making inferences as to the conditions responsible for the development of the stratigraphy. The results presented in chapter 4 suggest that different stratigraphic sequences, associated with point bar development, may arise depending on the relative sediment abundance in the river. These findings have implications for preserved sequences in the rock record where channel skewing may be representative of high-sediment systems, in which point bars were growing rapidly, and distorting the development of the bend. Authors often use preserved scroll bar complexes as a method of tracking historic meander migration across the floodplain (Durkin and Hubbard, 2016; Hickin

174

and Nanson, 1975; Jackson, 1976; Nanson, 1980; Russell, 2016), so explanations for differing rates of migration may be linked back to the mechanism of bend migration, and possible sediment loading conditions in the channel during that time. Indeed, the preservation of these facies is precluded by migration of the channel into the floodplain (Jackson, 1976) – which, as established in chapter 3, is more frequent in sediment-rich rivers. Therefore, it may be posited that systems characterised by poor preservation were more dynamic and perhaps indicative of systems with large sediment supplies.

Changes in alluvial architecture may have important implications for hydrocarbon reservoir potential. The alternating sequences of sand and mud characteristic of point bars and regions of fine sediment deposition in the floodplain serve as ideal hydrocarbon reservoirs (Berg, 1968). Fine material, deposited in the swales of point bars, forms impermeable caps preventing fluid migration, while the coarser grained sands comprising the bars allow for connectivity between bars in both the vertical and horizontal dimension. The added complexity introduced by infilled oxbow lakes – by fine material – also creates impermeable lenses that help isolate hydrocarbon prospects (Berg, 1968). Understanding the formation of these deposits is important for assessing their connectivity and therefore their reservoir potential (Davies et al., 1993). Knowledge of the dimensions and sinuosities of channels is useful for ascertaining the likely depth and continuity of hydrocarbons, which is essential for determining the financial viability of any project. Rivers with high sinuosities have been observed to construct point bars with larger extents, therefore increasing the potential reservoir size (Berg, 1968; Davies et al., 1993; Donselaar and Overeem, 2008). Moreover, highly dynamic rivers are likely to create complex floodplain stratigraphy with the potential for large

areas of connectivity and reservoir preservation where deposits are not frequently reworked by channel migration (e.g., large-scale channel avulsions) (Davies et al., 1993).

3) *Risk management* – Given the mobility of meandering rivers, it is pertinent to understand how these rivers change through time so as to make predictions for both reasons of safety and cost. The results presented in this thesis reinforce the requirement for an extensive understanding of the effect external conditions can have on planimetric channel changes. Our findings in chapter 4 suggest that the sediment flux characteristics of the river dictate the mechanisms by which meanders erode, and as such, require careful consideration when siting floodplain infrastructure, so as to limit damage losses (Bracic et al., 2014; Gilvear et al., 2000). Understanding how the mobility of river channels changes dependent upon sediment loading is important more broadly since we demonstrated (chapter 3) that the rates of floodplain material cycling are higher where migration rates and sediment supplies are greater. Moreover, the exceptional mobility of these rivers is likely to create more open water bodies (oxbow lakes) in the floodplains where it will be difficult to develop infrastructure.

Piegay et al. (2005) describe the ecological as well as economic benefits of allowing bank erosion and lateral migration to occur in place of hard engineering strategies. By creating erodible river corridors, the river is permitted to erode into the banks generating sediment and creating new floodplain habitats; this returns valuable habitat to the area serving as an ecosystem service (Piégay et al., 2005). The issue that arises with natural management strategies is the uptake by landowners who do not see a direct benefit from land loss and floodplain habitat creation. Improved education of the benefits of natural techniques such as the erodible river corridor alongside

more classic hard engineering strategies as well as the cost benefit associated with a nested management approach could see more widespread uptake of these schemes.

4) *Floodplain development, organic carbon and nutrient cycling* – One of the key functions meandering rivers provide is their ability to reorganise alluvial material. As meanders migrate, they extract older, stored material from the floodplain and redistribute it through the channel to create new, topographically lower floodplain surfaces at the inner bank (i.e., point bars) (Lauer and Parker, 2008). This inherent reorganisation of alluvial material also transforms the distribution of riparian species often transforming regions of low diversity into areas of high diversity as pioneer species replace mature ones (Salo et al., 1986). The constant removal of bank material and overriding vegetation delivers large quantities of organic carbon to meandering systems where it has been posited that they contribute a considerable flux to the atmosphere through biogenic metabolism (Aufdenkampe et al., 2011; Butman and Raymond, 2011; Mayorga et al., 2005; Ward et al., 2013). Although a large proportion of the organic material exported to river systems is young in age (< 5 years old), the recruitment of older floodplain sediments can also extract carbon up to 10,000 years old (Mayorga et al., 2005). Highly mobile rivers like those located in the Andes-Foreland Basin are capable of mobilising vast amounts of organic material as they excavate large areas of the floodplain over short timescales. Quicker rates of floodplain recycling will increase the net export of organic carbon to the river channel, which can undergo biodegradation and increase carbon dioxide (CO_2) emissions to the atmosphere (Ward et al., 2013). Alternatively, if rates of migration are high, the time for sufficiently large pools of organic carbon to develop in the floodplain will be reduced, therefore not necessarily increasing the volume of organic carbon exported to the channel. The degree to which rivers contribute

to atmospheric CO_2 budgets will depend on three main factors: 1) the rate at which floodplain material is eroded as set by the dynamism of the river (to some extent forced by the sediment load of the river); 2) the composition and density of floodplain vegetation, and; 3) the capacity for organic macromolecules to be degraded during downstream transport. A comprehensive understanding of meandering dynamics, in particularly vegetation-rich catchments, is required to make realistic estimates of river system contributions to local – and global – carbon budgets.

Unprecedented mining practices have had a marked influence on river channels across the planet with large amounts of contaminated sediment being directly discharged into these alluvial systems (Grayson and Plater, 2009; Pearson and Hanes, 2016; Pizzuto, 2014). Contaminants are transported by adsorption on to fine-grained sediments (e.g., clays), where they can be deposited in the floodplain during overbank floods or remain in the channel bed for up to a century or more (Terezinha Costa et al., 2006; Walling et al., 2003). Floodplain surfaces and oxbow likes are ideal sites for pollutant sequestration since they cause rapid deceleration to sediment-laden flood waters which promotes their deposition. This process has both positive and negative aspects associated with it: where floodplains remain pristine (i.e., devoid of human interference), contaminant storage effectively filters harmful molecules from the river, thereby improving downstream water quality. In situations where floodplain disturbance is expected – due to farming, land conversion, or infrastructure development – contaminant remobilisation could have detrimental consequences for those using the land, or by creating a mechanism by which contaminants are returned to the river. In dynamic river systems that constantly rework the floodplain, the potential for contaminant remobilisation will increase. This will be of concern for rivers with a history of mine workings.

Long-term floodplain development relies on the interactions between water and sediment as they are routed through the channel. The timing and magnitude of overbank flows controls the rate of vertical floodplain accretion and also creates a mechanism by which floodplain complexity can be smoothed (infilling swales and oxbow lakes) (Aalto et al., 2003; Shen et al., 2015; Wolman and Leopold, 1957). Meander migration forms the counteracting process that increases floodplain heterogeneity and complexity (Constantine et al., 2014; Lewin and Ashworth, 2014; van Dijk et al., 2012). The results presented in chapter 3 showed that rivers with high sediment loads were more proficient at both migrating and creating oxbow lakes to maintain a steady-state sinuosity through time. Therefore, if this observation is extrapolated to other highly dynamic river systems (e.g., Strickland River, Papua New Guinea) it can be expected that floodplain complexity and diversity will be greater; this may be an important consideration ecologically and societally as the world's wetlands are exposed to greater anthropogenic pressures (Tockner and Stanford, 2002).

5) *Numerical models* – The majority of morphodynamic flow models have adopted the classic curvature-velocity-driven meander migration model after the pioneering work of Ikeda (1981) and Parker (1982) among others (see references therein). Although this model makes good long-term predictions of migration and channel change (e.g., Sun et al. 2001), the theory underpinning the linear model of meander migration is not accurate. The work of Parker et al. (2011) and others has improved the theoretical structure of these models (as discussed in the introduction of chapter 5), but further insights into the link between sediment supplies and channel bedforms and their relation to planimetric changes will further improve them further. The results presented in this thesis add further knowledge to the theory describing how point bars affect processes of meander migration and floodplain habitat development.

These contributions offer further information to model developers who continue to constrain the many controls affecting the evolution of meandering channels (e.g., (Eke et al., 2014a)). In particular, the grain size distributions and bank erodibility are of importance in the context of this thesis since these two factors control the development of bedforms (i.e., point bars) and permit the excavation of sediment from the river bank, thereby determining planform reconfigurations. The results from chapter 5, suggest that where only bedload is present, point bars may be unable to accomplish downstream growth, but still manipulate the flow-field and increase rates of bank erosion.

6.4 Future Research Directions

The findings from this research stimulate a number of logical future research directions that require further attention. First, the development of a physical model in which sediment fluxes are altered in a realistic flume setting should be trialled. A number of workers (e.g., Braudrick, 2013; van de Lageweg et al., 2014) have already conducted experiments explicitly examining the effect of enhanced sediment loads on point bar evolution and channel change, but have a number of limitations associated with them. The development of a model in which the banks contain enough stability to permit steady meandering without avulsion or transitioning to a braided channel is desirable, although this has been reported as being very difficult to attain (Braudrick, 2013). The generation of realistic meandering systems in flume environments often require fixed walls, thus complicating the examination of the bar-push, bank-pull question. Further refinements to these models (e.g., flow variability and floodplain structure) may permit the development of representative rivers in which sediment variability can be examined with regards channel mobility and bar growth.

A field campaign conducted in mobile sand-bedded rivers such as those in the Amazon would assist in quantifying the contributions of barforms to both the force balance (after Dietrich and Smith (1983) and Legleiter et al. (2011)), and to near-bank

sediment excavation and point bar aggradation. Trying to quantify point bar accumulation rates would be logistically complex; although repeat low water high-resolution surveys (acquired by drone and laser scanner) may yield data to support the hypotheses and empirical evidence presented in this thesis. The rapid mobility of Andes-Foreland Basin rivers makes them ideal candidates for these experiments as they should display the most change over shorter timescales. To fully verify the findings described in this thesis, surveying of rivers from each of the physiographic provinces should be conducted; although, again, the logistical complexity of such a campaign would make it difficult to implement.

The data for the Amazon yielded several interesting future questions with regards responses to the installation of hydroelectric dams, particularly along the most dynamic rivers in the Andes region. Our results suggest that river network fragmentation should reduce dynamism downstream due to the restricted flow of sediment. A study examining whether these changes in dynamism can be detected and over what timescales following installation would further test the hypothesis of sediment-driven meander migration and guide future decision makers. Moreover, the reduced downstream sediment and discharge supplies should have detrimental effects on floodplain habitat development for two reasons: first, reduced dynamism will prevent sinuosity increases and therefore reduce the likelihood of cutoff formation, which will limit floodplain complexity and oxbow lake creation. Second, with a reduced sediment and water supply, overbank flow frequencies will decrease, potentially increasing the persistence of open water bodies and reducing floodplain species richness due to diminished nutrient fluxes. Reduced habitat renewal will also reduce the value and quality of river corridors.

An interesting finding from chapter 4 was the relationship between meander deformation, sediment flux, and sinuosity growth. The theory of resonance described extensively by Zolezzi and Seminara (2001) and Seminara et al. (2001) (and others)

is an area with which I believe the metrics defined in chapter 4 (extension and translation) could be used to explore this theory in more detail. Examining channel width and curvature relationships with respect to the types of meander translation could help reconcile resonance theory with observational data.

7. References

Aalto, R., Dunne, T., Guyot, J.L., 2006. Geomorphic controls on andean denudation rates. The Journal of Geology, 114(1), 85-99.

Aalto, R., Maurice-Bourgoin, L., Dunne, T., Montgomery, D.R., Nittrouer, C.A., Guyot, J.-L., 2003. Episodic sediment accumulation on Amazonian flood plains influenced by El Nino/Southern Oscillation. Nature, 425(6957), 493-497.

Aalto, R., Nittrouer, C.A., 2012. 210Pb geochronology of flood events in large tropical river systems. Philosophical Transactions of the Royal Society A: Mathematical, 				Physical and Engineering Sciences, 370(1966), 2040-2074.

Abad, J.D., Garcia, M.H., 2009a. Experiments in a high-amplitude Kinoshita meandering channel: 1. Implications of bend orientation on mean and turbulent flow structure. Water Resources Research, 45(2).

Abad, J.D., Garcia, M.H., 2009b. Experiments in a high-amplitude Kinoshita meandering channel: 2. Implications of bend orientation on bed morphodynamics. Water Resources Research, 45(2), n/a-n/a.

Abad, J.D., Garcia, M.H., 2009c. Experiments in a high-amplitude Kinoshita meandering channel: 2. Implications of bend orientation on bed morphodynamics. Water Resources Research, 45(2).

Abernethy, B., Rutherfurd, I.D., 1998. Where along a river's length will vegetation most effectively stabilise stream banks? Geomorphology, 23(1), 55-75.

Ahmed, J., Constantine, J.A., Dunne, T., Hales, T.C., In review. Point bars in the evolution of channel sinuosity in the Amazon Basin.

Allen, J.R.L., 1965. A review of the origin and characteristics of recent alluvial sediments. Sedimentology, 5(2), 89-191.

Allison, M.A., Nittrouer, C.A., Faria Jr, L.E.C., 1995. Rates and mechanisms of shoreface progradation and retreat downdrift of the Amazon river mouth. Marine Geology, 125(3–4), 373-392.

Allmendinger, N.E., Pizzuto, J.E., Potter, N., Johnson, T.E., Hession, W.C., 2005. The influence of riparian vegetation on stream width, eastern Pennsylvania, USA. Geological Society of America Bulletin, 117(1-2), 229-243.

Alsdorf, D., Bates, P., Melack, J., Wilson, M., Dunne, T., 2007. Spatial and temporal complexity of the Amazon flood measured from space. Geophysical Research Letters, 34(8), n/a-n/a.

Alsdorf, D., Han, S.-C., Bates, P., Melack, J., 2010. Seasonal water storage on the Amazon floodplain measured from satellites. Remote Sens. Environ., 114(11), 2448-2456.

Archer, A.W., 2005. Review of Amazonian Depositional Systems, Fluvial Sedimentology VII. Blackwell Publishing Ltd., pp. 17-39.

Armijos, E., Crave, A., Vauchel, P., Fraizy, P., Santini, W., Moquet, J.-S., Arevalo, N., Carranza, J., Guyot, J.-L., 2013. Suspended sediment dynamics in the Amazon River of Peru. Journal of South American Earth Sciences, 44(0), 75-84.

Asahi, K., Shimizu, Y., Nelson, J., Parker, G., 2013. Numerical simulation of river meandering with self-evolving banks. Journal of Geophysical Research: Earth Surface, 118(4), 2013JF002752.

Aufdenkampe, A.K., Hedges, J.I., Richey, J.E., Krusche, A.V., Llerena, C.A., 2001. Sorptive fractionation of dissolved organic nitrogen and amino acids onto fine sediments within the Amazon Basin. Limnology And Oceanography, 46(8), 1921-1935.

Aufdenkampe, A.K., Mayorga, E., Raymond, P.A., Melack, J.M., Doney, S.C., Alin, S.R., Aalto, R.E., Yoo, K., 2011. Riverine coupling of biogeochemical cycles

between land, oceans, and atmosphere. Frontiers in Ecology and the Environment, 9(1), 53-60.

Baby, P., Guyot, J.L., Hérail, G., 2009. Tectonic control of erosion and sedimentation in the Amazon Basin of Bolivia. Hydrological Processes, 23(22), 3225-3229.

Barke, R., Lamb, S., MacNiocaill, C., 2007. Late Cenozoic bending of the Bolivian Andes: New paleomagnetic and kinematic constraints. Journal of Geophysical Research: Solid Earth, 112(B1), n/a-n/a.

Barry, R.G., Chorley, R.J., 2010. Atmosphere, Weather and Climate. Routledge.

Bathurst, J.C., Thorne, C.R., Hey, R.D., 1977. Direct measurements of secondary currents in river bends. Nature, 269(5628), 504-506.

Benda, L., Dunne, T., 1997. Stochastic forcing of sediment supply to channel networks from landsliding and debris flow. Water Resources Research, 33(12), 2849-2863.

Berg, R.R., 1968. Point-bar origin of Fall River Sandstone reservoirs, northeastern Wyoming. AAPG Bull., 52(11 Part 1), 2116.

Bettess, R., White, W.R., 1983. Meandering and braiding of alluvial channels. Institution of Civil Engineers Proceedings, 75(3), 525-538.

Bishop, P., Hoey, T.B., Jansen, J.D., Artza, I.L., 2005. Knickpoint recession rate and catchment area: the case of uplifted rivers in Eastern Scotland. Earth Surface Processes and Landforms, 30(6), 767-778.

Blondeaux, P., Seminara, G., 1985. A unified bar-bend theory of river meanders. Journal of Fluid Mechanics, 157, 449-470.

Bluck, B.J., 1971. Sedimentation in the meandering River Endrick. Scot. J. Geol., 7(2), 93-138.

Bluck, B.J., 1982. Texture of gravel bars in braided streams In: R.D. Hey, J.C. Bathurst, C.R. Thorne (Eds.), Gravel-bed rivers. John Wiley & Sons, Chichester, pp. 339-355.

Blum, M.D., Roberts, H.H., 2009. Drowning of the Mississippi Delta due to insufficient sediment supply and global sea-level rise. Nature Geosci, 2(7), 488-491.

Boardman, J., 2015. Extreme rainfall and its impact on cultivated landscapes with particular reference to Britain. Earth Surface Processes and Landforms, 40(15), 2121-2130.

Bolla Pittaluga, M., Nobile, G., Seminara, G., 2009. A nonlinear model for river meandering. Water Resources Research, 45(4), n/a-n/a.

Bookhagen, B., Strecker, M.R., 2010. Modern Andean Rainfall Variation during ENSO Cycles and its Impact on the Amazon Drainage Basin, Amazonia: Landscape and Species Evolution. Wiley-Blackwell Publishing Ltd., pp. 223-241.

Bracic, J.J., Malcovish, C., Yaremko, E., 2014. Risk Management for Lateral Channel Movement at Pipeline Water Crossings. (46100), V001T004A012.

Braudrick, C.A., 2013. Meandering in gravel-bed rivers. Doctor of Philosophy, University of California, Berkeley, California, 208 pp.

Braudrick, C.A., 2016. Response of a fixed sinuous channel to a doubling of sediment supply, AGU Fall Meeting 2016. American Geophysical Union, San Francisco, CA.

Braudrick, C.A., Dietrich, W.E., Leverich, G.T., Sklar, L.S., 2009. Experimental evidence for the conditions necessary to sustain meandering in coarse-bedded rivers. Proceedings of the National Academy of Sciences.

Brice, J.C., 1964. Channel patterns and terraces of the Loup Rivers in Nebraska. U.S. Geological Survey profession paper 422-D, 1-41.

Brice, J.C., 1974. Evolution of Meander Loops. Geological Society of America Bulletin, 85(4), 581-586.

Bridge, J.S., 1993. The interaction between channel geometry, water flow, sediment transport and deposition in braided rivers In: J.L. Best, C.S. Bristow (Eds.), Geol. Soc. Spec. Pub., pp. 13-73.

Buer, K., 1994. Sacramento River bank erosion memorandum progress report: Red Bluff, California Department of Water Resources, Northern District, California.

Buer, K., Forwalter, D., Kissel, M., Stohler, B., 1989. The middle Sacramento River: human impacts on physical and ecological processes along a meandering river, USDA Forest Service General Technical Report, Berkeley, California.

Butman, D., Raymond, P.A., 2011. Significant efflux of carbon dioxide from streams and rivers in the United States. Nature Geosci, 4(12), 839-842.

Camporeale, C., Perona, P., Porporato, A., Ridolfi, L., 2005. On the long-term behavior of meandering rivers. Water Resour. Res., 41(12), W12403.

Camporeale, C., Perucca, E., Ridolfi, L., Gurnell, A.M., 2013. Modeling the interactions between river morphodynamics and riparian vegetation. Reviews of Geophysics, 51(3), 379-414.

Capitanio, F.A., Faccenna, C., Zlotnik, S., Stegman, D.R., 2011. Subduction dynamics and the origin of Andean orogeny and the Bolivian orocline. Nature, 480(7375), 83-86.

Caputo, M.V., 1991. Solimões megashear: Intraplate tectonics in northwestern Brazil. Geology, 19(3), 246-249.

Carling, P.A., 1991. An appraisal of the velocity-reversal hypothesis for stable pool-riffle sequences in the river severn, England. Earth Surface Processes and Landforms, 16(1), 19-31.

Chang, H.H., 1979. Minimum stream power and river channel patterns. Journal of Hydrology, 41(3–4), 303-327.

Church, M., 2006. Bed material transport and the morphology of alluvial river channels. Annual Review of Earth and Planetary Sciences, 34(1), 325-354.

Coe, M.T., Costa, M.H., Soares-Filho, B.S., 2009. The influence of historical and potential future deforestation on the stream flow of the Amazon River – Land surface processes and atmospheric feedbacks. Journal of Hydrology, 369(1), 165-174.

Coe, M.T., Latrubesse, E.M., Ferreira, M.E., Amsler, M.L., 2011. The effects of deforestation and climate variability on the streamflow of the Araguaia River, Brazil. Biogeochemistry, 105(1), 119-131.

Colombini, M., Tubino, M., Whiting, P., 1992. Topographic expressions of bars in meandering channels. In: P. Billi, R.D. Hey, C.R. Thorne, P. Tacconi (Eds.), Dynamics of Gravel-bed Rivers. John Wiley & Sons, pp. 457-474.

Constantine, C.R., 2006. Quantifying the connections between flow, bar deposition, and meander migration in large gravel-bed rivers, University of California, Santa Barbara, 191 pp.

Constantine, C.R., Dunne, T., Hanson, G.J., 2009. Examining the physical meaning of the bank erosion coefficient used in meander migration modeling. Geomorphology, 106(3-4), 242-252.

Constantine, J.A., Dieras, P.L., Hales, T.C., Piegay, H., In Review. The Fate of Oxbow Lakes as Determined by Mechanisms of Meander Cutoff.

Constantine, J.A., Dunne, T., 2008. Meander cutoff and the controls on the production of oxbow lakes. Geology, 36(1), 23-26.

Constantine, J.A., Dunne, T., Ahmed, J., Legleiter, C., Lazarus, E.D., 2014. Sediment supply as a driver of river meandering and floodplain evolution in the Amazon Basin. Nature Geosci, 7(12), 899-903.

Constantine, J.A., Dunne, T., Piégay, H., Mathias Kondolf, G., 2010a. Controls on the alluviation of oxbow lakes by bed-material load along the Sacramento River, California. Sedimentology, 57(2), 389-407.

Constantine, J.A., McLean, S.R., Dunne, T., 2010b. A mechanism of chute cutoff along large meandering rivers with uniform floodplain topography. Geological Society of America Bulletin, 122(5-6), 855-869.

Cook, K.L., Turowski, J.M., Hovius, N., 2013. A demonstration of the importance of bedload transport for fluvial bedrock erosion and knickpoint propagation. Earth Surface Processes and Landforms, 38(7), 683-695.

Costa, M.H., Foley, J.A., 1999. Trends in the hydrologic cycle of the Amazon basin. J. Geophys. Res., 104(D12), 14189-14198.

Costanza, R., d'Arge, R., de Groot, R., Farber, S., Grasso, M., Hannon, B., Limburg, K., Naeem, S., O'Neill, R.V., Paruelo, J., Raskin, R.G., Sutton, P., van den Belt, M., 1998. The value of the world's ecosystem services and natural capital. Ecological Economics, 25(1), 3-15.

Cox, K.G., 1989. The role of mantle plumes in the development of continental drainage patterns. Nature, 342(6252), 873-877.

Cox, P.M., Harris, P.P., Huntingford, C., Betts, R.A., Collins, M., Jones, C.D., Jupp, T.E., Marengo, J.A., Nobre, C.A., 2008. Increasing risk of Amazonian drought due to decreasing aerosol pollution. Nature, 453(7192), 212-215.

Crosby, B.T., Whipple, K.X., 2006. Knickpoint initiation and distribution within fluvial networks: 236 waterfalls in the Waipaoa River, North Island, New Zealand. Geomorphology, 82(1), 16-38.

Dadson, S.J., Hovius, N., Chen, H., Dade, W.B., Lin, J.-C., Hsu, M.-L., Lin, C.-W., Horng, M.-J., Chen, T.-C., Milliman, J., Stark, C.P., 2004. Earthquake-triggered increase in sediment delivery from an active mountain belt. Geology, 32(8), 733-736.

Damuth, J.E., Flood, R.D., Kowsmann, R.O., Belderson, R.H., Gorini, M.A., 1988. Anatomy and growth pattern of Amazon deep-sea fan as revealed by long-range side-scan sonar (GLORIA) and high-resolution seismic studies. AAPG Bull., 72(8), 885.

Daniel, J.F., 1971. Channel movement of meandering Indiana streams. United States Geological Survey Professional Paper 732, A, 17.

Darby, S.E., Alabyan, A.M., Van de Wiel, M.J., 2002. Numerical simulation of bank erosion and channel migration in meandering rivers. Water Resources Research, 38(9).

Darby, S.E., Trieu, H.Q., Carling, P.A., Sarkkula, J., Koponen, J., Kummu, M., Conlan, I., Leyland, J., 2010. A physically based model to predict hydraulic erosion of fine-grained riverbanks: The role of form roughness in limiting erosion. Journal of Geophysical Research-Earth Surface, 115.

David, S.R., Edmonds, D.A., Letsinger, S.L., 2016. Controls on the occurrence and prevalence of floodplain channels in meandering rivers. Earth Surface Processes and Landforms, n/a-n/a.

Davidson, E.A., de Araujo, A.C., Artaxo, P., Balch, J.K., Brown, I.F., C. Bustamante, M.M., Coe, M.T., DeFries, R.S., Keller, M., Longo, M., Munger, J.W., Schroeder, W., Soares-Filho, B.S., Souza, C.M., Wofsy, S.C., 2012. The Amazon basin in transition. Nature, 481(7381), 321-328.

Davies, D.K., Williams, B.P.J., Vessell, R.K., 1993. Dimensions and quality of reservoirs originating in low and high sinuosity channel systems, Lower Cretaceous Travis Peak Formation, East Texas, USA.

Decelles, P.G., Hertel, F., 1989. Petrology of fluvial sands from the Amazonian foreland basin, Peru and Bolivia. Geological Society of America Bulletin, 101(12), 1552-1562.

Dennis, I.A., Coulthard, T.J., Brewer, P., Macklin, M.G., 2009. The role of floodplains in attenuating contaminated sediment fluxes in formerly mined drainage basins. Earth Surface Processes and Landforms, 34(3), 453-466.

DHI, 2014a. MIKE 21 flow model hydodynamic module user guide. 130.

DHI, 2014b. MIKE 21C Curvilinear model for river morphology user guide. 193.

DHI, 2014c. MIKE 21C Curvilinear model scientific documentation. 112.

Dieras, P.L., Constantine, J.A., Hales, T.C., Piégay, H., Riquier, J., 2013. The role of oxbow lakes in the off-channel storage of bed material along the Ain River, France. Geomorphology(0).

Dietrich, W.E., Kirchner, J.W., Ikeda, H., Iseya, F., 1989. Sediment supply and the development of the coarse surface layer in gravel-bedded rivers. Nature, 340(6230), 215-217.

Dietrich, W.E., Smith, J.D., 1983. Influence of the point bar on flow through curved channels. Water Resources Research, 19(5), 1173-1192.

Dietrich, W.E., Smith, J.D., 1984. Bed Load Transport in a River Meander. Water Resources Research, 20(10), 1355-1380.

Dietrich, W.E., Smith, J.D., Dunne, T., 1979. Flow and Sediment Transport in a Sand Bedded Meander. The Journal of Geology, 87(3), 305-315.

Dietrich, W.E., Whiting, P., 1989. Boundary Shear Stress and Sediment Transport in River Meanders of Sand and Gravel, River Meandering. American Geophysical Union, pp. 1-50.

Donselaar, M.E., Overeem, I., 2008. Connectivity of fluvial point-bar deposits: An example from the Miocene Huesca fluvial fan, Ebro Basin, Spain. AAPG Bull., 92(9), 1109.

Dunne, T., Aalto, R.E., 2013. Large River Floodplains. In: J.F. Shroder (Ed.), Treatise on Geomorphology. Academic Press, San Diego, pp. 645-678.

Dunne, T., Constantine, J.A., Singer, M.B., 2010. The Role of Sediment Transport and Sediment Supply in the Evolution of River Channel and Floodplain Complexity. Transactions, Japanese Geomorphological Union, 31(2), 155-170.

Dunne, T., Mertes, L.A.K., Meade, R.H., Richey, J.E., Forsberg, B.R., 1998. Exchanges of sediment between the flood plain and channel of the Amazon River in Brazil. Geological Society of America Bulletin, 110(4), 450-467.

Durkin, P., Hubbard, S.M., 2016. The linkage between fluvial meander-belt morphodynamics and the depositional record improves paleoenvironmental interpretations, Western Interior Basin, Alberta, Canada, AGU Fall Meeting 2016, San Francisco.

Edmonds, D.A., Hajek, E.A., Downton, N., Bryk, A.B., 2016. Avulsion flow-path selection on rivers in foreland basins. Geology, 44(9), 695-698.

Einstein, A., 1926. Die Ursache der Mäanderbildung der Flußläufe und des sogenannten Baerschen Gesetzes. Naturwissenschaften, 14(11), 223-224.

Eke, E., Parker, G., Shimizu, Y., 2014a. Numerical modeling of erosional and depositional bank processes in migrating river bends with self-formed width: Morphodynamics of bar push and bank pull. Journal of Geophysical Research: Earth Surface, 119(7), 2013JF003020.

Eke, Esther C., Czapiga, M.J., Viparelli, E., Shimizu, Y., Imran, J., Sun, T., Parker, G., 2014b. Coevolution of width and sinuosity in meandering rivers. Journal of Fluid Mechanics, 760, 127-174.

Engel, F.L., Rhoads, B.L., 2012. Interaction among mean flow, turbulence, bed morphology, bank failures and channel planform in an evolving compound meander loop. Geomorphology, 163–164(0), 70-83.

Erskine, W., Melville, M., Page, K.J., Mowbray, P.D., 1982. Cutoff and Oxbow Lake. Australian Geographer, 15(3), 174-180.

Espinoza, J.C., Marengo, J.A., Ronchail, J., Carpio, J.M., Flores, L.N., Guyot, J.L., 2014. The extreme 2014 flood in south-western Amazon basin: the role of tropical-subtropical South Atlantic SST gradient. Environmental Research Letters, 9(12), 124007.

Fagherazzi, S., Gabet, E.J., Furbish, D.J., 2004. The effect of bidirectional flow on tidal channel planforms. Earth Surface Processes and Landforms, 29(3), 295-309.

Ferguson, R.I., Parsons, D.R., Lane, S.N., Hardy, R.J., 2003. Flow in meander bends with recirculation at the inner bank. Water Resources Research, 39(11), n/a-n/a.

Filizola, N., Guyot, J.L., 2009. Suspended sediment yields in the Amazon basin: an assessment using the Brazilian national data set. Hydrological Processes, 23(22), 3207-3215.

Finer, M., Jenkins, C.N., 2012. Proliferation of hydroelectric dams in the Andean Amazon and implications for Andes-Amazon connectivity. PLOS One, 7(4), e35126.

Fisk, H.N., 1947. Fine-grained alluvial deposits and their effects upon mississippi river activity. Waterways Experiment Station, 82.

Florsheim, J.L., Mount, J.F., Chin, A., 2008. Bank Erosion as a Desirable Attribute of Rivers. BioScience, 58(6), 519-529.

Frascati, A., Lanzoni, S., 2009. Morphodynamic regime and long-term evolution of meandering rivers. Journal of Geophysical Research: Earth Surface, 114(F2), F02002.

Frey, P., Church, M., 2009. How River Beds Move. Science, 325(5947), 1509-1510.

Frothingham, K.M., Rhoads, B.L., 2003. Three-dimensional flow structure and channel change in an asymmetrical compound meander loop, Embarras River, Illinois. Earth Surface Processes and Landforms, 28(6), 625-644.

Fryirs, K.A., Brierley, G.J., 2012. Sediment Movement and Deposition in River Systems, Geomorphic Analysis of River Systems. John Wiley & Sons, Ltd, pp. 81-115.

Furbish, D.J., 1988. River-bend curvature and migration - How are they related. Geology, 16(8), 752-755.

Furbish, D.J., 1991. Spatial autoregressive structure in meander evolution. Geological Society of America Bulletin, 103(12), 1576-1589.

Furbish, D.J., Zunka, J.P., Howell, S.M., Unpublished. Sediment conservation during river meandering, with implications for meandering behaviour. 23.

Gallen, S.F., Wegmann, K.W., Frankel, K.L., Hughes, S., Lewis, R.Q., Lyons, N., Paris, P., Ross, K., Bauer, J.B., Witt, A.C., 2011. Hillslope response to knickpoint migration in the Southern Appalachians: implications for the evolution of post-orogenic landscapes. Earth Surface Processes and Landforms, 36(9), 1254-1267.

Garcia, M., Niño, Y., 1993. Dynamics of sediment bars in straight and meandering channels: experiments on the resonance phenomenon. Journal of Hydraulic Research, 31(6), 739-761.

Gautier, E., Brunstein, D., Vauchel, P., Roulet, M., Fuertes, O., Guyot, J.L., Darozzes, J., Bourrel, L., 2007. Temporal relations between meander deformation, water discharge and sediment fluxes in the floodplain of the Rio Beni (Bolivian Amazonia). Earth Surface Processes and Landforms, 32(2), 230-248.

Gay, G.R., Gay, H.H., Gay, W.H., Martinson, H.A., Meade, R.H., Moody, J.A., 1998. Evolution of cutoffs across meander necks in Powder River, Montana, USA. Earth Surface Processes and Landforms, 23(7), 651-662.

Gerreaud, R.D., Aceituno, P., 2007. Atmospheric Circulation and Climatic Variability. In: T.T. Veblen, K.R. Young, A.R. Orme (Eds.), The Physical Geography of South America. Oxford University Press, pp. 45-59.

Gilvear, D., Winterbottom, S., Sichingabula, H., 2000. Character of channel planform change and meander development: Luangwa River, Zambia. Earth Surface Processes and Landforms, 25(4), 421-436.

Glinska-Lewczuk, K., 2005. Oxbow lakes as biogeochemical filters for nutrient outflow from agricultural areas. In: L. Heathwaite, B. Webb, D. Rosenberry, D. Weaver, M. Hayash (Eds.), Dynamics and biogeochemistry of river

corridors and wetlands. International Association of Hydrological Sciences 2005, Netherlands, pp. 55-65.

Gorycki, M.A., 1973. Hydraulic Drag: A Meander-Initiating Mechanism. Geological Society of America Bulletin, 84(1), 175-186.

Grayson, R.P., Plater, A.J., 2009. A lake sediment record of Pb mining from Ullswater, English Lake District, UK. Journal of Paleolimnology, 42(2), 183-197.

Grenfell, M., Aalto, R., Nicholas, A., 2012. Chute channel dynamics in large, sand-bed meandering rivers. Earth Surface Processes and Landforms, 37(3), 315-331.

Grenfell, M.C., Nicholas, A.P., Aalto, R., 2014. Mediative adjustment of river dynamics: The role of chute channels in tropical sand-bed meandering rivers. Sedimentary Geology, 301(0), 93-106.

Guyot, J.-L., Bazan, H., Pascal, F., Ordonez, J.J., Armijos, E., Laraque, A., 2007. Suspended sediment yields in the Amazon basin of Peru: a first estimation, Water Quality and Sediment Behaviour of the Future: Predictions for the 21st Century (Proceedings of Symposium HS2005 at IUGG2007, Perugia, July 2007). IAHS Publication.

Guyot, J.L., Bourges, J., Cortez, J., Olive, L., Loughran, R., Kesby, J., 1994. Sediment transport in the Rio Grande, an Andean river of the Bolivian Amazon drainage basin. IAHS Publications-Series of Proceedings and Reports-Intern Assoc Hydrological Sciences, 224, 223-232.

Guyot, J.L., Fillzola, N., Quintanilla, J., Cortez, J., 1996. Dissolved solids and suspended sediment yields in the Rio Madeira basin, from the Bolivian Andes to the Amazon. IAHS Publication, 55-64.

Hackney, C., Best, J., Leyland, J., Darby, S.E., Parsons, D., Aalto, R., Nicholas, A., 2015. Modulation of outer bank erosion by slump blocks: Disentangling the protective and destructive role of failed material on the three-dimensional flow structure. Geophysical Research Letters, 42(24), 10,663-610,670.

Hales, T.C., Roering, J.J., 2009. A frost "buzzsaw" mechanism for erosion of the eastern Southern Alps, New Zealand. Geomorphology, 107(3–4), 241-253.

Handy, R.L., 1972. Alluvial Cutoff Dating from Subsequent Growth of a Meander. Geological Society of America Bulletin, 83(2), 475-480.

Hasegawa, K., 1977. Computer simulation of the gradual migration of meandering channels Proceedings of the Hokkaido Branch, Japan Society of Civil Engineering (in Japanese), 197-202.

Hickin, E.J., 1969. A newly-identified process of point bar formation in natural streams. American Journal of Science, 267(8), 999-1010.

Hickin, E.J., 1974. Development of meanders in natural river-channels. American Journal of Science, 274(4), 414-442.

Hickin, E.J., Nanson, G.C., 1975. The Character of Channel Migration on the Beatton River, Northeast British Columbia, Canada. Geological Society of America Bulletin, 86(4), 487-494.

Hooke, J.M., 1977. The distribution and nature of changes in river channel patterns: The example of Devon. In: K.J. Gregory (Ed.), River channel changes. John Wiley & Sons, Chichester, pp. 265-279.

Hooke, J.M., 1979. Analysis of the processes of river bank erosion. Journal of Hydrology, 42(1-2), 39-62.

Hooke, J.M., 1984. Changes in river meanders. Progress in Physical Geography, 8(4), 473-508.

Hooke, J.M., 2004. Cutoffs galore!: occurrence and causes of multiple cutoffs on a meandering river. Geomorphology, 61(3–4), 225-238.

Hooke, J.M., 2007. Spatial variability, mechanisms and propagation of change in an active meandering river. Geomorphology, 84(3–4), 277-296.

Hooke, J.M., Harvey, A.M., 1983. Meander changes in relation to bend morphology and secondary flows. International Association for Sedimentology Special Publication, 6, 121-132.

Hooke, R.L.B., 1975. Distribution of Sediment Transport and Shear Stress in a Meander Bend. The Journal of Geology, 83(5), 543-565.

Hoorn, C., Guerrero, J., Sarmiento, G.A., Lorente, M.A., 1995. Andean tectonics as a cause for changing drainage patterns in Miocene northern South America. Geology, 23(3), 237-240.

Hoorn, C., Wesselingh, F.P., ter Steege, H., Bermudez, M.A., Mora, A., Sevink, J., Sanmartín, I., Sanchez-Meseguer, A., Anderson, C.L., Figueiredo, J.P., Jaramillo, C., Riff, D., Negri, F.R., Hooghiemstra, H., Lundberg, J., Stadler, T., Särkinen, T., Antonelli, A., 2010. Amazonia Through Time: Andean Uplift, Climate Change, Landscape Evolution, and Biodiversity. Science, 330(6006), 927-931.

Howard, A.D., 1992. Modeling channel migration and floodplain sedimentation in meandering streams. In: P.A. Carling, G.E. Petts (Eds.), Lowland floodplain rivers: Geomorphical perspectives. John Wiley & Sons Ltd, pp. 41.

Howard, A.D., 2009. How to make a meandering river. Proceedings of the National Academy of Sciences, 106(41), 17245-17246.

Howard, A.D., Knutson, T.R., 1984. Sufficient conditions for river meandering - A simulation approach. Water Resources Research, 20(11), 1659-1667.

Hudson, P.F., Kesel, R.H., 2000. Channel migration and meander-bend curvature in the lower Mississippi River prior to major human modification. Geology, 28(6), 531-534.

Ikeda, H., 1989. Sedimentary controls on channel migration and origin of point bars in sand-bedded meandering rivers. In: H. Ikeda, G. Parker (Eds.), River meandering. American Geophysical Union, Water Research Monograph, pp. 51-68.

Ikeda, S., Parker, G., Sawai, K., 1981. Bend theory of river meanders .1. Linear development. Journal of Fluid Mechanics, 112(NOV), 363-377.

IPCC, 2013. Climate Change 2013: The Physical Science Basis. Contribution of Working Group I to the Fifth Assessment Report of the Intergovernmental Panel on Climate Change, Cambridge, United Kingdom and New York, NY, USA.

Isacks, B.L., 1988. Uplift of the Central Andean Plateau and bending of the Bolivian Orocline. Journal of Geophysical Research: Solid Earth, 93(B4), 3211-3231.

Iwasaki, T., Shimizu, Y., Kimura, I., 2016. Numerical simulation of bar and bank erosion in a vegetated floodplain: A case study in the Otofuke River. Adv. Water Resour., 93, Part A, 118-134.

Jackson, R.G., 1975. Velocity–bed-form–texture patterns of meander bends in the lower Wabash River of Illinois and Indiana. Geological Society of America Bulletin, 86(11), 1511-1522.

Jackson, R.G., 1976. Depositional model of point bars in the lower Wabash River. Journal of Sedimentary Research, 46(3), 579-594.

Jarvis, A., Reuter, H.I., Nelson, A., Guevara, E., 2008. Hole-filled SRTM for the globe Version 4, available from the CGIAR-CSI SRTM 90m Database: http://srtm.csi.cgiar.org.

Jerolmack, D.J., Paola, C., 2010. Shredding of environmental signals by sediment transport. Geophysical Research Letters, 37(19), n/a-n/a.

Junk, W.J., Furch, K., 1993. A general review of tropical South American floodplains. Wetlands Ecology and Management, 2(4), 231-238.

Kasvi, E., Vaaja, M., Alho, P., Hyyppä, H., Hyyppä, J., Kaartinen, H., Kukko, A., 2012. Morphological changes on meander point bars associated with flow structure at different discharges. Earth Surface Processes and Landforms, n/a-n/a.

Kean, J.W., Smith, J.D., 2006a. Form drag in rivers due to small-scale natural topographic features: 1. Regular sequences. Journal of Geophysical Research F: Earth Surface, 111(4).

Kean, J.W., Smith, J.D., 2006b. Form drag in rivers due to small-scale natural topographic features: 2. Irregular sequences. Journal of Geophysical Research: Earth Surface, 111(F4), F04010.

Keller, E.A., 1971a. Areal Sorting of Bed-Load Material: The Hypothesis of Velocity Reversal. Geological Society of America Bulletin, 82(3), 753-756.

Keller, E.A., 1971b. Pools, Riffles, and Meanders: Discussion. Geological Society of America Bulletin, 82(1), 279-280.

Keller, E.A., 1972a. Areal Sorting of Bed-Load Material: The Hypothesis of Velocity Reversal: Reply. Geological Society of America Bulletin, 83(3), 915-918.

Keller, E.A., 1972b. Development of Alluvial Stream Channels: A Five-Stage Model. Geological Society of America Bulletin, 83(5), 1531-1536.

Keller, E.A., 1974. Development of Alluvial Stream Channels: A Five-Stage Model: Reply. Geological Society of America Bulletin, 85(1), 150-152.

Keller, E.A., Melhorn, W.N., 1978. Rhythmic spacing and origin of pools and riffles. Geological Society of America Bulletin, 89(5), 723-730.

Kendon, E.J., Roberts, N.M., Fowler, H.J., Roberts, M.J., Chan, S.C., Senior, C.A., 2014. Heavier summer downpours with climate change revealed by weather forecast resolution model. Nature Clim. Change, 4(7), 570-576.

Kingsford, R.T., 2000. Ecological impacts of dams, water diversions and river management on floodplain wetlands in Australia. Austral Ecology, 25(2), 109-127.

Kleinhans, M.G., 2010. Sorting out river channel patterns. Progress in Physical Geography, 34(3), 287-326.

Knighton, D., 1998. Fluvial forms and processes: A new perspective. Arnold Publishing.

Kondrat'yev, N.Y., 1968. Hydromorphological principles of computations of free meandering. Soviet Hydrology, 309(4), 309-335.

Kuehl, S.A., DeMaster, D.J., Nittrouer, C.A., 1986. Nature of sediment accumulation on the Amazon continental shelf. Continental Shelf Research, 6(1–2), 209-225.

Lane, S.N., Tayefi, V., Reid, S.C., Yu, D., Hardy, R.J., 2007. Interactions between sediment delivery, channel change, climate change and flood risk in a temperate upland environment. Earth Surface Processes and Landforms, 32(3), 429-446.

Langbein, W.B., Leopold, L.B., 1966. River meanders-theory of minimum variance. U. S. Geological Society professional paper 424-H, 1-15.

Lanzoni, S., Seminara, G., 2006. On the nature of meander instability. Journal of Geophysical Research: Earth Surface, 111(F4), n/a-n/a.

Larsen, E.W., Premier, A.K., Greco, S.E., 2006. Cumulative effective stream power and bank erosion on the sacramento river, California, USA. JAWRA Journal of the American Water Resources Association, 42(4), 1077-1097.

Latrubesse, E.M., Amsler, M.L., de Morais, R.P., Aquino, S., 2009. The geomorphologic response of a large pristine alluvial river to tremendous deforestation in the South American tropics: The case of the Araguaia River. Geomorphology, 113(3–4), 239-252.

Latrubesse, E.M., Cozzuol, M., da Silva-Caminha, S.A.F., Rigsby, C.A., Absy, M.L., Jaramillo, C., 2010. The Late Miocene paleogeography of the Amazon Basin and the evolution of the Amazon River system. Earth-Science Reviews, 99(3–4), 99-124.

Latrubesse, E.M., Restrepo, J.D., 2014. Sediment yield along the Andes: continental budget, regional variations, and comparisons with other basins from orogenic mountain belts. Geomorphology, 216, 225-233.

Latrubesse, E.M., Stevaux, J.C., Sinha, R., 2005. Tropical rivers. Geomorphology, 70(3-4), 187-206.

Lauer, J.W., Parker, G., 2008. Net local removal of floodplain sediment by river meander migration. Geomorphology, 96(1-2), 123-149.

Lauer, J.W., Viparelli, E., Piégay, H., 2016. Morphodynamics and sediment tracers in 1-D (MAST-1D): 1-D sediment transport that includes exchange with an off-channel sediment reservoir. Adv. Water Resour., 93, Part A, 135-149.

Lazarus, E., Constantine, J.A., 2013. Generic theory for channel sinuosity. Proceedings of the National Academy of Sciences.

Legleiter, C.J., Harrison, L.R., Dunne, T., 2011. Effect of point bar development on the local force balance governing flow in a simple, meandering gravel bed river. Journal of Geophysical Research-Earth Surface, 116.

Leopold, L.B., Langbein, W.B., 1962. The concept of entropy in landscape evolution. u. S. Geological Society professional paper 500-A, A1-A20.

Leopold, L.B., Maddock, T.J., 1953. Hydraulic geometry of stream channels and some physiographic implications. U. S. Geological Society professional paper, 252, 55.

Leopold, L.B., Wolman, M.G., 1957. River channel patterns: meandering, braided and straight. U.S. Geological Survey profession paper 282-B.

Leopold, L.B., Wolman, M.G., 1960. River meanders. Geological Society of America Bulletin, 71(6), 769-&.

Leopold, L.B., Wolman, M.G., Miller, J.P., 1964. Fluvial processes in geomorphology. W. H. Freeman and Company, New York.

Lewin, J., 1972. Late-stage meander growth. Nature Physical Science, 240(101), 116-116.

Lewin, J., 1976. Initiation of bed forms and meanders in coarse-grained sediment. Geological Society of America Bulletin, 87(2), 281-285.

Lewin, J., 1978. Meander development and floodplain sedimentation: A case study from mid-Wales. Geological Journal, 13(1), 25-36.

Lewin, J., Ashworth, P.J., 2014. The negative relief of large river floodplains. Earth-Science Reviews, 129(0), 1-23.

Lewin, J., Ashworth, P.J., Strick, R.J.P., 2016. Spillage sedimentation on large river floodplains. Earth Surface Processes and Landforms, n/a-n/a.

Leyland, J., Darby, S.E., Teruggi, L., Rinaldi, M., Ostuni, D., 2015. A self-limiting bank erosion mechanism? inferring temporal variations in bank form and skin drag from high resolution topographic data. Earth Surface Processes and Landforms, 40(12), 1600-1615.

Lima, J.E.F.W., Lopes, W.T.A., de Oliveira Carvalho, N., Vieira, M.R., de Silva, E.M., 2005. Suspended sediment fluxes in th large river basins of Brazil, International Symposium on Sediment Budgets. IAHS, pp. 355-363.

Lobón-Cerviá, J., Hess, L.L., Melack, J.M., Araujo-Lima, C.A.R.M., 2015. The importance of forest cover for fish richness and abundance on the Amazon floodplain. Hydrobiologia, 750(1), 245-255.

Lotsari, E., Vaaja, M., Flener, C., Kaartinen, H., Kukko, A., Kasvi, E., Hyyppä, H., Hyyppä, J., Alho, P., 2014. Annual bank and point bar morphodynamics of a meandering river determined by high-accuracy multitemporal laser scanning and flow data. Water Resources Research, 50(7), 5532-5559.

Luchi, R., Hooke, J.M., Zolezzi, G., Bertoldi, W., 2010a. Width variations and mid-channel bar inception in meanders: River Bollin (UK). Geomorphology, 119(1-2), 1-8.

Luchi, R., Zolezzi, G., Tubino, M., 2010b. Modelling mid-channel bars in meandering channels. Earth Surface Processes and Landforms, 35(8), 902-917.

Mainville, N., Webb, J., Lucotte, M., Davidson, R., Betancourt, O., Cueva, E., Mergler, D., 2006. Decrease of soil fertility and release of mercury following

deforestation in the Andean Amazon, Napo River Valley, Ecuador. Science of The Total Environment, 368(1), 88-98.

Mann, M.E., Bradley, R.S., Hughes, M.K., 1999. Northern hemisphere temperatures during the past millennium: Inferences, uncertainties, and limitations. Geophysical Research Letters, 26(6), 759-762.

Marani, M., Lanzoni, S., Zandolin, D., Seminara, G., Rinaldo, A., 2002. Tidal meanders. Water Resources Research, 38(11), 7-1-7-14.

Marengo, J., Tomasella, J., Soares, W., Alves, L., Nobre, C., 2012. Extreme climatic events in the Amazon basin. Theoretical and Applied Climatology, 107(1-2), 73-85.

Marengo, J.A., Alves, L.M., Soares, W.R., Rodriguez, D.A., Camargo, H., Riveros, M.P., Pabló, A.D., 2013. Two Contrasting Severe Seasonal Extremes in Tropical South America in 2012: Flood in Amazonia and Drought in Northeast Brazil. Journal of Climate, 26(22), 9137-9154.

Marengo, J.A., Nobre, C.A., Tomasella, J., Cardoso, M.F., Oyama, M.D., 2008a. Hydro-climatic and ecological behaviour of the drought of Amazonia in 2005. Philosophical Transactions of the Royal Society B: Biological Sciences, 363(1498), 1773-1778.

Marengo, J.A., Nobre, C.A., Tomasella, J., Oyama, M.D., Sampaio de Oliveira, G., de Oliveira, R., Camargo, H., Alves, L.M., Brown, I.F., 2008b. The Drought of Amazonia in 2005. Journal of Climate, 21(3), 495-516.

Marengo, J.A., Tomasella, J., Alves, L.M., Soares, W.R., Rodriguez, D.A., 2011. The drought of 2010 in the context of historical droughts in the Amazon region. Geophysical Research Letters, 38(12), n/a-n/a.

Marshall, M.R., Ballard, C.E., Frogbrook, Z.L., Solloway, I., McIntyre, N., Reynolds, B., Wheater, H.S., 2014. The impact of rural land management changes on soil hydraulic properties and runoff processes: results from experimental plots in upland UK. Hydrological Processes, 28(4), 2617-2629.

Maslin, M.A., 2009. Review of the timing and causes of the Amazon-Fan mass transport and avulsion deposits during the latest Pleistocene. External controls on deep-water depositional systems, 92, 133-144.

Matsuoka, N., 2008. Frost weathering and rockwall erosion in the southeastern Swiss Alps: Long-term (1994–2006) observations. Geomorphology, 99(1–4), 353-368.

Mayer, L.M., Keil, R.G., Macko, S.A., Joye, S.B., Ruttenberg, K.C., Aller, R.C., 1998. Importance of suspended participates in riverine delivery of bioavailable nitrogen to coastal zones. Global Biogeochem. Cycles, 12(4), 573-579.

Mayorga, E., Aufdenkampe, A.K., Masiello, C.A., Krusche, A.V., Hedges, J.I., Quay, P.D., Richey, J.E., Brown, T.A., 2005. Young organic matter as a source of carbon dioxide outgassing from Amazonian rivers. Nature, 436(7050), 538-541.

Meade, R.H., 1994. Suspended sediments of the modern Amazon and Orinoco rivers. Quat. Int., 21(0), 29-39.

Meade, R.H., Dunne, T., Richey, J.E., De M. Santos, U., Salati, E., 1985. Storage and Remobilization of Suspended Sediment in the Lower Amazon River of Brazil. Science, 228(4698), 488-490.

Meggers, B.J., 1994. Archeological evidence for the impact of mega-Niño events on Amazonia during the past two millennia. Climatic Change, 28(4), 321-338.

Mertes, L.A.K., 1997. Documentation and significance of the perirheic zone on inundated floodplains. Water Resources Research, 33(7), 1749-1762.

Mertes, L.A.K., Dunne, T., 2007. Effects of Tectonism, Climate Change, and Sea-level Change on the Form and Behaviour of the Modern Amazon River and its Floodplain, Large Rivers. John Wiley & Sons, Ltd, pp. 115-144.

Mertes, L.A.K., Dunne, T., Martinelli, L.A., 1996. Channel-floodplain geomorphology along the Solimões-Amazon River, Brazil. Geological Society of America Bulletin, 108(9), 1089-1107.

Michalkova, M., Piegay, H., Kondolf, G.M., Greco, S.E., 2011. Lateral erosion of the Sacramento River, California (1942-1999), and responses of channel and floodplain lake to human influences. Earth Surface Processes and Landforms, 36(2), 257-272.

Micheli, E.R., Kirchner, J.W., 2002. Effects of wet meadow riparian vegetation on streambank erosion. 1. Remote sensing measurements of streambank migration and erodibility. Earth Surface Processes and Landforms, 27(6), 627-639.

Micheli, E.R., Kirchner, J.W., Larsen, E.W., 2004. Quantifying the effect of riparian forest versus agricultural vegetation on river meander migration rates, Central Sacramento River, California, USA. River Research and Applications, 20(5), 537-548.

Micheli, E.R., Larsen, E.W., 2010. River channel cutoff, Sacramento River, California, USA, River Research and Applications. Wiley InterScience.

Mikkelsen, N., Maslin, M., Giraudeau, J., Showers, W., 1997. Biostratigraphy and sedimentation rates of the Amazon Fan. In: R.D. Flood, D.J.W. Piper, A. Klaus, L.C. Peterson (Eds.), Proceedings of the Ocean Drilling Program, Scientific Results, pp. 577-594.

Millar, R.G., 1999. Grain and form resistance in gravel-bed rivers. Journal of Hydraulic Research, 37(3), 303-312.

Milliman, J.D., Meade, R.H., 1983. World-Wide Delivery of River Sediment to the Oceans. The Journal of Geology, 91(1), 1-21.

Milliman, J.D., Syvitski, J.P.M., 1992. Geomorphic/tectonic control of sediment discharge to the ocean: the importance of small mountainous rivers. The Journal of Geology, 525-544.

Motta, D., Langendoen, E.J., Abad, J.D., García, M.H., 2014. Modification of meander migration by bank failures. Journal of Geophysical Research: Earth Surface, 119(5), 1026-1042.

Mueller, J.E., 1972. Re-evaluation of the Relationship of Master Streams and Drainage Basins. Geological Society of America Bulletin, 83(11), 3471-3474.

Murray, A.B., Paola, C., 2003. Modelling the effect of vegetation on channel pattern in bedload rivers. Earth Surface Processes and Landforms, 28(2), 131-143.

Mégard, F., 1984. The Andean orogenic period and its major structures in central and northern Peru. Journal of the Geological Society, 141(5), 893.

Naiman, R.J., Decamps, H., 1997. The ecology of interfaces: Riparian zones. Annu. Rev. Ecol. Syst., 28, 621-658.

Naiman, R.J., Decamps, H., Pollock, M., 1993. The Role of Riparian Corridors in Maintaining Regional Biodiversity. Ecological Applications, 3(2), 209-212.

Nanson, G., Hickin, E., 1983. Channel Migration and Incision on the Beatton River. Journal of Hydraulic Engineering, 109(3), 327-337.

Nanson, G.C., 1980. Point bar and floodplain formation of the meandering Beatton River, northeastern British Columbia, Canada. Sedimentology, 27(1), 3-29.

Nanson, G.C., Beach, H.F., 1977. Forest Succession and Sedimentation on a Meandering-River Floodplain, Northeast British Columbia, Canada. J. Biogeog., 4(3), 229-251.

Nanson, G.C., Page, K., 1983. Lateral Accretion of Fine-Grained Concave Benches on Meandering Rivers, Modern and Ancient Fluvial Systems. Blackwell Publishing Ltd., pp. 133-143.

Nearing, M.A., Pruski, F.F., O'Neal, M.R., 2004. Expected climate change impacts on soil erosion rates: A review. J. Soil Water Conserv., 59(1), 43-50.

Nicholas, A., 2013. Morphodynamic diversity of the world's largest rivers. Geology, 41(4), 475-478.

Nicoll, T.J., Hickin, E.J., 2010. Planform geometry and channel migration of confined meandering rivers on the Canadian prairies. Geomorphology, 116(1–2), 37-47.

Nittrouer, C.A., Curtin, T.B., DeMaster, D.J., 1986a. Concentration and flux of suspended sediment on the Amazon continental shelf. Continental Shelf Research, 6(1–2), 151-174.

Nittrouer, C.A., DeMaster, D.J., 1996. The Amazon shelf setting: tropical, energetic, and influenced by a large river. Continental Shelf Research, 16(5–6), 553-573.

Nittrouer, C.A., Kuehl, S.A., Demaster, D.J., Kowsmann, R.O., 1986b. The deltaic nature of Amazon shelf sedimentation. Geological Society of America Bulletin, 97(4), 444-458.

Nittrouer, C.A., Kuehl, S.A., Sternberg, R.W., Figueiredo Jr, A.G., Faria, L.E.C., 1995. An introduction to the geological significance of sediment transport and accumulation on the Amazon continental shelf. Marine Geology, 125(3–4), 177-192.

Norris, R.M., Webb, R.W., 1990. Geology of California. John Wiley, New York.

Odgaard, A.J., 1984. Bank erosion contribution to stream sediment load.

Odgaard, A.J., 1987. Streambank erosion along 2 rivers in Iowa. Water Resources Research, 23(7), 1225-1236.

Osman, A., Thorne, C., 1988. Riverbank Stability Analysis. I: Theory. Journal of Hydraulic Engineering, 114(2), 134-150.

Owens, P.N., Batalla, R.J., Collins, A.J., Gomez, B., Hicks, D.M., Horowitz, A.J., Kondolf, G.M., Marden, M., Page, M.J., Peacock, D.H., Petticrew, E.L., Salomons, W., Trustrum, N.A., 2005. Fine-grained sediment in river systems: environmental significance and management issues. River Research and Applications, 21(7), 693-717.

Parker, G., 1976. On the cause and characteristic scales of meandering and braiding in rivers. Journal of Fluid Mechanics, 76(3), 457-480.

Parker, G., Sawai, K., Ikeda, S., 1982. Bend theory of river meanders. Part 2. Nonlinear deformation of finite-amplitude bends. Journal of Fluid Mechanics, 115, 303-314.

Parker, G., Shimizu, Y., Wilkerson, G.V., Eke, E.C., Abad, J.D., Lauer, J.W., Paola, C., Dietrich, W.E., Voller, V.R., 2011. A new framework for modeling the migration of meandering rivers. Earth Surface Processes and Landforms, 36(1), 70-86.

Peakall, J., Ashworth, P.J., Best, J.L., 2007. Meander-Bend Evolution, Alluvial Architecture, and the Role of Cohesion in Sinuous River Channels: A Flume Study. Journal of Sedimentary Research, 77(3), 197-212.

Pearson, A., Hanes, D.M., 2016. How much sediment have we added to a floodplain? Preliminary results of using contaminated sediments to tease out enhanced deposition to a floodplain of the lower Meramec River, MO, AGU Fall Meeting 2016, San Francisco, CA, USA.

Pizzuto, J.E., 1994. Channel adjustments to changing discharges, Powder River, Montana. Geological Society of America Bulletin, 106(11), 1494-1501.

Pizzuto, J.E., 2014. Long-term storage and transport length scale of fine sediment: Analysis of a mercury release into a river. Geophysical Research Letters, 41(16), 5875-5882.

Pizzuto, J.E., Meckelnburg, T.S., 1989. Evaluation of a linear bank erosion equation. Water Resources Research, 25(5), 1005-1013.

Piégay, H., Darby, S.E., Mosselman, E., Surian, N., 2005. A review of techniques available for delimiting the erodible river corridor: a sustainable approach to managing bank erosion. River Research and Applications, 21(7), 773-789.

Potter, P.E., 1978. Significance and Origin of Big Rivers. The Journal of Geology, 86(1), 13-33.

Pyrce, R.S., Ashmore, P.E., 2005. Bedload path length and point bar development in gravel-bed river models. Sedimentology, 52(4), 839-857.

Reuter, H.I., Nelson, A., Jarvis, A., 2007. An evaluation of void filling interpolation methods from SRTM data. International Journal of Geographical Information Science, 21(9), 983-1008.

Rice, S., 1994. Towards a model of changes in bed material texture at the drainage basin scale. In: M.J. Kirkby (Ed.), Process models and theoretical geomorphology. Wiley, Chichester, pp. 159-172.

Richards, K.S., 1976. The morphology of riffle-pool sequences. Earth Surface Processes, 1(1), 71-88.

Richey, J.E., Hedges, J.I., Devol, A.H., Quay, P.D., Victoria, R., Martinelli, L., Forsberg, B.R., 1990. Biogeochemistry of Carbon in the Amazon River. Limnology and Oceanography, 35(2), 352-371.

Richey, J.E., Meade, R.H., Salati, E., Devol, A.H., Nordin, C.F., Santos, U.D., 1986. Water Discharge and Suspended Sediment Concentrations in the Amazon River: 1982–1984. Water Resources Research, 22(5), 756-764.

Richey, J.E., Mertes, L.A.K., Dunne, T., Victoria, R.L., Forsberg, B.R., Tancredi, A.C.N.S., Oliveira, E., 1989. Sources and routing of the Amazon River Flood Wave. Global Biogeochem. Cycles, 3(3), 191-204.

Riebesell, U., Zondervan, I., Rost, B., Tortell, P.D., Zeebe, R.E., Morel, F.M.M., 2000. Reduced calcification of marine plankton in response to increased atmospheric CO_2. Nature, 407(6802), 364-367.

Roddaz, M., Baby, P., Brusset, S., Hermoza, W., Maria Darrozes, J., 2005. Forebulge dynamics and environmental control in Western Amazonia: The case study of the Arch of Iquitos (Peru). Tectonophysics, 399(1–4), 87-108.

Rollet, A.J., Piégay, H., Dufour, S., Bornette, G., Persat, H., 2014. Assessment of consequences of sediment deficit on a gravel river bed downstream of dams in restoration perspectives: Application of a multicriteria, hierarchical and spatially explicit diagnosis. River Research and Applications, 30(8), 939-953.

Rominger, J.T., Lightbody, A.F., Nepf, H.M., 2010. Effects of Added Vegetation on Sand Bar Stability and Stream Hydrodynamics.

Rowland, J.C., Dietrich, W.E., Day, G., Parker, G., 2009. Formation and maintenance of single-thread tie channels entering floodplain lakes: Observations from three diverse river systems. Journal of Geophysical Research: Earth Surface, 114(F2), n/a-n/a.

Russell, C., 2016. The complex shapes of fluvial meanders and the distribution of heterogeneity in point bar deposits, Rain, rivers and reservoirs. The Geological Society, Edinburgh Conference Centre, Heriot-Watt University, Edinburgh.

Räsänen, M., Neller, R., Salo, J., Jungner, H., 1992. Recent and ancient fluvial deposition systems in the Amazonian foreland basin, Peru. Geol. Mag., 129(03), 293-306.

Räsänen, M.E., Salo, J.S., Jungnert, H., Pittman, L.R., 1990. Evolution of the Western Amazon Lowland Relief: impact of Andean foreland dynamics. Terra Nova, 2(4), 320-332.

Safran, E.B., Bierman, P.R., Aalto, R., Dunne, T., Whipple, K.X., Caffee, M., 2005. Erosion rates driven by channel network incision in the Bolivian Andes. Earth Surface Processes and Landforms, 30(8), 1007-1024.

Salo, J., Kalliola, R., Hakkinen, I., Makinen, Y., Niemela, P., Puhakka, M., Coley, P.D., 1986. River dynamics and the diversity of Amazon lowland forest. Nature, 322(6076), 254-258.

Schumm, S.A., Khan, H.R., 1972. Experimental Study of Channel Patterns. Geological Society of America Bulletin, 83(6), 1755-1770.

Schuurman, F., Shimizu, Y., Iwasaki, T., Kleinhans, M.G., 2016. Dynamic meandering in response to upstream perturbations and floodplain formation. Geomorphology, 253, 94-109.

Schwendel, A.C., Nicholas, A.P., Aalto, R.E., Sambrook Smith, G.H., Buckley, S., 2015. Interaction between meander dynamics and floodplain heterogeneity in a large tropical sand-bed river: the Rio Beni, Bolivian Amazon. Earth Surface Processes and Landforms, n/a-n/a.

Schöngart, J., Junk, W.J., 2007. Forecasting the flood-pulse in Central Amazonia by ENSO-indices. Journal of Hydrology, 335(1–2), 124-132.

Sear, D.A., 1996. Sediment transport processes in pool-riffle sequences Earth Surface Processes and Landforms, 21(3), 241-262.

Seminara, G., Tubino, M., 1992. Weakly nonlinear theory of regular meanders. Journal of Fluid Mechanics, 244, 257-288.

Seminara, G., Zolezzi, G., Tubino, M., Zardi, D., 2001. Downstream and upstream influence in river meandering. Part 2. Planimetric development. Journal of Fluid Mechanics, 438(-1), 213-230.

Shen, Z., Törnqvist, T.E., Mauz, B., Chamberlain, E.L., Nijhuis, A.G., Sandoval, L., 2015. Episodic overbank deposition as a dominant mechanism of floodplain and delta-plain aggradation. Geology.

Shields, A., 1936. Application of similarity principles and turbulence research to bed load movement. 167.

Singer, M.B., 2008a. A new sampler for extracting bed material sediment from sand and gravel beds in navigable rivers. Earth Surface Processes and Landforms, 33(14), 2277-2284.

Singer, M.B., 2008b. Downstream patterns of bed material grain size in a large, lowland alluvial river subject to low sediment supply. Water Resources Research, 44(12), W12202.

Singer, M.B., Dunne, T., 2001. Identifying eroding and depositional reaches of valley by analysis of suspended sediment Transport in the Sacramento River, California. Water Resour. Res., 37(12), 3371-3381.

Singer, M.B., Dunne, T., 2004. Modeling decadal bed material sediment flux based on stochastic hydrology. Water Resources Research, 40(3), n/a-n/a.

Sioli, H., 1975. Amazon tributaries and drainage basins In: J. Jacobs, O.L. Lange, J.S. Olson, W. Wieser (Eds.), Ecological Studies-Analysis and Synthesis. Springer-Verlag, New York, pp. 199-213.

Sioli, H., 1984. The Amazon and its main affluents: Hydrography, morphology of the river courses, and river types. In: H. Sioli (Ed.), The Amazon. Monographiae Biologicae. Springer Netherlands, pp. 127-165.

Slingerland, R., Smith, N.D., 1998. Necessary conditions for a meandering-river avulsion. Geology, 26(5), 435-438.

Slingerland, R., Smith, N.D., 2004. River avulsions and their deposits. Annual Review of Earth and Planetary Sciences, 32(1), 257-285.

Smith, C.E., 1998. Modeling high sinuosity meanders in a small flume. Geomorphology, 25(1–2), 19-30.

Stallard, R.F., 1988. Weathering and Erosion in the Humid Tropics. In: A. Lerman, M. Meybeck (Eds.), Physical and Chemical Weathering in Geochemical Cycles. Springer Netherlands, Dordrecht, pp. 225-246.

Stoffel, M., Tiranti, D., Huggel, C., 2014. Climate change impacts on mass movements — Case studies from the European Alps. Science of The Total Environment, 493, 1255-1266.

Stone, H., 1968. Iterative Solution of Implicit Approximations of Multidimensional Partial Differential Equations. SIAM Journal on Numerical Analysis, 5(3), 530-558.

Struiksma, N., Olesen, K.W., Flokstra, C., De Vriend, H.J., 1985. Bed deformation in curved alluvial channels. Journal of Hydraulic Research, 23(1).

Stølum, H.-H., 1996. River Meandering as a Self-Organization Process. Science, 271(5256), 1710-1713.

Stølum, H.-H., 1997. Fluctuations at the self-organized critical state. Physical Review E, 56(6), 6710-6718.

Stølum, H.-H., 1998. Planform geometry and dynamics of meandering rivers. Geological Society of America Bulletin, 110(11), 1485-1498.

Sun, T., Meakin, P., Jøssang, T., 2001a. A computer model for meandering rivers with multiple bed load sediment sizes: 1. Theory. Water Resources Research, 37(8), 2227-2241.

Sun, T., Meakin, P., Jøssang, T., 2001b. A computer model for meandering rivers with multiple bed load sediment sizes: 2. Computer simulations. Water Resources Research, 37(8), 2243-2258.

Sun, T., Meakin, P., Jøssang, T., Schwarz, K., 1996. A Simulation Model for Meandering Rivers. Water Resour. Res., 32(9), 2937-2954.

Sutherland, D.G., Ball, M.H., Hilton, S.J., Lisle, T.E., 2002. Evolution of a landslide-induced sediment wave in the Navarro River, California. Geological Society of America Bulletin, 114(8), 1036-1048.

Swanson, K.M., Watson, E., Aalto, R., Lauer, J.W., Bera, M.T., Marshall, A., Taylor, M.P., Apte, S.C., Dietrich, W.E., 2008. Sediment load and floodplain deposition rates: Comparison of the Fly and Strickland rivers, Papua New Guinea. Journal of Geophysical Research: Earth Surface, 113(F1), F01S03.

Słowik, M., 2016. The influence of meander bend evolution on the formation of multiple cutoffs: findings inferred from floodplain architecture and bend geometry. Earth Surface Processes and Landforms, 41(5), 626-641.

Tal, M., Paola, C., 2007. Dynamic single-thread channels maintained by the interaction of flow and vegetation. Geology, 35(4), 347-350.

Tal, M., Paola, C., 2010. Effects of vegetation on channel morphodynamics: results and insights from laboratory experiments. Earth Surface Processes and Landforms, 35(9), 1014-1028.

Talmon, A.M., 1992. Bed topography of river bends with suspended sediment

transport. Ph.D thesis, Delft University of Technology.

Tanner, W.F., 1960. Helicoidal flow, a possible cause of meandering. Journal of Geophysical Research, 65(3), 993-995.

Terezinha Costa, A., Arias Nalini, H., de Tarso Amorim Castro, P., Carvalho de Lena, J., Morgenstern, P., Friese, K., 2006. Sediment contamination in floodplains and alluvial terraces as an historical record of gold exploitation in the Carmo River basin, Southeast Quadrilátero Ferrífero, Minas Gerais, Brazil. Acta hydrochimica et hydrobiologica, 34(3), 245-256.

Thorne, C.R., 1982. Processes and mechanisms of river bank erosion. In: R.D. Hey, B.J. C, C.R. Thorne (Eds.), Gravel-bed rivers. Wiley, Chichester, UK, pp. 227-271.

Thorne, C.R., 1990. Effects of vegetation on riverbank erosion and stability. In: J.D. Thornes (Ed.), Vegetation and erosion. John Wiley & Sons, Chichester, pp. 125-144.

Thorne, C.R., 1991. Bank erosion and meander migration of the Red and Mississippi Rivers, USA. Hydrology for the water management of large river basins (Proceedings of the Vienna symposim), 201, 301-313.

Thorne, C.R., Tovey, N.K., 1981. Stability of composite river banks. Earth Surface Processes and Landforms, 6(5), 469-484.

Thorne, C.R., Zevenbergen, L.W., Pitlick, J.C., Rais, S., Bradley, J.B., Julien, P.Y., 1985. Direct measurements of secondary currents in a meandering sand-bed river. Nature, 315(6022), 746-747.

Tockner, K., Stanford, J.A., 2002. Riverine flood plains: present state and future trends. Environmental Conservation, 29(03), 308-330.

Tomasella, J., Borma, L.S., Marengo, J.A., Rodriguez, D.A., Cuartas, L.A., A. Nobre, C., Prado, M.C.R., 2011. The droughts of 1996–1997 and 2004–2005 in Amazonia: hydrological response in the river main-stem. Hydrological Processes, 25(8), 1228-1242.

van de Lageweg, W.I., van Dijk, W.M., Baar, A.W., Rutten, J., Kleinhans, M.G., 2014. Bank pull or bar push: What drives scroll-bar formation in meandering rivers? Geology, 42(4), 319-322.

van de Lageweg, W.I., van Dijk, W.M., Kleinhans, M.G., 2013. Channel belt architecture formed by a meandering river. Sedimentology, 60(3), 840-859.

Van De Wiel, M.J., Darby, S.E., 2007. A new model to analyse the impact of woody riparian vegetation on the geotechnical stability of riverbanks. - 32(- 14), - 2198.

van Dijk, W.M., van de Lageweg, W.I., Kleinhans, M.G., 2012. Experimental meandering river with chute cutoffs. Journal of Geophysical Research: Earth Surface, 117(F3), F03023.

Vermeulen, B., Hoitink, A.J.F., Zolezzi, G., Abad, J.D., Aalto, R., 2016. Multiscale structure of meanders. Geophysical Research Letters, 43(7), 3288-3297.

Walling, D.E., 2006. Human impact on land–ocean sediment transfer by the world's rivers. Geomorphology, 79(3–4), 192-216.

Walling, D.E., Owens, P.N., Carter, J., Leeks, G.J.L., Lewis, S., Meharg, A.A., Wright, J., 2003. Storage of sediment-associated nutrients and contaminants in river channel and floodplain systems. Appl. Geochem., 18(2), 195-220.

Ward, N.D., Keil, R.G., Medeiros, P.M., Brito, D.C., Cunha, A.C., Dittmar, T., Yager, P.L., Krusche, A.V., Richey, J.E., 2013. Degradation of terrestrially derived macromolecules in the Amazon River. Nature Geosci, advance online publication.

Whipple, K.X., Gasparini, N.M., 2014. Tectonic control of topography, rainfall patterns, and erosion during rapid post–12 Ma uplift of the Bolivian Andes. Lithosphere, 6(4), 251.

Whiting, P.J., 1997. The effect of stage on flow and components of the local force balance. Earth Surface Processes and Landforms, 22(6), 517-530.

Whiting, P.J., Dietrich, W.E., 1993. Experimental constraints on bar migration through bends: Implications for meander wavelength selection. Water Resources Research, 29(4), 1091-1102.

Whittaker, A.C., Boulton, S.J., 2012. Tectonic and climatic controls on knickpoint retreat rates and landscape response times. Journal of Geophysical Research: Earth Surface, 117(F2), n/a-n/a.

Wiberg, P.L., Smith, J.D., 1987. Calculations of the critical shear stress for motion of uniform and heterogeneous sediments. Water Resources Research, 23(8), 1471-1480.

Wickert, A.D., Martin, J.M., Tal, M., Kim, W., Sheets, B., Paola, C., 2013. River channel lateral mobility: metrics, time scales, and controls. Journal of Geophysical Research: Earth Surface, 118(2), 396-412.

Wilkinson, S.N., Keller, R.J., Rutherfurd, I.D., 2004. Phase-shifts in shear stress as an explanation for the maintenance of pool–riffle sequences. Earth Surface Processes and Landforms, 29(6), 737-753.

Wittmann, H., von Blanckenburg, F., Guyot, J.L., Maurice, L., Kubik, P.W., 2009. From source to sink: Preserving the cosmogenic 10Be-derived denudation rate signal of the Bolivian Andes in sediment of the Beni and Mamoré foreland basins. Earth and Planetary Science Letters, 288(3–4), 463-474.

Wolman, M.G., Leopold, L.B., 1957. River flood plains: some observations on their formation. Geological Survey professional paper 282-C, 87-107.

Wood, A.L., Simon, A., Downs, P.W., Thorne, C.R., 2001. Bank-toe processes in incised channels: the role of apparent cohesion in the entrainment of failed bank materials. Hydrological Processes, 15(1), 39-61.

Yang, C.T., 1971a. On river meanders. Journal of Hydrology, 13(0), 231-253.

Yang, C.T., 1971b. Potential Energy and Stream Morphology. Water Resources Research, 7(2), 311-322.

Zinger, J.A., Rhoads, B.L., Best, J.L., 2011. Extreme sediment pulses generated by bend cutoffs along a large meandering river. - 4(- 10), - 678.

Zolezzi, G., Luchi, R., Tubino, M., 2012. Modeling morphodynamic processes in meandering rivers with spatial width variations. Reviews of Geophysics, 50(4), n/a-n/a.

Zolezzi, G., Seminara, G., 2001. Downstream and upstream influence in river meandering. Part 1. General theory and application to overdeepening. Journal of Fluid Mechanics, 438(-1), 183-211.

Appendix 1

Reach images (in order of appearance in the subsequent pages)

Araguaia (flow direction is south to north)
Vaupes (flow direction is north to south)
Branco (flow direction is north to south)
Iriri (flow direction is south to north)
Xingu (flow direction is south to north)
Purus1 (flow direction is west to east)
Purus2 (flow direction is south to north)
Jurua (flow direction is south to north)
Jutai (flow direction is south to north)
Itui (flow direction is south to north)
Nanay (flow direction is south to north)
Curuca (flow direction is south to north)
Putumayo (flow direction is west to east)
Mamore0 (flow direction is south to north)
Mamore1 (flow direction is south to north)
Mamore2 (flow direction is south to north)
Beni (flow direction is south to north)
Madre de Dios (flow direction is west to east)
Ucayali (flow direction is south to north)
Huallaga (flow direction is south to north)

A summary of the reach characteristics can be found at the end of Appendix 1
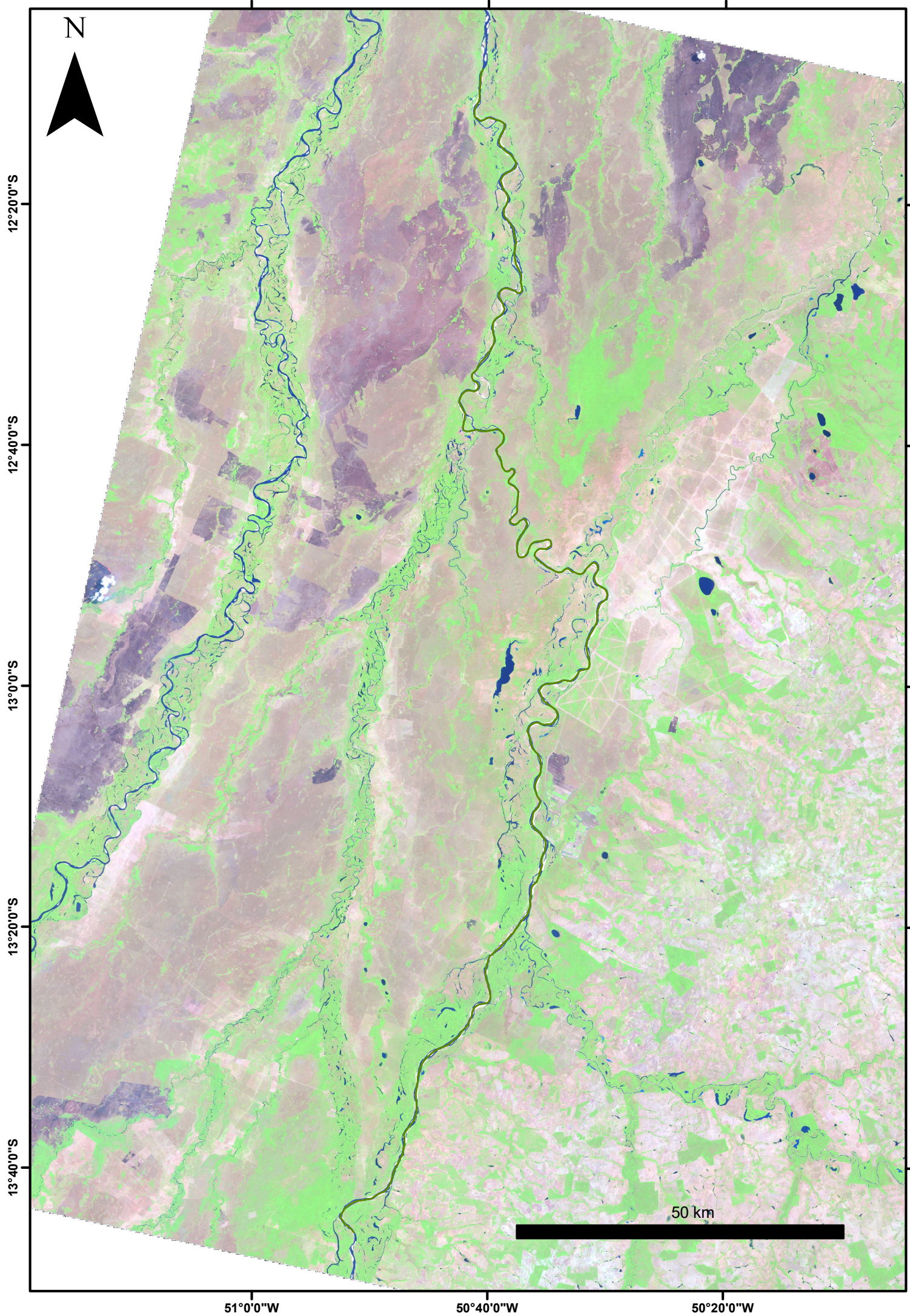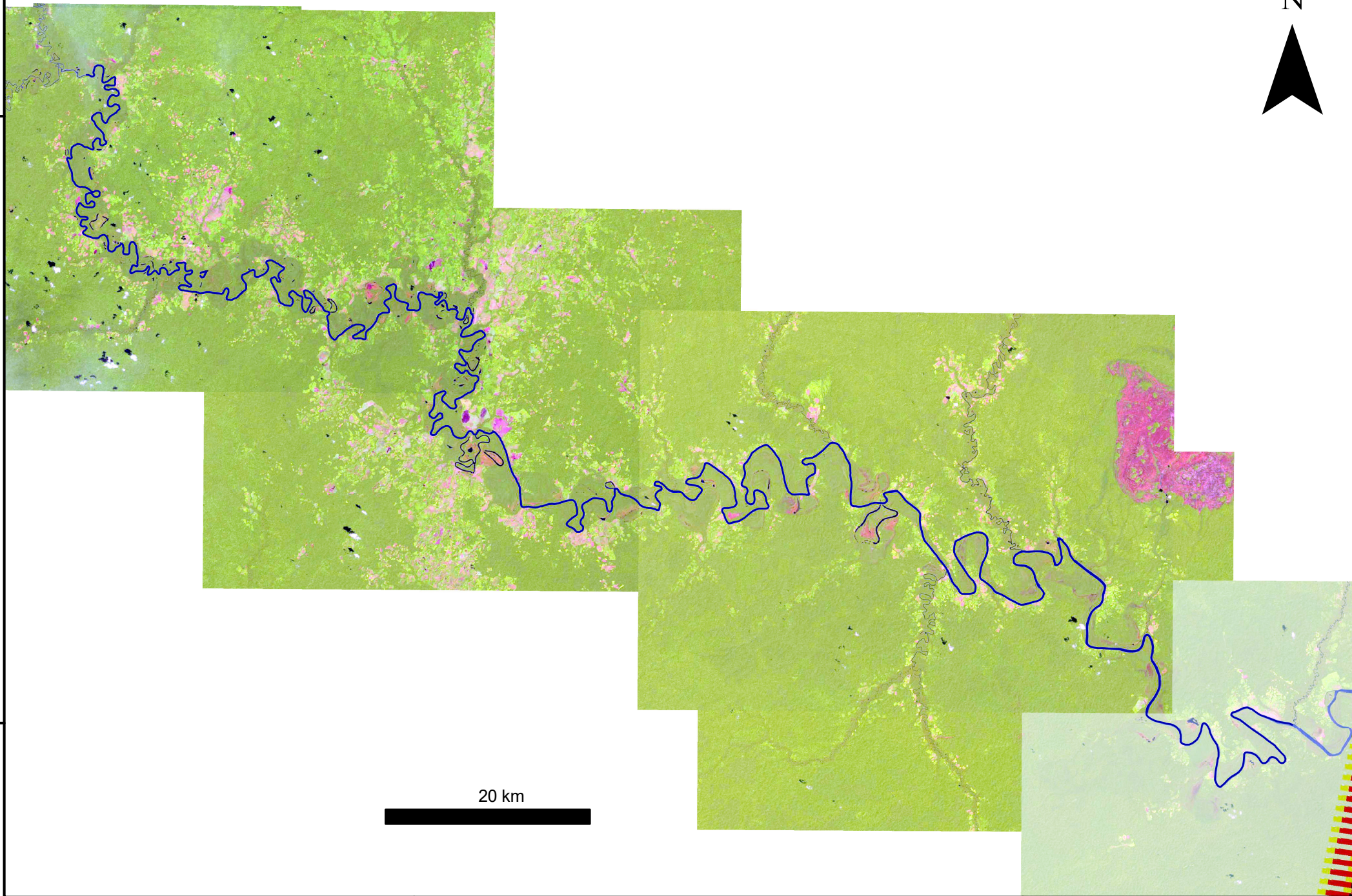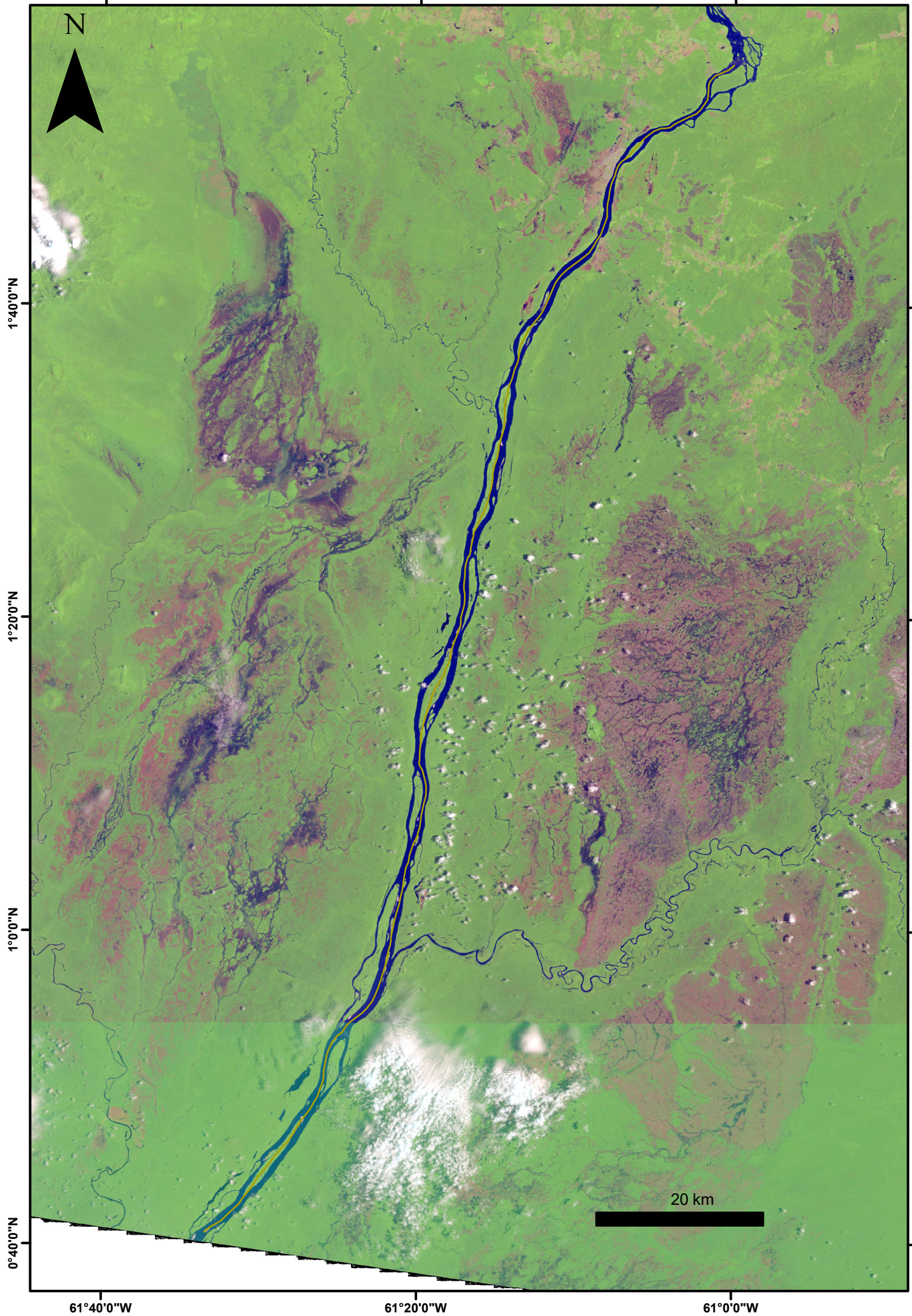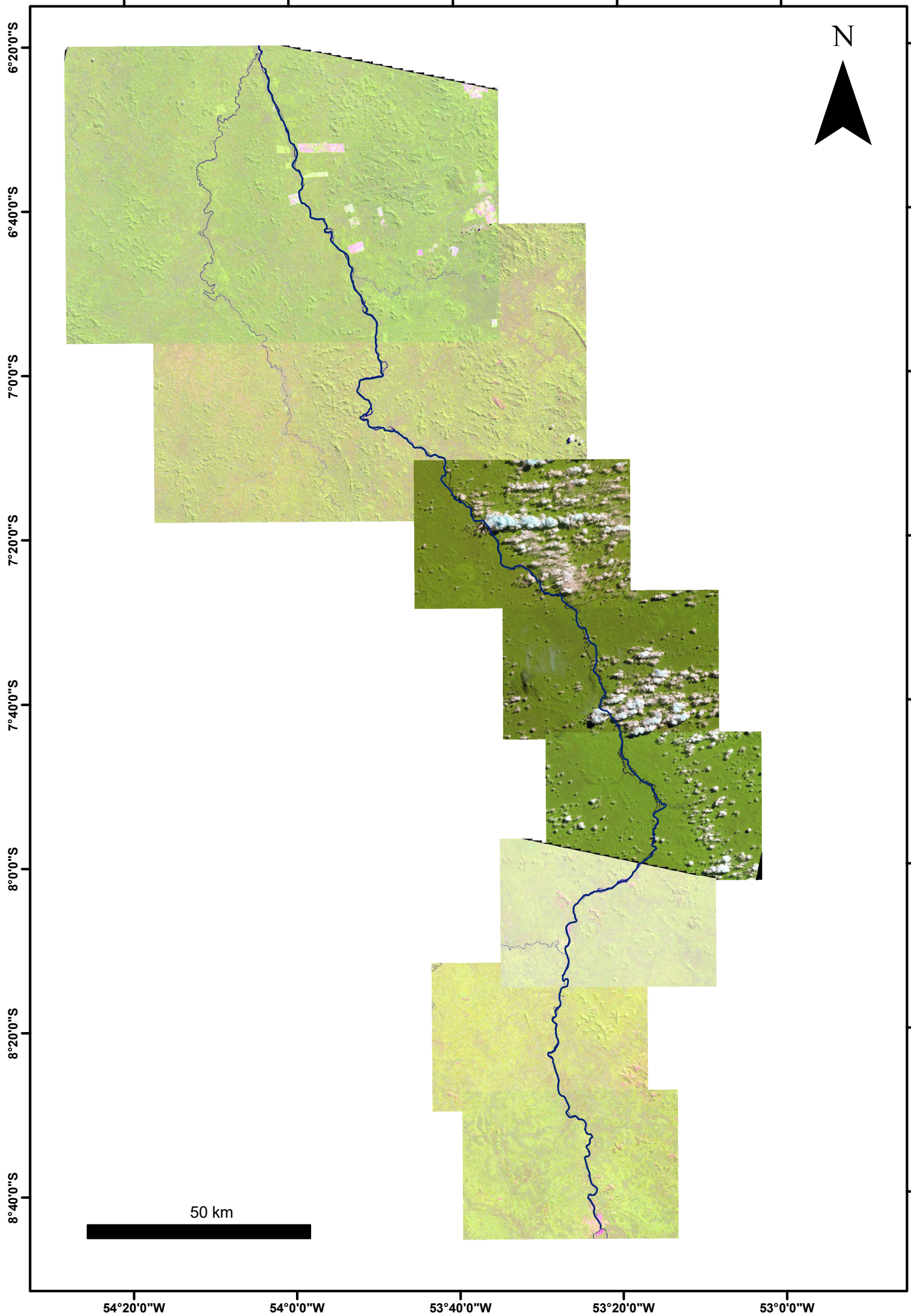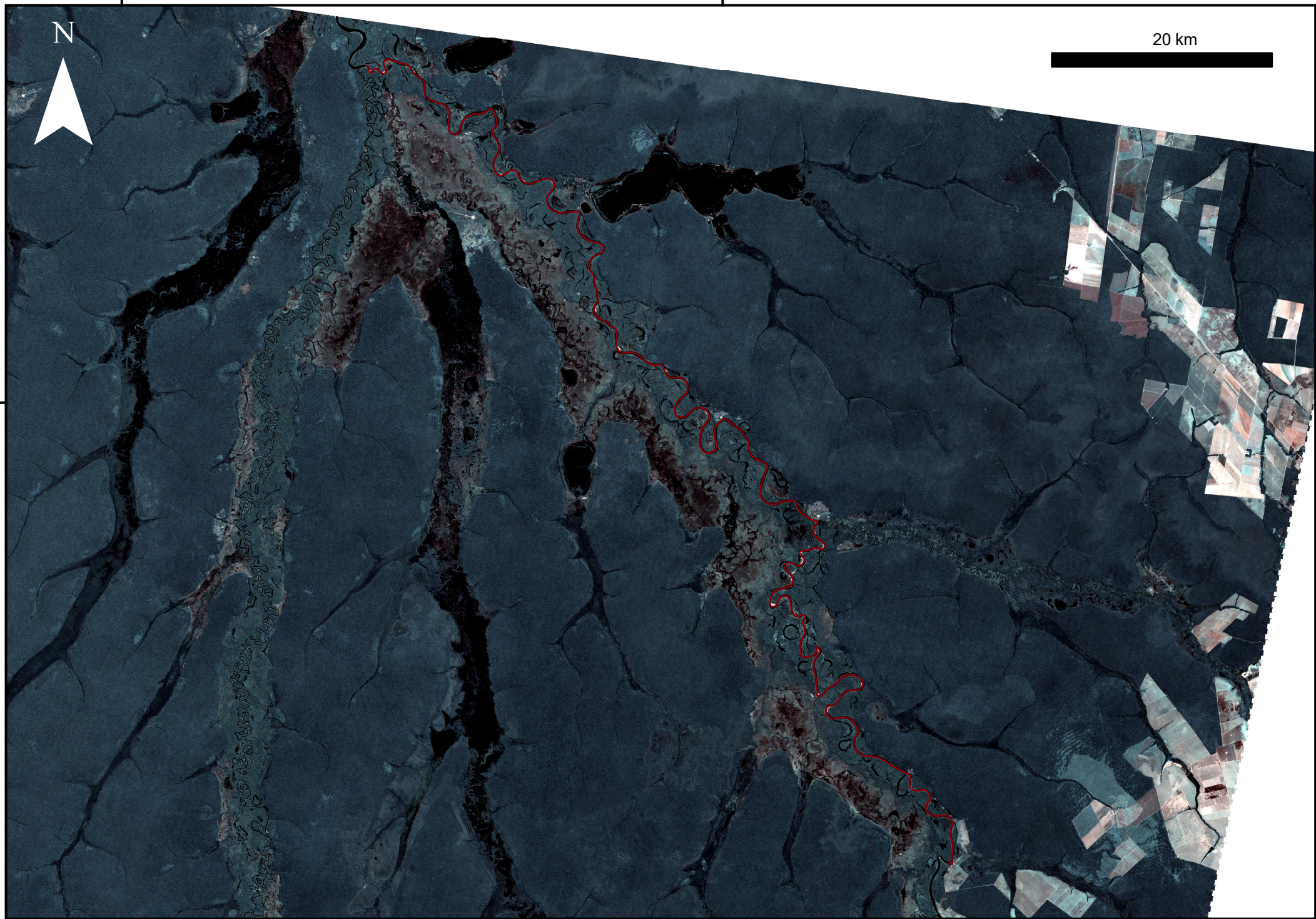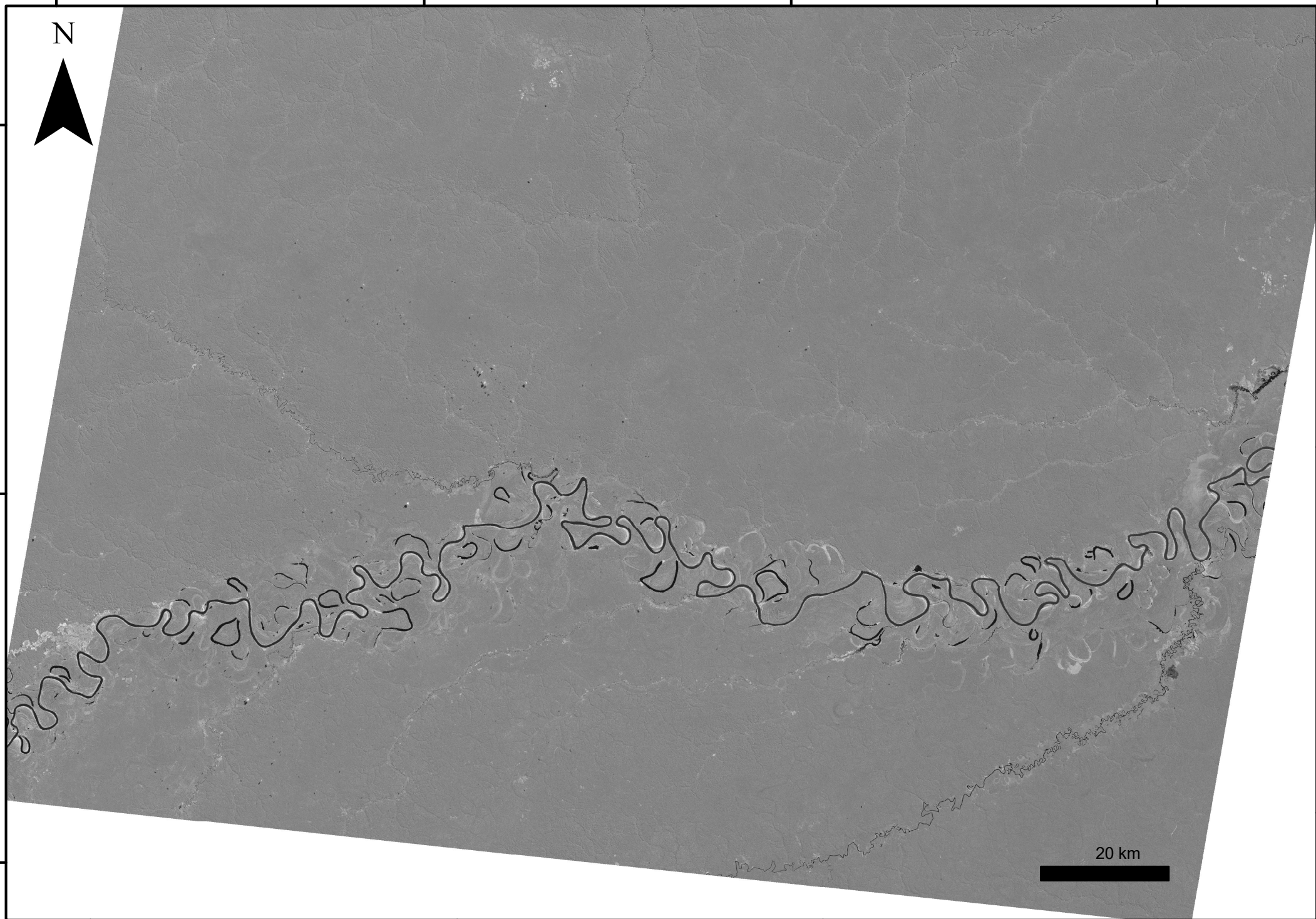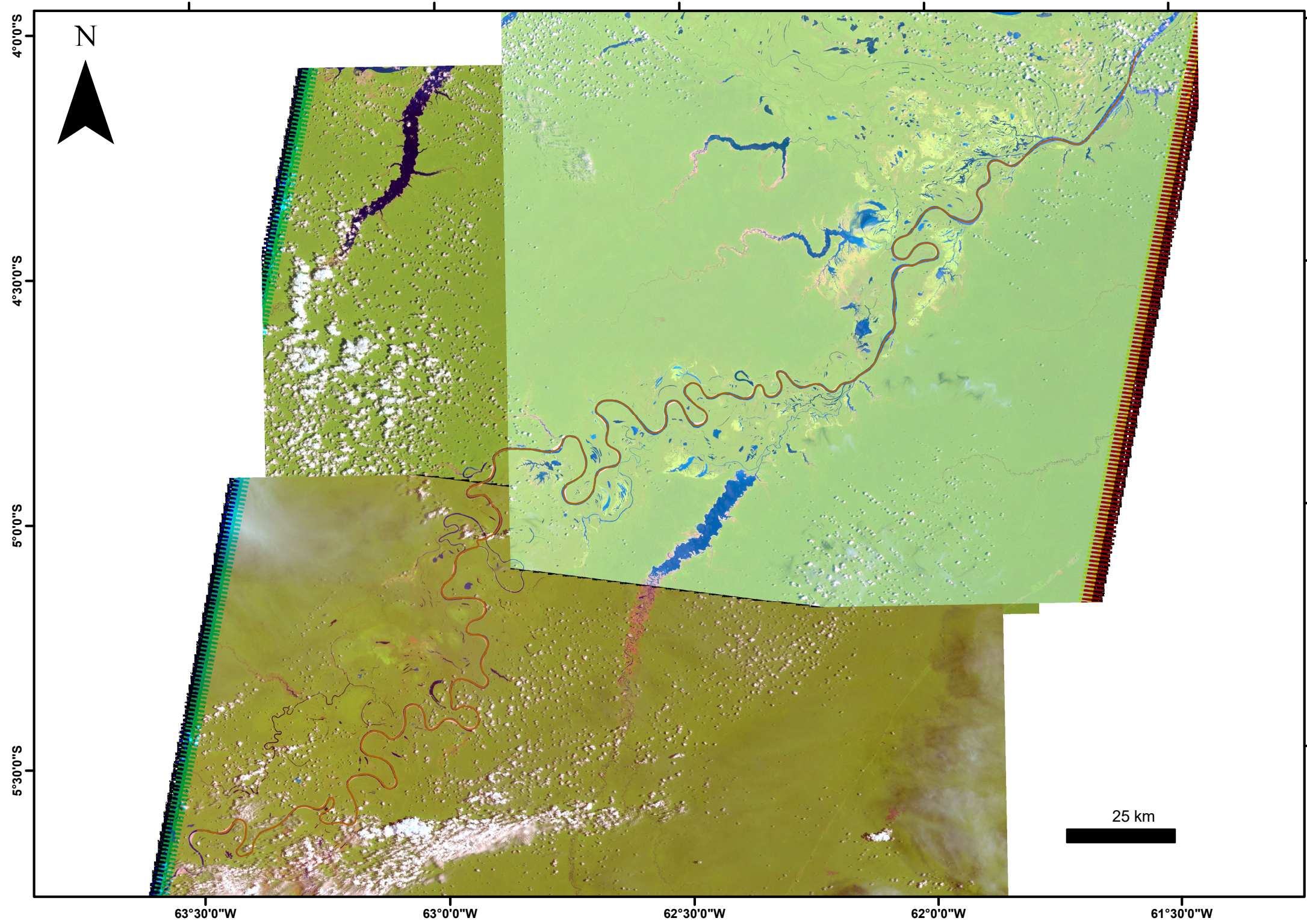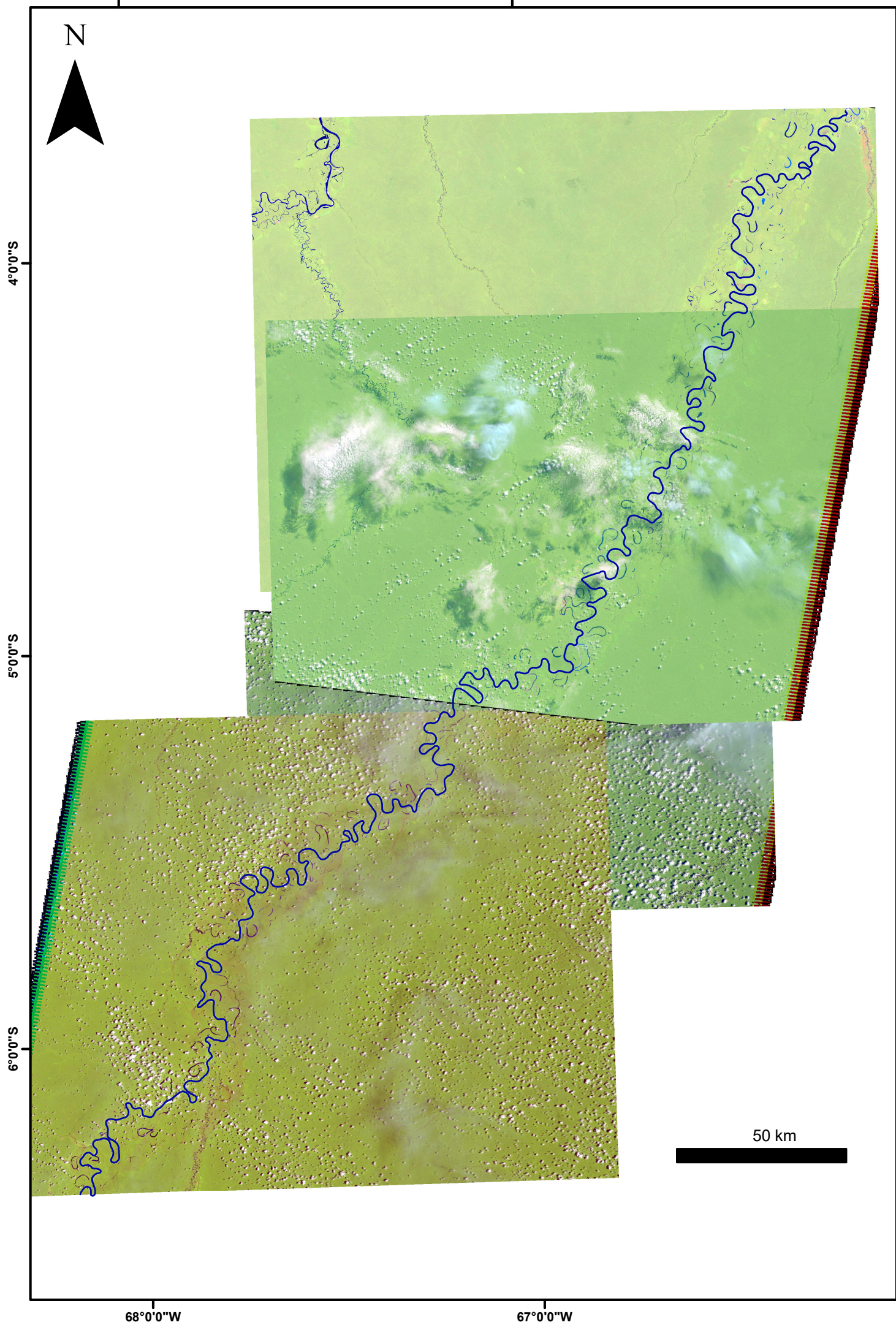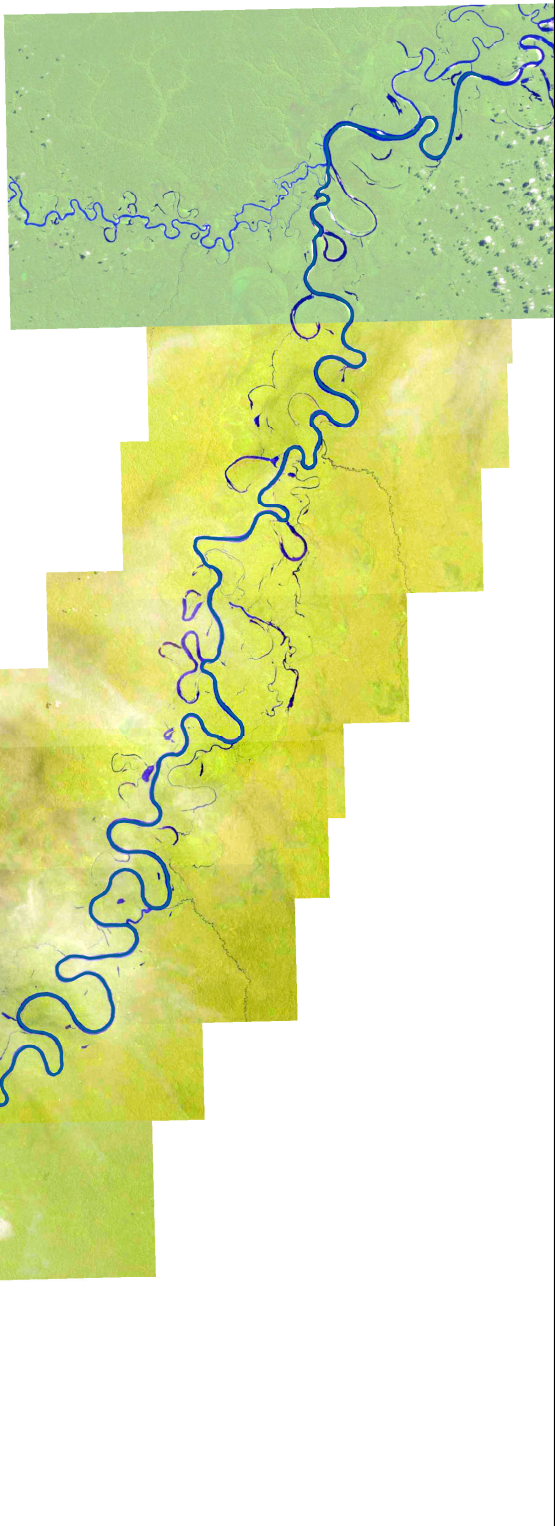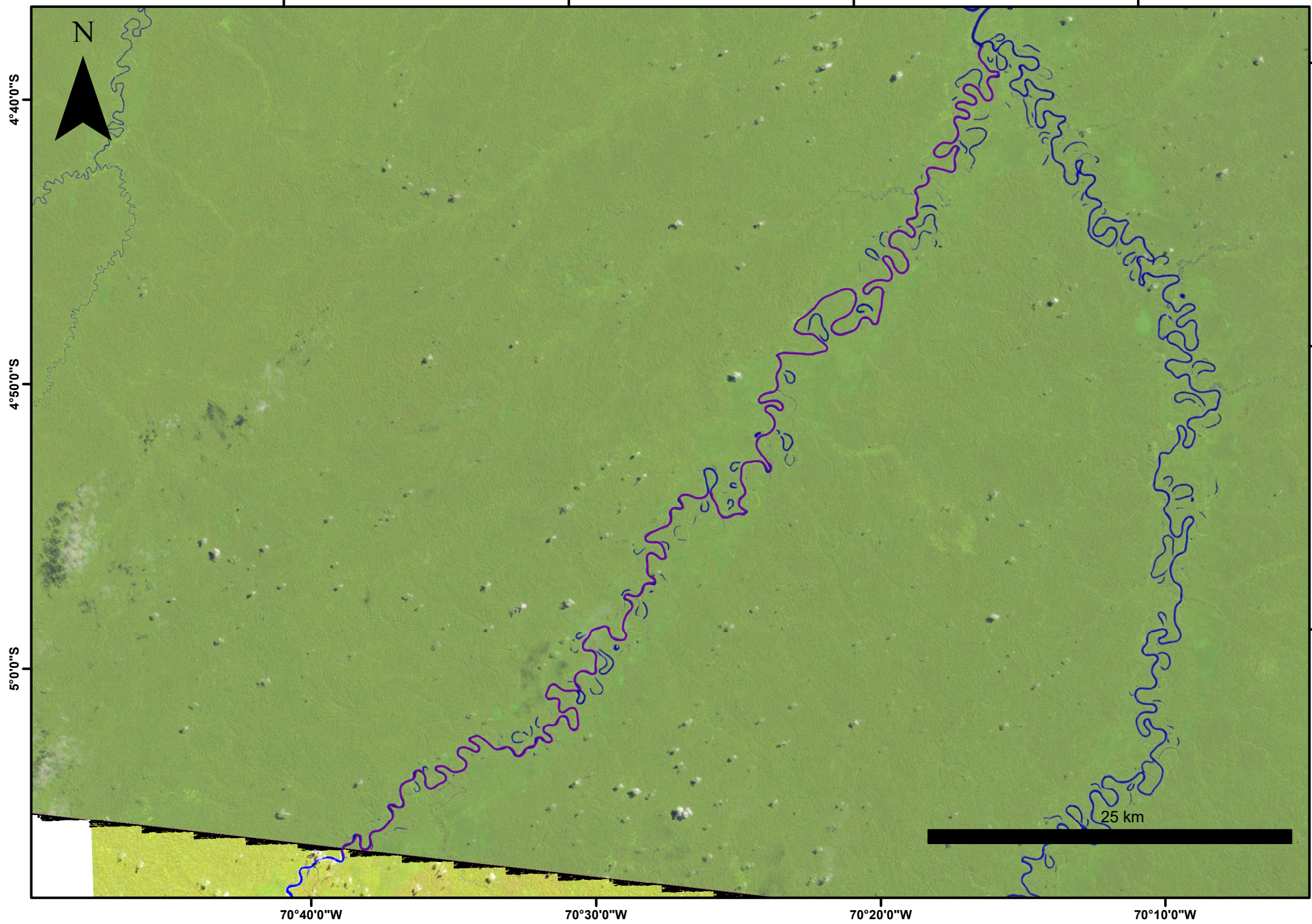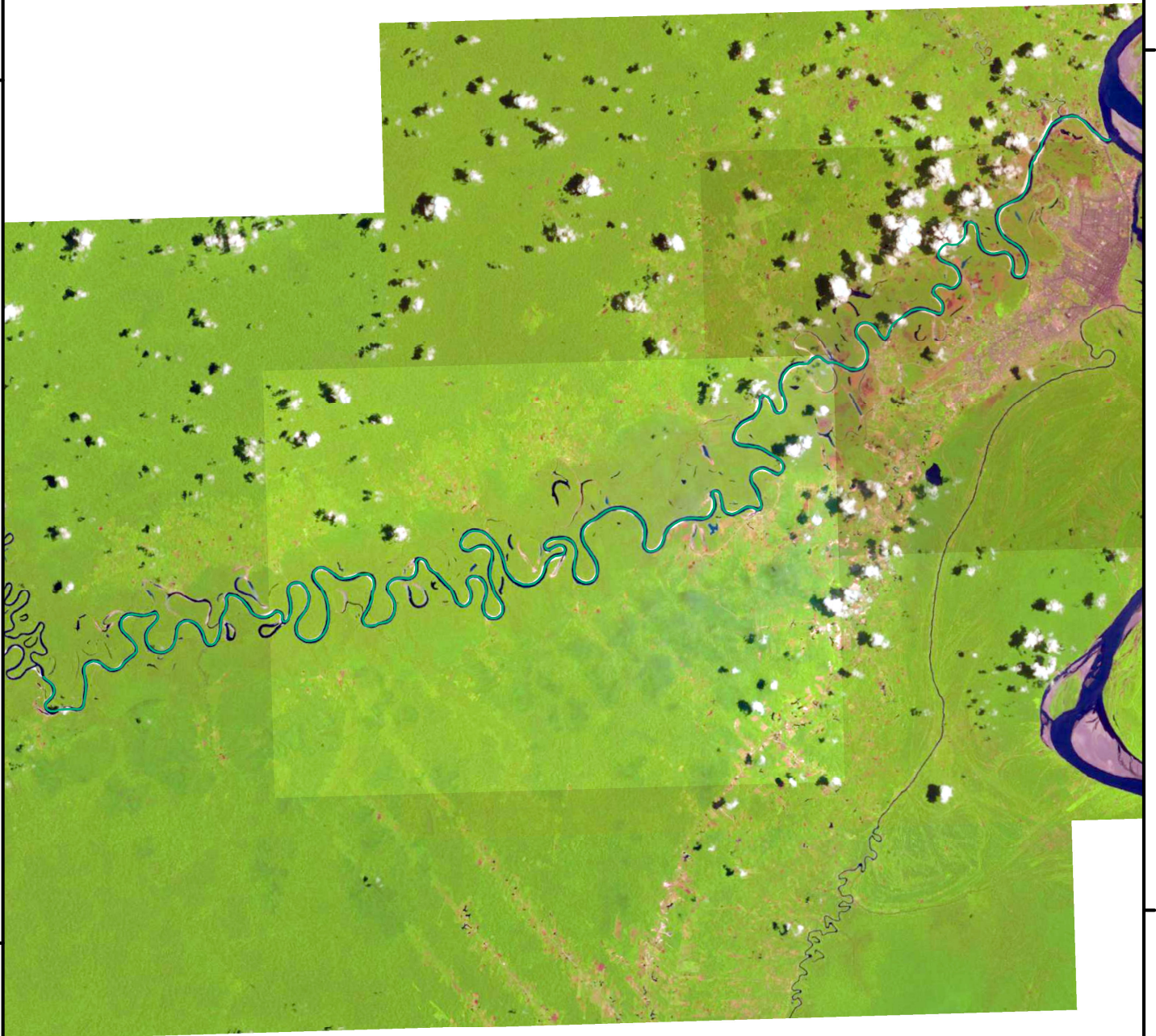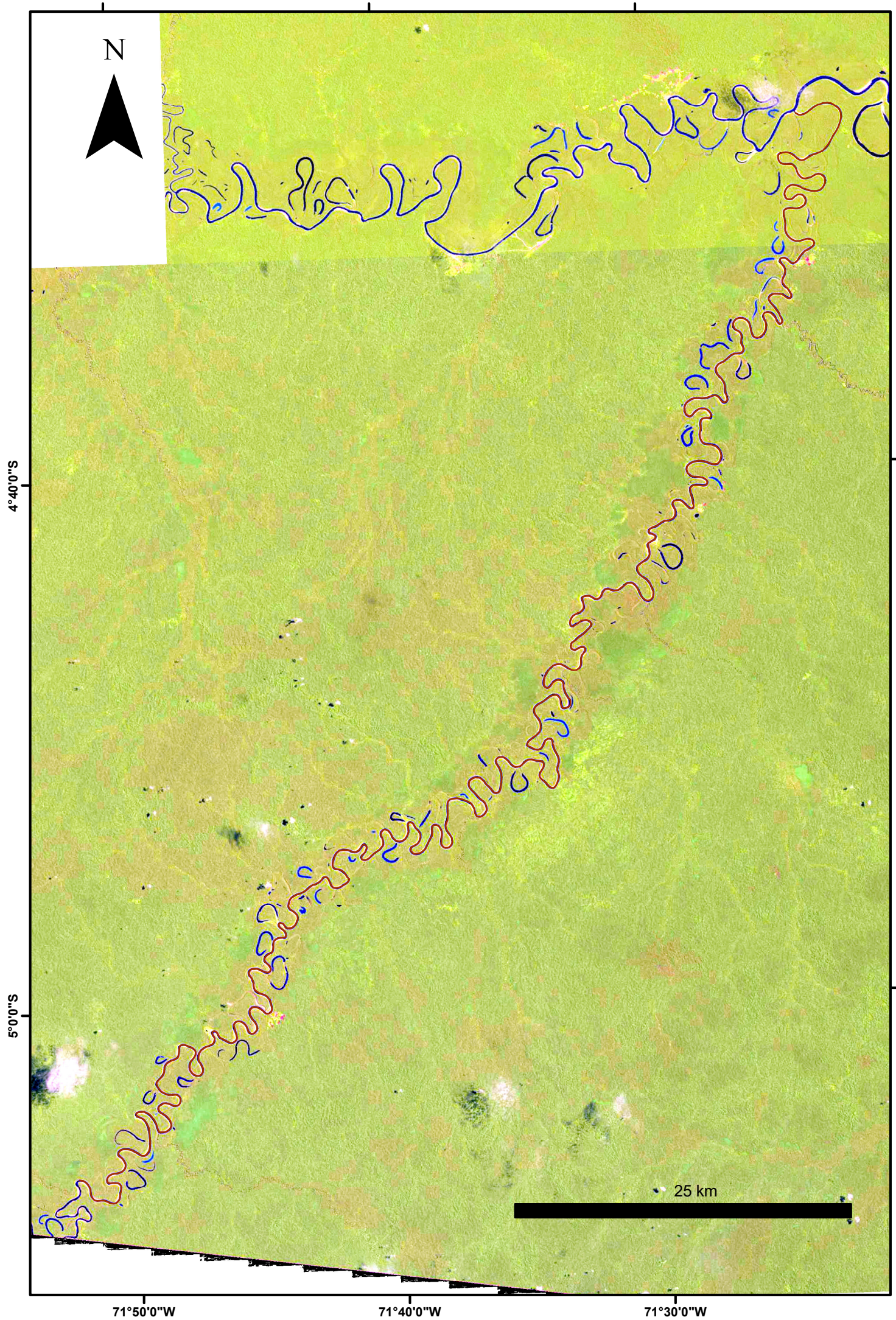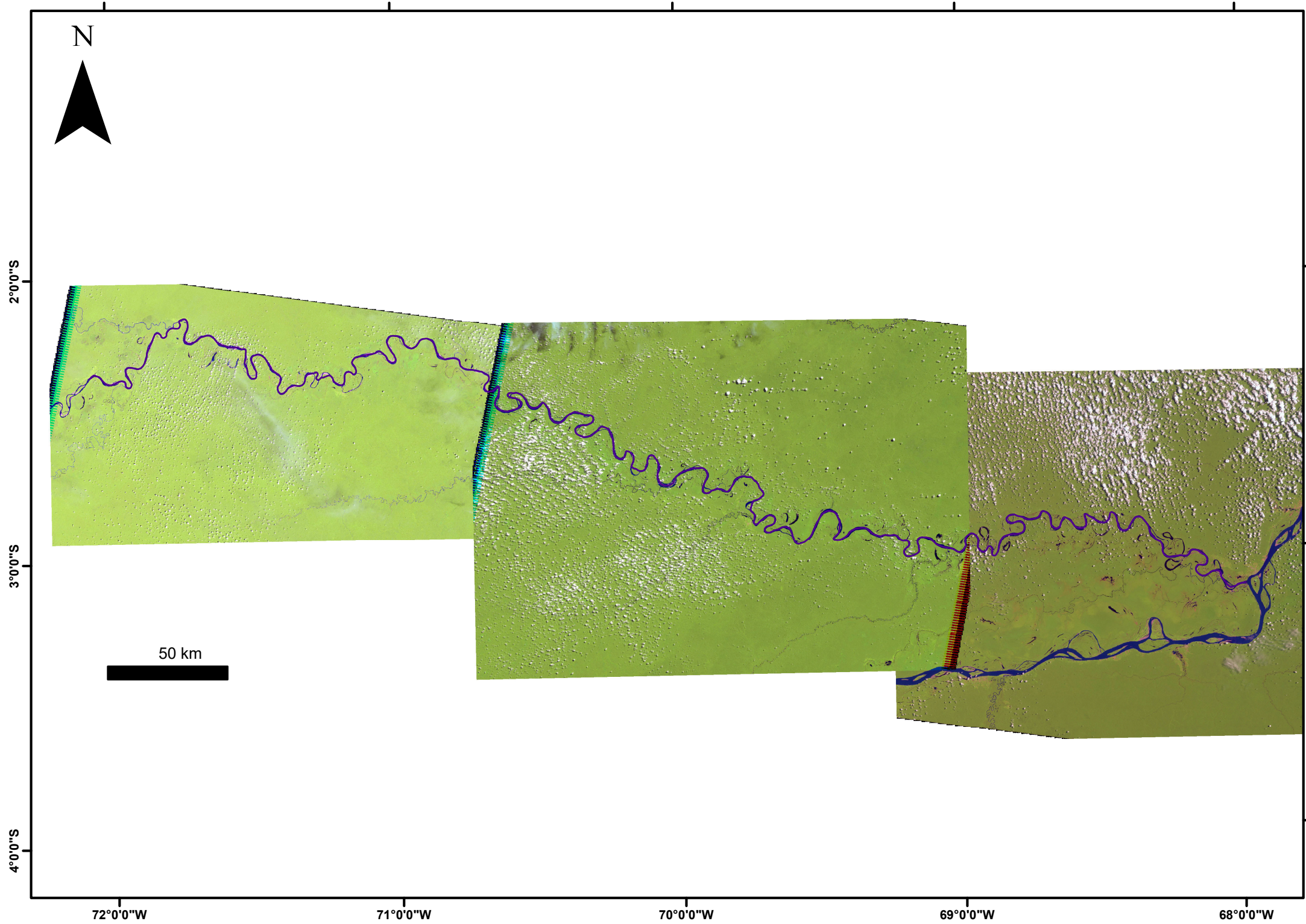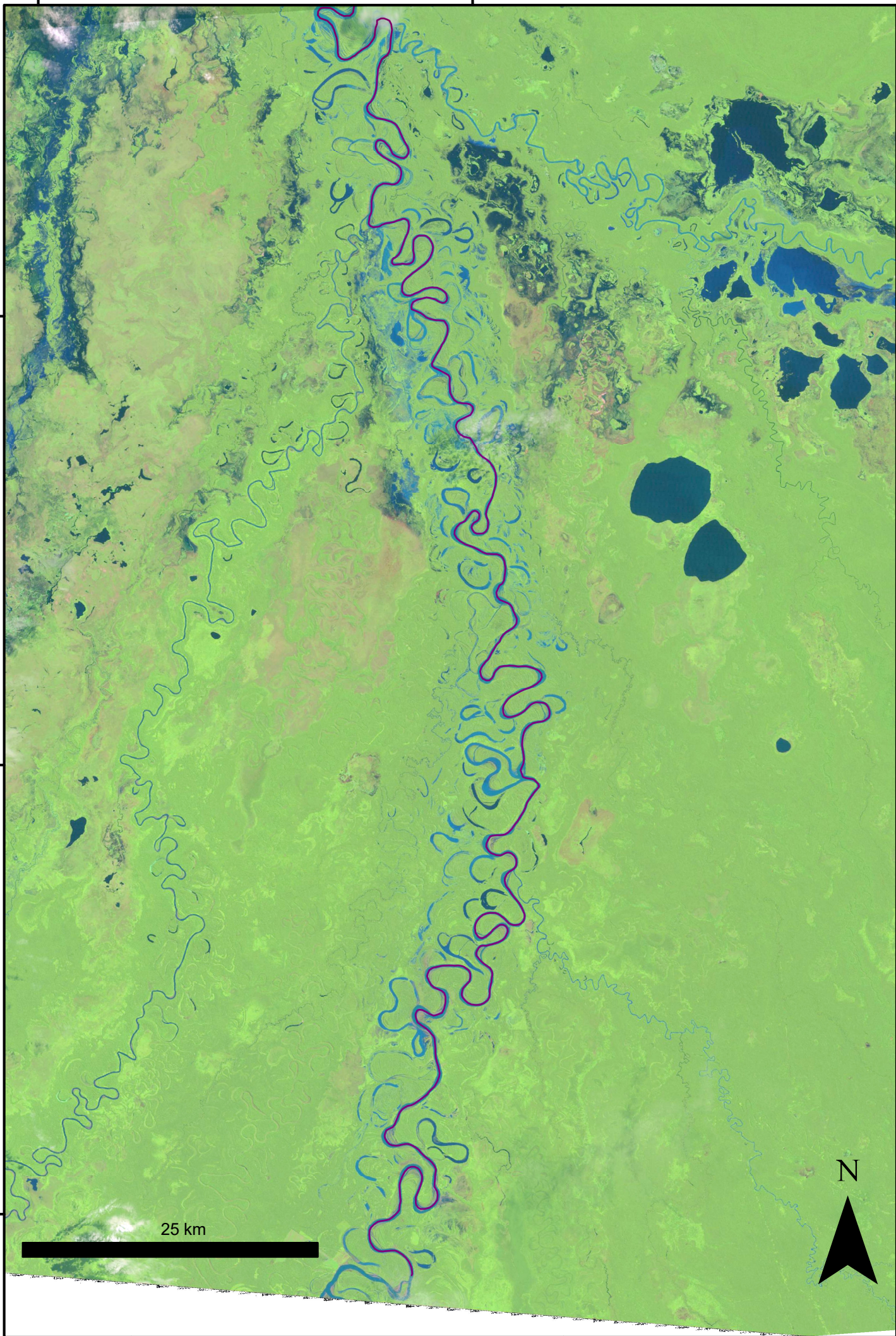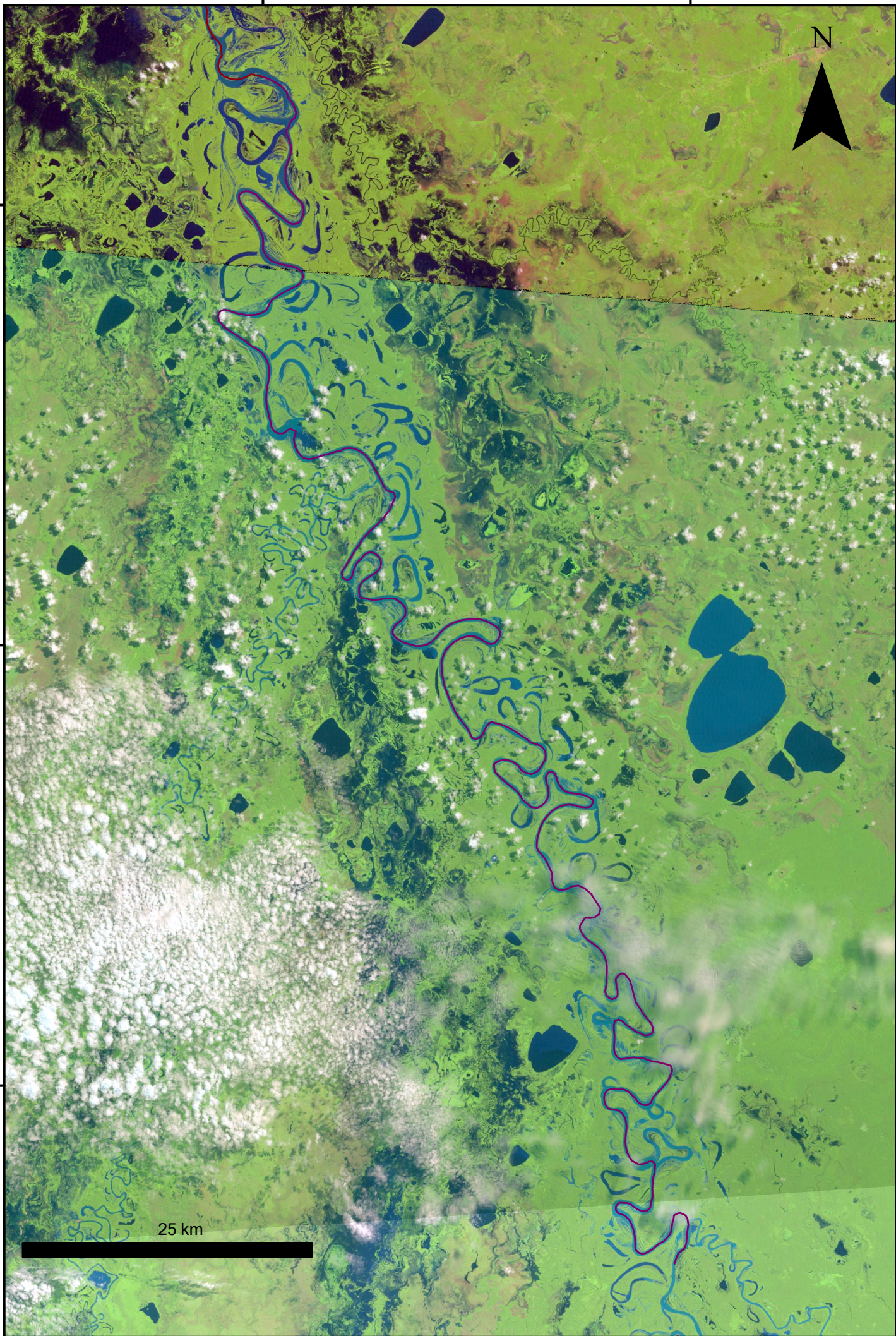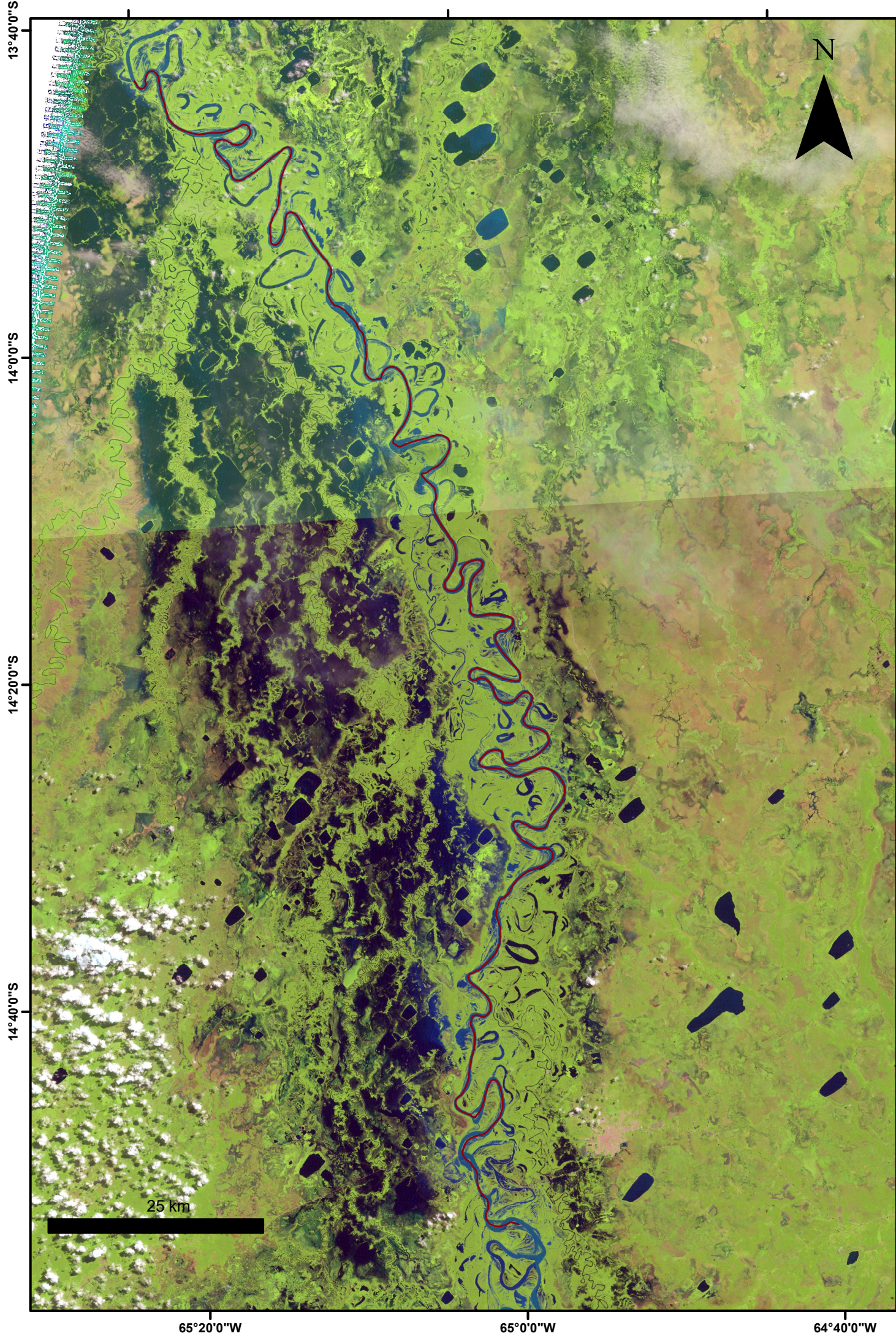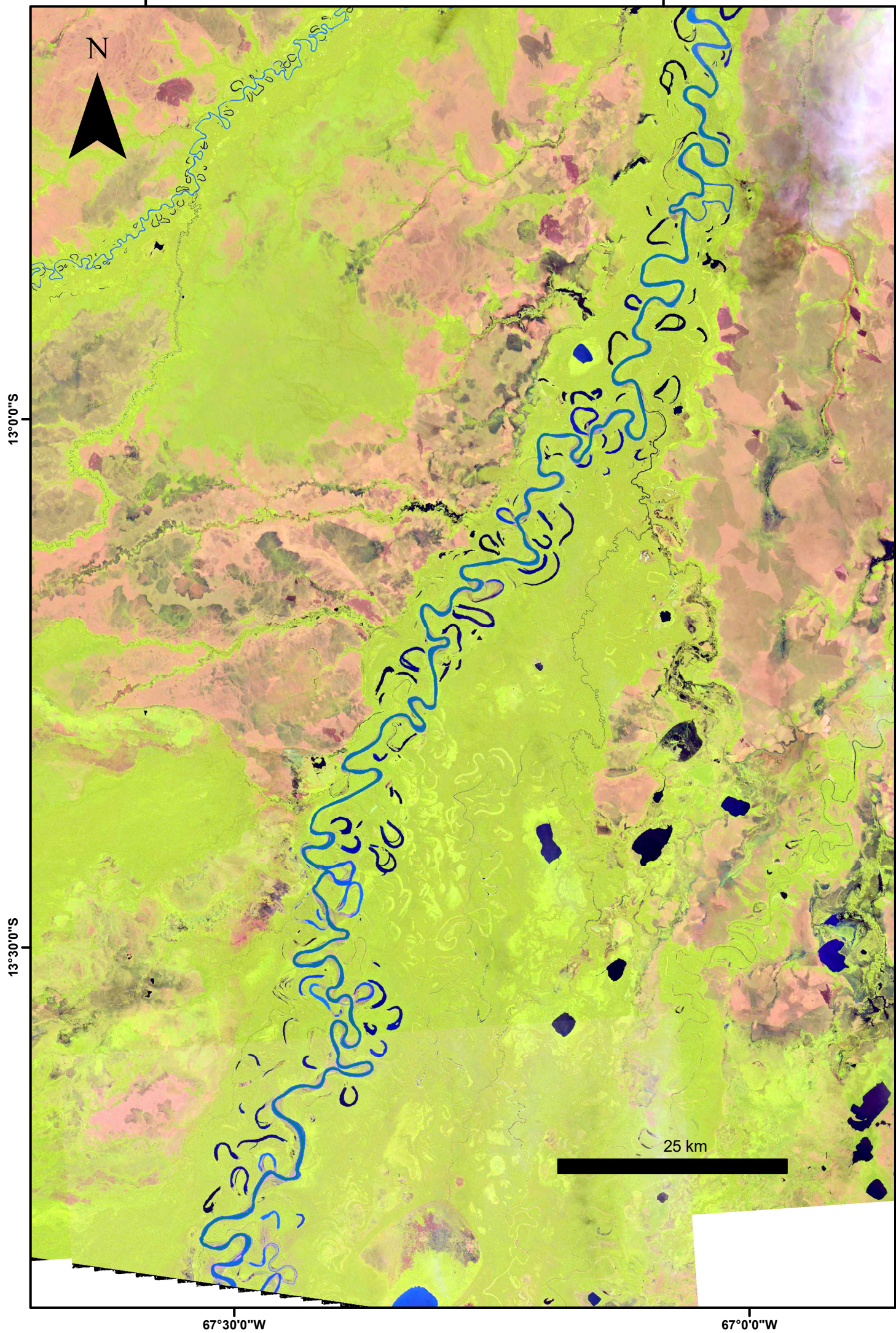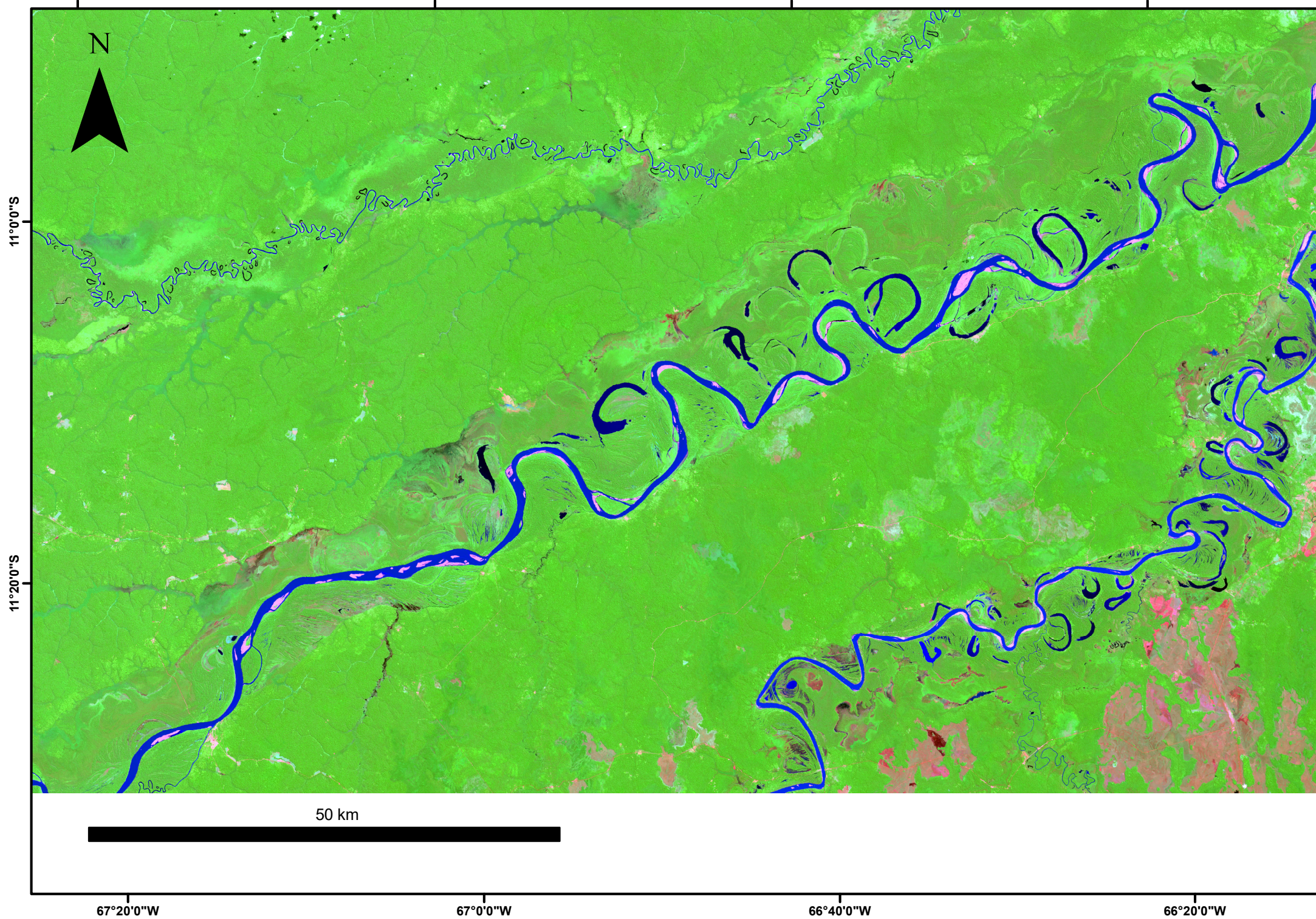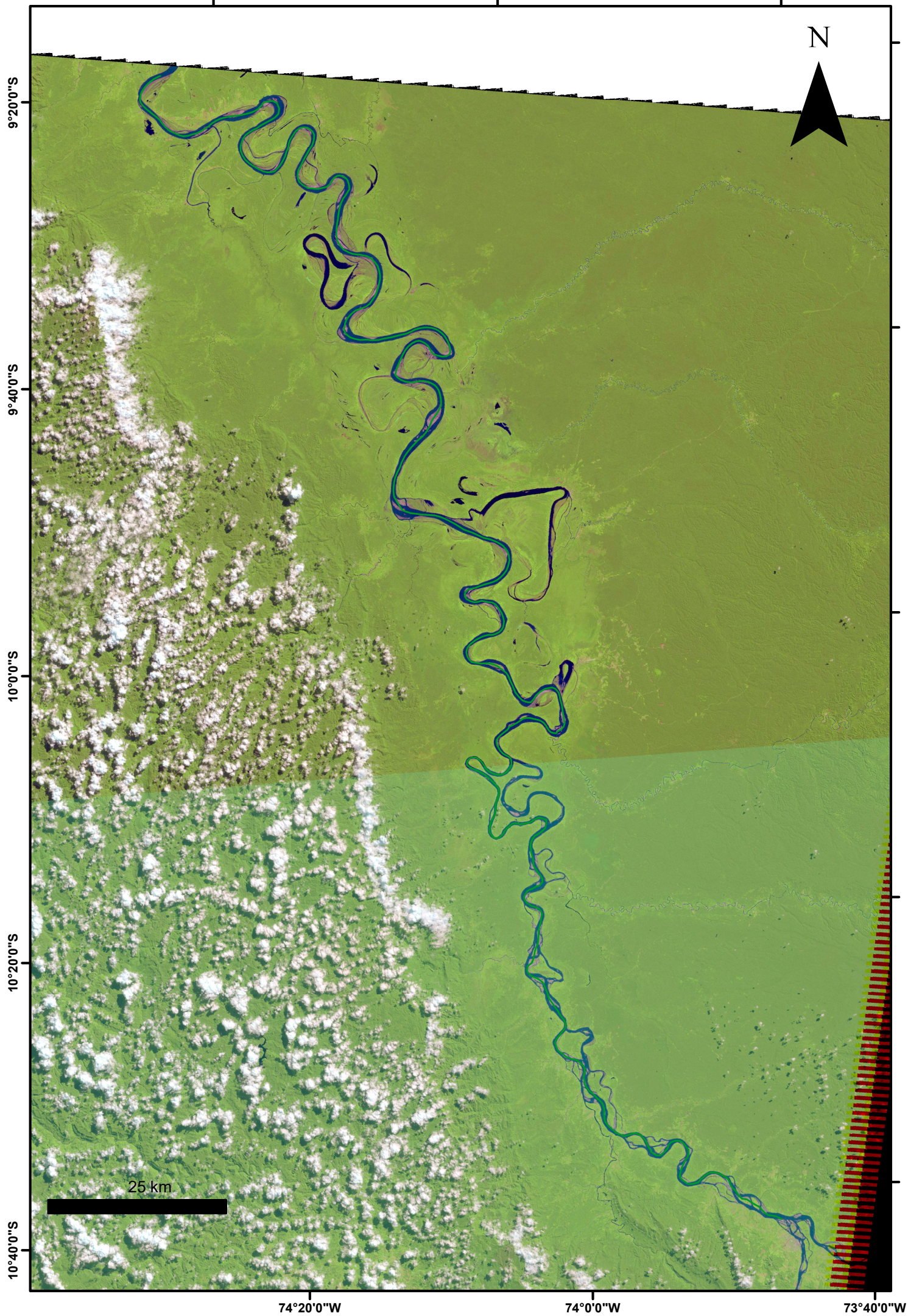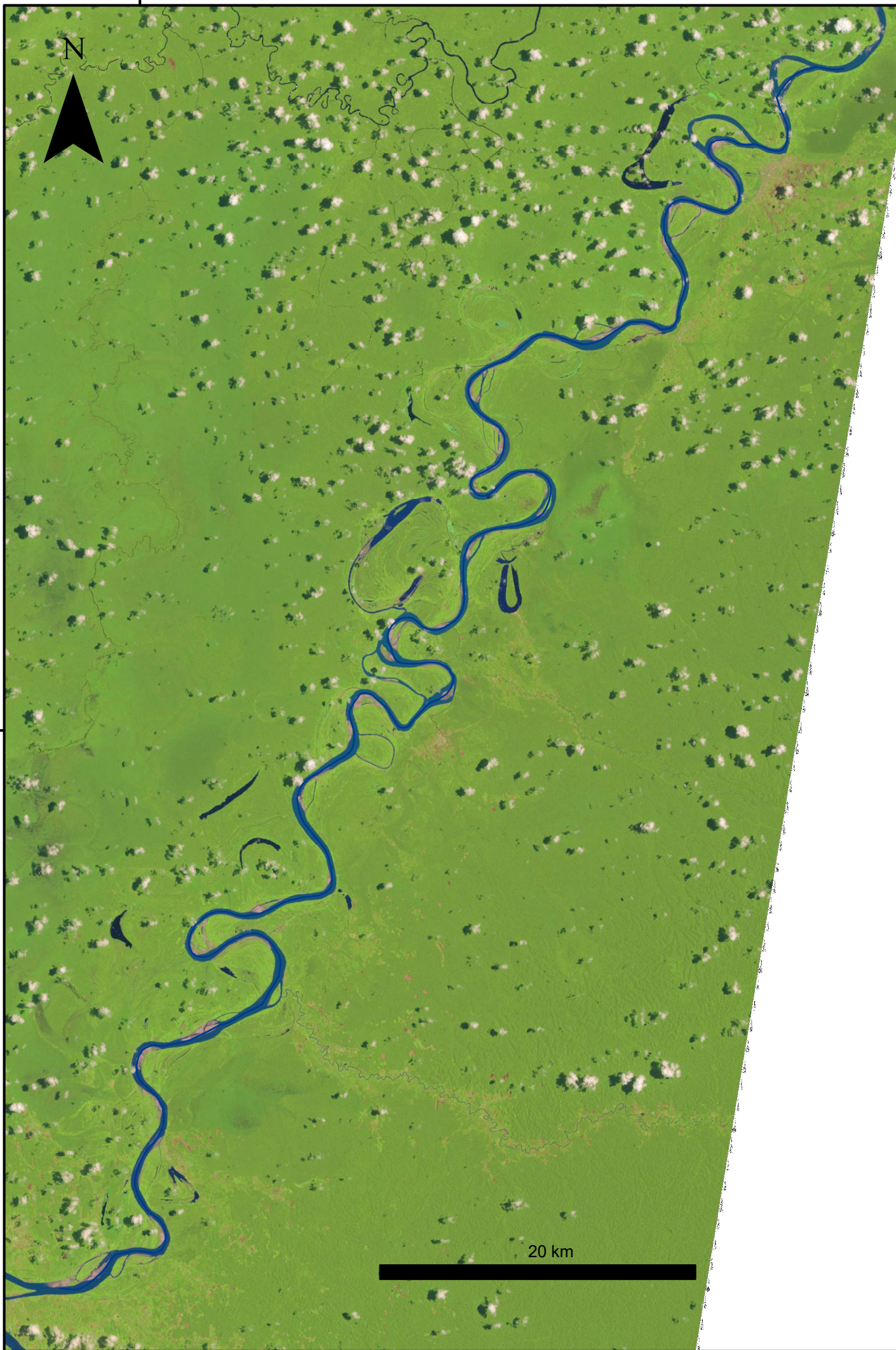
Reach	Physiographic province	Upstream reach coordinates	Downstream reach coordinates	Length (km)	Av. Channel width (m)	Sinuosity	Av. Channel belt width (m)	Estimated channel slope
Araguaia	Shield	13:45:24 S, 50:51:21 W	12:08:50 S, 50:40:28 W	260	420	1.31	5142	0.00010
Vaupes	Shield	01:32:03 N, 72:16:33 W	00:58:55 N, 71:14:26 W	374	150	2.40	1503	0.00003
Branco	Shield	01:55:27 N, 61:00:00 W	00:40:44 N, 61:33:28 W	160	1210	1.03	1759	0.00008
Iriri	Shield	08:44:13 S, 53:22:48 W	06:22:50 S, 54:02:53 W	361	290	1.23	701	0.00021
Xingu	Shield	12:52:59 S, 52:49:02W	12:13:38 S, 53:17:46 W	152	190	1.44	3012	0.00012
Purus1	Central Trough	07:49:25 S, 67:07:16 W	07:32:52 S, 65:23:14 W	469	360	2.28	12608	0.00008
Purus2	Central Trough	05:37:47 S, 63:30:38 W	03:58:44 S, 61:28:36 W	579	700	1.76	8815	0.00003
Jurua	Central Trough	06:22:29 S, 68:10:38 W	03:41:28 S, 66:10:29 W	878	330	2.10	11002	0.00005
Jutai	Central Trough	04:49:07 S, 68:33:36 W	03:55:24 S, 67:43:02 W	330	290	2.16	5144	0.00009
Itui	Central Trough	05:06:59 S, 70:38:47 W	04:39:06 S, 70:15:33 W	153	150	2.16	3980	0.00002
Curuca	Central Trough	05:06:17 S, 71:52:15 W	04:26:47 S, 71:24:01 W	219	180	2.33	2691	0.00005
Nanay	Central Trough	03:53:52 S, 73:39:48 W	03:42:00 S, 73:14:34 W	128	180	2.27	1953	0.00010
Putumayo (Ica)	Central Trough	02:21:48 S, 72:04:34 W	03:08:13 S, 67:58:28 W	882	720	1.72	6964	0.00005
Mamore0	Andes-Foreland Basin	16:44:01 S, 64:46:52 W	15:50:13 S, 64:44:34 W	260	270	2.05	9894	0.00012
Mamore1	Andes-Foreland Basin	15:50:13 S, 64:44:34 W	14:54:53 S, 65:00:00 W	231	330	2.06	9131	0.00010
Mamore2	Andes-Foreland Basin	14:54:53 S, 65:00:00 W	13:43:26 S, 65:19:47 W	280	430	1.85	8558	0.00005
Beni	Andes-Foreland Basin	13:48:05 S, 67:29:07 W	12:42:21 S, 66:57:48 W	300	410	2.00	12575	0.00008
Ucayali	Andes-Foreland Basin	10:41:55 S, 73:46:08 W	09:18:42 S, 74:23:25 W	393	600	1.81	10051	0.00013
Madre de Dios	Andes-Foreland Basin	11:32:18 S, 67:20:35 W	11:01:23 S, 66:15:17 W	216	650	1.57	18101	0.00010
Huallaga	Andes-Foreland Basin	05:47:23 S, 76:04:13 W	05:10:26 S, 75:38:07 W	143	420	1.72	6569	0.00010